Modelling Integrated Biomass and Photovoltaic Generators for Rural Electrification

Efosa Osaghae

Submitted in accordance with the requirements for the degree
of
Doctor of Philosophy

The University of Leeds
School Chemical and Process Engineering
Faculty of Engineering

May, 2020

The candidate confirms that the work submitted is his own. The candidate confirms that appropriate credit has been given within the thesis where reference has been made to the work of others. This copy has been supplied on the understanding that it is copyright material and that no quotation from the thesis may be published without proper acknowledgement.

PUBLICATIONS AND CONFERENCES

Conference:

1. E. Osaghae, B. Chong. R. Crook, and A. Heyes, ‘‘The effect of demand variability and generating cost on the deployment of integrated renewable energy systems,’’ in Conf. 12th International conference on sustainability, Portland, USA Jan. 21 – 23, 2016.

ACKNOWLEDGEMENTS

While trying to write this section, the memories of these years with all its ups and downs were reminisced in my mind, reminding me that without the support of many people, it was impossible to go this distance alone. Yet it is not possible to mention all the names here and I hope that I will be excused by those whose names are not here.

First, I would like to express the utmost appreciation to my project supervisors Dr. Rolf Crook, Dr. Benjamin Chong and Professor Andrew Heyes, for their positive attitude, encouragement, useful critiques and constant availability. Without their supervision and constant guidance this thesis would not have been possible. I also want to thank my previous supervisors Professor Mohamed Pourkashanian, Professor Derek Ingham, Professor Lin Ma and Dr. Kevin Hughes for their valuable comments, guidance and suggestions during the early years of my research. I am also grateful to University of Leeds for the training they provided and the financial assistance I received towards my third-year tuition fee payment.

I sincerely appreciate University of Benin, Nigeria and Tertiary Education Trust Fund, Nigeria for granting me a PhD scholarship.

A special thanks to my family (Osaghaes and Inegbedion) for their sacrifices and prayers. At the end I would like to express my deepest appreciation to my beloved wife (Dr. Isimemen) for her continuous support and encouragement, and to my children (Dominion and David). Their presence motivated me each day

ABSTRACT

Renewable energy technologies can be used for clean electricity generation, rapid rural electrification and cost-effective supply of reliable electricity. In this thesis, the study of the effect of integrating biomass and photovoltaic generators for rural electrification will involve survey and modelling of rural households load profiles, investigation of the optimal combination of PV, biomass and battery energy systems for reliable supply of electricity and a power flow study of the impact of load aggregation on the operation of a regional grid. The studied location solar radiation and biomass availability data are used when selecting the optimal combination of components in the hybrid renewable energy system (HRES) design space.

An occupancy-based stochastic load profile model is developed with the use of survey data on the number of bedrooms in a household, household population and classification, occupant' activity schedule and appliance ownership. Analysis of simulated load profiles show that the studied location average daily energy consumption was 3.13 kWh. During solar radiation assessment, performance evaluation of meteorological parameters used for constructing solar radiation estimation models show that temperature is an important meteorological parameter that should be used to estimate studied location solar radiation. Whilst, the minimum required duration of measured data to estimate past solar radiation shows that 2 years of recent data is required to achieve R^2 greater than 0.75, and more than 5 years of recent solar radiation data is required to achieve R^2 greater than 0.9. Biomass availability assessment shows that the quantity of recoverable household and animal bio-waste in the studied location is limited. To reduce the quantity of outsourced bio-waste and minimize anaerobic digester volume, biogas generator is only used when energy demand is greater than 50% of its rated capacity. Study on how different combinations of PV, biogas generator and battery systems affect the optimal sizing of battery shows that an optimally designed HRES requires a much smaller battery capacity than when a biogas generator and battery or a PV and battery are integrated for rural electrification in the studied location.

Techno-economic analysis of the HRES shows that for 0% loss of power supply probability (LPSP), the levelized cost of energy (LCOE) is $0.1657/kWh, but the

LCOE for a diesel alone energy system was $0.62/kWh. Despite the national grid unreliability, its 2019 residential customers reflective tariff (i.e., a tariff without subsidizes) for the studied location was $0.164/kWh. HRES analysis also shows that if the HRES LPSP is increased to 3.7%, its LCOE is reduced to $0.1623/kWh. So, for a LPSP of 3.7%, the HRES LCOE is less than the LCOE of the national grid. Power flow study of the effect of aggregating 5 regional loads show that load aggregation reduced the 5 regions peak load by 23%. Furthermore, power flow study of the regional grid shows that power losses minimization will be achieved when installed generators are not centralized but distributed in terms of the amount of apparent power drawn by each of the regional grid load buses. Overall, this study shows that integrated biomass and photovoltaic generators can be used for rural electrification because the HRES guarantees the supply of clean and sustainable electricity and its LCOE can compete with national grid LCOE. Meanwhile, future work will profit from the development of an electricity pricing plan that allows for the shifting of peak loads and a study of how the electricity pricing plan affects LCOE.

TABLE OF CONTENTS

LIST OF FIGURES

LIST OF TABLES

NOMENCLATURE

Symbol	Meaning	Unit
G_{SC}	Solar constant	kWm^{-2}
H_g	Daily horizontal surface global solar radiation	$kWm^{-2}day^{-1}$ or $MJm^{-2}day^{-1}$
H_o	Daily horizontal surface extra-terrestrial global solar radiation	$kWm^{-2}day^{-1}$ or $MJm^{-2}day^{-1}$
K_T	Clearness index	
S	Daily average sunshine duration	h
S_o	Maximum sunshine duration or day length	h
G_{SC}	Solar constant	kWm^{-2}
N_{day}	Day number of a year	
Γ	Day angle	°
H_{meas}	Measured daily global solar radiation	$kWm^{-2}day^{-1}$ or $MJm^{-2}day^{-1}$
H_{pred}	Predicted daily global solar radiation	$kWm^{-2}day^{-1}$ or $MJm^{-2}day^{-1}$
η	Efficiency	
E_{PV}	PV installation hourly electricity generation	kWh
P_{PV}	PV installation peak power or rated capacity	kW_P
$P_{PV,1m^2}$	Peak power of a meter squared PV panel	kW_P
I_g	Hourly global solar radiation on a horizontal surface	$kWm^{-2}h^{-1}$
I_γ	Hourly global solar radiation on an inclined surface	$kWm^{-2}h^{-1}$
I_{STC}	Solar irradiance under standard test conditions	$kWm^{-2}h^{-1}$
k_{temp}	Temperature power correction coefficient	$\%°C^{-1}$
DF_{PV}	PV installation derating factor	%
η_{PV}	PV panel electrical efficiency	
η_{ref}	PV panel manufacturer's reference efficiency	
γ_o	Irradiance level correction coefficient	
Δt	Change in time	
T_{PV}	PV temperature	°C
T_a	Ambient temperature	°C
T_{STC}	Temperature under standard test condition	°C
NOCT	Nominal operating cell temperature	°C
k_α	Ross coefficient	$°C\ m^2W^{-1}$
A_{PV}	Effective collection area of a PV installation	m^2
A_{mod}	Effective collection area of a PV module	m^2
N_{PV}	Total number of PV modules in a PV installation	
ϕ	Latitude	°
δ	Sun declination angle	°
ω	Hour angle	°
ω_S	Sunrise hour angle	°
T_S	Solar time	mins
T_{st}	Standard or local clock time	h
L_{st}	Standard meridian for the local time zone	°
L_{loc}	Longitude of the location	°
E_t	Equation of time	mins
θ	Solar incidence angle	°
θ_z	Solar zenith angle	°
γ	Surface azimuth angle	°

β	Tilt angle	°
ρ_r	Reflectivity or ground albedo	
η_{Conv}	Efficiency of the power converter	
η_{mod}	Module efficiency of the PV material type	
$C_{ann,tot}$	Annualized total cost of the system	$
$C_{ann,cap}$	Annualized capital cost	$
$C_{ann,rep}$	Annualized replacement cost	$
$C_{ann,O\&M}$	Annualized operation and maintenance cost	$
$C_{ann,fuel}$	Annualized fuel cost	$
ir_{nom}	Nominal interest rate	
ir	Real interest rate	
f_r	Inflation rate	
P	Real power	kW
Q	Reactive power	kV_{ar}
S	Apparent power	kVA
V	Voltage	Volts
δ°	Phase angle	rad
Y	Admittance	Ω^{-1}
G	Conductance	Ω^{-1}
B	Susceptance	Ω^{-1}
Z	Impedance	Ω
Z_{TX-PU}	Impedance normalised per unit value	Ω
$Z_{TX-actual}$	Actual impedance of the line	Ω
Z_{base}	Base impedance	Ω
ΔP	Real power mismatch	kW
ΔQ	Reactive power mismatch	kV_{ar}
N_{ss}	Survey sample size	
Z_{score}	The value of the confidence level on a Z-table	
e	Margin of error	
N_{pop}	Population size	
$E_{app,j}$	The energy consumption of an appliance	kWh
$P_{app,j}$	The power rating of an appliance	kW
$N_{app,j}$	The quantity of an appliance in a household	
P_{Bio}	Biogas generator rated capacity	kW
E_{Bio}	Biogas generator hourly electricity generation	kWh
Y_{biogas}	Biogas generator hourly biogas consumption	m^3
η_{bio}	Biogas generator electrical conversion efficiency	
H_{LHV}	Lower heating value	MJ m^{-3}
f_{energy}	Mechanical to electrical energy conversion factor	MJ kWh^{-1}
bmc	Biogas methane content of a bio-waste	%
k_o	Energy to biogas conversion factor	m^3 kWh^{-1}
HRT	Hydraulic retention time	day
Q_{rate}	Substrate influent flow rate	m^3 day^{-1}
TS	Total solid	%
VS	Volatile solid	%
C_i	Influent volatile solids (VS) content	kg_VS $kg^{-1}_{wet\_weight}$
S_{biogas}	Specific biogas production	m^3 kg_VS^{-1}
ρ_s	Substrate density	kg m^{-3}
M_{waste}	Bio-waste quantity or mass	kg
Vol_W	Digester (reactor) working volume	m^3
Vol_{actual}	Digester (reactor) actual volume	m^3

u	Digester (reactor) non-working volume	m^3
E_{DC_net}	DC bus net energy	kWh
E_{AC_net}	AC bus net energy	kWh
E_{BSD}	Battery self-discharge	kWh
E_{BSS}	Battery storage capacity	kWh
R_{BSD}	Battery self-discharge rate	$\%h^{-1}$
E_{Load}	Electrical load	kWh
$E_{B/SOC}$	Battery state of charge	kWh
$E_{B/charging}$	Battery charging energy	kWh
$E_{B/discharging}$	Battery discharging energy	kWh
E_{AC/DC_net}	AC/DC net energy	kWh
P_{Conv}	Rated capacity of converter	kW
η_{Conv}	Converter efficiency	
CP_{ST}	State transition conditional probability	
MAE	Mean absolute error	$kWm^{-2}day^{-1}$
RMSE	Root mean square error	$kWm^{-2}day^{-1}$
MPE	Mean percentage error	
MARE	Mean absolute relative error	
RRMSE	Relative root mean square error	
RMSRE	Root mean square relative error	
erMax	Maximum absolute relative error	
U_{95}	Uncertainty at 95%	$kWm^{-2}day^{-1}$
R^2	Coefficient of determination	
UML	Un-met load	kW
n	Project lifetime	Year
n_j	System component lifetime	Year

Abbreviations

IEA	International energy agency
SSA	Sub-Saharan Africa
Tx	Transmission line
T&D	Transmission and distribution
SHS	Solar home system
DG	Distribution generation
GHG	Greenhouse gas
FGN	Federal government of Nigeria
REA	Rural electrification agency
SHP	Small hydropower
LGA	Local government area
LCOE	Levelized cost of energy
PV	Photovoltaic
REMP	Renewable energy master plan
IRENA	International renewable energy agency
FAO	Food and agriculture organization
UNIDO	United nation industrial organization
CHP	Combined heat and power
AD	Anaerobic digestion
CAD	Centralized anaerobic digestion
MSW	Municipal solid waste
ECN	Energy commission of Nigeria
NiMet	Nigerian meteorological agency
IEC	International electro-technical commission

NREEEP	National renewable energy and energy efficiency policy
FIT	Feed-in tariff
HRE	Hybrid renewable energy
ESS	Energy storage system
VFA	Volatile fatty acids
C/N	Carbon to nitrogen ratio
PHES	Pumped hydro energy storage
FES	Flywheel energy storage
BESS	Battery energy storage system
CAES	Compressed air energy storage
SWOT	Strength, weakness, opportunity, and threat
SMES	Superconducting magnetic energy storage
$DISCO_S$	Distribution companies
TD	Top-down
BU	Bottom-up
TUS	Time use survey
LSPS	Loss of power supply probability
EENS	Expected energy not supplied
SOC	State of charge
LOLP	Loss of load probability
NPC	Net present cost
PoPA	Power pinch analysis
CBN	Central bank of Nigeria
MPP	Maximum power point
STC	Standard test condition

Chapter 1 INTRODUCTION

This chapter introduce the research works performed in this thesis. The chapter begins by presenting a background to the research, then the motivation for the research and a clear definition of the scope of the research. Next, the research aim and research objectives are presented. But before the research objectives are presented in this chapter, a series of un-answered research questions are presented. Finally, this chapter ends with an outline of the research focus of the remaining chapters.

1.1 Research background

1.1.1 Energy and growth in demand consumption

Energy is a vital instrument that enables sustainable economic prosperity and improves the standard of living of a nation. The desire for energy can be expressed by the continuous growth in world energy consumption. According to British Petroleum (BP) 2018 international energy outlook, global primary energy demand will increase from 13.276 billion tonnes of oil equivalent (btoe) in 2016 to 17.983 btoe in 2040 [1]. Therefore, global primary energy demand increased at a rate of 1.27% per annum (p.a.). The key energy demand drivers used to underpin projected growth in primary energy demand are energy demand trends data, population growth data, and global prosperity data [1]. Past and projected growth in primary energy demand is presented in Fig. 1.1.

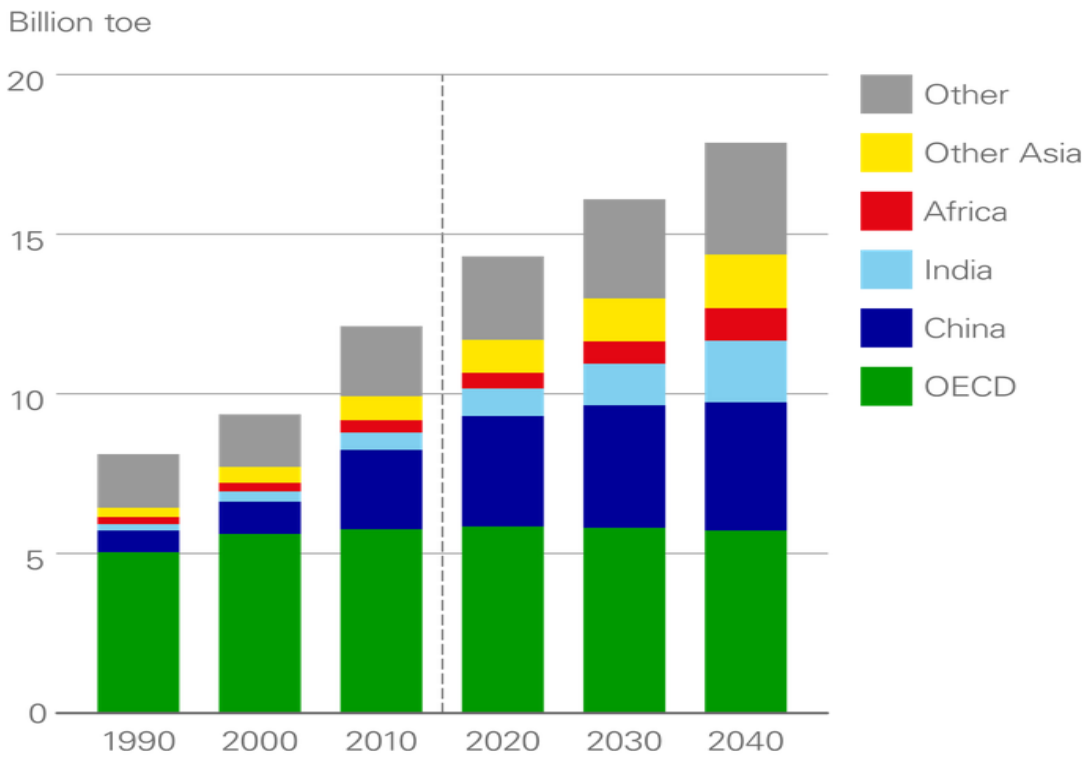

Fig. 1.1. Global primary energy demand (billion toe) [1]

Fig. 1.1 shows that the rise in global primary energy demand is linked to fast-growing emerging economies increased demand for energy. By 2040, Asia Pacific countries (i.e., China, India and other emerging Asia countries) will account for two-thirds of the growth in global primary energy demand [1]. This is because Asia Pacific countries primary energy demand increase by 57% between 2016 and 2040. Fig. 1.1 also shows that Organization for Economic Co-operation and Development (OECD) countries has a flat primary energy demand growth during the projected period.

Non-OECD countries strong economic growth and the desire by these countries to improve their standard of living are responsible for the rapid growth in primary energy demand [1]. International Monetary Fund (IMF) economic growth chart shows that since the millennium, non-OECD countries have maintained a faster economic growth rate in comparison to the economic growth rate of the world and OECD economies [2]. Specifically, 2018 IMF report shows that the economic growth rate – as measured by the gross domestic product (GDP) – for non- OECD countries

is 4.9%, while the economic growth rate for the world and OECD countries are 3.9% and 2.5% respectively [2].

1.1.2 Electricity outlook

Electricity is the world fastest-growing form of end-use energy [1]. Electricity plays an important role in the development and industrialization of a country. As the world continues to electrify, the rapid increase in electricity generation (specially in developing countries) is motivated by the desire to supply electricity to growing demand and/or the desire to improve electricity access. BP 2018 international energy outlook reports that global electricity consumption will rise from 64942 terawatt hour (TWh) in 2017 to 102507 TWh by 2040 [1]. The rise in electricity consumption is at a rate of 1.9% per annum (p.a.). Over this period, the growth in electricity demand will be three times more than the growth in other end-use energy demands [1].

International energy agency (IEA) 2018 report shows that global electricity demand experienced a rapid growth in 2017 because global electricity demand grew by 3.1% or 780 terawatt hours (TWh) over the previous year [3]. IEA 2018 report also show that in 2017, global energy demand grew by 2.1%, the energy demand of non-OECD countries grew by 2.5% and the energy demand of OECD countries (with more matured infrastructure and relatively slow or declining population growth) grew by 1.2% [3]. The higher growth rate recorded in 2017 for global electricity demand in comparison to global energy demand was because of the increased demand for electricity. Cleaner electricity generation resources such as renewable energy sources, natural gas, and nuclear power are expected to make substantial contribution in meeting the increase demand for electricity [1]. Past and projected share of generation resources that are used to supply global electricity is presented in Fig. 1.2.

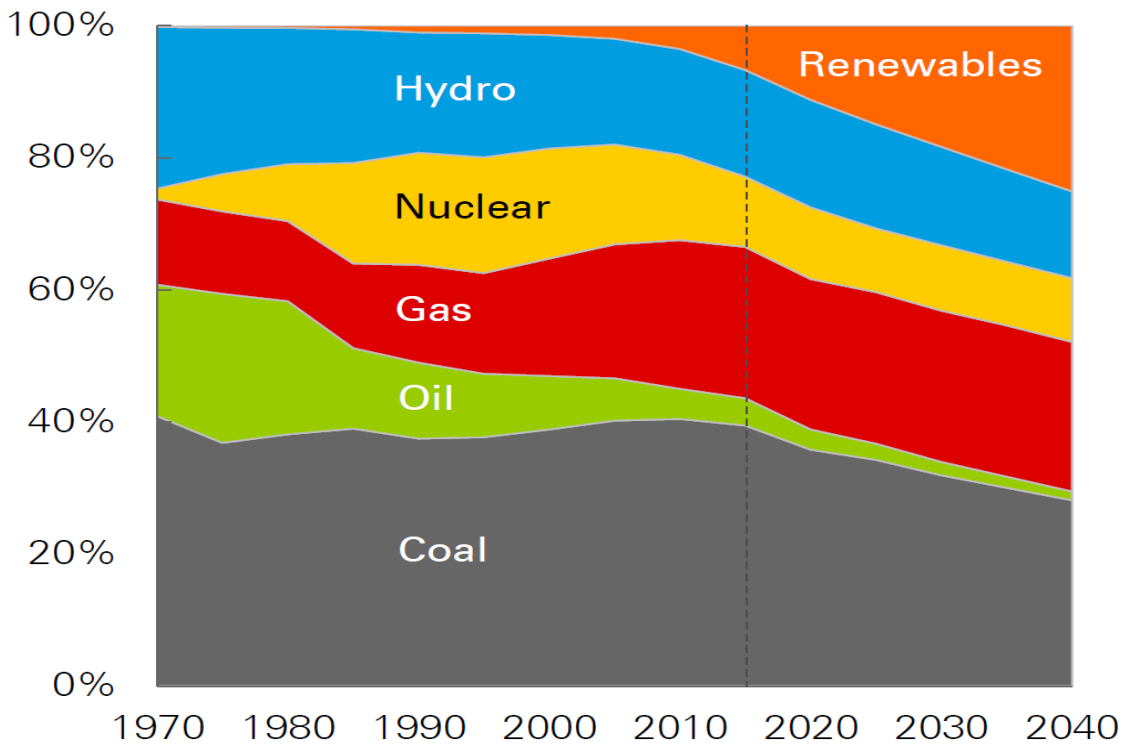

Fig. 1.2. 1970 – 2040 global share of electricity generation resources [1].

Due to global environmental concerns and the desire to reduce global greenhouse gas (GHG) emissions, Fig. 1.2 shows that there will be more drastic shift towards the use of renewables for electricity generation. Over the projected period, half of the newly installed generators will be powered by renewables, therefore, global percentage use of renewables for electricity generation will increase from 7% in 2016 to a quarter in 2040.

It is evident from Fig. 1.2 that the increase in renewables will have the most impact on the usage of coal because in comparison to the previous 35 years where coal accounts for 40% of newly installed generators, coal will account for 13% of newly installed generators in the projected period [1]. The continuous rise experienced over the past 35 years in natural gas share will be affected by renewables usage during the projected period because natural gas share will flatten during this period.

1.1.3 Trends in global electricity access

The pace of progress in universal electricity access has accelerated, resulting in the number of people without electricity access falling from 1.6 billion people in 2000

to about 1.1 billion for the first time in 2016, and with nearly 1.2 billion people having gained access since 2000 [4]. Despite the impact of growing world population, global desire to ensure access to affordable, reliable and modern energy for all by 2030 will generally be successful in most regions, due to the pace of progress in universal electricity access [4]. Between 2000 and 2016, global progress made and the progress made by some locations with high number of people without electricity is presented in Fig. 1.3.

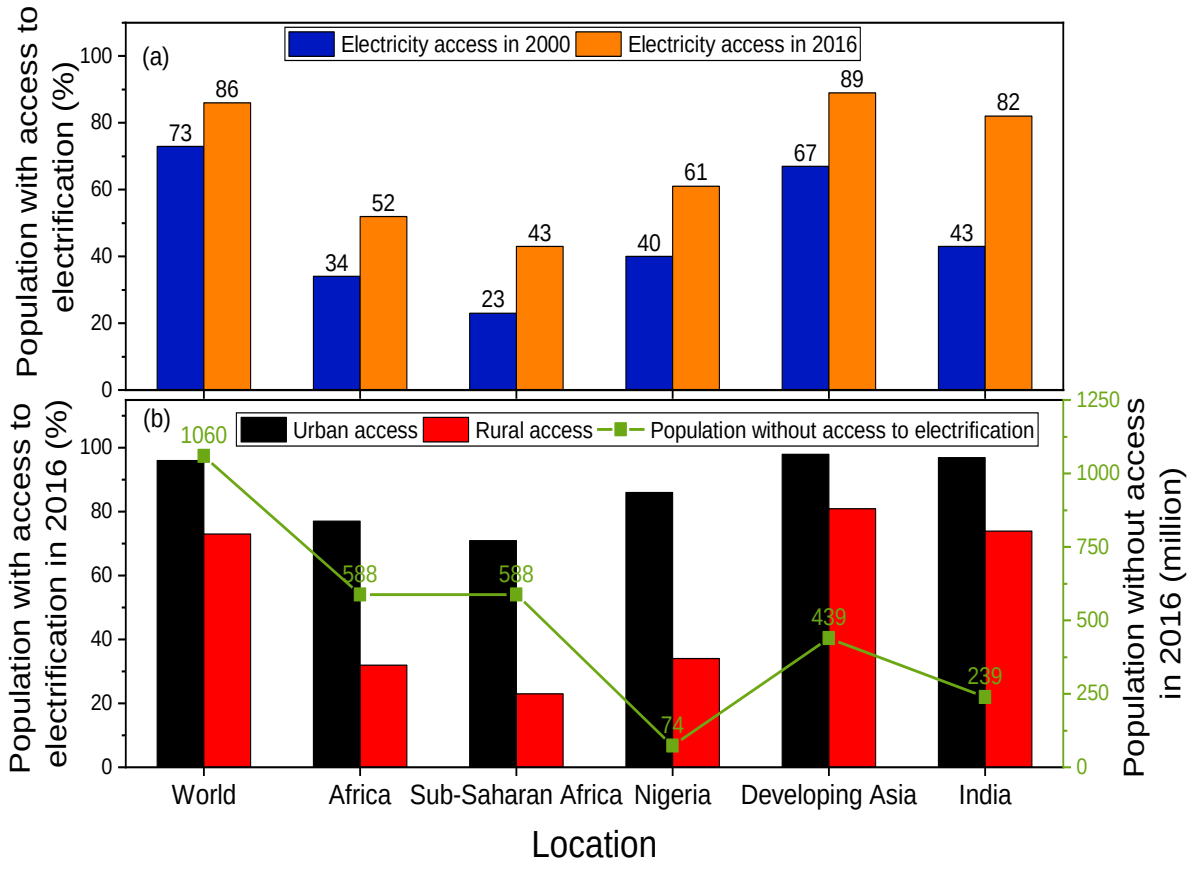

Fig. 1.3. Aggregates of electricity access, (a) Electrification access in the world and some developing nations/regions, (b) 2016 electricity access in urban and rural areas in the world and some developing nations/regions. Data source: [5]

Trends in global electricity access collected from IEA database shows that significant progress has been made globally. For example, nearly 1.2 billion people have gained access to electricity between 2000 and 2016, out of which 870 million people gained access in developing Asia, with India alone accounting for 500 million of those that gained access [4]. As a result, many countries in developing Asia are on course in reaching universal electricity access by 2030, while India is on course in reaching

the global goal of having 100% electricity access by the early 2020s. However, 674 million people of global population are expected to remain without electricity access in 2030 because of growing population, and sub-Saharan Africa (SSA) is where 90% of them will live [4]. It is worrying that SSA projected percentage contribution to the population without electricity access will increase from 50% in 2016 to 90% in 2030.

Meanwhile, electricity access rate is not low for all SSA countries because in countries such as Mauritius, Seychelles, Cape Verde and Gabon, national electricity access rate was more 90% as at 2016 [5]. Significant progress have also been made in improving the rate of electricity access by many SSA countries because between 2000 and 2016, Fig. 1.3 shows that electricity access rate in SSA grew by 87%. Continuous growth in SSA electricity access rate has made its annual increase to outpace its fast growing population rate since 2014 [4]. Due to rapid growth in population, electricity access rate in many SSA countries is uneven and slow, hence, there were more people without electricity in 2016 (588 million people) than there were in 2000 (516 million people) [5]. The use of electricity access rate for comparing the electrification levels of countries might be a misleading because the number of people without electricity access in a country can be more than in another country despite having a higher electricity access rate than the other country.

In Nigeria (this study country of focus), although the percentage of people with electricity access grew from 40% in 2000 to 61% in 2016, there are still more people without electricity in 2016 than there were in 2000 because Nigeria population grew from 122 million in 2000 to 190 million in 2016 [5]. Other challenges with Nigeria drive towards universal access for all is the poor quality of electricity supply to customers [6], and the uneven electricity distribution between Nigeria urban and rural areas. Whilst it is far from complete, Fig. 1.3 shows 2016 uneven electricity distribution between urban and rural areas in Nigeria. Low electricity access rate in rural areas is a global concern because 84% of the 1.06 billion people without electricity access in 2016 live in rural areas [4].

The wide disparity between urban and rural areas electricity access rate is evident in many SSA countries. For example, 90% of Gabonese had electricity access in 2016,

but the percentage of urban and rural dwellers with electricity access were 97% and 38% respectively [5]. Similarly, Fig. 1.3 shows that 61% of Nigerians had electricity access in 2016, but the percentage of urban and rural dwellers with electricity access were 86% and 34% respectively. Because rural areas are usually least electrified, research on rural electrification solutions can help achieve universal electricity access for all.

1.1.4 Rural electrification: Benefits, challenges and way forward

Direct and indirect benefits of rural electrification spurs rural development because it creates an avenue for increase income generation, greater educational attainment, improve health services, higher quality of life, access to information, increased gender equality, and several other social welfare benefits required for sustainable economic and social development [7]–[15]. Daily benefits of rural electrification are evident in different sectors of life. In the agricultural sector, rural electrification directly spurs high productivity with the use of electric motors and pumps driven machines, and the indirect benefit of rural electrification includes the use of information received from television and radio to make informed planning decisions on weather conditions and crop prices. Despite the many benefits of rural electrification, the rate of rural electrification in developing countries is still slow [13]. Lack of commitment by many developing countries is often seen as responsible for the slow progress in rural electrification [16].

Regional crises such as development imbalance, excessive rural to urban migration and rapid failure of existing infrastructures, that arise from population growth can be mitigated by rural electrification, therefore, overloading of the already stressed electricity network can be avoided [17], [18]. Scaling up electricity access in developing economies is an enormous responsibility [16]. More so, it makes less business sense to supply electricity to a country's poorest population. An understanding of the diverse challenges affecting rapid rural electrification is important for spurring rapid rural electrification growth in many developing countries.

Several factors have been reported as responsible for the slow progress in rural electrification. For example, Yadoo and Cruickshank [19] reported that there are usually limited financial investment on rural electrification because rural electrification projects often offer little or no market incentives to profit-seeking private companies. Some other barriers that limits rapid rural electrification include low population density, roughness of terrains, low load densities, low economic activities, irregular subsidies, poor performance on the part of contractors, little or no supervision, and procurement difficulties [9], [12], [13], [20]–[23]. These challenges can be grouped into technical, financial, institutional and governance barriers [24]. Meanwhile, different country-wide studies on rural electrification emphasise that there are no short-cut solutions, therefore, the ideal pathway for providing electricity services in rural areas involves the design of a well-structured local context-based support schemes that offers financial, training and advisory support at a micro-level, and offers broader level support, by ensuring that there is favourable policy environment, an effective regulatory mechanisms that considers diversity in local needs and wider institutional level subsidies is appropriate [13], [19], [25], [26].

Design of a localised rural electrification scheme is vital because it can enable energy system cost reduction, accurate load prediction, and the deployment of renewable energy technologies. For example, lessons from successful rural electrification programs show that optimal design and sizing of an energy system can reduce the energy system cost by 20-30% [27]. Therefore, technical strategy of a rural electrification program is important for the optimal design of an energy system because the total losses of an energy system influence its unit cost of energy. For example, World Bank (with a history of several successful planned, designed and commissioned rural electrification projects) have reported that technical related issues can make up to 50% of the total energy generated by a system to be lost; as was the experience in Albania and Rajasthan in India [11]. Typically, grid extension and off-grid systems are the two technical approaches for increasing the rate of electricity access in rural area. Also, the two design options for off-grid electrification are communal grids and stand-alone/individual microgeneration systems. The selection of the most suitable approach for rural electrification is

dependent on several factors such as the closeness of the rural area from the national grid, the surrounding terrain of the area, and load density [11], [28].

Generally, grid extensions are recommended when the rural area has high load density, when it is close to the high voltage (HV) national transmission lines (Tx) and when its surrounding terrain is economically viable to extend the national grid lines [28]. Unlike grid extension, where an HV transmission line architecture is required, communal grid or small autonomous electricity network requires a low voltage (LV) power architecture to supply electricity that can be used for productive engagement. Furthermore, communal grid is recommended when there are clusters of loads, there is no nearby national grid lines and the surrounding terrain is not viable for national grid extension. Stand-alone microgeneration systems are small power off-grid systems, and are recommended for rural areas, where potential electricity customers are few, dispersed and their main electricity use is domestic lighting [28].

Despite the urge upfront investment of centralised energy systems, many developing countries selects grid extension as their preferred option for rural electrification, because centralised energy systems can offer a better economies of scale [29]. Therefore, off-grid systems are sometimes less appealing in many countries [30]. However, off-grid systems are the quickest approach to achieve United Nation's Sustainable Energy for All (SE4ALL) initiative because of the challenges of electrify many remote areas by grid extension. Sometimes, off-grid systems compliment the national grid, by ensuing that in remote areas, electricity is available many years in advance and there is the existence of an energy customer base [11].

To spur rapid rural electrification, decentralised electricity infrastructures can use available renewable energy resources in a rural area to generate useable electricity. One of the advantages of a decentralised electricity infrastructures is that they can be interconnected. This implies that electrical load aggregation and local energy control can be performed on the network. Globally, for easy integration of decentralised technologies into existing centralized energy system, many governments have made urge investment so that centralized grid infrastructure are

retrofit into decentralized energy system, [31]. Meanwhile, in rural areas with unreliable electricity supply or no access to electricity, decentralized energy systems can compete technically and economically against centralized energy systems.

1.1.5 Communal grid electrification

Communal grid is a localised electricity infrastructure. In rural areas, it can be deployed because of its flexible design architecture. As a decentralised installation, communal grids generates electricity near customer load, therefore, it can spur the growth of rural areas economy, aggregation of loads, energy system reliability, environmental sustainability and mitigates electricity supply imbalance in a country [28].

1.1.5.1 Communal grid techno-economic advantage

Typically, grid-extension electrification solutions are used for electrifying many countries rural areas but grid-extension electrification solutions will be less desirable when the cost of transmitting electricity to rural areas exceeds decentralised solutions [28]. Also, grid-extension electrification solutions are associated with a higher transmission and distribution (T&D) line losses, therefore, there is an increase in the unit of electricity. For instance, Kenya average cost for connecting a household to the grid is $1900 (USD), but the cost of connecting remote and sparsely populated areas to the grid is much higher [32]. Therefore, due to the high cost of transmitting electricity to remote and sparsely populated areas, communal grid can be a cost effective solution for rural areas electrification [33], [34].

Furthermore, communal grid system has comparative advantage over other decentralized technologies such as solar home systems (SHS), because their flexible architecture allows for load aggregation. Also, larger electrical network can be created by either integrating a communal gird and the national grid or integrating communal grids [14]. Therefore, there is an opportunity for the integrated grids to sell their excess generated electricity in a larger network and avoid less profitable electricity generation by buying electricity from the larger network. Apart from

buying and selling generated electricity in a larger network, electrical load aggregation in a larger network unlocks greater economies of scale and provide an opportunity for better management of generated electricity. Meanwhile, because of communal grid architectural flexibility, there can be an improvement in energy system security if the energy system is designed with the required functionality that allows it operate in islanded mode whenever it is interconnected [14]. So, the prevalent blackouts that occurs when electricity is supplied by an unreliable national grid can be mitigated by operating the decentralized energy system in islanded mode.

1.1.5.2 Communal grid and development

In rural areas, national grid-quality electricity generated by communal grid energy systems can be applied for productive energy use or to drive sustainable development. However, pseudo-electricity generated by decentralized energy technologies such as SHS, cannot be applied to drive sustainable development. Because national grid-quality electricity has the potential to drive poverty alleviation and food self-sufficiency in rural areas, some developing countries like India, recommends the use of communal grid energy systems for rural electrification [8].

Report on lighting electrification experience show that SHS initiatives can be used to spur rapid lighting electrification of rural areas. For example, between 2012 and 2016, a company called M-KOPA, electrified 300,000 homes in East Africa through the use of their small 8W SHS initiative [35]. The 8W SHS initiative was designed to supply electricity to LED lights, a cell phone charger, and a radio. However, electricity generated by the small SHS initiatives is limited, therefore, the pseudo-electricity generated cannot be used to power productive engagements such as refrigeration, mills and food processing, sewing machines, and electric tools for carpentry and construction, that stimulate rural economies and enable poverty reduction [14]. Another advantage of grid-quality electricity generated by communal grid energy systems is that it helps to avert extreme customer dissatisfaction that would accompany decentralised energy installations in the

future when grid-quality electricity is supplied to a nearby location from the national grid [36].

1.1.5.3 Communal grid and environment

Globally, there is growing concern that human activities, especially burning fossil fuels, results in the increase of the level of carbon dioxide (CO_2) and other greenhouse gas (GHG) in the atmosphere. Increasing the level of GHG emission leads to rising temperature of the Earth's atmosphere, ocean, and land surface. Most of the GHG release from human activities are from the energy sector [37]. For example, it is reported that 2018 global energy-related CO_2 emission was 1.7% higher than 2017 global energy-related CO_2 emission, therefore, reaching a historic high of 33.1 giga tonnes (Gt) of CO_2 [3]. The power sector was responsible for 67% of the CO_2 emitted in 2018 because there was an increase in the use of fossil fuels for electricity generation [3].

The amount of GHG emitted by developing countries is usually low when compared to developed countries, but if developing countries are to use fossil fuel-based solutions for supplying electricity to their growing energy demands, global environment concerns with climate change will be exacerbated by the continuous growth in developing countries energy demand [38]. Currently, developing countries are facing the greatest consequences of climate change because they are less prepared to combat the impact of climate change [14]. The use of communal grid energy systems for rural electrification can mitigate CO_2 emission from centralized energy system, because the design architecture of communal grid energy systems allows the use of local renewable energy resources such as wind, solar, small hydropower and biomass systems. Consequently, the use of renewable energy technologies by communal grid energy systems provides an opportunity for the supply of environmentally friendly and grid-quality electricity for rural electrification.

1.1.6 Nigeria rural electrification and communal grid

Nigeria is Africa most populous nation and the 7th most populous nation in the world [39]. The country is a developing nation with a rising population growth. In 2018,

the population of Nigeria was 195.9 million [6]. Based on current population growth rate, Nigeria is projected to move from the 7th most populous country in 2018 to the 3rd most populous country by 2050 [40]. Nigeria population are spread across the country six geo-political zone or across the 36 states and federal capital territory of the country. A map showing Nigeria 36 states and federal capital territory is presented in Fig. 1.4.

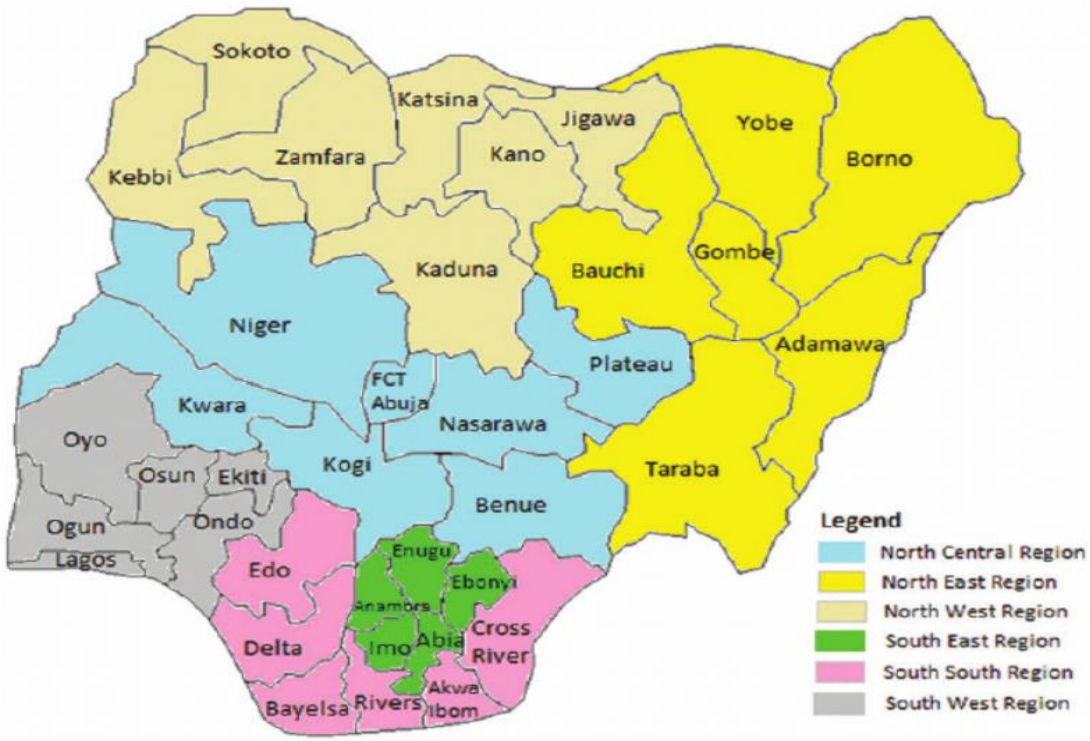

Fig. 1.4. Map of Nigeria showing 36 states and the Federal Capital Territory (FCT) [41]

As earlier mentioned, there is fast growth in Nigeria population, but there has not been corresponding growth in developmental infrastructures like electricity generation. For instance, a study on the electricity consumption per capital of 21 African countries shows that Nigeria with an electricity consumption per capital of 164 kWh is at the lower end of the spectrum in Africa [42]. In rural areas where about 51% of the population live in 2017 [6], electricity consumption per capital will be lower because these areas of the country has much lower electricity assess rate [5].

Rapid electrification of rural areas through grid extension is less likely in Nigeria, because it is perhaps more techno-economically sensible for a national grid operator to channel most, if not all, of the available electricity to urban areas with high load density and greater economy potentials than to rural areas with difficult terrain and low demand density. Transmission energy losses during national grid extension will aggravate the pressure on the deplorable power network. It is a serious concern because Nigeria electricity transmission losses is high (i.e. a network transmission loss of 7.4% loss as compared to the benchmark of 2 – 6% for developing countries) [43]. Nigeria power network is also confronted by incessant energy system failures, and this is a critical operational challenge affecting the efficient supply of electricity from the national grid [43]. Beyond the incessant system failures, the growing gap between electricity generation capacity and demand, has increases the pressure on Nigeria power network. For example, over the past two decades, the national grid supplies unstable and epileptic electricity to household for less than 6 hours per daily [44].

Currently, 85% of the total electricity generated in the national grid is from fossil fuel [43]. From an environmental perspective, electricity generation from unclean energy sources and extending the national grid to rural areas with no electricity access, will increase the amount of GHG emitted from the country power sector. So, if the national grid were to be extended to rural areas with no electricity access, it will be difficult to comply with international donors request that clean energy resources (with low CO_2 emission) are used for rural electrification because the integration of renewable energy technologies into the national grid comes at a higher cost.

Nigeria large population without access to electricity and/or low electricity consumption per capital, and the national grid deplorable state, shows that the country power sector is in a crisis. Research on the benefits of using alternative electrification solution for rapid rural electrification is necessary because the unreliable national grid is perhaps not an efficient way for rapid rural electrification in Nigeria. Off-grid energy systems are viable electrification options for rapid rural electrification, and they also allows for easy deployment of cleaner energy

technologies [14], [26], [45], [46]. As earlier mentioned, communal grid energy system is a more viable off-grid option for rural electrification than other off-grid energy systems because the national grid-quality electricity it supplies can be applied for productive energy use (i.e. beyond lighting) and to drive sustainable development.

1.1.7 Renewable energy technologies for rural electrification

Rural electrification with renewable energy technologies is used to drive environment sustainability since rural areas of developing countries are least prepared to combat the challenges of climate change. Furthermore, financial incentives required to spur rapid rural electrification can be secured because many international donors prefer rural electrification with renewable energy technologies. Evidence from literature show that renewable energy technologies can be used to drive rural electrification because they can compete with conventional energy technologies [47]–[49]. To resolve Nigeria power sector crises and minimise the release of GHG emission, there is growing clamour for the deployment of renewable energy technologies into the country energy mix. 2016 report on the roadmap to solving Nigeria's power sector crises state that incremental growth in electricity capacity is achievable when all generated megawatts of electricity are efficiently harnessed and distributed to customers, then after, the push for steady supply of electricity, and finally the supply of uninterrupted electricity [50].

In Nigeria, the agency responsible for the electrification of rural and unserved communities is called Nigerian Rural Electrification Agency (REA). To achieve incremental growth in electricity capacity, REA also recommends that all generated megawatts of electricity are efficiently harnessed and distributed to customers. Urge progress has been made by REA on the deployment of renewable energy technologies for rural electrification [51]. Furthermore, to provide electricity access to economic clusters such as markets, shopping complexes and agricultural/industrial clusters, REA has recently launched the energizing economies initiative (EEI) [51]. REA mainly emphasises the use of PV systems for electricity generation [51].

In literature, many authours support the use of renewable energy technologies for electricity generation. For example, Shaaban and Petinrin [52] recommended that renewable energy technologies should be deployed for the supply of reliable electricity to rural areas and to avoid the immenient collapse of the power network because the available fossil fuel used for national grid electricity generation is near depletion. Due to Nigeria rapid population growth, increase need for industrial growth and rising energy consumption levels, Agbongiarhuoyi [53] recommended that renewable energy technologies should be deployed into Nigeria energy mix in order to avoid the devastating environmental pollution and survive current economic realities.

Despite clamour for increase deployment of renewable energy technologies, its integration into Nigeria energy mix is still in its nascent stage [53]. The reason for the slow deployment of renewable energy technologies is attributed to technological and economic drawbacks, as well as deep rooted policy inertia [52]–[54]. Despite renewable energy technologies slow deployment, Nigeria renewable energy master plan provide the required assurance that federal government of Nigeria (FGN) is committed towards the deployment of solar, wind, hydro-power and biomass resources in the short, medium and long term [55], [56]. A brief assessment of Nigeria's solar, hydro, wind and biomass resources are presented below:

Nigeria lies within a high sunshine belt [57], [58]. Therefore, the deployment of PV energy systems has the potential of improving Nigeria energy security and reliability as well as enlarging Nigeria solar market. Several studies states that PV energy system is technically and economically viable energy technology for rural electrification [59]–[61]. Furthermore, authors such as Chakrabarti and Chakrabarti [62] and Moharil and Kulkarni [63] have argued that when the unit cost of national grid electricity is low, the deployment of off-grid PV energy system can be justified on the basis of its indirect benefits in the social, economic and environmental spheres.

Large hydropower systems account for 15% of Nigeria national grid generation capacity [43]. The current large hydropower system installed capacity in Nigeria can be increased by adequate mapping of available water resources into large and small hydropower system [64], [65]. Annual rainfall is about 3400mm depth in the south central shores of the Niger Delta, about 1400mm around the Plateau in the mid-belt region and about 500mm over the northern boundaries of the country [55]. Precipitation last over 8 months of the year in the southern areas, whereas at the extreme north annual rainfall duration can be less than 3 months. Small hydropower (SHP) has the potential of driving rapid rural electrification, but its deployment in Nigeria is limited because it is drought-sensitive, weather and season dependent, and requires site specific design [55]. Therefore, if SHP are deployed for rural electrification in Nigeria, it can only operate all year round in the southern and the south-eastern regions of Nigeria because their rivers and streams flows are perennial [55].

Nigeria wind speed is generally low. Peak wind speed for most locations in Nigeria occurs between April and August [57]. Nigeria annual wind resource is dependent to the rain-bearing south-western winds that blow strongly from the month April to the month of October and the dry and dusty north-east trade winds which blow strongly from the month of November to the month of March [55]. Because of Nigeria low wind speed, wind power is projected to contribute the least amount of renewable energy into Nigeria energy mix [57]. In Nigeria, the drawbacks with the deployment of wind power for rural electrification are wind power intermittency and the country low wind speed, therefore, all year electricity generation in many locations is either unlikely or very expensive [55].

Biomass energy resources includes fuelwood, animal wastes, agricultural residues, and energy crops [57]. Nigeria biomass resources assessment shows that biomass can be used to increase Nigeria electricity generation capacity and supply clean domestic cooking fuel [66], [67]. Large deposits of biomass resources are distributed across Nigeria different regions [68]. When the water content of bio-waste is high, anaerobic digester is the most suitable technology for producing biogas [52]. For efficient anaerobic digestion, all necessary system inputs and

outputs such as feedstock (bio-waste) and digester waste (i.e. for fertilizer production) should be coordinated to avoid inefficient biogas production and the disruption of living things food supply chain.

1.2 Research motivation

Most of the people without access to electricity live in rural areas. For example, 84% of the 1.06 billion people without electricity access in 2016 live in rural areas [4]. Low electricity access rate is usually experience in rural areas because they are the least electrified areas of developing countries. Therefore, development of rural electrification solutions is required to guarantee universal electricity access for all. In developing countries like Nigeria, alternative solution to national grid extension is required because the national grid is in a deplorable state and incessant blackout is experienced in the power network. Communal grid energy systems are attractive off-grid energy solutions because they can be used for supplying grid-quality electricity, the deployment of renewable energy technologies and the aggregation of load [14], [34], [36].

In literature, studies on the viability of renewable energy driven communal grid energy systems have been conducted [47]–[49], but the development of a stochastic load profile that is representative of the energy consumption behaviour of rural areas occupants was not existent, nor was the investigation of the impact of load aggregation on a communal or regional grid considered in these studies. So, it will be useful to develop a household occupancy demand model for rural areas, before calculating the minimum cost of supplying clean energy to rural households and studying the effect of load aggregation in a communal and regional grid. It is therefore hoped that outcomes from this research will contribute to on-going research geared towards the development of clean alternative solutions for rapid rural electrification.

1.3 Scope

This research studies the optimal combination of PV, biomass and battery energy systems that guarantees reliable supply of electricity to rural households at

minimum system cost. To simulate the energy consumption pattern of rural households, a household survey that investigate occupants' activity schedule is performed so that the effect of occupancy behaviour on energy consumption patterns can be predicted. In this research, high-resolution models are developed because of the stochastic nature of load profiles and solar radiation data. The effect of load aggregation on a communal grid and a regional grid is also investigated in this thesis.

In this study, Nigeria is selected as the reference country. Although located within a high sunshine belt [57], [58], the amount of solar radiation that can be harnessed from different locations in Nigeria varies widely. Out of Nigeria 36 states and federal capital territory, research data collected from Edo state are used in this study, because Edo state is one of the states with the least solar radiation potentials in the country. Household occupancy and appliance ownership survey is carried out in Esan North-East local government area (LGA) of Edo state. Biomass availability is assessed by calculating the quantity of recoverable household and animal bio-waste in the studied location. Household and animal bio-waste were selected because they are usually disposed indiscriminately in rural areas. Therefore, the use of household and animal bio-waste for energy production will not disrupt living things food supply chain. Household and animal bio-waste has high moisture content, so, anaerobic digester is the most suitable technology for converting these bio-wastes into biogas [52].

1.4 Aim and objectives

To study the effect of integrating biomass and photovoltaic generators for rural electrification, the aim of this research is the survey and modelling of households load profiles, investigation of the optimal combination of PV, biomass and battery energy systems for reliable supply of electricity and a power flow study of the impact of load aggregation on the operation of a regional grid.

To formulate this thesis research objectives, relevant research questions were considered. For the research questions and research objectives presented below, the research questions align one-to-one with the research objectives.

1.4.1 Research questions

i) What is Nigeria renewable energy potential and how does Nigeria energy policies influence the deployment of renewable energy technologies?

ii) What is the energy consumption behaviour of rural areas?

iii) What is the amount of solar radiation that can be received in the studied location when a PV panel is permanently fixed horizontally, permanently fixed at its optimal annual angle, or adjusted seasonally to its optimal angle?

iv) What is the studied location biomass potential?

v) Can the integrated PV, biomass, and battery energy system LCOE compete with the LCOE of a diesel only energy system and the LCOE of the national grid?

vi) What is the effect of load aggregated on a regional grid?

1.4.2 Research objectives

i) An assessment of Nigeria renewable energy potential and evaluation of how Nigeria energy policies influence the deployment of renewable energy technologies.

ii) Survey of rural household's energy consumption patterns and development of a stochastic household load profile model.

iii) Estimation of the studied location hourly global solar radiation data and evaluation of the minimum time span of measured meteorological dataset that is required to estimate the solar radiation of the studied location.

iv) Assessment of the studied location biomass potential

v) Investigation of the optimal size of PV, biogas generator and battery capacities that should be integrated in order to guarantee cost-effective supply of reliable electricity.

vi) Study of the effect of load aggregated on a regional grid and evaluation of the best approach for siting generators in a regional grid in order to ensure power losses minimization.

1.5 Contributions of the research

Some of the specific contributions of this thesis can be summarized as:

i) Survey and development of an occupancy-based stochastic load model. The developed load model can be used to simulate the load profiles of households when measured national time use data is not available in developing countries.

ii) Evaluation of the minimum time span of measured meteorological dataset that is required to accurately estimate hourly global solar radiation.

iii) Development of a power flow study model that can study the effect of load aggregated on a regional-grid and evaluate the best approach for siting generators in a regional grid in order to ensure power losses minimization.

1.6 Thesis outline

This thesis is divided into 8 chapters, and the thesis structure is such that it follows a normal step by step progression, from problem formulation to the presentation of research findings.

Chapter 1 presents an introduction of the research work discussed in this thesis. It sets out with an overview of the background of the research problem, in order to provide a justification for the research. The chapter clearly articulates the problem and purpose statements, as well as the research questions that emanate from the research problem. This chapter also presents the research objectives and concludes with an outline of the remaining chapters in this thesis.

Chapter 2 sets out with an overview of renewable energy potential in Nigeria, to ascertain renewable resource potential in supplying electrical demand beyond lighting. Also, it contains the review of the existing renewable energy potential and policies, in order to determine the driver and drawback of using renewable technologies in Nigeria's energy mix.

Chapter 3 build on Chapter 1 and Chapter 2 by providing a critical review of literature in relation to the research context and method used in this thesis. The

literature review covers the review of the different forms of hybrid renewable energy system configurations, the review of the general operating characteristic of PV technology and the different approaches for modelling solar radiation, the review of anaerobic digestion process and anaerobic digester design, the review of techno-economic characterization of energy storage systems, the review of load profile modelling approaches, the review of different hybrid energy systems design indicators, and the review of the different hybrid energy system design and simulation optimization techniques.

Chapter 4 build on Chapter 3 by presenting the methodology adopted in designing the hybrid energy sub-systems. This chapter also presents the methodology employed for generating some of the hybrid energy sub-system synthetic inputs such as load consumption input data, and solar radiation input data. Furthermore, boundary conditions, assumptions and limitations applied in the design of the hybrid energy system are also presented in this chapter.

Chapter 5 the methodology for constructing a stochastic occupancy-based load profile model presented in Chapter 4 was applied. Therefore, the survey outcomes for household occupancy behaviour and appliance ownership, and the modelling outcomes for households and community load profiles were presented in this chapter.

Chapter 6, assessment of the hourly global solar radiation that can be harnessed for photovoltaic application is performed. This involves a study to determine if there are mathematical expressions and meteorological parameters that should be considered when developing a new solar radiation estimation model. The duration of data to purchase from a weather station or the duration that an installed weather station should monitor data to guarantee accurate estimation of solar radiation is calculated. Assessment of the optimal angle to position panels for maximum solar radiation yield was also performed.

In Chapter 7, the studied community daily biogas production is estimated. Then, the estimated daily biogas production, modelled community residential load profile in Chapter 5, and estimated hourly global solar radiation in Chapter 6 are to study how

an integrated PV, biomass and battery storage community project can compete economically against a diesel only system, and against a subsidized and unreliable national grid, as well as to study how the aggregation of communities' residential loads affects the sizing and operation of a regional grid.

Finally, Chapter 8 summarizes the work done in this thesis. Therefore, research outcomes from the study of Nigeria renewable energy market, survey of rural household's energy consumption patterns, development of household load model, estimation of hourly global solar radiation, evaluation of the minimum time span of measured meteorological dataset required to estimate solar radiation, assessment of the studied location bio-waste potential, investigation of the optimal size of PV, biogas generator and battery capacities that should be integrated, study of the effect of load aggregated on a regional grid and evaluation of the best approach for siting generators in a regional grid were summarized in this chapter. Recommendations of future works to be carried out were also presented in this chapter.

Chapter 2 NIGERIA RENEWABLE ENERGY RESOURCE ASSESSMENT

In this chapter, Nigeria's renewable energy potential is studied, and existing renewable energy policy is reviewed in order to determine the possibility of using renewable energy technologies to resolve existing energy crises in the country. In this chapter, the studied renewable energy technologies are selected based on the country renewable energy master plan.

2.1 Overview

Globally, conventional technologies that burns fossil fuel are still commonly used for electricity generation because fossil fuel has high energy capacity and can easily be transported from one location to another [1], [3], [69]. However, the drawback to the continuous use of fossil fuel for electricity generation include its negative contribution to ozone depletion, acid rain and global warming [70], [71]. Renewable energy resources can be used to generate clean and affordable electricity, therefore, it can serve as a viable alternative to fossil fuel [69], [72]–[74]. For example, it is reported that over 17 countries generated more than 90% of their annual electricity consumption in 2017 from renewable energy technologies [75]. Studies have shown that the use of renewable energy technologies is a technically developed option [76]–[79]. Some other studies performed from a social, economic and environmental perspectives have also reported that the use of renewable energy technologies for electricity generation is a viable alternative to conventional technologies [73], [80], [81].

Some of the advantages of using renewable energy technologies for electricity generation is to guarantee energy security and promote economic advancement [74], to minimise fossil fuel running costs and conserve its finite fuel deposit [72], to develop a sustainable approach for meeting growing global energy demand [82], and to enable environmental sustainability [73]. Therefore, the favorable deployment of renewable energy technologies in Nigeria can be a clean and sustainable way of developing Nigeria energy sector. However, because current

trends in Nigeria population show that there is rapid increase in the country population growth and there are few installations of new technologies into the country national grid, existing crises in the country energy sector might not be resolved soon without a committed effort by all energy players.

Nigeria rural areas are the most affected, with 65% of the people having no access to electricity in 2016 [5]. This does not suggest that Nigeria urban areas; with a higher percentage of electricity access, are exempted since electricity supply from the country national grid is very unreliable, that is electricity supplied from the national grid is characterized by long-duration of no electricity availability. For example, survey outcomes of a research carried out in the urban area of Ibadan, shows that over 50% of grid-connected households received less than 4 hours of electricity on a daily basis [83]. Because national grid-supplied electricity is unreliable, many persons use diesel generators to generate their electrical energy despite the high negative environmental and social impact that arises from fumes and noise produced during the operation of diesel generators. From an economic perspective, Nigerian government recent removal of subsidy from the sales of diesel fuel has made the use of diesel generator for electricity generation less desirable in the country because diesel generator users will have to pay for the high diesel fuel cost [84]. In fact, Ohijeagbon and Ajayi [85] reported that because of the high cost of purchasing diesel fuel, the levelized cost of energy of a diesel standalone systems is 0.62 USD/kWh.

2.2 Nigeria's renewable resource potential

The Federal Government of Nigeria (FGN) has identified the use of renewable energy technologies as a means of addressing Nigeria's energy crises. Consequently, the renewable energy master plan (REMP) was developed in 2005 with set targets to drive the deployed of renewable energy technologies [55]. Table 2.1 outlines the proposed renewable power targets that are expected to contribute to overcoming Nigeria power shortage.

Table 2.1. Nigeria renewable power targets [56], [86]

Resources	Short term (MW) (2008)	Medium term (MW) (2015)	Long term (MW) (2030)
PV	5	120	36,750
Wind	1	20	50
Large Hydro	1930	5930	11,250
Small Hydro	100	734	3,500
Biomass	1	100	1,300
Total	2,038	6,906	68,350

As shown in Table 2.1 there is a renewable power target frame work in Nigeria, but actualization of renewable energy expectation has remained unfilled or slowly be met over the years based on international renewable energy agency (IRENA) renewable energy capacity statistics [87]. Therefore, this research will benefit from studying the renewable energy resources presented in Table 2.1 and from a review of Nigeria current renewable energy support system, since the progress in the country renewable energy system is slow when compared with the progress made by many countries. Reduction in manufacturing cost, technology improvements and the deployment of favourable policies are some of the factors that have spurred a fast pace increase in global renewable power generation capacity. 2011 – 2017 global installed renewable power generation capacity is presented in Fig. 2.1.

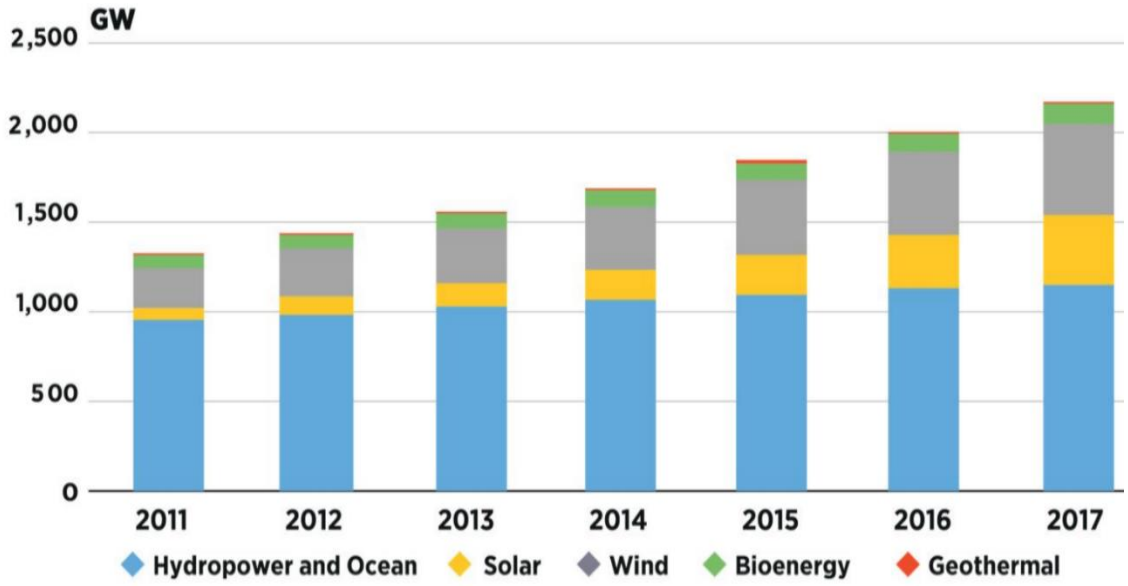

Fig. 2.1. Global renewable power generation capacity [87]

Current trends show that annual growth of about 8.3% was experienced in 2017, as global renewable power generation capacity increased by 167 GW and reached 2,179 GW worldwide [87].

2.2.1 Biomass resource potential for modern energy generation

Biomass is a chemically biodegradable material with the characteristic of producing energy carriers, which can be transformed into electricity, heat or fuel. Bioenergy[1] is a versatile energy source because, in comparison to other energy sources, biomass can be converted into solid, liquid and gaseous fuels. Globally, biomass is the largest renewable contributor to total final energy consumption (TFEC) as well as the 4th largest primary energy source, providing nearly 13% of the final energy consumption in 2017 [75]. Traditional use of biomass in developing countries (for cooking and heating) accounts for almost 8% of the total, and modern use accounts for the remaining 5%. Specifically, modern use of bioenergy for electricity generation experienced an annual increase of 11% in 2017 [75]. Globally, Brazil, USA, China, India, and Germany are taking the lead in the use of bioenergy for electricity generation, with a combined share of about 53% of the 109,213 MW total generation capacity in 2017 [87]. Whilst African nations are not part of the leading nations in the use of bioenergy for power generation, however, substantial progress has been made in Ethiopia, South Africa, and Sudan, with a combined share of 38% within the region [87].

In Nigeria, according to statistics on world bank development indicators, biomass accounts for above 80% of TFEC [6], but biomass consumption is mainly through traditional means. Specifically, for electricity generation, a 2018 report by the international renewable energy agency (IRENA) shows that bioenergy is currently not a part of Nigeria energy mix for grid power generation [87]. However, there is the possibility of harvesting significant amount of modern bioenergy from the

[1] Bioenergy is the energy derived from biofuels, which are fuels derived from biomass

country's biomass energy resources which includes agricultural crop and residues, animal waste, forest waste and municipal solid waste [56], [86]. In terms of electricity generation, Nigeria renewable energy master plan offers the assurance that bioenergy has the potentials to contribute to improving Nigeria electricity sector. Therefore, the government of Nigeria believe that electricity generated from biomass can be as high as 13,140 GWh by 2035 [88].

2.2.1.1 Agricultural crop residues

Agricultural crop residues are organic matters, which are produced either by harvesting or processing of agricultural products. As an agrarian nation, Nigeria has the potential of generating substantial quantities of agricultural crop residues from their large arable land. According to statistics from World Bank development indicators, the country has 34 million hectares of arable land, which is about 48% of their agricultural land [6]. Despite the fact that crop residues are usually generated at different stages of a crop production cycle, residues are usually discarded, mostly by onsite burning or allowed to rot, with consequent release of greenhouse gases [89]. Within a household, some of the crop residues generated from crop processing activities are used as domestic fuel, especially in rural communities. For example, for direct burning in a traditional 3-stone scheme. While the remaining portion, which makes up a fraction of domestic municipal solid waste, are disposed at formal and informal dump sites [67]. Annual production quantity of different crops in Nigeria varies significantly from one crop to another, which means that the quantity of residue produced by different crops also varies. So, Food and Agriculture Organization (FAO) of the United Nations' statistics on the production quantity (in kg) of Nigeria main crop residues between 2000 and 2016 are presented in Table 2.2.

Table 2.2. Production quantity (kg) of Nigeria main crops residues [90]

Year	Maize	Millet	Rice	Sorghum	Soybeans
2000	43,958,883	73,044,550	67,544,402	1.25E+08	9,838,695
2001	48,125,988	65,079,930	61,749,748	1.16E+08	9,923,136
2002	50,311,670	69,207,068	64,411,625	1.23E+08	10,414,611
2003	53,434,388	73,371,372	66,345,071	1.27E+08	10,852,511
2004	56,188,023	78,265,880	70,669,303	1.32E+08	11,526,157
2005	59,558,468	83,468,352	75,262,510	1.39E+08	12,013,027
2006	69,409,450	89,651,855	83,353,435	1.44E+08	12,703,310
2007	66,773,772	93,956,448	71,490,605	1.44E+08	12,580,781
2008	72,321,253	104,453,187	77,862,609	1.43E+08	12,333,422
2009	68,987,063	58,013,217	62,549,900	85,576,642	10,704,553
2010	74,740,008	61,262,762	81,102,794	1.01E+08	6,503,661
2011	89,221,865	16,943,648	79,069,980	87,721,445	11,366,929
2012	89,101,876	15,439,523	96,776,652	93,221,397	13,546,978
2013	87,122,360	11,545,946	93,346,750	92,978,118	12,538,579
2014	1.02E+08	16,926,703	1.05E+08	1.07E+08	12,902,375
2015	1.07E+08	17,962,134	1.08E+08	1.10E+08	12,315,847
2016	1.05E+08	17,933,737	1.04E+08	1.08E+08	12,353,150

The data presented in Table 2.2 shows that substantial crop residues are generated annually in Nigeria. With the year 2016 statistics taken from Table 2.2 as the base year, Table 2.3 summarise the energy potential of the base year crops residues

Table 2.3. Energy potential of crops residues for 2016

Crop	Residue (10^3 kg)	Residue type	Moisture content (%)	Energy content ($MJkg^{-1}_{dry\_matter}$)	Energy potential (TJ)
Maize	105,262[a]	Stalk	15[b]	19.66[b]	1759
Millet	17,934[a]	Straw	15[b]	12.38[b]	189
Rice	104,236[a]	Straw	12.71[b]	16.02[b]	1458
Sorghum	108,312[a]	Straw	15[b]	12.38[b]	1140
Soybeans	12,353[a]	Straw	15[b]	12.38[b]	130

Source: [a] [90] [b] [66] where $kg^{-1}_{dry\_matter}$ is the mass of dry matter

From this empirical analysis in Table 2.3, the total estimated energy potential for these five crops residues is 4676 TJ. Currently, there is an increased use of agricultural residues such as bagasse (sugarcane residue) in cogeneration plants to increase electricity generation. Successful cases have been recorded in Asia (e.g. India) and in countries such as Mauritius, Kenya, and Ethiopia in Africa, where there is government supported policy [75]. Also, evidence from Brazil's agricultural residues usage shows that out of the 49 TWh electricity generated from their 14.6 GW total bioelectricity capacity in 2017, bagasse (sugarcane residue) accounts for nearly 80% of the biofuel employed [75]. Apart from bagasse, other agricultural residues have also been used in countries with substantial residue deposit. For example, a 1.8 MW plant fuelled with rice residue (rice husk) is being developed in the Ayeyarwady region of Myanmar [75]. The increased use of agricultural residues for electricity generation can generally be attributed to the fact that modern energy production has little or no threat to food security as well as the fact that bioenergy systems are becoming more cost competitive [89].

In Nigeria, agricultural residues fuelled power plants is currently not common, especially for rural household electrification, due to economic and technological constraints [91]. However, for industrial purpose, a 32 kW demonstration off-grid power plant fuelled by rice husk was established in Ebonyi State, by United Nation Industrial Organisation (UNIDO) in collaboration with the Ebonyi state government to supply electricity to a palm kernel processing outfit, information and communication technology (ICT) centre, local cottage health centre, and for street lighting [92]. Consequently, the Ebonyi state government intends to implement a 5 MW power plant project worth $ 14.6 million (USD) in the state [92]. However, due to economic and technological bottlenecks the 5 MW plant is yet to be implemented. In view of the substantial deposit of agricultural residue in Nigeria coupled with the advances made worldwide in its use for power generation, it, therefore, means that research-based policies can reduce the economic and technological bottlenecks restraining the use of agricultural residues for power generation.

2.2.1.2 Animal Waste

Animals waste are obtained in the process of animal husbandry as well as during livestock consumption. In general, daily animal wastes are generated from animal dungs as well as from abattoirs in Nigeria. The quantity of manure produced from livestock usually depends on the type of feed consumed, the quality of the feed, and the weight of the animal [66]. The main livestock reared in Nigeria are cattle, pigs, goats, chicken, and sheep [54]. In rural areas of Nigeria, livestock rearing is one of the main sources of income, with most rural households having at least 3 different types of these common domesticated animals [67]. Food and Agriculture Organization (FAO) of the United Nations statistic for the quantity of livestock production in Nigeria since 2000 is presented in Fig. 2.2.

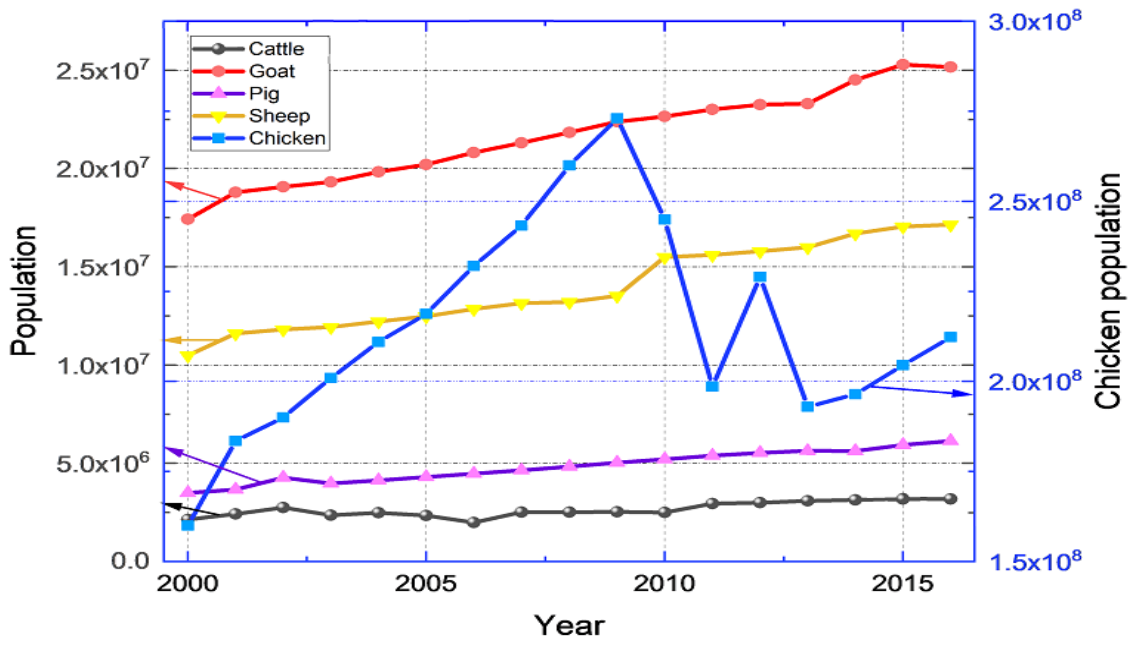

Fig. 2.2. Nigeria livestock production. Data source: [90]

It is evident from Fig. 2.2 that apart from chicken, there were noticeable increment in the population of the livestock between 2000 and 2016. For the chicken, noticeable incremental growth was also mainly experience except for the years between 2009 and 2013. Using 2016 as the reference year, the energy potential from Nigeria livestock can be estimated as follow:

For the reference year (2016), the population of livestock were 3,193,334 (cattle), 212,335,000 (chicken), 25,167,866 (goat), 6,139,547 (pig), and 17,141,531 (sheep). The equivalent dry dung output in kilograms per head per day are 1.8 (cattle), 0.06 (chicken), 0.4 (goat), 0.8 (pig), and 0.4 (sheep) [67]. While the corresponding caloric values for cattle, chicken, goat, pig and sheep are 18.5 GJt^{-1}, 11.0 GJt^{-1}, 14.0 GJt^{-1}, 11.0 GJt^{-1}, and 14.0 GJt^{-1} respectively [67]. Thus, the total energy potentials for cattle, chicken, goat, pig and sheep for the reference year corresponds to 38.8 PJ, 51.2 PJ, 51.4 PJ, 19.7 PJ and 35 PJ respectively. It is evident from the FAO statistics and the empirical analysis that Nigeria's goat and chicken population of 25,167,866 and 212,335,000 respectively, have greater potentials for producing manure. However, Cattle, generates the highest total energy per tonnes, therefore, greater energy potentials can be derived from cattle when they are reared in larger numbers.

For modern energy generation purposes, the manure is best utilized by first converting it to a methane-rich fuel called biogas through anaerobic digestion [93], [94]. Anaerobic digestion is a matured technology and it is well suited for treating the organic matter from animals during energy production, despite animal waste high moisture content [94]. This is because it has the potential for manure stabilization, sludge reduction, odour control, and energy production [95]. In the anaerobic digestion process, biogas is produced alongside anaerobically organic manure. The manure produced is often very rich fertilizers and they can be applied to an agricultural field after drying [96], [97]. The biogas can either be used for household cooking or for generating heat and electricity in a combined heat and power (CHP) plant, as widely used in European countries.

Anaerobic digestion is different from the traditional approach of burning livestock waste for heat energy production, a practice that is widely used in Nigeria [67]. Although traditional approach of drying and burning animal residues in locally constructed three-stone stoves for a direct source of energy is common, experimental evidence from comparative analysis of the traditional approach (direct burning) and anaerobic digestion, reveals that the traditional approach produces about 2.5 times lesser final heat energy than anaerobic digestion [98].

Because of the high moisture content, he traditional approach of direct burning has very low conversion efficiency (10% to 20%) [89]. Therefore, efficient utilization of livestock waste through modern approaches is required.

To optimise the amount of biogas produced in rural areas, centralised anaerobic digestion (CAD) scheme can be adopted [99], since it might not make techno-economic sense for all households to have a digester. Thus, taking advantage of CAD scheme, because it has the potential benefits of technological improvement, effective management of the digester by more skilled personnel within or outside the community as well as the fact that large bio-digesters benefit from economies of scale [100], [101]. Also, CAD affords the opportunity for the digester to be operated as a corporative scheme [102], which reduce the capital expenses of a biogas plant investment as well as supply a large number of consumers at domestic level or to run a bigger generator for electricity production.

In Nigeria rural areas, where households engage in animal husbandry that involves more than 3 different forms of domesticated animals [67], substantial waste can be generated from a corporative scheme operating CAD system. The corporative scheme is such that many farmers combine in feeding a single, large-scale digester with a single or varieties of substrates [99], [102]. The process of combining different feedstocks for the operation of CAD is known as a co-digestion process. Apart from wider reach to feedstock, co-digestion increases biogas yield in comparison with single digestion, by enhancing the biodegradation of long chain fatty acid, increasing the rate of organic loading, synergistically effecting micro-organisms as well as improving buffer capacity and the balance of nutrients [96], [103], [104].

2.2.1.3 Forest Biomass

Forest biomass is another biomass resource for bioenergy generation. The most recent World Bank documentation on Nigeria development indicators reveals that, in 2015, Nigeria forest area covers 7.4% (69,930 km^2) of the country's land area [6]. Woods can be generated from diverse forest products (e.g. branches, stump, roots, low-grade and/or decayed wood, slashing etc.) as well as from different industrial

activities such as sawmilling, plywood production, and particleboard production. Typically, several forms of wood, such as fuelwood, industrial round wood, and sawn wood are used for bioenergy production. Fuelwood is the most used resource for cooking as well as the most widely used bioenergy resource in Nigeria [105], [106]. It is estimated that fuelwood is used by over 70% of Nigerians living in the rural areas and the country use more 50 million tonnes of fuelwood annually [105]. Mohammed et al. [91] argued that the high reliance on conventional biomass for energy stems from Nigeria's energy crises, which has forced millions of people to depend directly on forest-based biomass thereby causing adverse effect on the ecosystem.

Despite the use of forest-based biomass for bioenergy production, the worrying rate of deforestation arising from the excessive harvesting of fuelwood, coupled with illegal logging, mining, and seasonal fire is a major concern to the current levels of dissertation in the country, since reforestation is estimated at only about 10% of the deforestation rate [105]. This is because development indicators statistics reveals that the country's forest area has reduced drastically from 172,340 km^2 in 1990 to 69,930 km^2 in 2015 and specifically from 74,026 km^2 in 2014 to 69,930 km^2 in 2015 [6], at a deforestation rate of 3.54% and 5.53% respectively. Thus, with the assumption that the country's population remains the same, annual deforestation of forest area remains 4096 km^2, and that there is a commitment to ensure annual reforestation of 10% of 2015 deforested area, Nigeria might have no forest area as early as 2035, If the current trends of deforestation persist.

The high reliance on forest-based biomass is the major cause of the unsustainable rate of deforestation, therefore, more sustainable solutions should be provided in order to limit or address the current devastating effect of desertification on the country's environment [107]. Similarly, Oyedepo [105] has argued that the sourcing of fuelwood for domestic and commercial uses is a major cause of desertification in the arid-zone states and erosion in the southern part of Nigeria. Therefore, to combat environmental degradation arising from the high reliance on conventional forest-based biomass for bioenergy generation, rapid reforestation and afforestation should be emphasized along with the push for the use of alternative

(modern) bioenergy generation technologies with little or no impact on the environment.

2.2.1.4 Municipal Solid Wastes

Municipal solid waste (MSW) is another biomass resource, with the potential of generating a substantial amount of bioenergy from the country's household, commercial, and industrial sectors. It is estimated that approximately 74,428.85 tonnes of MSWs are generated in Nigeria daily, which has the potential of generating 2.04 million m^3 of biogas daily [108]. However, these solid wastes are disposed indiscriminately or in landfills, from which biogenic waste methane and CO_2 are emitted uncontrollably into the atmosphere, as the biodegradable fraction of the waste decomposes anaerobically [91], [106], [108]. Renewable energy recovery technology options have become a sustainable mitigating solution in developed and developing economies for improving waste management and energy generation, as well as the potential of controlling anthropogenic gases emissions from MSW [75], [91].

In China, for improved waste management, producing energy from waste is a common practice, and the deployment of waste-to-energy plants in other parts of Asia and in Africa is on the increase [75]. For example, in Addis Ababa, Ethiopia, construction of a waste-to-energy plant that will process 1,400 tonnes of waste per day and generate 185 GWh of electricity annually began in 2017 [75]. Specifically for electricity generation, in 2017, solid waste was used for generating 89,992 MW of electricity worldwide, which was 82.4% of the total bioenergy generating capacity for the same year [87]. Also, in 2017, global annual electricity generating capacity from solid waste increased by 5% [87]. Thus, accounting for 90.44% of the total increase in bioenergy generating capacity for the same year.

In Nigeria, studies have shown that substantial energy can be generated from the solid waste, in resolving the country's energy crises. For example, by using 0.53 $kgcap^{-1}day^{-1}$ as the average MSW generation, Somorin et al. [109] showed that electricity generating potential from MSW in Nigeria is 3,053 MW. An amount that is about one-quarter of the total grid installed capacity of 12,522 MW [43]. The

electricity generating potential was calculated with the assumption that incineration with energy recovery was the preferred choice of thermal treatment [109]. Because of the low industrial activities in Nigeria, there is also high methane generating potential from the country's highly biodegradable waste [110]. For instance, it is reported that 87% of Nigeria MSWs are biodegradable [66].

Mohammed et al. [91] showed that 913.44 Gg of methane is the estimated amount of methane that can be emitted from Nigeria major cities landfill sites and at a plant efficiency of 30%, 482.4 MW of electrical power can be generated from the landfill sites [91]. However, sustainable management and utilization of Nigeria MSWs that can boost the country's bioenergy generation have been limited by drawbacks such as poor legal framework, unclear vision and strategies, and imbalance of corporation between the various entities of government [106], [108], [109].

2.2.2 Hydropower resource potential

Hydropower is the process of harnessing energy from falling water to create electricity. This is achieved by controlling the flow of water through a turbine, thereby rotating the turbine blades. The capacity of the hydropower plant is a function of the height of fall and the volume of water discharged. Thus, run-of-the-river (ROR) are used for small-scale hydropower plants while for large-scale hydropower plants dams are constructed to confine a large volume of water within a barrage. Hydroelectric power is the largest and most used renewable resource for electricity generation by a wide margin. In 2017, 22 GW of hydropower was added worldwide, bringing total capacity to about 1,270 GW, thereby accounting for 58% of global renewable power capacity for 2017 [87]. China remained the perennial leader in commissioning new hydropower capacity, accounting for about 40% of new installations in 2017, and was followed by Brazil, India, Angola and Turkey [75], [87]. The commissioning of new hydropower systems in China and other emerging and/or developing economies will enable the increase in the utilization of global untapped hydropower technical potential.

In developed countries, there is the extensive implementation of hydropower (over 50% utilization of the technically feasible hydropower potential) in comparison to

emerging economies were about 20% to 30% of technically feasible hydropower potential has been utilized [111]. Therefore, there is a possibility for more utilization of hydropower technology in developing than in developed economies. Africa is an extreme case of the uneven development of hydropower technical potential, where only 7% of economically feasible hydropower potential has been developed (see Fig. 2.3).

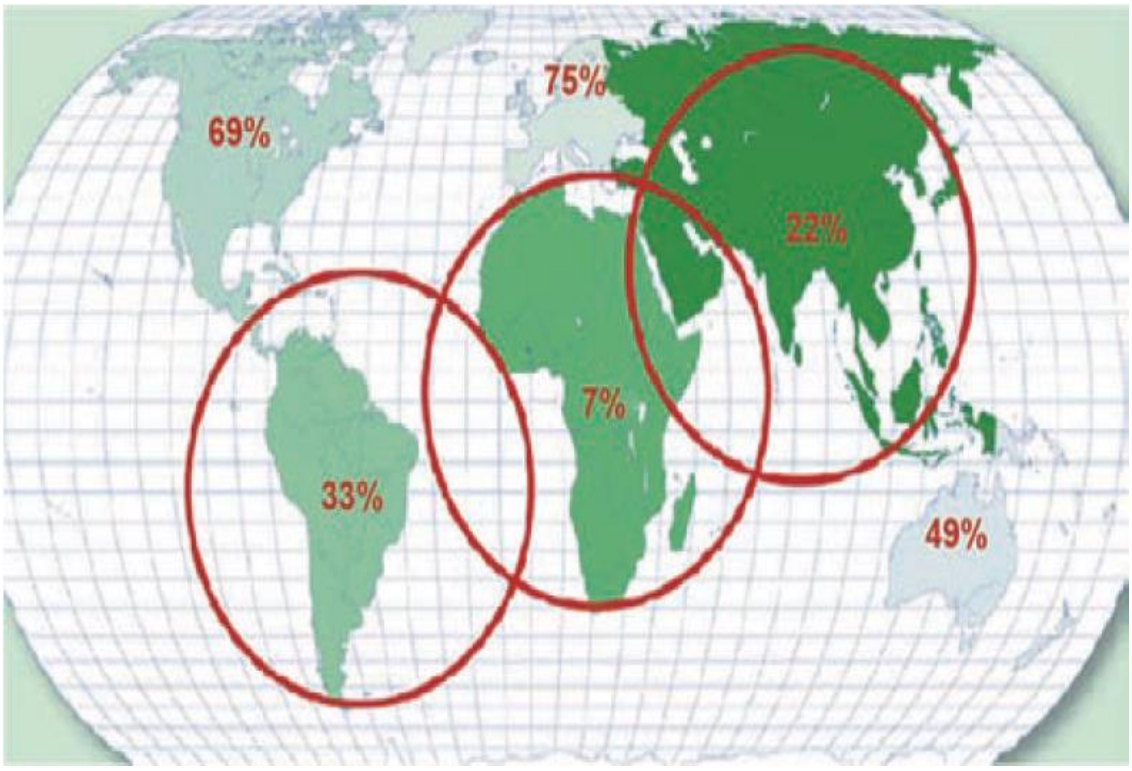

Fig. 2.3. Regional development of hydropower as a percentage of hydropower potential [111]

Therefore, since developed countries have already exploited most of their hydropower potential, emphasis on hydropower utilization can be directed towards emerging and/or developing countries with more hydropower utilization potentials. Nigeria is significantly endowed with hydropower resources from a topographical and hydrological perspective [112]–[114]. The development of hydropower systems has a great economic prospect in the country due to its high system efficiency, and long lifespan [91]. The rivers Niger and Benue and their several tributaries constitute the core of the Nigerian river system. River Niger is Africa third longest river and fifth largest in terms of discharge, and it flows across

several regions of the country (such that about two-thirds of the country lies in its watershed) before it empties into the Atlantic in the Niger Delta region [44].

Kainji, Jebba, and Shiroro power stations are Nigeria hydropower stations and they commenced operation in 1968, 1985 and 1900 respectively [91]. These stations account for the entire 1,930 MW of hydroelectric power connected to Nigeria national grid [42], [43], [115]. This constitutes about 15% of the country's total installed capacity of 12,522 MW [43]. However, based on assessments of the potential of the different sites across the Nigerian river basins for small and large-scale hydropower, only a small fraction of the country's potential for hydropower generation has been utilized [65], [112], [114]. According to energy commission of Nigeria (ECN), although the total exploitable hydropower potential for large and small systems are estimated at about 14,120 MW and 3,500 MW respectively, only about 13.5% and 1.7% of the estimated potential for large and small systems have been developed [57].

The rate of development of hydropower system in Nigeria has been slow and this is due to challenges such as the lack of local research and development strategies, lack of technical knowledge for equipment manufacturing, difficulties in financing energy infrastructure, lack of intensive feasibility studies [91]. Although large hydropower systems have been mostly used in Nigeria because of its economies of scale, small hydropower system which is geographically dispersible systems can enable rapid electrification of rural areas [65], [113]. The deployment of small hydropower (SHP) for rural electrification offers the possibility for the supply of power for productive engage, which in turn spur development. Also, SHP has the potential limiting ecological and environmental footprint associated with large hydropower systems [116]. Whilst from a social and ecological perspective, SHP reduces operational issues such as those associated with large hydropower plants (e.g. loss of habitat by several plant and animal species, displacement of human population, soil erosion, a difference in oxygen levels and water warmth) that could potentially create an imbalance in the ecosystem. Furthermore, in comparison to large hydropower, SHP enables the reduced production of methane gas, a highly potent greenhouse gas [65], [113].

2.2.3 Solar resource potential

Solar energy is the energy produced from the sun's radiant light and heat energy. Thus, a substantial amount of solar energy strikes the surface of the earth crust on daily basis. However, the magnitude of solar energy received at a point on the earth surface (i.e. solar radiation), depends on parameters such as the sunshine duration, cloud cover index, geographical location of the receiving spot and atmospheric absorption or reflection behaviours [117]–[119]. Solar energy can be converted into thermal or electrical energy depending on the system of conversion available and the purpose of utilization. Examples of suitable technologies for converting solar energy to thermal or electrical energy includes solar thermal technologies, solar architectural system, and solar photovoltaic module. On a global scale, solar energy applications have increased over the past decade. Specifically, electricity generating solar photovoltaic (PV) capacity grew from about 8 GW in 2007 to 402 GW in 2017 (see Fig. 2.4).

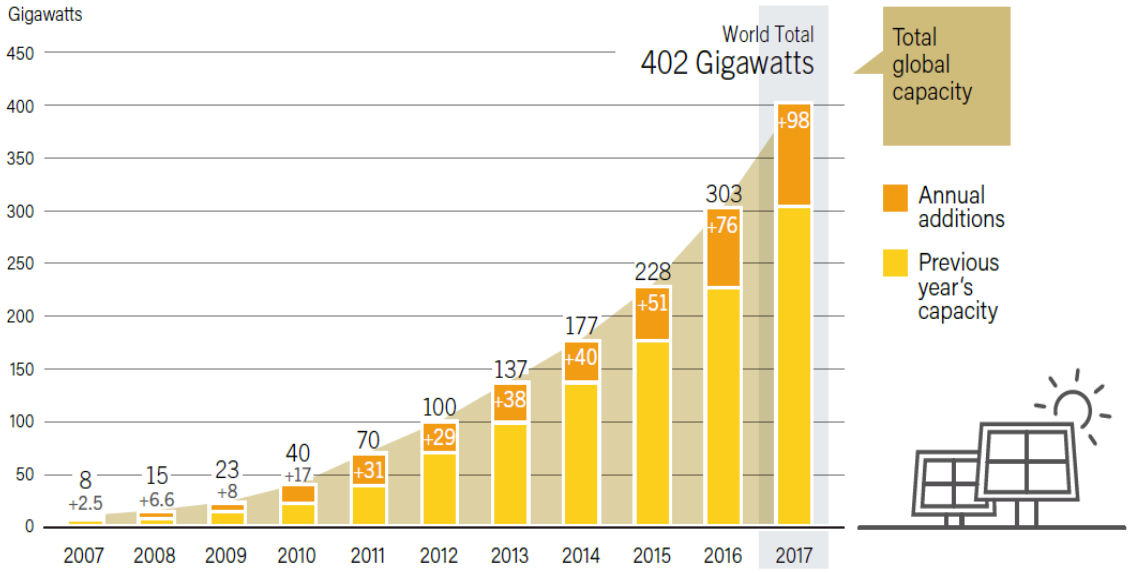

Fig. 2.4. PV global capacity and annual additions [75]

In 2017, the world witnesses a landmark capacity addition of 98 GW, increasing total capacity to nearly one-third of the capacity of 2016, which was more than the addition from any other type of power generating technology. In fact, more PV was installed in 2017 than the net capacity additions of fossil fuels and nuclear power combined [75]. The global acceptance of solar energy was again echoed by the fact

that by the end of 2017, every continent had installed at least 1 GW and at least 29 countries had 1 GW or more of capacity [75]. Despite the significant market increase in new installations in Asia (about 75% of global additions), and the market doubling recorded in China and India to be specific, so, the leading countries for PV capacity per inhabitant in 2017 remains Germany, Japan, Belgium, Italy and Australia [75].

By Nigeria's position (9.0820 °N, 8.6753 °E) near the equator, the country is in a high sunshine belt, with the potential of exploiting a substantial amount of solar energy. Nigeria irradiation values varies from north to south (See Fig. 2.5). Specifically, the north-eastern axis of Nigeria has the highest global irradiation potential, while the south-south has the lowest global irradiation potential.

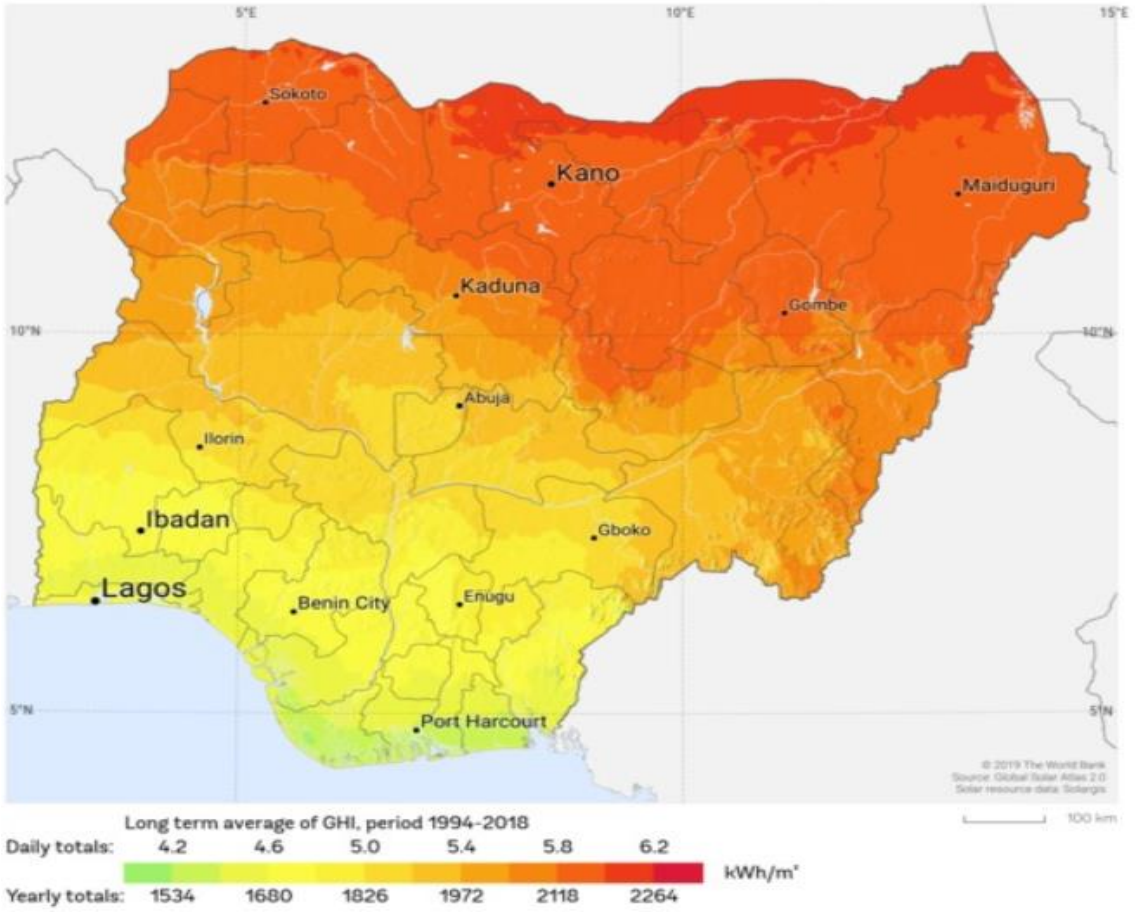

Fig. 2.5. Nigeria global horizontal irradiation [120]

Nigeria solar radiation varies from one location to another. Based on long term average global horizontal irradiation (GHI) data, Fig. 2.5 shows that average annual

GHI ranges between 1534 and 2264 kWh m^{-2}. Therefore, for a PV system of 1 kW_P and a performance ratio[1] of 0.75, electricity between 1150 and 1700 kWh kW_P^{-1} can be generated annually. Several factors such as PV panel temperature, inefficient system components, PV panel soiling, and PV panel shading affect the performance ratio (PR) of PV systems [121]–[124]. In this study, PR of 0.75 was selected because Nigeria has high temperature, the potential of accumulating dust on PV panels and the potential of using substandard system installation components such as wires and inverters.

In literature, there are noticeable discrepancies in Nigeria reported GHI values. For example, Nigerian renewable energy master plan reported that Nigeria daily GHI is 3.5 – 7.0 kWh m^{-2} day^{-1} [55], but in [119], it was reported that Nigeria daily GHI is 3.5 – 6.5 kWh m^{-2} day^{-1}, while Fig. 2.5 shows that Nigeria daily GHI is 4.2 – 6.2 kWh m^{-2} day^{-1}. These discrepancies also exist in the values reported for average daily GHI. For example, the average daily GHI for Nigeria was estimated in [84], [125] as 5.25 kWh m^{-2} day^{-1}, while in [48] it was estimated as 5.75 kWh m^{-2} day^{-1}. Despite these discrepancies in reported GHI values, Nigeria has substantially high solar potential, and when adequately deployed, it can improve Nigeria's deplorable state of electricity. So, for a PV system PR of 0.75, a solar panel efficiency of 17% and a daily averaged GHI of 4.2 kWh m^{-2} day^{-1}, more than 4 times the current peak operational generation of 4811MW can be generated from 0.1% of Nigeria's land area of 910,770 km^2 [6].

Although the commitment of all energy players (i.e. the government, policymakers, investors and researchers) is necessary for optimum utilization of solar energy technology, solar assessment of the energy potential of a location is important because it helps authorities make informed policy and investment decisions as well

[1] Performance ratio (PR) is a quality factor that compare the energy output of a power system with that of other systems by calculating the overall effect of energy losses on a system output. PR is independent of the system location and it is defined by the ratio between an energy system final yield and its reference yield.

as to underscore the techno-economic and environmental benefits of solar energy technology. In Nigeria were the government intends to disburse $225 million (USD) out of the $350 million (USD) electricity fund received from world bank in 2018 on solar technology related off-grid electricity project [126], [127], accurate assessment of the country solar radiation has the potential to spur increased access to rural electrification. Consequently, estimation of the studied rural community solar radiation will be carried out in Chapter 6 in order to ensure accurate design.

2.2.4 Wind resource potential

Wind turbines convert the kinetic energy of moving air to electricity by rotating the turbine blades. Wind turbines are scalable and substantially space efficient. Thus, depending on the available wind speed, electricity is generated from a single turbine or from a group of turbines in a wind farm. Wind power had its third strongest year ever in 2017, with more than 52 GW added (29% of newly installed renewable power capacity in 2017, thus occupying the 2nd position behind PV) to the year total install capacity to 539 GW [75]. Specifically, European and India achieved wind power installation record year in 2017, while at least 13 countries – including Costa Rica, Nicaragua and Uruguay, and several countries in Europe – met 10% or more of their electricity consumption with wind power during 2017 [75].

Onshore wind power has become one of the most competitive sources of new generation, with the levelized cost of energy (LCOE) of onshore wind power projects falling to as low as USD 0.03 per kWh in locations with excellent resources and low installation cost, while global weighted average was USD 0.06 per kWh [75], [128]. The margin between the minimum and maximum weighted LCOE attest to the tie between the cost viability of wind power and the potential wind resource that can be harvested from a location. Thus, the basis for carrying out wind resource assessment before implementing wind power generation. In Nigeria, a reasonable amount of work has been carried out on the characterization of wind speed and pattern in order to identify the best locations for wind energy conversion. Studies on the country's wind resource assessment can be classified into regional and countrywide investigations.

Ohunakin [129] carried out a wind assessment of 5 sites (Bauchi, Nguru, Maiduguri, Yola, and Potiskum) in the North-Eastern geopolitical zone of Nigeria using measured data by Nigerian meteorological agency (NiMet) at a height of 10m, for a period of 37 years. He reported that although the wind speeds for the 5 sites range from 3.18 to 7.04 ms^{-1}, the average annual wind speed in Bauchi, Nguru, Maiduguri, Yola, and Potiskum were 4.83, 4.12 ms^{-1}, 5.31 ms^{-1}, 4.16 ms^{-1}, and 4.80 ms^{-1} respectively. In addition, Ohunakin [129] suggested that the probability of harvesting a wind speed of over 4 ms^{-1} all through a year in Maiduguri, Potiskum, Nguru, and Yola was 100%, 75%, 50%, and 50% respectively. While for Bauchi, the probability of harvesting over 4 ms^{-1} was reported as 80% and 100% in a dry and rainy season respectively. In a separate study within the same geopolitical zone, based on a NiMet measured data over a 15 years period, Ngene et al. [131] reported that the annual wind speed for Maiduguri was 5.3 ms^{-1}. A wind speed value that corroborated Ohunakin [129] reported wind speed for Maiduguri.

In Sokoto, North-Western geopolitical zone of Nigeria, Ngene et al. [131] reported that from their analysis of NiMet measured data over a period of 15 years, the annual average wind speed at a height of 10 m was 7.2 ms^{-1}. For the same region, Ohunakin [132] studied seasonal variation in wind speed data recorded by NiMet over a period of 37 years, and reported that the average annual wind speed for Gusau, katsina, Kaduna and Kano were 6.093 ms^{-1}, 7.446 ms^{-1}, 5.274 ms^{-1} and 7.767 ms^{-1} respectively. Despite noticeable seasonal variation in the studied locations wind speed data, Ohunakin [132] stated that wind turbines installed at a height of 10 m can guarantee an all year electricity generation in Katsina and Kano, but in Gasau, wind turbines installed at a height slightly greater than 10 m guarantees an all year electricity generation, while in Kaduna, wind turbines installed at a height of 10 m can only guarantee occasional supply of electricity in some seasons of a year.

Wind speed assessment of 5 sites in North-Central geopolitical zone of Nigeria was carried by Adaramola et al. [133] based on data recorded by NiMet over a period of 37 years, and concluded that the annual average wind speed for these sites (Bida, Ilorin, Lokoja, Makurdi, and Minna) were 2.75 ms^{-1}, 4.39 ms^{-1}, 3.16 ms^{-1}, 4.57 ms^{-1} and 4.29 ms^{-1} respectively. Ngene et al. [131] corroborated the research of

Adaramola et al. [133] when they reported that the average wind speed for Bida is 2.6 ms^{-1}. In this geopolitical zone, the wind speed of Jos (Nigeria Plateau region) was studied at an elevation of 10 m by Ohunakin and Akinnawonu [134] and Ajayi et al. [135]. Whilst Ohunakin and Akinnawonu [134] stated that the average annual wind speed for Jos was 8.6 ms^{-1}, Ajayi et al. [135] stated that the average annual wind speed for Jos ranges between 6.7 ms^{-1} and 11.8 ms^{-1}.

In South-Eastern geopolitical zone of Nigeria, Oriaku et al. [136] investigated data recorded by Statistics Department of National Root Crops Research Institute (NRCRI) over a period of 10 years, at a height of 10 m for Umudike, and reported that the average wind speed for Umudike was 2.31 ms^{-1}, with a 98% chance of obtaining a 2.0 ms^{-1} hourly wind speed. By investigating the same data measured by NRCRI over a period of 10 years, Asiegbu and Iwuoha [137] corroborated the findings of Oriaku et al. [136], when they reported that the average wind speed for Umudike at a height of 10 m is 2 ms^{-1}. Wind speed assessment of Owerri an Onitsha in South-Eastern Nigeria was performed by Oyedepo et al. [138]. By analysing data collected by NiMet at a height of 10m over a 24 years period, Oyedepo et al. [138] reported that the annual average wind speeds at Owerri and Onitsha were 3.36 ms^{-1} and 3.59 ms^{-1} respectively.

Amoo [139] carried wind assessment of Abeokuta and Ijebu Ode, South-Western geopolitical zone of Nigeria, and reported from the analysis of NiMet collected data over a period of 37 years that the average wind speed for Abeokuta and Ijebu Ode were 2.54 ms^{-1} and 3.44 ms^{-1} respectively. Similarly, Ajayi et al. [140] corroborated the findings of Amoo [139] by reporting that the average wind speed for Abeokuta and Ijebu Ode at an elevation of 10m were 2.5 ms^{-1} and 3.4 ms^{-1} respectively. In Akure, South-West Nigeria, based on analysis of data recorded by NiMet at a height of 10m over a period of 11 years (1999 – 2009), Okeniyi et al. [141] reported that the annual average wind speed for Akure was 2.7 ms^{-1}. Metrological data collected by Statistics Department of International Institute of Tropical Agriculture (IITA) at a height of 10 m over a period of 10 years (1995 – 2004) in Ibadan was investigated by Fadare [142], and he reported that the annual average wind speeds at Ibadan were 2.75 ms^{-1}.

In Calabar, South-Southern Nigeria, Na et al. [143] presented data recorded by NiMet at a height of 10m over a period of 4 years and reported that the annual average wind speed in Calabar was 3.2 ms^{-1}. The neighbouring city of Uyo, Ohunakin [144] investigated data recorded by NiMet at a height of 10m over a period of 21 years (1986 – 2007) and reported that the average wind speed for Uyo was 3.17 ms^{-1}. Within the same region, Adaramola et al. [133] reported that the annual average wind speed in Warri was 3.08 ms^{-1} while Ngene et al. [131] reported that the annual average wind speed in Benin was 3.2 ms^{-1}. Nationally, the annual wind speed regime at an elevation of 10 m above the ground is reported to have a mean wind speed value of 5.88 ms^{-1}, 4.34 ms^{-1}, 4.00 ms^{-1}, 3.16 ms^{-1}, 3.50 ms^{-1} and 3.00 ms^{-1} in the country's North-East, North-West, North-Central, South-East, South-West and South-South region respectively [112].

It is evident from the literature review that there are noticeable discrepancies in the measurement duration of data used to estimate Nigeria wind speed, and this can lead to misleading presentation of national estimated wind speed data [112]. To avoid misleading presentation of estimated wind speed, a normalised graphical representation of estimated wind speed regime in Nigeria is presented in Fig. 2.6.

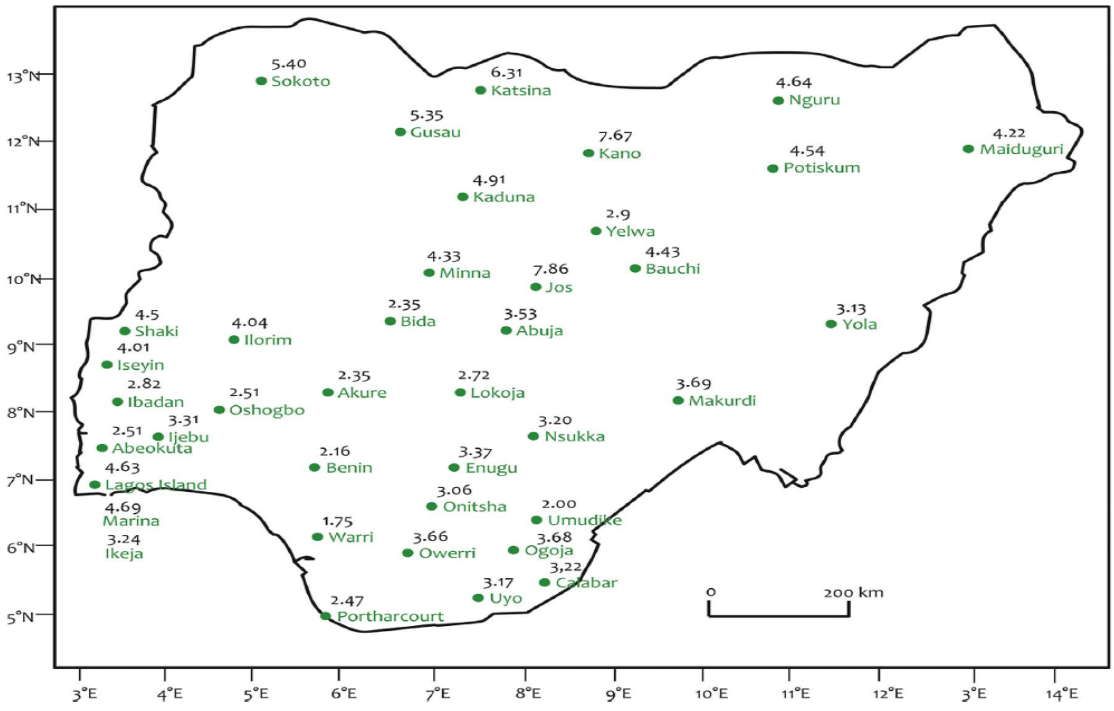

Fig. 2.6. Wind speed ($\mathbf{ms^{-1}}$) regime in Nigeria locations [112]

Brimmo et al. [112] calculated the normalised wind speed data in Fig. 2.6 by applying weights that were based on the measurement duration of data used to estimate wind speed. Meanwhile, an update to Fig. 2.6 might be required in future studies because NiMet measured dataset are mainly used for estimating Nigeria wind speed. The challenge with NiMet measured wind speed dataset is that its wind speed dataset can be less accurate because NiMet measured wind speed synoptically at a very low frequency, i.e., a couple readings a day, with a cup-generator anemometer [134]. Although this claim was refuted by the work of Adaramola et al [145] who presented hourly wind speed data from the same source, it is possible that the frequency of measurement of wind speed in a NiMet weather station varies across its 43 stations [112].

Based on international electrotechnical commission (IEC) standards for classifying the wind regime, evidence from literature show that Nigeria wind regime is classified as low in the south and moderate in the north; with peak values found in the north-western and plateau part of the country. Despite the possibility of moderate wind regime locations to generate substantial amount of energy, the pace of development of wind energy system in moderate wind regime location has been slow [91], [147]. Meanwhile, terrain features such as tall buildings and up-rise infrastructures can impede the flow of wind into a wind farm and then limit the power capacity of the wind turbine [146]. So, it is perhaps more profiting to deploy wind technology for rural electrification in locations with moderate wind regimes because tall buildings and up-rise infrastructures are not common features of a rural areas.

Unlike developed and emerging economies, such Germany, USA, UK and China that are actively promoting and developing electricity generation from wind energy [75], [87], the few visible wind power project in the country includes a 5 kW and power system installed in Sayya Gidan-Gada (Sokoto state) and a 0.75 kW power system installed in Danjuwa (Sokoto state), while about 1 kW of wind power system is installed in Bauchi (Kedada) and Katsina (Goronyo) for water pumping [91], [148]. On a larger scale, a pilot scale wind farm with a generating capacity of 10 MW that was conceptualised in 2007 is still under construction in Katsina state [112], [148].

Currently, Nigeria government is determined to deliver the project by the last quarter of 2019 [149]. Whilst it is hoped that at the completion and operation of the pilot scale wind farm would encourage the development of wind power technology in locations with moderate wind energy generating potentials, there are fundamental challenges restricting the penetration of wind power into the country's energy mix. Some of these challenges include low financing, lack of awareness and encouragement to embrace wind technologies and technical capacities [147], [148]. However, it expected that increased financing as well as more specific developmental policies and regulations, that is flexible, and research-driven would assist in addressing some of the mentioned challenges.

2.3 Nigeria's renewable energy policies

Nigeria renewable energy resource assessment in Section 2.2 has shown that renewable energy resources have the potential to resolve the rising environmental challenges as well as the country's energy crises. To enhance the deployment of renewable energy into Nigeria's energy mix, a national renewable energy masterplan (REMP) has been developed since 2005 [55]. To reduce the high initial cost of investment associated with renewables, the 2005 REMP was revised and a new REMP draft that covered economic and financial incentives that would stimulate renewable energy deployment was proposed in November 2012 [56]. Unfortunately, the targets, supportive and regulatory policies proffered in the new REMP is not yet binding as the new REMP draft still requires to be approved by the National assembly and signed into law by the Executive Government. However, a National Energy Policy called National Renewable Energy and Energy Efficiency Policy (NREEEP), with the aim of adopting renewable energy technologies and energy efficiency best practices in Nigeria was developed in 2014 [57] and was approved by the country Federal Executive Council (FEC) in 2015.

Nigeria is not lacking energy policies and implementation strategies, as several energy policies and implementation strategies to spur rapid renewable energy deployment have been developed over time [88], [150]. However, these policies have either not connected with the issues limiting the deployment of renewable

energy technologies into the country's energy mix or lack sufficient implementation regulations [151], [152], thereby failing to develop an action plan that will stimulate renewable energy deployment. For example, the government keeps offering subsidies to fossil fuel rather than discouraging fossil-fuel driven technologies as means of penalizing fossil-fuel negative externalities, as well as the high-risks stigma and high initial capital cost attached to renewable energy investments by financial institution, makes the deployment of clean technologies in a free market driven by demand and supply impossible.

On a more specific perspective note, the short-coming in government's financial commitment towards NREEEP document was highlighted by Ozoegwu et al. [153]. They argued that although NREEEP initiated strategies for supporting investment in renewable energy, the policy document lacked obligatory quantitative figures of government commitment in the policy [153]. Consequently, as an off-shoot of the poorly framed energy policies and implementation strategies, deployment of renewable energy technologies in Nigeria have been stymied by financial constraints, organizational and managerial weaknesses, lack of technological capabilities, and adverse political and economic contextual factors [91], [147]. Therefore, well-tailored renewable energy policy will be required to drive renewable energy deployment into the country energy mix.

In countries with rapid renewable energy deployment, the growths are simulated by well-tailored national renewable energy policy or support systems, with a clearly defined financial and regulatory obligation from the government [75]. The different support systems provided to renewable energy-sourced electricity (RES-E) worldwide can be classified mainly as a price-based system (feed-in system) and quantity-based system (quota system). The difference between these two support systems is that the price-based system set the price of RES-E unit and thus leave the determination of the RES-E quantity to the market, while the quantity-based system set an obligation upon consumers or utilities to consume/generate to a certain amount of RES-E, leaving the determination of its price to the market [75]. Thus, the quantity-based system appears to be more compatible with the liberalisation of the electricity market. Although the support system adopted by the different national

and sub-national government are usually motivated by political and economic needs, the feed-in systems seem to have encouraged higher RES-E deployment and technology diversity than quota system [154]. The reason while feed-in system encourages higher RES-E deployment can be explained by the perceived belief that it offers safer investment, better predictability, and a more stable policy framework, as well as lower projection transaction costs.

Evidence from the European market has shown that a feed-in system has proven to have the highest impact in promoting solar technology in Germany and Italy in particular [119]. In fact, Schallenberg-Rodriguez [154] reported that amongst member states of the European Union, countries with the higher efficiency and deployment status tendency adopts the feed-in system. However, a quota system is also a successful support system based on the level of renewable energy penetration in countries such as USA, UK, Belgium, and Australia that employs the quota system as their main support system. For example, USA with a renewable energy capacity of 229,913 MW is the second highest worldwide [87]. Also, Belgium and Australia are the 3rd and 5th leading countries for PV capacity per inhabitant [75].

The choice of a support system is not always restricted to either feed-in system and quota system as different countries such as US, UK Canada, China, and India have integrated both the feed-in system and quota system to differentiate among RES-E technologies or size [155]. In 2010, the UK introduced a feed-in tariff (FIT) system for small-scale renewable energy producers (up to 5 MW). Lessons from India's with a co-existing support system shows that beyond the support system nomenclature, well-tailored legislation and government policy, that emphasise renewable purchase obligation to obligated entities is vital in enhancing renewable energy development [75]. Therefore, to spur rapid renewable energy deployment in Nigeria's abysmal energy system, a co-existing support system that can stimulate rapid rural electrification as well as enable the actualisation of the on-going liberalisation of the electricity market.

To help the government develop relevant renewable purchase obligation in rural areas, this study through subsequent chapters will contribute to the on-going

discourse by studying what is the expected LCOE in areas with the least solar potential. The choice of PV is based on its substantial availability across all region in the country as well as the fact that PV systems can leverage on the government financial commitment and policy direction. Currently, PV is receiving the most of government commitment towards renewable energy technologies development. For example, based on Nigeria renewable power target (see Table 2.1), the projected installed capacity for PV by 2030 is 36,750 MW, a capacity that accounts for 54% of the total projected renewable electricity supply by 2030. Again, in securing approval of a $350 million (USD) loan from World Bank to boost the country's clean energy infrastructure, the government emphasised that $225 million (USD) out of the $350 million (USD) electricity fund received from world bank in 2018, will be disbursed on solar technology related off-grid electricity project [126], [127].

In pursuing a country-wide PV electrification scheme, the cost of PV electrification is expected to vary, since the lower the solar resource potential, the less competitive a PV system becomes. So, for a location with a lower solar radiation potential, the use of integrated PV and battery system to supply reliable electricity might not be a viable economic option. For example, in south-southern Nigeria, with the least solar energy potential (see Fig. 2.5), to pursue 100% solar energy driven renewable energy technology for rural electrification, the integration of PV and battery with non-intermittent generation technology such as biopower for bio-waste, will possibly compete better and reduce the amount of un-met load in the distributed network. The conversion of bio-waste into biopower (through anaerobic digestion) has the potential to foster corporation amongst rural dwellers and in turn, secure commitment since the rural dwellers can benefit from the electricity generated and the fertilizer that could be produced from the digestate.

2.4 Chapter summary

Nigeria pursuit of rapid rural electrification with 100% renewable energy technology (mainly solar) can be achieved based on the resource potentials highlighted in Section 2.2. However, before the design of solar power technology, further assessment study of the solar radiation potential in any reference location is

vital. Assessment of solar radiation potential is vital in Nigeria because there is discrepancy in literature on Nigeria solar radiation potentials. Also, in regions with least solar energy potential, the use of PV and battery system for reliable supply of power to electrical load beyond lighting is less competitive and less desirable from an economic perspective. Therefore, integration of PV system without renewable energy technologies might be useful in these areas.

Improved energy security and community participation might be achieved by integrating anaerobic digester and biogas generator (non-intermittent power system) with the PV and battery system, but the performance of the integrated system will be dependent on several factors such as the load profile of the community, RE resource availability, unit cost of system components, and the energy system configuration. Therefore, a detailed study will be required to assess how well the newly integrated renewable energy system will compete from a techno-economic perspective since it might be misleading to determine the performance of the hybrid system based on intuition (spot diagnosis). So, the next chapter presents a review of the literature on PV technology and solar radiation estimation models, biogas energy generation and anaerobic digester, energy storage systems, electrical load models and hybrid energy system design metrics The literature review in Chapter 3 is vital because it is expected to further articulate the research problem and provide justification approaches adopted in the design methodology chapter (Chapter 4) and the subsequent results chapters (Chapter 5 to Chapter 7).

Chapter 3 LITERATURE REVIEW OF HYBRID ENERGY SYSTEM

In Chapter 1, an integrated photovoltaic (PV) and biomass energy system was proposed as a sustainable means of supplying reliable electricity beyond lighting to a rural community. Whilst in Chapter 2, a background study of Nigeria renewable energy potential, policies and implementation strategies was performed. Therefore, in this chapter literature review of different HRES configurations, HRES components, load profile models and approaches that can be used for the optimal sizing of HRES will be carried out. Outcomes from the review of literature are expected to serve as justification for the design methodology defined in Chapter 4, and implement in Chapters 5, Chapter 6, and Chapter 7.

3.1 Hybrid renewable energy (HRE) systems

As mentioned in Section 1.6, single source generation and hybrid sources generation are the two renewable energy generating options for off-grid electrification. A hybrid renewable energy system (HRES) can serve as a viable generating option for rural electrification when renewable energy resources are optimally integrated. HRES has the potential of overcoming single source renewable energy systems challenges such as; the high cost of energy, system inefficiency, and energy insecurity [156]–[158]. Recently, the possibility of developing HRES with a high energy system efficiency and an increase system flexibility is higher because of current development in power converter technology [159]–[164].

Despite the several advantages of HRES, its design is more complex because it requires careful analysis to avoid over-sizing of system components. For example, it is more complex to calculate the total annualized capital, maintenance, replacement and fuel cost of a HRES than a single source energy system. HRES design complexity can also be attributed to the challenges of carrying out resource assessment of its energy sources and deciding on the best combination of energy system components that will guarantee reliable supply of electricity at minimum cost.

3.2 Hybrid renewable energy system configurations

Renewable energy technologies power outputs are either alternative current (AC) or direct current (DC) outputs. Therefore, the optimal combination of renewable energy technologies is vital in minimizing mismatch between the supply and the load. Whenever energy storage systems (ESSs) are integrated into HRES, the configuration of the HRES is important in ensuring an optimal supply of AC load as well as the effective charging of the DC battery storage. The 3 main configurations of HRES are DC-coupled, AC-coupled and hybrid-coupled HRES configuration [165]–[167].

3.2.1 DC-coupled HRES configuration

In DC-coupled HRES configuration of an off-grid, renewable energy technologies and storage are connected to the AC load with the aid of a DC bus. A DC/DC power converter is used to connect DC renewable energy technologies and battery storage to the DC bus while an AC/DC power converter is used to connect AC renewable energy technologies to the DC bus. Hence, the expected AC load to be met is supplied from the DC bus through a DC/AC converter [166], [167]. A schematic representation of a DC-coupled HRES configuration option for an off-grid application is presented in Fig. 3.1.

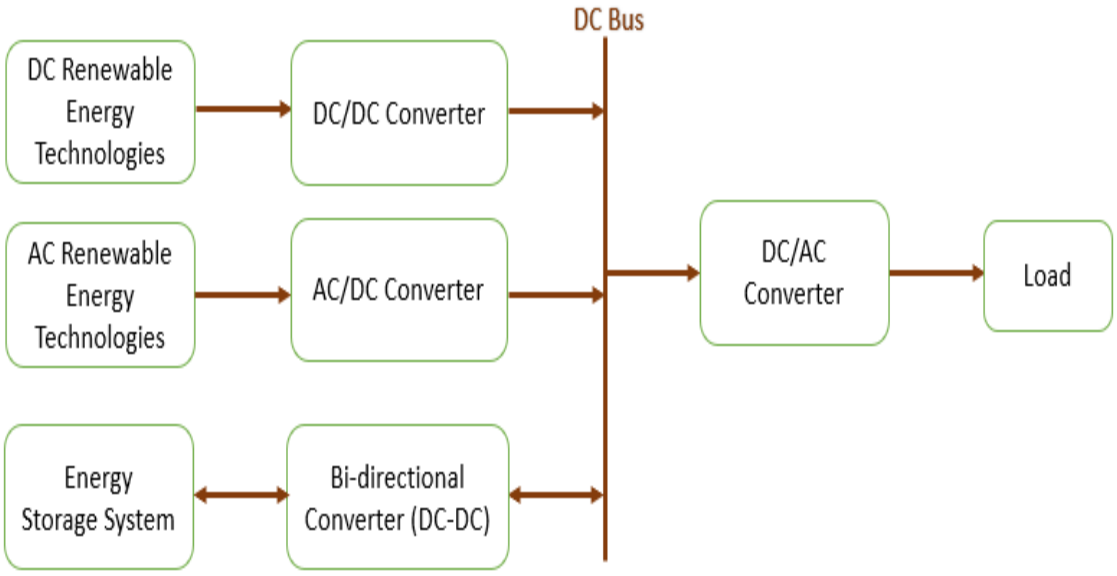

Fig. 3.1. DC-coupled HRES configuration [168]–[171]

Some of the advantages of this configuration option include reducing systems integration complexities as well as the avoidance of power quality issues, such as harmonics and reactive power [166], [167]. The main drawbacks include the possibility of the total blackout that would arise in the event of the loss of the DC/AC converter and the reduction of overall system efficiency as a result of the conversion of AC generators power outputs to DC power before re-converting to AC power to supply AC load. However, the issue of total blackout due to failure of DC/AC converter can be mitigated by connecting several DC/AC converters in parallel [167], [172], but this will lead to an increase in the total system cost, the system complexity, and the area occupied [167].

3.2.2 AC-coupled HRES configuration

The architecture of AC-coupled HRES configuration option for off-grid renewable energy application is such that renewable energy technologies and storage are connected to the integrated communal AC load with the aid of an AC bus. A DC/AC power converter is used to connect DC renewable energy technologies and battery storage to the AC bus while an AC/AC power converter is used to connect AC renewable energy technologies to the AC bus. Hence, period AC loads are met by the power supplied to the AC bus [166], [167]. A schematic representation of an AC-coupled configuration option for an off-grid application is presented in Fig. 3.2.

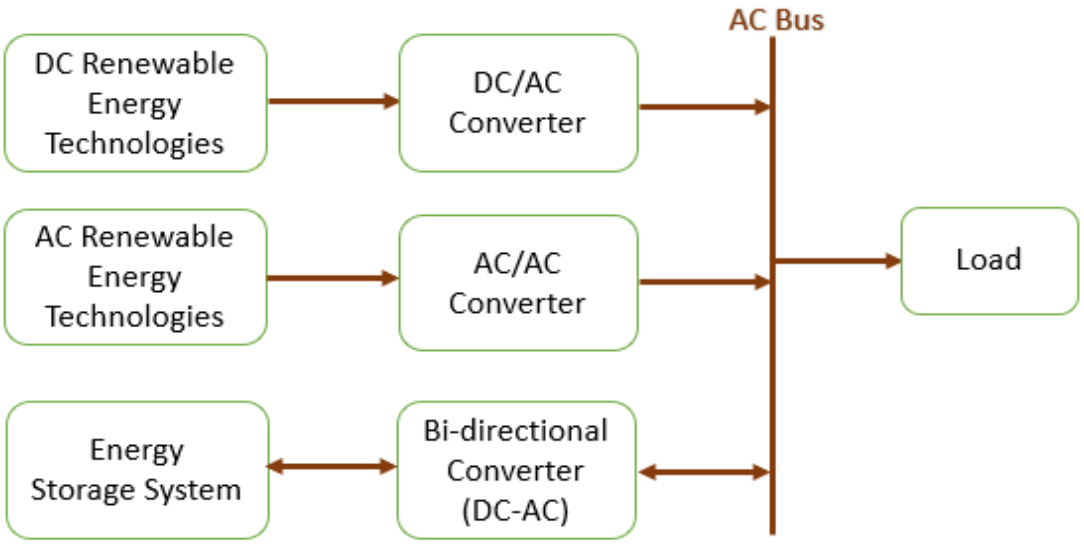

Fig. 3.2. AC-coupled HRES configuration [173]–[175]

This HRES configuration option has been employed for optimal sizing of HRES components in the literature [173]–[175]. This configuration option guarantees improved energy security in comparison to the DC-coupled configuration option because of the direct connection of the load to the AC bus. However, the complexity of synchronizing the power generated from renewable energy resources with the AC bus as well as power quality issues, such as harmonics and reactive power are some of the drawbacks of this HRES configuration option [165]–[167].

3.2.3 Hybrid-coupled HRES configuration

Hybrid-coupled configuration option for off-grid renewable energy application has both a DC bus and an AC bus in its architecture. A bi-directional converter is used to link the DC bus to the AC bus. DC renewable energy technologies and battery storage are connected to the DC bus through a DC/DC converter while AC renewable energy technologies and the AC loads are connected to the AC bus directly or through an AC/AC converter when necessary [176]–[181]. A schematic representation of a hybrid-coupled configuration option for an off-grid application is presented in Fig. 3.3.

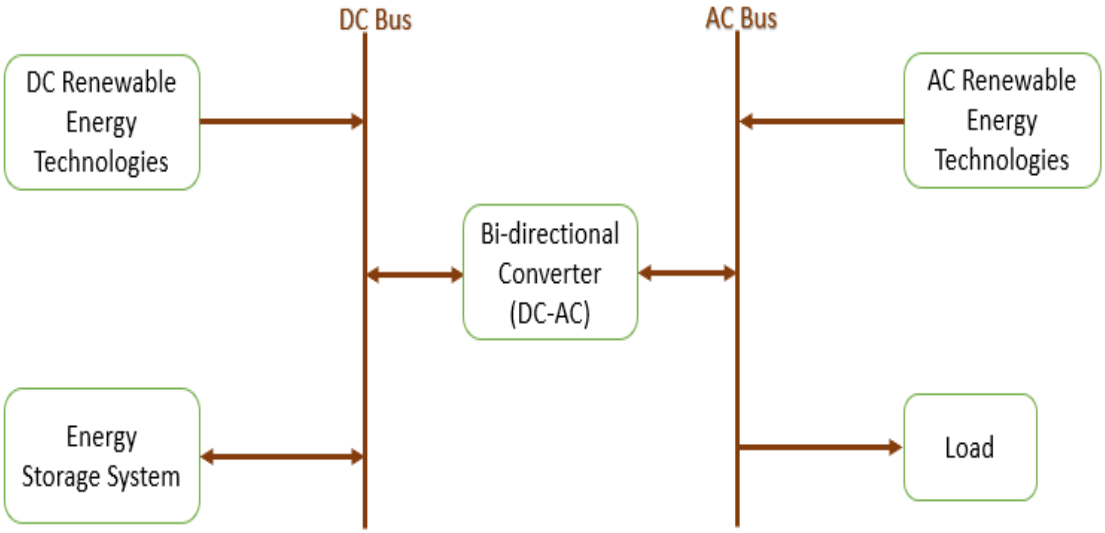

Fig. 3.3. Hybrid-coupled energy systems configuration [176]–[181]

Hybrid-coupled configuration option enables improve system efficiency in comparison to the DC and AC coupled configurations [166], [167] since this configuration option offers the possibility of connecting AC energy system and DC

energy system separately, so, unnecessary energy conversion is avoid. Therefore, it results in the reduction in energy conversion losses and the unit cost of energy. In terms of the control and energy management of this configuration option, it is the most complex option [165], [166]. However, the complexity in hybrid-coupled energy systems configuration can be minimized by the recent development in power converter technology [159]–[162]. In this study, the hybrid-coupled configuration option is selected as the HRES configuration. Therefore, DC renewable energy technology, AC renewable energy technology, and energy storage system in Fig. 3.3 will be PV, Biogas generator, and battery respectively.

3.3 Hybrid renewable energy system components

As earlier mentioned, PV, biomass generator and battery are the main HRES components. Because the effect of integrating HRES in locations with lower solar radiation potential is studied here, biomass generator is used to reduce the effect that PV intermittent energy supply has on the HRES energy security and to prevent excessive battery charge and discharge. This is because the excessive use of the battery lead to an increase in energy losses and a reduction in the life span of the battery. Therefore, whenever the PV system is unavailable, the biogas generator is used to supply the load, while the battery is only used for peak power shaving. Furthermore, the local collection of biowaste can encourage the direct participation of the community in biogas energy production.

To calculate the minimal cost of energy generation, a design space search is performed to determine the optimal combination of generator capacities. The HRES design space can be compared to a 2-D graph. Therefore, “x,y” coordinates in the design space represents combinations of PV and biogas generator capacities. The peak load is used to estimate the maximum capacity of the PV and the biogas generator (i.e. maximum x-axis and y-axis values of the HRES design space). The area of the design space whereby combinations of PV and biogas generator, can reliably supply the load is the feasible region. While the area of the design space whereby combinations of PV and biogas generator cannot reliably supply the load is the infeasible region.

In the feasible region, the optimal combination of PV and biogas generator is the combination with the lowest unit cost of energy. Because energy mismatch arises from the variability in solar irradiance and in load profile, the estimation of the battery optimal capacity can reduce over-sizing of PV and biogas generator in the feasible region. Hence, the optimal battery energy capacity is estimated from the maximum cumulative energy deficit between the energy generated and the load profile. In the sections of this chapter, literature review is performed on HRES components design and operation, load profile models and different modelling approaches.

3.4 Photovoltaics (PV) electricity generation

PV are semiconducting materials that convert sunlight into electrical energy. The PV system generated electrical energy is dependent on the photo-electric effect of the PV material, and on the amount of photons/incident radiations that is received by the PV material [117], [182]–[185].

3.4.1 Photovoltaic technology

PV semiconductor materials are designed in the form of a p-n junction. Whenever incident photons are absorbed by the semiconductor material, electron-hole pairs are generated, therefore, when these materials are connected in a closed circuit, the excited electrons (electric current) flows through the circuit [117], [183], [184]. The electrical output of a PV system is dependent on the design characteristics of the PV material/technology. Some of the electrical parameters used by manufacturers to define the characteristics of a PV system are presented in Table 3.1.

Table 3.1. Definition of PV system electrical parameters [117], [184], [186]

PV parameters	PV parameters definition
Efficiency, η	It is defined as the ratio of the energy output from the solar cell to the input energy from the sun. So, it is a measure of the percentage of received solar energy that a PV panel converts into electricity.
Open-circuit voltage, V_{OC} V_{OC}	It is defined as the maximum voltage supplied at no-load or no-current. It's due to cell junction bias by the light-generating current
Short-circuit current, I_{SC}	It is defined as PV module supply current when the module voltage is zero or short-circuited. Unlike many other electrical generators, PV module can be short-circuited.
Voltage at maximum power point, V_{MPP}	It is defined as the PV module voltage for maximum power supply or the ideal voltage to generate maximum power
Current at maximum power point, I_{MPP}	It is defined as the PV module current for maximum power supply or the ideal current to generate maximum power
Power at maximum power point, P_{MPP}	It is defined as the point in which the highest power can be achieved on the PV module I-V characteristic curve or the point whereby the PV module can supply maximum power to the load.
Fill factor, FF	It is the ratio of the maximum power point power (P_{MPP}) to the power obtained by multiplying open-circuit voltage by the short-circuit current

Current-voltage (I-V) characteristic curve of a PV module can be used to illustrate short-circuit current (I_{SC}), open-circuit voltage (V_{OC}), current at maximum power point (I_{MPP}), voltage at maximum power point (V_{MPP}), and power at maximum power point (P_{MPP}) of a PV module. For example, from Canadian solar manufactured CS6U-355 poly crystalline silicon module datasheet [187], the PV module I_{SC}, V_{OC}, I_{MPP}, V_{MPP}, and P_{MPP} values are shown in its I-V characteristic curve in Fig. 3.4.

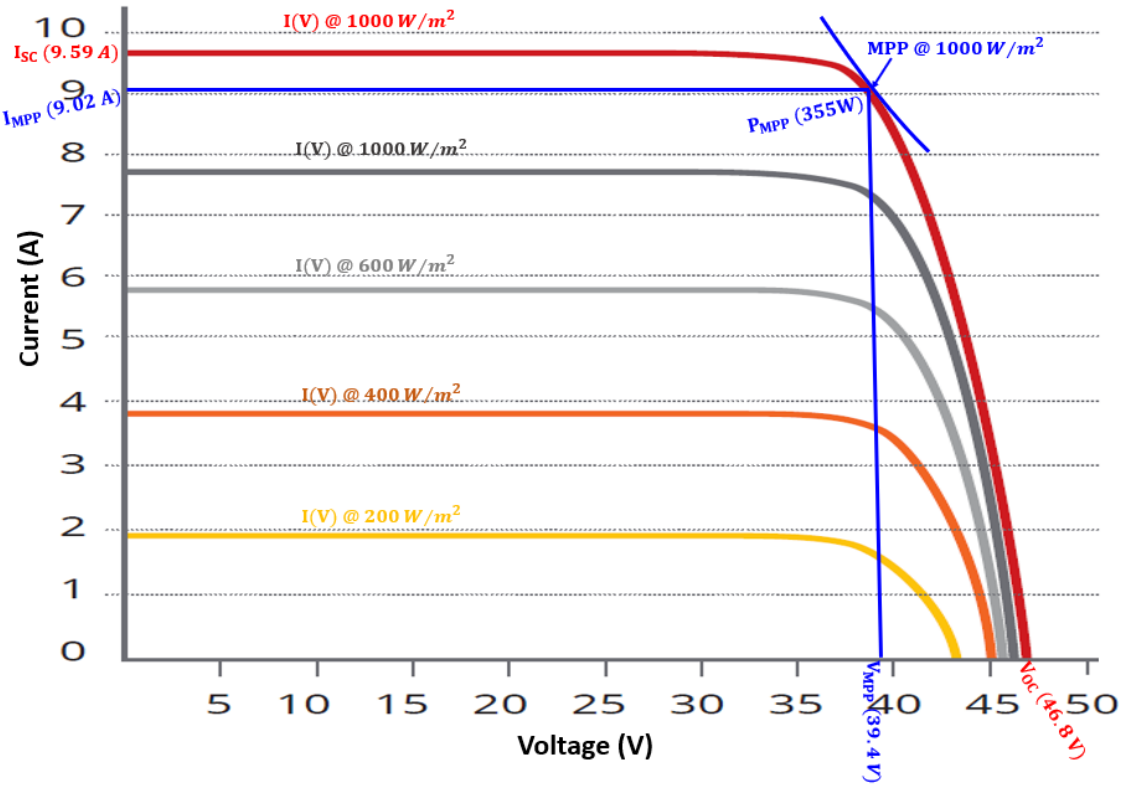

Fig. 3.4. CS6U-355 poly crystalline silicon module I-V curve [187]

The performance characteristics of a PV module I-V characteristic curve are measured under standard test conditions (i.e. a cell temperature of 25°C and an irradiance of 1000 Wm^{-2} at an air mass of 1.5 spectra) [186]. Therefore, the power output of a PV panel is dependent on the irradiance received by the PV panel (see Fig. 3.4) and on the operating temperature of the PV panel. Fig. 3.4 shows that the fill factor defines the rectangularity of the I-V curve because it is the ratio of the product of the current and voltage at the maximum power point to the product of the short-circuit current and the open-circuit voltage. The fill factor of the PV module in Fig. 3.4 was 0.79. The power at maximum power point (P_{MPP} or P_{max}) is the maximum power a PV panel supply to a load for a given irradiance. So, the energy generated by a PV module varies from a zero value to a maximum value, because energy generated is dependent on PV module efficiency, PV module area, and on the available radiance [185], [186].

A PV module comprises of several PV cells. Typically, PV cells are connected in series within a PV module because the output voltage of a single PV cell is usually too small

for meaningful energy application [186]. Similarly, to increase the electricity generated from a PV system, the next PV system hierarchy (design) involves the aggregation of PV modules into a PV array as shown in Fig. 3.5.

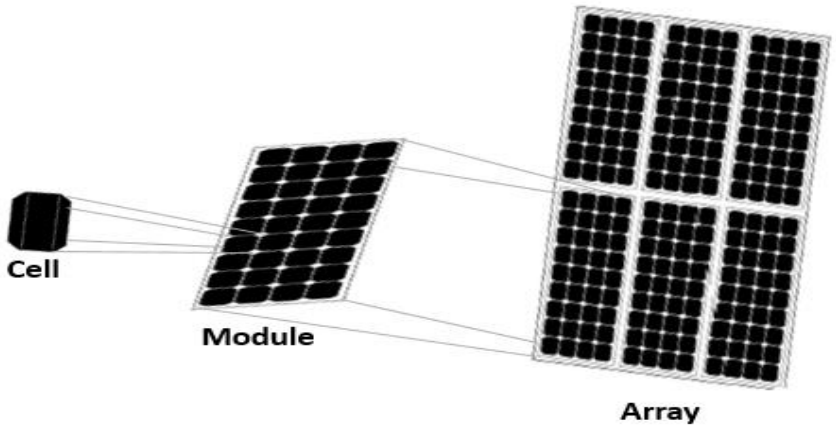

Fig. 3.5. PV system hierarchy

There are different generations of PV materials, and the performance characteristics of the different generations of PV materials have improved over the years. Recent progress in PV research and applications has been reported in [188]. Under standard test condition (STC), performance characteristics of PV modules which are recently manufactured by different generations of PV materials is presented in Table 3.2.

Table 3.2.PV module characteristics at STC [188]

Module classification	η (%)	A (cm^{-2})	V_{OC} (V)	I_{SC} (A)	FF (%)
Crystalline silicon	24.4±0.5	13177[da]	79.5	5.04	80.1
Multi-crystalline silicon	19.9±0.4	15143[ap]	78.87	4.795	79.5
GaAs thin film	25.1±0.8	866.45[ap]	11.08	2.303	85.3
CIGS thin film	19.2±0.5	841[ap]	48	0.456	73.7
CdTe thin film	18.6±0.5	7038.8[da]	110.6	1.533	74.2
Amorphous silicon	12.3±0.3	14322[t]	280.1	0.902	69.9
Perovskite	11.6±0.4	802[da]	23.79	0.577	68.0
Organic	8.7±0.3	802[da]	17.47	0.569	70.4

Abbreviations: η – nominal efficiency; A – Area; V_{OC} – open circuit voltage; I_{SC} – short circuit current; FF – fill factor; t[1]- total area; ap[2]- aperture area; da[3]- designated illumination area; GaAs – gallium arsenide; CIGS – copper indium gallium selenide; and CdTe – cadmium telluride.

The thermal properties of the different generations of PV materials are different, so, their operating temperature affects the electrical efficiency of PV panels [185]. The nominal operating cell temperature (NOCT) of a PV module is usually specified on a PV module datasheet. NOCT is defined as the temperature of the PV panel when it is subjected to a solar radiation of 800 Wm^{-2}, air mass of 1.5 spectra, wind speed of 1 ms^{-1}, ambient temperature of 20°C, and to a no-load operation (i.e. open circuited) [117], [184]. Consequently, the operating temperature of a PV panel is dependent on several factors, such as ambient temperature, local wind speed, solar radiation, glazing cover transmittance, and plate absorptance [117], [185], [189].

Apart from PV module NOCT, other temperature related characteristics of a PV module that are specified in the datasheet of a PV module include temperature coefficient of P_{max} in $\%°C^{-1}$ the temperature coefficient of V_{OC} in $\%°C^{-1}$, and temperature coefficient of I_{SC} in $\%°C^{-1}$. Meanwhile, because Nigeria is a tropical country (hot climatic condition), temperature coefficient of P_{max} can be used determine the impact of temperature on the maximum power output from a PV module. Power losses whenever the ambient temperature (°C) is more than PV module reference temperature (25°C) [117], [119], [175], [190], [191]. The amount of power losses is also dependent on the PV material because temperature coefficient of P_{max} varies amongst the different generations of PV materials.

---

[1] Total area is the projected area of the module and this includes the frame area.

[2] Aperture area is the portion of the module total area that takes into account essential components such as active materials, and interconnections. Thus, during testing, illumination is restricted to this portion of the total area.

[3] Designated illumination area refers to the portion of the module total area, where electricity is generated. Therefore, the contacting components are excluded from this area.

3.4.2 Solar radiation modelling techniques

During the design and evaluation of solar energy technologies, solar radiation data is an important input that is required to assess the solar energy potential of the studied location. Because of the movement of the earth and the chaotic nature of the atmosphere, measurement of solar radiation is a complex process. So, solar radiation is measured by satellite image processing or by group measuring instruments such as pyranometer or pyrheliometer [192], [193]. Typically, measured solar radiation data are not available for many locations in developing countries like Nigeria because the measurement and analysis of solar radiation data is a tedious and costly exercise [192], [193]. So, in these locations with no ground measured solar radiation data, an alternative approach is to estimate the global solar radiation data empirically from long-term measured meteorological parameters [192]–[195].

Several solar radiation estimation models have been developed in the literature [193], [196], [197]. Developed solar radiation estimation models can be classified based on [195]:

- Output (global, beam or diffuse radiation)
- Input(s) (meteorological data, climatological data or other radiation components)
- Time scale (daily, monthly average daily, hourly, monthly average hourly or even minutely basis)
- Time coverage (all-year or seasonal)
- Spatial coverage (site-dependent or global model)
- Methodology (stochastic or time-series modelling)
- Approach (physical, semi-physical or empirical)
- Surface inclination (horizontal, tilted or tracking surfaces)
- Type of sky (all sky or clear sky conditions)
- Algorithm used (statistical analysis or machine-learning algorithms).

Specifically, the input parameters for estimating solar radiation can be categorized into [193], [194]:

- Astronomical parameters (e.g. solar constant, earth-sun distance, solar declination, and hour angle)
- Geographical parameters (latitude, longitude, and elevation of the site)
- Geometric parameters (e.g. azimuth angle of the surface, tilt angle of the surface, sun elevation angle, sun azimuth angle)
- Physical parameters (e.g. scattering of air molecules, water vapour content, the scattering of dust and other atmospheric constituents such as O_2, N_2, CO_2, O, etc.)
- Meteorological parameters (e.g. extra-terrestrial solar radiation, sunshine duration, ambient temperature, precipitation, relative humidity, effects of cloudiness, soil temperature, evaporation, the reflection of the environs).

The accuracy of the estimated solar radiation data is dependent on the accuracy and influence of the estimating parameter(s) employed on the global solar radiation since the range of estimation error amongst the different estimation parameters varies from one parameter to another [192]. Sunshine duration is the most commonly used parameter for estimating global solar radiation [193]. The first sunshine duration model for estimating solar radiation was proposed in [198]. In this model, the ratio between actual daily horizontal surface global solar radiation (H_g) and clear day horizontal surface global solar radiation (H_c) was linearly correlated to the sunshine fraction (SF). Meanwhile, because of the uncertainty in the definition of a clear day, the original correlation developed in [198], was modified by replacing the clear day global solar radiation term with horizontal surface extra-terrestrial global solar irradiation (H_o).

Over the years, several authors have also estimated global solar radiation for different location by refitted the modified Angstrom model since Angstrom coefficients vary significantly with respect to the location and type of climates [192], [194], [195]. Furthermore, to enhance the accuracy of the modified Angstrom model, authors have proposed different mathematical expressions (such as quadratic, cubic, square root, logarithmic, exponential, and power expressions) to correlate the actual daily global horizontal irradiation (H_g) with the horizontal extra-terrestrial irradiation (H_o) [194]. Similarly, more complex artificial intelligent techniques such

as artificial neural network [199]–[202], fuzzy logic [203]–[205], and support vector machine [204], [206]–[208] have also been proposed for estimating solar radiation. However, evidence from the error estimation study by Zhang et al. [192] reveals that the more complex modelling techniques such as artificial neural network, did not show sufficient improvement in comparison to some empirical models but they argued that the rate of error of a model increases with respect to the shortness of the model life span. Zhang et al. [192] also stated that although artificial intelligence techniques have become popular in recent years, there is still the need for careful examination of their practical effectiveness and superiority in estimating solar radiation.

For Nigeria, several solar radiation estimation models exist in the literature that are either derived with the use of empirical or artificial intelligent technique. Some of the empirically derived models for estimating global solar radiation in Nigeria include: the modification of Hargreaves and Sammani [209] model to estimate the solar radiation of Ibadan [210]. In another study, Kolebaje et al. [211] derived an empirical model to estimate the solar radiation of Ikeja and Port-Harcourt by correlating global solar radiation with relative humidity and temperature. A multi-variant parameters solar radiation model that can be applied across Nigeria was developed in [212]. Another nation-wide estimation model was proposed by [213] by incorporating Garcia model into Angstrom-Prescott model, and the newly proposed model offered better performance accuracy compared with Garcia model and Angstrom-Prescott model.

Also, examples of artificial intelligent models developed for estimating global solar radiation of localities in Nigeria include: an artificial neural network (ANN) model that utilizes sunshine hours, maximum temperature, cloud cover, and relative humility daily data to estimate the global solar radiation for Makurdi was proposed in [214]. By using adaptive neuro-fuzzy interference approach, Olatomiwa et al. [215] derived an artificial intelligence model for estimating the global solar radiation of Iseyin. In an another study by the authors, an artificial intelligence model that hybridized support vector machine and firefly algorithm was developed to estimate the global solar radiation of Iseyin, Maiduguri, and Jos [216]. The

hybridized artificial intelligent model was found to offer better performance accuracy than both artificial neural network and genetic programme modelling techniques. In summary, both empirical and artificial intelligence techniques are acceptable approaches for estimating the solar radiation of a location without measured solar radiation data. However, when long term meteorological parameters are available, the prefer approach for estimating a location solar radiation is the empirical estimation technique because the more complex artificial intelligence estimation techniques could not guarantee lesser estimation error for a study where long term meteorological parameters was available [192].

Meanwhile, even though solar radiation estimation models are derived from meteorological dataset, it is very difficult to determine the rationale and influence that measured meteorological parameter(s) have on solar radiation estimation models. Also, empirical and artificial intelligence solar radiation estimation models for Nigeria are often derived to estimate horizontal surface global solar radiation, therefore, these Nigeria derived models might not be suitable to estimate the global solar radiation received by a PV panel at an inclined surface. However, solar radiation estimation models are not limited to the estimation of horizontal surface global solar radiation because many models have been developed for other countries to estimate inclined surface global solar radiation [217]–[219]. Despite the fact that Nigeria meteorological agency weather stations do not measure diffuse solar radiation; which is required by most estimation models to estimate inclined surface global solar radiation [220]–[228], in Chapter 4 Olmo et al. [229] estimation model which does require diffuse solar radiation data to estimate inclined surface global solar radiation is used. An alternative approach is to estimate the diffuse solar radiation of the location but most of the estimation models include numerical definitions with numerous coefficients, which are mainly valid for a location [230]. However, the alternative approach in this study desirable here because it is a more complex approach and it requires the use of measured diffuse solar radiation data; which is un-available for the location, to derive the modelling coefficients and to evaluate the most suitable diffuse solar radiation estimation model for the location.

3.5 Biogas electricity generation

Biogas electricity generation is a 2-stage conversion process. The first conversion stage involves the conversion of bio-waste into biogas, while the second conversion stage involves the conversion of biogas into electrical energy, with the use of a biogas generator. During the conversion of biogas into electrical energy, the operation of the biogas generator at full loading condition is essential for the optimal operation of the biogas generator [231]–[233] as well as to guarantee healthy engine operation and long engine life. This is because the operation of a generator at lower load ratio over a long duration of time can lead to exhaust manifold slobber or wet stacking [234].

Bio-waste can be converted into biogas by either a biochemical conversion technique or by a thermo-chemical conversion technique [235]. For organic waste with high moisture content, biochemical conversion technique is a more suitable option for the production of biogas [235]–[237]. The amount of biogas produced is dependent on the degradability of the organic waste or the microbial activities within the digester [235], [238], [239]. Meanwhile, the design and operation of an anaerobic digester for biogas production is dependent on several factors [238], [239].

3.5.1 Biogas production

Anaerobic digestion is an environmentally friendly technique used for producing biogas that can help to cut down both waste and greenhouse gas emission. Anaerobic digestion (AD) is the biological decomposition (fermentation) of organic materials by a consortium of microorganisms in the absence of oxygen [240], [241]. Anaerobic digestion occurs in a well-controlled enclosure called digester. Biogas (i.e. combination of mainly methane and CO_2) and digestate (i.e., fibrous end product that can serve as a bio-fertilizer) are two main output from an anaerobic digester [238], [239]. Whilst, little amount of other gases and trace elements such as nitrogen, hydrogen, hydrogen sulfide, ammonia, and water vapour are also produced [238]. The biochemical reactions for AD are similar to that of landfill gas, but the composition of the produced biogas from AD process is such that there are

higher methane composition (50 - 80%) than carbon dioxide (CO_2) composition (30 – 50%) [238], [241], [242]. Typically, the composition of methane (i.e. the actual energy constituent in biogas) and CO_2 in the produced biogas is dependent on the type of feedstock fed to the digester and on the digester operating conditions [238].

Anaerobic digestion is currently been used for wide range of applications such as the treatment of animals and crop residues, as well as for other industrial and commercial waste [241], [243]. In fact, anaerobic digestion has great potential for organic waste reduction, biomass energy recovery, as well as for biofuel and bio-energy production [241], [242]. The process of converting organic matter into biogas by microorganisms is achieved through a sequence of conversion phases or anaerobic digestion food chain. The conversion phases is carried out in series, such that the end products of one phase become the substrate for another phase [244]. Because of the dependence of one digestion phase on digestion another, the rate of metabolism at each digestion phase is vital for maintaining the stability of the AD process and for optimal biogas production [244], [245].

The four fundamental phases for anaerobic conversion of organic waste into biogas are hydrolysis, acidogenesis (combination of hydrolysis and acidogenesis is also called fermentation), acetogenesis and methanogenesis [246]–[248]. In the hydrolysis phase, complex degradable matters such as proteins, lipids, and organic complex carbohydrates (polysaccharides) are hydrolysed and converted into the simple or soluble organic substance or monomers such as fatty acids, monosaccharides, sugar, amino acids, and alcohols [235], [238]. End-products such as acids and simple carbohydrates from the hydrolysis phase are further broken-down in the acidogenesis phase into hydrogen, carbon dioxide, and simple acids [235]. During the acetogenesis, alcohols and volatile fatty acids (VFAs) are anaerobically oxidized by hydrogen-producing acetogenic bacteria into acetate, H_2, and CO_2. Acetate can also be formed from H_2, and CO_2 by hydrogen-oxidizing acetogenic bacteria known as homoacetogens [240], [249]. Hydrogen (H_2), CO_2, and acetate are vital for methane formation [235].

In the methanogenesis phase, a consortium of methanogens is responsible for methane formation. These methanogens are categorized broadly into acetate-utilizing (aceticlastic) methanogens and hydrogen-utilizing (hydrogenotrophic) methanogens, and acetogens [235]. Aceticlastic methanogens produce methane and CO_2 whenever their respective methyl and carboxyl groups act upon acetate. Hydrogen-utilizing methanogens produce methane by using CO_2 and hydrogen as an electron acceptor and donor, respectively [235], [238].

3.5.2 Anaerobic digester design

Although the process of anaerobic digestion has been in existence for several centuries, but as years went by, several breakthroughs such as the discovery of methane, establishment of the chemical constituent of methane, the use of biogas for heating and lighting, and the design and operation of different configuration of digesters for biogas production were achieved [238], [241], [250]. Apart from more complex and technically advance digesters such as anaerobic contact reactor, up-flow anaerobic sludge blanket reactor, fluidized bed reactor, and anaerobic filters, the most efficient form of conventional digesters are fixed dome, floating drum and plug flow digester [238], [251], [252]. These 3 forms of conventional digesters are mainly used by developing countries [251].

Conventional anaerobic digestion system usually comprises of a mixing tank, gas holder, inlet pipe, outlet pipe, gas pipeline, and outlet tank [238], [252], [253]. Typically, organic waste is mixed in a tank before it is fed into a anaerobic digester for microbial activities [252], [253]. During the mixing of organic waste, water is added so that a homogenous slurry can be formed from the mixture of organic waste. The homogenous slurry flows through the inlet pipe to the digester tank. In the digester tank (i.e. anaerobic reactor chamber), the slurry is retained for several days (i.e. hydraulic retention time) to undergo microbial digestion [238], [239], [251]. On completion of the digestion process, digestate is discharged from the chamber through the outlet pipe into the outlet tank and the solid effluent in the outlet can be used as fertilizer. While, biogas produced from the digestion process

goes into the gas holder of the digester before it is supplied through the biogas pipeline to be burnt as fuel for electricity generation.

The fixed dome digesters are constructed underground. Some of the advantages of fixed dome digesters include low initial design cost, long lifespan, space-saving, low maintenance, no moving or rusting parts [250], [251], [254]. The drawbacks of fixed dome digester include: the need for highly skilled workers during gas-tight construction, the challenge of repairing leakages in fixed dome digester, and the difficulty of determining the amount of gas produced since the produced gas is not immediately visible [250], [251], [254].

The operating features of floating dome digesters are like that of fixed dome digesters, but a floating gas holder is incorporated, and the gas holder is supported by a guide frame [251], [254]. In comparison to fixed dome digester, floating dome digesters are easier to construct but their material cost is high and their lifetime is shorter, because an extra steel drum is installed as a guide frame, and the steel drum will require continuous (regular painting) to avoid corrosion [250], [251], [254].

The tubular digesters can be constructed underground like fixed dome digesters, but they are constructed with polyethylene tubing [251], [254]. A separate polyethylene tubing or bag is also used for storing the biogas. The advantages of tubular digesters include: lesser need for highly skilled workers during tubular digester installation, easier operation of the digester, relatively easier to attain high digester temperature and low initial cost [250]–[252], [254]. However, this digester main drawbacks are their relatively short lifetime, high susceptibility to damage, and little possibility for effective repairs [251], [252], thus, resulting in higher cost in the long-run. Consequently, in a rural area, for long-term project construction, fixed dome digester is the preferred option because it has no moving or rusting part (i.e. it is robust), guarantee longer life span, and it is the cheapest digester construction option for a long-term project.

3.5.3 Effect of AD process parameters on biogas production

Anaerobic digestion of organic waste into biogas is a complex process [238], [239]. Therefore, biogas production from an anaerobic digestion process is dependent on several parameters such as temperature, pH, carbon to nitrogen (C/N) ratio, organic loading rate (OLR), hydraulic retention time (HRT), alkalinity and concentration of volatile fatty acid (VFA). Temperature affects the performance of an AD process. Detailed explanation on how temperature affects the rate of reaction and the stability of an AD process has been reported in [235], [238]. Typically, the 3 operating temperature regimes of an anaerobic digester are: psychrophilic, mesophilic, and thermophilic [235], [238], [239]. For optimum operation, the temperature regime for psychrophilic bacteria, mesophilic bacteria, and thermophilic bacteria is 12 – 18 °C, 25 – 40 °C, and 55 – 65 °C respectively [235].

Mesophilic and thermophilic temperature operating conditions are the most suitable for anaerobic digestion [235], [238], [239], [255], [256]. The operation of a digester under mesophilic temperature regime guarantees better digester stability, bacteria enrichment, and lesser sensitivity to inhibitors, while operation of a digester under thermophilic temperature regime guarantees higher solubility of organic compounds, faster reaction rates, and higher organic load rate [235], [239], [256]. Although, the operation of a digester under thermophilic temperature regime will lead to higher biogas production than when the digester is operating under mesophilic temperature regime, but because methane is the energy content of biogas, and the effect of temperature increase will result in higher CO_2 production than methane [256], so, the effect of operating a digester under a thermophilic temperature regime rather than under a mesophilic temperature regime, might not be too significant. In fact, some studies have shown that there is no significant difference in methane production when a digester is operating under a thermophilic temperature regime rather than under a mesophilic temperature regime [255], [256]. For a rural community, the operation of a digester under mesophilic temperature regime is perhaps the most preferred option because it requires lesser temperature and offers higher robustness to AD process [257]; which is necessary for withstanding the complications that might arise from a less controlled digester

in a rural area. Furthermore, there is less need for a CHP; which are more expensive than a power only generator, because Nigeria temperature is close to mesophilic operating temperature regime.

The pH of a digester affects the growth of microorganism and the subsequent methane production [239], [258]. Typically, several microorganisms have a preference for neutral pH range [259]. In fact, for optimal operation of a digester, the pH value across the four phases of an anaerobic digestion process ranges from 6.8 – 7.2 [238], [259].

The ratio of Carbon to Nitrogen (C/N) affects the quality of nutrients [235], and it essential for the growth and biocatalytic activities of microorganism in a digester [238], [239], [259]. C/N ratio for many feedstocks are reported in [96], [259], [260], and it is evident that C/N varies from one feedstock to another. For example, a protein rich feedstock has high methane and energy generation potential [261], but too much total ammonia might be generated that can lead to the instability or eventual collapse of the digester process [239], [259]. Co-digestion of feedstocks is one of the ways of regulating a digester C/N ratio because the optimum C/N ratio for a digester is between of 20 – 30 [239], [259]. The reason why a definite value is not used is because a digester C/N ratio is affected by different factors such as the feedstock type, composition of trace elements, chemical composition, and biodegradability [259].

Organic loading rate (OLR) is the daily amount of volatile solids (VS) fed into a digester. Its optimal selection is necessary to enhance optimal methane production [238], [262], [263], as well as to avoid microbial imbalance or instability of the digester process [238], [239], [247]. Typically, anaerobic co-digestion of substrate offers greater potentials for increase OLR than single digested system [238], [247], [262]. Several OLR values has been reported as the optimum values for an AD process [247], [264], but to allow easy flow of feedstock into a low cost anaerobic digester, Kinyua et al. [251] recommended that an organic loading rates beyond 2.8 3.5 – 7.0 $kgVS\ m^{-3}\ day^{-1}$ is less desirable because the feedstock will likely be manually mix in a feed tanks.

Hydraulic retention time (HRT) is the average time that a given volume of sludge stays in the digester [238], [239], [251]. It is one of the most import design parameter that determines the size and cost of the digester. HRT of a digester is usually influenced by the microbial growth rate, process temperature, OLR and substrate composition [239], [251]. Under mesophilic temperature regime, a digester hydraulic retention time is between 15–30 days [239].

In summary, it is evident from the review of parameters that affects the design and operation of an anaerobic digester, that organic loading rate of a digester is necessary for evaluating if the available feedstock with the studied location is enough to generate the required amount of biogas for the biogas generator, while the hydraulic retention time is necessary for calculating the volume of the digester.

3.6 Energy storage systems

An electrical energy storage system is defined as an energy technology that stores electrical energy when it is not needed and supply electrical energy when it is needed. In the literature, there is a growing research on energy storage systems (ESSs), which might be because of the several applications of ESSs [265]. These applications of ESSs include: energy management, load leveling or peak shaving, remote and vehicle load supply, power bridging, and power quality improvements [265]–[267]. Specifically, for renewable energy systems, ESSs are used for storing and smoothing renewable energy in order to improve energy security and energy reliability of renewable energy systems [267]–[269]. Meanwhile, the growing research in ESSs is not driven by only the positive impacts of ESSs on global energy mix, but also the need to address the challenges of ESSs. Some of the challenges of ESSs include: reduction in efficiency because of the reconversion of energy from one form to another, pumped hydro energy storage (PHES) adverse effect on climate change; that arise from PHES artificial construction of lakes, and chemical pollution from battery storage technologies [265].

From a historical perspective, the use of energy storage began in the early 20th century with the emergence of devices that could store electrical energy in the form of charges and conveniently discharge the stored energy when it is needed [270].

The lead-acid accumulator was the first energy storage device to be developed and it was used to supply residual loads on a direct current electricity network [270]. Over the years, research breakthroughs and technological developments have led to the storage of electrical energy in different energy forms such as chemical, electrochemical, electrical, mechanical and thermal energy form [265], [267], [271]. Therefore, the classification of energy storage systems based on their stored energy form is presented in Fig. 3.6.

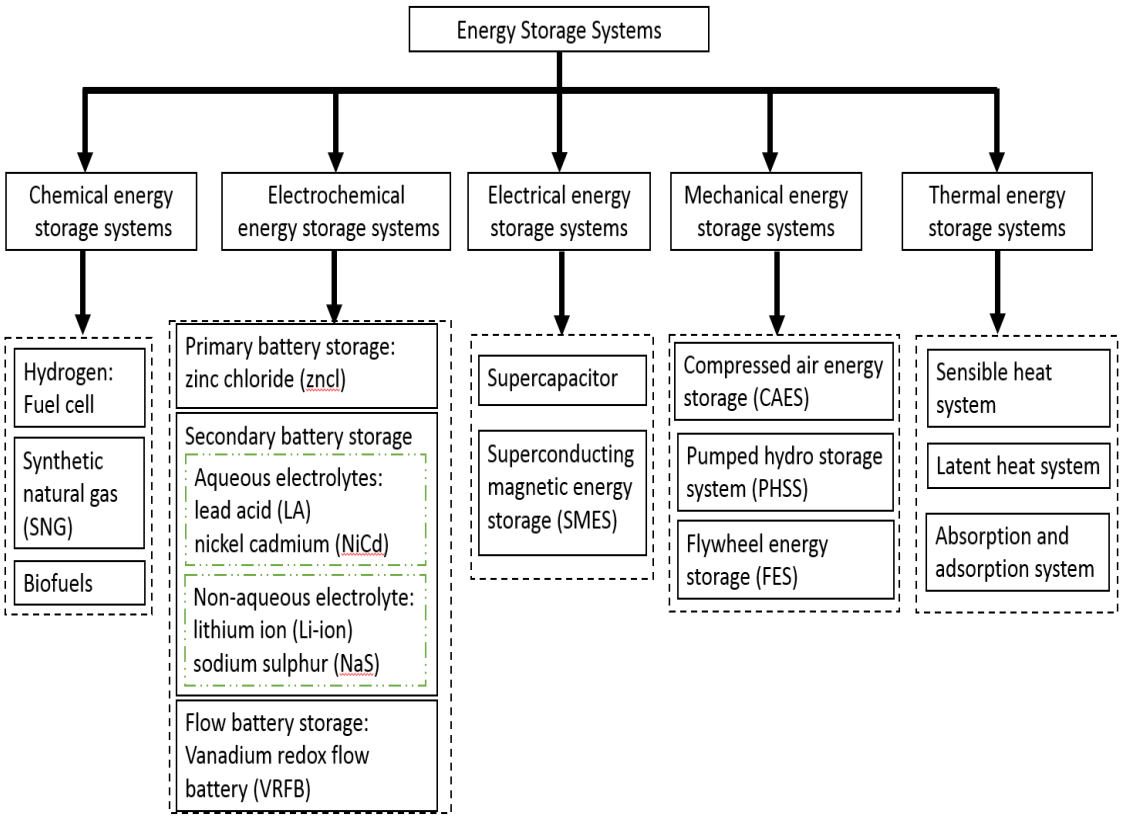

Fig. 3.6: Energy storage systems classification [265], [267], [271]

Some of the ESSs presented in Fig. 3.6 are either still technically under development or developed but still not widely used for power applications. In literature, the level of maturity for different types of ESSs has been presented by Zhao et al. [271], in the course of their review of different types of energy storage systems. Again, the physics and design features for the different types of ESSs have been presented by many authors in the literature [265], [267], [270]–[272], but it is noteworthy to mention from a system design level, that ESSs have unique properties and operating features that influence their use in different applications. Consequently, the

characteristics of ESSs can be defined in terms of capital cost, power rating, discharge time, power density, energy density, years, cycles, efficiency, self-discharge rate and response time [267], [271]. An overview of the techno-economic features of ESSs is presented in Table 3.3.

Table 3.3. Techno-economic features of energy storage systems [267], [271], [273]

Capacity	Super-capacitor	SMES	Flywheel	PHSS	CAES	Lead acid	Li-ion	NaS	VRFB
	Wh to kWh			MWh to GWh		kWh to GWh (modular)			
Energy density (Wh/l)	2 - 20	0.5 -10	20 - 200	0.27 - 1.5	3 - 6	50 - 100	200 - 350	150 - 250	20 - 70
Power density (Wh/l)	15000 - 50000	1000 - 5000	5000 - 15000	0.5 - 1.5	0.5 - 2	10 - 500	10 - 350	140 - 180	<2
Cycle efficiency	77 - 83	80 - 90	80 - 95	75 - 82	60 - 70	70 - 75	90 - 99	68 - 75	70 - 80
Storage duration	Seconds to minutes			Hours to weeks					
Self-discharge rate (%/day)	≈ 10 - 20	10 - 15	70 - 100	0.005 - 0.02	0.5 - 1	0.1 - 0.4	0.1 - 0.3	≈ 10	0.1 - 0.4
Response time (ms)	<10	1 - 10	>10	> 3 min	3 - 10min	3 - 5	3 - 5	3 - 5	>1sec
lifetime (years)	15	20	15	≈ 80	≈ 25	5 - 15	5 - 20	10 - 15	10 - 15
Cycle lifetime (full cycles)	up to 1 million	> 1 million	> 1 million	10000 - 30000	8000 - 120000	500 - 2000	2000 - 7000	5000 - 10000	>10000
Costs ($/kWh)	10000 - 20000	1000 - 10000	≈ 1000	5 - 20	40 - 80	100 - 250	300 - 800	500 - 700	300 - 500

It is evident from the ESSs techno-economic features presented in Table 3.3 that because of supercapacitors' high power density and cycle lifetime, they can be employed in applications where the minimization of the effect of fluctuations is required but they are only useful for low energy applications. Due to flywheel energy storage (FES) high energy and power density, as well as its lightweight, they are mainly employed for the starting and braking of locomotives. Wide range electrical application of FES is limited by its low energy generating capacity, high self-discharging rate as well as its relatively high unit cost of energy. Unlike flywheel energy storage, compressed air energy storage can be used for large energy

application because of its high energy generating capacity, high storage duration and low unit cost of energy but its low efficiency and slow response time makes it less desirable. Pumped hydro energy storage (PHSS) system is perhaps the most effective ESS for large-scale power application because of its high energy generating capacity, ideal efficiency, very low self-discharge rate and unit cost of energy. However, some of the drawbacks of PHSS include [265]: geographical dependence, massive capital cost, soil erosion, land flooding, and silting up of dams.

Battery energy storage systems (BESSs) is the most technically manured energy storage and are available in scalable sizes [267], [271]. Therefore, they can be used for either small-scale energy applications or integrated for large-scale energy applications (distributed generation systems). BESSs techno-economic features in Table 3.3 shows that each of the different battery technologies offer at least a comparative advantage over another. Lithium ion battery is usually a more expensive battery technology, but from a technical perspective, Table 3.3 shows that it offers more comparative advantage that is required for the deployment of renewable energy technologies. Over the years, there have been significant reduction in the cost of lithium ion battery, and more significant reduction is projected to occur in the future [87].

The different types of ESSs in Table 3.3 can be categorized into 2 groups. The first group is made up of ESSs such as supercapacitor, SMES, and FES with high power density, high cycle lifetime, and relatively higher efficiency, have low energy generation capacity, high self-discharge rate, and short storage duration. Thus, these types of ESSs are restricted to mainly high power demand applications, as well as for controlling systems with transient and/or fast fluctuating loads. While the second group is made up of ESSs such as PHSS, CAES, and BESSs with higher energy generation capacity, lower self-discharge rate, and longer storage duration, have lesser power density, and lower cycle lifetime. Thus, suitable for large-scale energy applications.

Technically, these 2 groups of ESSs can complement each other. Therefore, their hybridization can help optimize the size, improve the efficiency, and elongate the

life span of energy storage systems [267], [274], [275]. However, hybrid energy storage systems (HESSs) is accompanied by an increase in the complexity of the conditioning circuitry [275], which will result in an additional energy system cost. In rural areas, with poor technical expertise and limited financial resources, HESSs might not be suitable because of the increase complexity in conditioning circuitry and less technical manurity of the first of ESSs. Meanwhile, the 3 most technically matured ESSs are BESSs, PHSS and CAES [271]. A comparison of these 3 matured ESSs, in terms of their respective SWOT[1] characteristics, is presented in Table 3.4.

Table 3.4. SWOT analysis of long-term storage possibilities [265]

Technology	Strengths	Weaknesses	Opportunities	Threats
Compressed air energy storage (CAES)	High capacity, Low cost per kWh. Less need for power electronic converters	Need for underground cavities and the need for fuel	Potentials for its use as distributed storage	The popularity of thermal power plants
Pumped hydro storage system (PHSS)	High capacity, Low cost per kWh. Less need for power electronic converters	Suited for centralized storage application and can be geographically restricted	Lower reservoirs under seabed will be useful in offshore wind parks	Less attractive or perhaps it becomes obsolete for distributed storage applications
Battery energy storage system (BESS)	Good configuration and well-suited for distributed storage applications	High investment cost, low cycle life, and temperature dependent	Can be integrated with emerging technologies	Raw material limitations and selection issues that arise from the constant development phase

In summary, BESSs are the most suitable for distributed storage applications. Also, because Li-ion battery has very good technical features and require little or no maintenance, it is perhaps the best BESS for distributed storage applications.

3.7 Electrical load demand

As earlier mentioned in Chapter 1, load profile study is vital for energy planning as well as for evaluating the suitability of renewable energy technologies for rural

[1] SWOT is an acronym for strength, weakness, opportunity and threat

electrification beyond lighting. In this section, review of load profile modelling techniques that can be applied to study Nigeria rural communities load profiles is performed. Typically, to study domestic load profiles, national time use survey (TUS) data is used [276]–[280]. However, national time use survey data on electricity consumption is non-existent in some countries like Nigeria, and this makes the study of domestic load profiles more restricted and challenging. This is because in studies without national TUS data such as presented in [59], [281], fewer details are usually captured during survey. Consequently, the developed demand models are either un-able to predict households' energy consumption behaviour or there is increase complexity in developing demand model. Review of energy consumption drivers and load profile modelling techniques is necessary to ensure well-tailored data gathering and the development of a demand model that can predict households' energy consumption behaviour.

3.7.1 Households' energy consumption drivers

In modelling load profiles, knowledge of energy consumption drivers assists model construction [277], [282], [283]. Many energy consumption drivers are reported in literature. For example, the time it takes to perform an activity, availability of appliance, age of a house, and occupants' behavioural patterns have been listed as energy consumption drivers [284]. In another study, the value of a house (worth of the house), household income, house age (year the house was built), composition of occupants (age variation of household occupants), tenure (owned, rented), social status (e.g. skilled, semi-skilled, unskilled etc.), dwelling type (detached, semi-detached), house location (city versus rural area), and years lived in the house were listed as energy consumption drivers [283].

Based on the frequency of citations in literature, McLoughlin et al. [277] stated that the commonly reported dwelling and occupant-related energy consumption drivers include dwelling type, household income, appliance holdings, number of occupants, location, household composition, appliance rating, head of household (HoH) age, floor area, time of use, heating type, weekday/weekend, external/internal temperature, dwelling age, number of rooms, employment status, tenure type,

dwelling value, disposable income, social group, number of rooms, education level, electricity price, dwelling surface area, and period of residency.

These different households energy consumption drivers can be categorized into four major groups: external conditions (e.g. location and weather), physical characteristics of dwelling, appliance ownership, and of most importance the occupants' activity schedule [285]–[288]. Although there are many energy consumption drivers that influence households' energy consumption, only few energy consumption drivers are selected during load profile modelling. This is because the more the number of energy consumption drivers selected, the more the complexity of the model design.

Typically, the research boundary of a proposed load profile model is considered when selecting the main energy consumption drivers in literature. For example, Huebner et al. [286] argued that when electric powered heating systems are not used by the studied households, the main energy consumption drivers for modelling load profiles are dwelling size, household population, and appliance ownership and usage. For households where electric powered heating systems are used, studies have shown that building related variables is a main energy consumption driver. For example, Kavousian et al. [287] stated that the main energy consumption driver for modelling load profiles are floor area (building related variable), weather, location, number of occupants, and high energy consumption appliance such as electric water heating. To an extent, Xie et al. [285] collaborated the finding of Kavousian et al. [287] because they stated that the number of occupants and floor area are amongst the main energy consumption drivers. But they also mentioned that the use of split air conditioner during summer months is another main energy consumption driver.

During the questionnaire design, Huebner et al. [286] main energy consumption drivers are selected because Nigeria is in a tropical region, hence, it is unlikely that electric powered heating systems will be used by households. So, question on the "number of bedrooms in the house" and question on the "number of occupants" in the demographic (first) section of the questionnaire, are used to generate the dwelling size and the household population respectively. Huebner et al. [286] remaining main energy consumption driver, i.e., appliance ownership and usage can

be separated into appliance ownership and appliance usage. Here, modelling of appliance usage is important because the impact of occupants' behaviour on energy consumption is considered. Also, without appliance usage data, appliance ownership data has minimal influence on households' energy consumption [289]. In fact, from a study of 323 households in Netherland, Bedir et al. [290] reported that appliance usage resulted in 37% variation in the households' energy consumption.

To model how occupants' behaviour influence household appliance usage, data relating to occupants' activity schedule will be collected from the household occupants' behaviour section and the household activities section of the questionnaire. To acquire data on household appliance ownership, a list of household appliances was tabulated in the fifth section of the questionnaire. The data acquired from the energy usage and power availability (fourth) section of the questionnaire are met for the in-direct validation of the developed load profile model because existing data to validate the developed load profile model are limited. Although the fourth questionnaire section is for model validation and not the model design, it is not presented as the last section because the fifth questionnaire section was design as a table, it is perhaps more presentable to end the questionnaire design with a table.

3.7.2 Review of load profile models

The science or art of modelling load profiles is a complex process that depends on several factors. However, forecasting of load profile is vital to ensure adequate demand-supply balancing in the energy industry. Consequently, the design of a load model that can mimic the behaviour of the actual load as well as predict future load consumption is the underlying motivation for continuous research into load profile modelling [291]–[293]. Typically, load models are representations of energy consumption patterns and they are designed with the aid of mathematical techniques. The design of load models is dependent on several predicting variables such as time factor, weather condition, customer factor and economic factor [294]. These predicting variables serve as inputs and/or operational elements that influences the accuracy of the generated synthetic load data. Therefore, the accuracy of load model design is primarily a function of the suitability of the modelling

technique adopted, the accuracy of the predicting variable as well as on the acceptability of relevant assumptions [295].

In representing energy consumption patterns, several models have been developed in the literature. Over the years, to allow for ease of understanding and ease of application of load models, researchers have attempted to classify load models into groups and sub-groups, but none of the available forms of load model classifications is the best or of universal significance [296]. According to Suganthi and Samuel [297] the different load forecasting models can be categorized into traditional modelling techniques (e.g. time series, regressions, and autoregressive integrated moving average models) and soft computing modelling techniques (e.g. fuzzy logic, genetic algorithm, and neural network models). Similarly, based on load models development tendency, Hong [298] stated that there are two forms of load modelling techniques: traditional and soft computing (artificial intelligent) modelling techniques, but Hong [298] also mentioned that another (third) group of load models are designed by the hybridization of different statistical and artificial intelligence modelling techniques. Apart from the classification of load models based on the type of forecasting techniques employed, researchers have also attempted to classify load models with more specific attributes of the load models. Some of these classifications are presented below:

An earlier classification in Grubb et al. [299] recommended that energy models should be categorized based on research headings such as: top down and bottom up, time horizon, sectoral coverage, optimization and simulation techniques, level of aggregation and geographical coverage. In [300], the research headings recommended for load model classification includes: general and specific purpose, structure (internal and external assumptions), analytical approach (top down and bottom up approaches), underlying methodology, mathematical approach, geographical coverage (global, regional, national, local or project), sectoral coverage, time horizon (short, medium and long term) and data requirements. Herbst et al. [301] argued that since the design of the load model are usually dependent on prediction variables, therefore prediction variables such as the target group (policymakers, research bodies or energy companies), intended use

(forecasting, simulation, optimization etc.), scope of coverage (regional, national or multinational), conceptual framework (top down or bottom up), and availability of information (data inputs) should be used for load models classification.

In literature, because domestic energy consumption patterns are dependent on several modelling parameters such as dwelling characteristics, lifestyle, affluence, and occupancy [302], authors have attempted to categorize domestic load models into groups. For example, Widén et al. [303] stated that since the range of coverage of domestic models varies distinctively, domestic load model can be classified in terms of the load model's resolution in space and time. So, Widén et al. [303] recommended that domestic load models should be classified as: high time and low spatial models (e.g. load forecasting models), high spatial and low time resolution models (e.g. econometric models), and high time and high spatial resolution models. In this study, because there is no access to extensive electrical load data, the accurate design of the rural domestic load model will mainly depend on the determinant used for modelling the load profile. So, for accurate load modelling, it will be useful to take advantage of the approaches employed in similar studies. These approaches can be grouped under the conceptual framework or the analytical modelling approach [300], [301].

3.7.3 Analytical modelling approach

The analytical modelling approach is concerned with the way the input data of the domestic load model is processed in order to take advantage of the available information. Historically, the two traditional approaches employed for modelling domestic demand models from input data are top-down (TD) and bottom-up (BU) modelling approach [291], [292], [301], [304], [305]. It is important that although TD and BU modelling approaches are historical approaches for modelling domestic load profiles, over the years, researchers sometimes employs another (third) analytical modelling approach called hybrid modelling approach. Typically, when load models are built with hybrid modelling approach, the strengths of TD and/or BU modelling approaches are usually combined [291], [296].

Top-down models are developed by the fission of macroscopic load input data into different housing stocks, in order to analyze the housing stock data more critically [292], [304], [306]. TD model construction is less complex than BU model construction because they are less reliant on households' occupancy consumption behaviour. TD models take a whole-system view of demand [307]. Thus, they are also known as high system-level models and they can be used for determining the relationship between the power sector and other top-level functions such as macroeconomic indicators (e.g. gross domestic product, and inflation), energy price, and general climate [292], [304], [306], [308]. However, because of the variation in households' occupant's consumption behaviour, TU models are less suitable for modelling household load profiles.

Bottom-up load models are developed by the fusion of microscopic load data of a household or group of households, and extrapolate the resultant energy consumption to a regional or national housing stock [291], [304], [308], [309]. In synthesizing regional or national energy consumption, BU load models are often accomplished by the use of weighted average, which are allotted based on the representation of the household types [310]. BU load models are sometimes referred to as statistical, probabilistic, empirical, time use or building physical modelling approaches [291], [304].

The two BU modelling techniques used for evaluating the energy consumption of end-uses are statistical models and engineering models [296], [304], [308]. Statistical models apply a variety of statistical techniques to regress the relationship between end-uses and energy consumption. Some of the techniques adopted in the literature by statistical models includes regression [311], [312], conditional demand analysis [313]–[315], and neural networks [316], [317]. Engineering models applies information on building characteristics and end-uses to estimate energy consumption characteristics. Engineering method can be used to model electricity consumption of households' without relying on historical data on electricity use. Strengths and weaknesses of TU models, statistical models and engineering models are presented in [296], [304]. Engineering modelling techniques can be classified are: distribution [276], [318], archetypes [319], [320], and samples [321], [322].

Typically, BU engineering models are more suited for modelling current and prospective technological options [296], [304]. This is because each end-use of BU engineering models have their respective sub-models, which allows the aggregated model to easily track the effect that changes made on any of the sub-models will have on the total energy consumption. However, one of the limitations with BU engineering models is that occupant behaviour is estimated, which is rather difficult as behaviour is unpredictable and can vary greatly [296], [304]. Thus, there is the possibility that inaccurate conclusion might be reached. This limitation has encouraged researchers to develop engineering models equipped with improved occupant behaviour models. For instance, Capasso et al. [276] applied Monte Carlo method to capture the relationship between residential energy demand and behavioural factors of household occupants. Richardson et al. [323] employed a Markov Chain technique to synthesize active occupancy patterns based on the survey data on people's time use in the UK. Highly resolved synthetic demand data were created in their study by using a stochastic model that maps occupant activities to appliance uses.

Markov Chain technique was also employed by Widén and Wäckelgård [279] to synthesize active occupancy patterns from time use and electricity consumption database in Sweden, in order to relate residential power demand to occupancy profiles. Widén and Wäckelgård [279] study showed that realistic demand patterns can be generated from simulated sequences of human activities. Furthermore, Muratori et al. [310] proposed a similar approach, where by Markov process technique was integrated with a physics-based engineering heating, ventilation, and air conditioning (HVAC) systems. The Markov process technique was used to synthesize the activity patterns of households from American Time Use Survey (ATUS) data. Muratori et al. [310] study concluded that their synthesized outputs were statistically similar to metered residential electricity data.

Despite the wide use of bottom-up modelling approach for modelling household's energy consumption, the use of bottom-up modelling approach for modelling Nigeria households' energy consumption are rarely reported in the literature. This is perhaps because of the lack of national TUS data for Nigeria. For instance, Ayodele

et al. [309] assumed that the lifestyle amongst city around the world are similar, so that household active occupancy data synthesized by Richardson et al. [323] for the United Kingdom could be applied for modelling households' energy consumption for the city of Ibadan, Nigeria. Household occupancy time use survey (TUS) data is an essential parameter for modelling households' energy consumption. For instance, Yao and Steemers [324] stated that households' load profile is highly dependent on the occupancy behaviour. This opinion was collaborated by Stokes et al. [325], because they reported that when household's occupancy behaviour is considered in a model, there is an improvement in the modelling of diversity.

3.7.4 Bottom-up modelling approach

The ability of bottom-up engineering models to generate synthetic load data without relying on observed or historical data of interest in this study. However, since the accuracy of the developed load model is dependent on the way the housing input data are combined within a hierarchical structure, the resolution of the BU load model is vital in accessing the load model complexity as well as its accuracy [278], [279], [292]. In the next sub-section, review of some bottom-up load models is presented. For ease of representation, the reviewed bottom-up load models are classified into low-resolution and high-resolution models. The high-resolution models are the more detailed models and are perhaps more preferred. This is because more details of the input data can be captured by them in comparison to low-resolution models.

3.7.4.1 Low-resolution models

Notable amongst the earlier studies on the modelling of domestic load profile with bottom-up approach was the study by Capasso et al. [276]. The essence of the study was to determine how working days' electricity consumption influences peak winter electricity consumption of the Italian electricity network. Outcomes from this study revealed that households' appliances time of use synthetic data can be generated by analyzing the electricity consumption behaviour of household occupants. However, due to the amount of input data that is required by Capasso et al. [276] model, the model is less practicable.

An extensive two-part model was developed in [326], unlike in [276]. The model's input data were gotten from available appliance data and households' electricity consumption statistics. The first part of the demand model is used to captures electricity consumption fluctuation as well as store appliance ratings, while the second part of the load model is used to generate the individual load curves for each appliance. However, due to the underestimation of the mean daily electricity consumption during the model construction, the accuracy of the developed model was undermined in [326]. Yao and Steemers [324] developed a comprehensive bottom-up model called the simple method for formulating load profile (SMLP). This model had the flexibility of generating synthetic data for different conditions such as building types and occupancy time of use. However, the drawback with the SMLP is that its comprehensive nature results in an increase in the amount of input data required as well as on modelling complexity. Therefore, SMLP is less suitable for modelling load profiles that require several input data.

3.7.4.2 High-resolution models

The high-resolution models or time of use load models makes use of high-resolution time steps (i.e. time step lesser 30 minutes) when modelling load profiles [292]. Several load models are built on high-resolution times steps and because of the increased use of this modelling approach in literature, they should be referred to as a separate modelling approach [327]. Amongst the developed time of use models is the comprehensive three-step model that was developed with a high time resolution in [328]. The developed 3-step Stokes' model had the potential of determining how the number of household occupancy and the size of the floor area affects a load profile. Stokes model is regarded as a very extensive load model because of the model's comprehensive nature and ability to generated synthetic data at a high time resolution. In fact, Widén et al. [329] stated that Stokes [328] model is arguably the most detailed domestic load model.

Stokes [328] model is not only well acknowledged and used by several researchers for generating synthetic load profiles but several authors such as in [293], [330], [331] also use Stokes [328] model to validate their developed model. Apart from Stokes [328] model, Richardson's model [278], [323], [332] and Widén's model

[279], [303], [333], are examples of a well-developed high-time resolution load models. The two essential building blocks used by Richardson's model and Widén's models for generating synthetic load profiles are time use survey (TUS) data and Markov-chain process. The Markov-chain process is essentially a conditional probability-based technique, and it is used to synthesise the missing information in a time use survey data. This is achieved by constructing the transition probability matrix for households' active occupancy and the time of use of appliances [279]. One of the benefits of using Markov-chain technique to generate extensive occupancy behavioural patterns is that it reduces the challenges of acquiring the extensive behavioural data used for modelling a high-time resolution load profile.

3.8 Hybrid energy system design metrics

The hybrid energy system design metrics are performance indicators or control apparatus that help energy providers or stakeholders make an informed decision during optimum sizing of energy system components. Hybrid energy system design metrics are usually employed to determine the reliability and financial viability of a system-level energy project design. To determine the operational reliability of an energy system, performance indicators such as economic dispatch, and power flow analysis are examples of reliability metrics that are used in the literature. Description of some of the metrics used for studying hybrid energy systems is presented as follow:

The total annualized system cost $(C_{ann,tot})$ is an economic criterion, that can be used for the optimal sizing of components of an energy project [170], [334]–[336]. It compares the different cost functions (i.e., capital cost, replacement cost, operation and maintenance cost, and fuel cost) of the energy project in terms of their annualized related cost [170]. This criterium is useful because it helps to relate the different sub-system cost of an energy project that occurs at the different stages of the energy project lifetime. Therefore, the energy project annualized total cost is dependent on the energy project annuity factor [168]. Levelized cost of energy (LCOE) and net present cost (NPC) are another two useful economic metrics that can used to determine the suitability of an energy project, and they can be derived

from the energy project total annualized system cost [170], [334]–[336]. LCOE is defined as the ratio of the average cost per kilowatt-hour of useful electrical energy produced by the energy system or the constant price per unit of energy that ensures that the return on investment break even, while the NPC is defined as the summation of the discounted present costs throughout the useful lifetime of the energy system [85], [170], [177], [334]–[336].

The loss of power supply probability (LPSP) is one of the most commonly use reliability criteria, and it can be used during energy system to provide a trade-off between the reliability and the total cost of an energy project [337]. LPSP is defined by the probability that an energy project is unable to continuously supply its electrical load because of insufficient power supply, or defined by the ratio of the total unmet electrical load of the energy project to the total electrical load of the energy project over a period of time [166], [167], [190], [337]. Some other reliability metrics that can be used to determine the suitability of an energy project include: the expected energy not supplied (EENS), the battery state of charge ($E_{B/SOC}$), and the level of autonomy (LA).

The expected energy not supplied (EENS) is used to determine the periodic reliability of a stochastic renewable energy source. Therefore, for each time step, EENS measures the amount of expected energy that will not be supplied because the electrical load exceeds the available electricity supplied [170]. The battery state of charge ($E_{B/SOC}$) is a reliability criterium that can be used to determine the excess energy that can be added or drawn from the battery per time. It can be used to determine the optimal size of battery [338]–[340], as well as can be used to calculate the expected energy not supplied of an energy project with 0% loss of load probability. The level of autonomy (LA) is a reliability criterium that is used to select the optimal capacity of an energy storage (back-up energy system) that will be able to ensure continuous supply during periods of limited or no energy generation in the energy system [49], [171].

The reliability criteria mentioned in this section are usually employed to ascertain the reliability of design on a system-level basis. However, performance indicators

such as economic dispatch, and load flow analysis are measures that are applied in literature to ascertain the operational reliability of an energy system. Depending on the network operational constraints, economic dispatch is used to determine generators unit commitments (generator to turn on) in order to ensure reliable supply of electricity at minimum system cost [341]–[345]. Unlike economic dispatch study; which is concern with the optimal selection of generators to minimise energy system cost, power flow study is concern with the healthy operation of an electrical network [346]–[350]. The healthy operation of an energy system will result to more saving in the future. Furthermore, power flow studies provide more information about the operating characteristics of an energy system.

Unlike, traditional circuit analysis methods; whose usage are limited as the complexity of the power network increases, power flow study are used to analyse complex network because it utilizes simplified notations such as one-line diagram and per-unit system, to compute power system bus parameters (e.g. reactive, apparent, phase angle etc) at steady state condition [350]–[353]. So, power flow study can be used to identify power system issues such as low voltage and excessive load on the transmission line, in order to correct suspected fault before they escalate into a major network problem [350]. Outcome of a power flow study is relevant to power system engineers because power flow analysis is performed based on the steady-state characteristics of a balanced three-phase power network [354]. Furthermore, outcomes from power flow study are used to plan for future expansion of the power network and used to determine the best operating approach for the existing network [353].

Power flow study is a complex numerical analysis, and it is mainly simulated with the use of iterative techniques in a computer. Iterative techniques/methods used for power flow study simulation include: Jacobi, Gauss-Siedel, and Newton-Raphson methods [350], [352]. Gauss-Siedel model and Newton-Raphson method are the two commonly used methods [350]. Gauss-Siedel method is used to solves power flow equations in rectangular coordinates until the difference in bus voltage from one iteration to another is sufficiently small, while Newton-Raphson method can be used to solve linear and non-linear problems [350], [352], [353]. Taylor's series

expansion are used in Newton-Raphson method, its power flow equations are solved in polar forms, while its optimal solution is reached when real and reactive power mismatches (ΔP and ΔQ) at all buses are within specified tolerance level [350], [352]. Newton-Raphson method is reported as the best iterative method for power flow study because it converges in some cases when Jacobi and Gauss-Siedel methods diverge [350], [352]. Furthermore, the number of iteration required for convergence by Newton-Raphson method is independent of the number of buses in the power network, but for Jacobi and Gauss-Siedel methods, the iteration increases with increase in the number of buses in the power network [350], [352], [353]. So, in terms of computational space savings, Newton-Raphson method is more economical.

Typically, a power network comprises of many network buses. A network bus is a node that can interconnect transmission lines, electrical loads and electrical generators [350], [353]. The electrical characteristics of a network bus are defined by voltage magnitude (V), phase angle (δ°), real or active power (P), and reactive power (Q) [350], [353], [355]. In power flow analysis, 2 of these 4 electrical parameters of a network bus are specified, while the other 2 un-specified electrical parameters of a network bus are simulated [350]. Depending on the 2 electrical parameters of a network bus that is specified, a network bus is classified as a swing or slack ($V < \delta^{\circ}$) bus, a voltage controlled (PV) bus, or a load (PQ) bus [350], [352], [353]. Characteristics of these 3 classifications of network buses has been presented in [350], [353].

3.9 Hybrid energy system optimization techniques

Optimal sizing of a hybrid energy system is required to ensure reliable supply of electricity at minimum system cost [356]. Therefore, for reliable supply of electricity at minimum system cost, different optimization techniques are used for the design and analysis of hybrid energy systems. Optimization techniques are a mathematical representation of system component parameters so that the effect of changing system component parameters can be observed and analyzed. The different optimization techniques used for optimal sizing of hybrid energy system can be

classified into: computer software tools, classical (traditional) techniques, and artificial intelligent (modern) techniques [166], [167], [357]. Meanwhile, Hybrid optimization techniques, which are derived from the combination of optimization techniques, are sometimes referred to as another optimization technique classification.

3.9.1 Computer software tools

In literature, computer software tools are commonly used to simulate the performance of a hybrid energy system. This is because computer software tools can help reduce the time and the cost spent on the design and analysis of a hybrid energy system [356]. Computer software tools that can be used for hybrid energy system design and analysis include: H2RES, HOMER, HYBRID2, HYBRIDS, HYDROGEMS, iHOGA, INSEL, RETScreen, SOLMIM, SOMES, TYNSYS, etc. The performance of computer software tools usually varies in terms of their functionality and adaptability [156], [358]. The inputs and outputs, as well as the strengths and weakness of some selected hybrid energy system computer software tools are presented in Table 3.5 and Table 3.6 respectively.

Table 3.5. Inputs and outputs of some selected hybrid energy system computer software tools [156], [357]–[359]

Software	Input	Output
HOMER	Load demand	Optimal unit sizing
	Relevant resource input	Cost of energy and net present cost
	Capital, maintenance and replacement cost	Renewable energy fraction
	System control	Multi-objective optimization
HYBRID2	Load demand	Unit sizing with cost optimization
	Relevant resource input	Cost of energy
	Systems initial investment and O&M cost	Percentage emission of different GHG
	Components details	Total payback period of the system
TRNSYS	Inbuilt input and modular structure library	Dynamic simulation of electrical output
	Meteorological data input	Dynamic simulation of thermal output
iHOGA	Load data	Cost of energy
	Relevant resource input	Life cycle emission
	Component and economic details	Energy buying and selling analysis
RETScreen	Load data	Energy production and saving
	Size of solar array	System component and fuel costs
	Product database are required	Comparative reduction in emission
	Climate database	Project financial viability
		Project sensitivity and risk analysis

Table 3.6. Strength and weakness of some selected hybrid energy system computer software tools [156], [356], [357]

Software	Strength	Weakness	Developed by:
HOMER	Suitable for optimal sizing of all renewable sources along with diesel generators, battery, or H2 storage for both electrical and thermal loads. Also, suited for technical and economic analysis	It only minimizes a single objective (net present cost) during optimal sizing. Thus, it cannot perform multi-objective optimization. Its simulation flexibility is limited (a black-box simulation tool)	U.S National Renewable Energy Laboratory (NREL) in 1992; www.homerenergy.com
HYBRID2	Useful for performing a techno-economic simulation of the optimal size of system components. Suited for accounting for inter time-step variations in data with the use of probabilistic methods	It requires a large quantity of input data and its simulation flexibility is limited (a black-box simulation tool)	Uni of Massachusetts; https://hybrid2-simulation-program.software.informer.com/
TRNSYS	Suited for simulating energy system behaviours that varies with time. Also, it performs extensive electrical and thermal analysis	It is more complex and less user-friendly than the other black-box simulation tools.	University of Wisconsin; http://sel.me.wisc.edu/trnsys
IHOGA	It can be used to simulate both single and multi-objective problems, that is, technical, economic and environmental analysis. It also has easy user's implementation functionalities	It cannot be used to perform sensitivity and probability analysis and modification of the daily load profile is also limited. Its simulation flexibility is limited (a black-box simulation tool)	University of Zaragoza, Spain; https://ihoga.unizar.es/en/descarga/
RETScreen	Suitable for assessing the benefit of a comparative study between a base (diesel) case and a proposed (renewable) case. It's also useful for carrying out an extensive economic and environmental study as well as for performing risk and sensitivity analysis	Time-series data cannot be imported into this software. The effect of temperature on PV module performance is not considered. Its simulation flexibility is limited (a black-box simulation tool)	National resources Canada in 1996; www.nrcan.gc.ca/energy/software-tools/7465

3.9.2 Classical optimization techniques

They are also known as traditional optimization techniques. They are developed by users to optimally size a hybrid energy system or to find the optimum solution of a hybrid energy system objective function. Classical optimization techniques can be categorized into: graphical method, probabilistic method, analytical method, and iterative method [167], [359].

3.9.2.1 Graphical method

Graphical methods provides a design space solution or graphical solution to optimization problems [360]. During the optimal hybrid energy system sizing, graphical methods are either used as a single optimization (standalone) tool; such as presented in [361]–[363] or combined with other numerical methods to form a hybrid optimization tool; such as presented in [339], [340], [364]–[366]. Furthermore, during the construction of a graphical simulation model, two decision variables are usually considered [171], [367]. For example, a standalone graphical tool called outsourced and storage curves was developed to predict the energy allocation of a hybrid energy system, determine the minimum outsourced electricity, and perform a demand side management [363]. In another study, a graphical and numerical integrated visualization tool (hybrid optimization tool) called modified extended power pinch analysis (MEPoPA) tool was developed to optimally size the energy storage of an integrated renewable energy systems in order to minimise the energy system losses [340].

3.9.2.2 Probabilistic method

It is also referred to as statistical method. It is suitable for carrying out hybrid energy system variability study with multiple possible outcomes, varying degrees of certainty or uncertainty of occurrence [368]. To optimize wind power imbalance that results from a varying wind speed, a probabilistic method was used to estimate wind reserve and to differentiate between the different categories of wind reserves that influence wind power imbalance [369].In another study, probabilistic method was used to generate synthetic wind speed data that was used to perform a hybrid energy system techno-economic study [370]. Outcomes from the probabilistic study shows that the use of battery energy storage can substantially reduce the ramp rate of an auxiliary heat generator.

3.9.2.3 Analytical method

In comparison to other classical optimization techniques, whereby no specified route is followed in arriving at an optimal solution, analytical method uses computational techniques, such as Fourier transform or introduce series of logical

steps that should be followed to determine the optimal size of a hybrid energy systems [167], [359]. For optimal sizing of a hybrid energy system component, discrete Fourier transform (analytical method) was used to decompose (match) the energy generated by time-varying components with time varying cyclic taxonomy such as energy market, load following, regulation process [371]. In another study, an analytical model was developed to minimize the cost of electricity purchase from the grid as well as to minimize the battery energy storage losses, in order to ensure reliable supply of demand at minimal hybrid energy system cost [372].

3.9.2.4 Iterative methods

An An iterative method is a recursive procedure that terminates or concludes its selection of the optimal combination of a hybrid energy system at the instant when the pre-defined decision conditions are met [359], [360], [368]. This optimization method simulates the optimal solution of an optimization problem by using linearly changing decision variables [360]. An iterative method was used to evaluate a standalone hybrid energy system minimum total cost of energy that can supply reliable electricity to four regions in Iran [191]. Loss of load expectation (LOLE) and loss of energy expectation (LOEE) assessment metrics were used to ensure that the expected reliability of the hybrid energy system was met. Similarly, an iterative method was also used to determine the minimum cost that a hybrid energy system can supply reliable energy to a seawater desalination unit installed in Kerkennah Island of Southern Tunisia [373].

Strength and weakness of all these four traditional optimization methods are presented in Table 3.7.

Table 3.7. Strength and weakness of traditional optimization techniques

Classical techniques	Strength	Weakness	References
Graphical method	It is a simple and quick optimization method. Simulated output is very descriptive	Few objectives can be simulated at a time. It cannot be used to simulate specific details of a hybrid energy system. For example, the tilt angle of a PV system	[171], [339], [340], [361]–[367]
Probabilistic method	It is a simple and quick optimization method. It requires only few input data because it can use sample data to represent a population.	It often fails to select the best possible solution. It cannot be used to optimize hybrid energy system dynamic nature.	[369], [370], [374], [375]
Analytical method	High simulation precision and accuracy	Increase computational time	[371], [372], [376], [377]
Iterative method	It is easy to use and understand. It is capable of tracking modelling defects at an early phase.	Each iteration phase is rigid with no overlaps	[191], [373], [378], [379]

3.9.3 Artificial intelligence techniques

Artificial intelligence (AI) techniques are developed intelligent computer programs, and they are built by the application of science and engineering procedures in order to represent natural occurrence. AI technique can be defined as the ability of a machine to perform functions or activities that characterize human thought [359], [360]. Examples of AI optimization techniques include: genetic algorithm (GA), particle swarm optimization (PSO), simulated annealing (SA), harmony search algorithm (HSA), ant colony algorithm (ACA), bacterial foraging algorithm (BFA), artificial bee colony (ABC) algorithm, bio-geography based optimization (BBO), gravitational search algorithm (GSA) cuckoo search (CS), and a hybrid of different AI techniques. One of the advantages of AI methods is their ability to investigate the non-linear variations of renewable energy system components and perform multi-objective optimization, but AI optimization techniques are usually a more complex technique to implement than traditional optimization techniques [167], [360], [368]. Key features (characteristics, strength, and weakness) of selected artificial intelligence optimization techniques are presented in Table 3.8.

Table 3.8. Features of artificial intelligent optimization techniques [167], [356], [360], [367], [368]

Techniques	Characteristic	Strength	Weakness
Genetic Algorithm (GA)	Mimics the different processes of natural evolution, such as inheritance, mutation, selection, and crossover	Efficient for finding the global optimum and suitable for complex problems with a great number of parameters and multiple solutions	Convergence speed is slower than most stochastic algorithms. There is also no assurance of having a constant optimization response time
Particle swarm optimization (PSO)	Mimics bird and fish movement behaviour	It has a fast convergence speed and its coding is also simple in comparison with most other methods with more equations	Not suitable for non-coordinate system problems. PSO can also suffer from partial optimism.
Simulated annealing (SA)	It is a trajectory random investigation that mimics the way in which a metal cools and freezes into a minimum energy crystalline structure (the annealing process)	Analyses non-linear, chaotic and noisy data with many constraints without been trapped in local minima. It is also a robust technique for determining global optimum without relying on any restrictive property	The quality of the optimal solutions is dependent on the computation time. Fine-tuning of model parameters can be complicated and it does significantly affect the quality of the outcome
Ant colony algorithm (ACA)	The algorithm is inspired by the foraging behaviour of ants in nature. That is, finding the shortest path between their source and their nests	Performs a local and global search. It is useful for carrying out global search as well as analyzing different optimization problems. It has high convergence speed	It is a complex process that requires the fine-tuning of its parameters, random initialization, and long-term memory space.
Artificial bee colony (ABC) algorithm	This algorithm is inspired by the intelligent foraging behaviour of honey bee	Performs a local and global search. More so, it can be combined with other available algorithms and it is useful for optimizing different problems	Random initialization, as well as fine-turning of its several parameters, is required. Also, a probabilistic approach is used for performing the local search
Harmony search algorithm (HSA)	It is a derivative-free, real-parameter optimization algorithm that is inspired by the improvisation process of jazz musicians	Performs a global and local search. it is free from divergence and It does not require differential gradients, the setting of variables initial value and. It is also suited for discontinuous and continuous functions as well as for discrete and continuous variables.	Complex solving process

Table 3.8 continues

Techniques	Characteristic	Strength	Weakness
Biogeography-based optimization (BBO)	Mimics the behaviour of species in nature against time and space by using stochastic and iterative approaches to find the optimal solution of a given measure of quality or fitness function	Its computation time is fast, and it has a good convergence accuracy	Not suitable for selecting the best member within each generation, thereby some of the solutions generated might not be the optimal solution
Gravitational search algorithm (GSA)	It is inspired by Newton's law of gravitation and Newton's second law of motion. GSA's optimal solution is obtained from the principle that a larger entity or force emergences when particles attract and bond together	It offers good calculation accuracy and faster convergence speed	It sometimes suffers from premature convergence problem
Hybrid optimization techniques	Developed by using two or more algorithms	They are usually more robust and offer better calculation accuracy for multi-objective problems than individual methods. More so, they sometimes converge quickly	Hybridization of algorithms result in increased optimization complexity and the difficulty of developing the algorithm

3.10 Chapter summary

Literature review in this study began with a review of the characteristics and applications of the different forms of hybrid renewable energy system (HRES) configuration. In comparison with other HRES configuration options, hybrid-coupled configuration option was reported to offer to improve system efficiency and in turn, increase cost minimization due to the current state of developments in converter technologies. Section 3.3 presents a review of the different hybrid energy sub-systems. For the photovoltaic (PV) electricity generation, review of the general operating characteristic of PV technology, as well as some of the benchmarks used by manufacturers in rating different classification of photovoltaics under standard test conditions has been emphasized. Furthermore, because the intensity of solar radiation for PV electricity generation is location dependent, the different approaches for modelling solar radiation was also reviewed.

Different stages of converting bio-waste into biogas as well as the different types of anaerobic digester design has been reviewed. Also, due to the complexity of anaerobic digestion, vital parameters that influence anaerobic digestion of biogas production has been reviewed in Section 3.5. Types of energy storage systems (ESSs) as well as the techno-economic characterization of the different energy storage systems were presented in Section 3.6. An extensive comparative analysis; in terms of the strength, weakness, opportunity, and threat, of long-term energy storage possibilities was also reviewed. Based on technical and economic consideration from the ESSs review, battery storage systems (BSSs), which is the most developed ESSs technology, was the most suitable for this study.

In Section 3.7, load profile review began with an outlook into the different context in which load profiles are modelled. However, because of the dearth in information on rural load consumption, load profile modelling context in this study was narrowed to an analytical modelling approach. Also, the characteristics, strength, and weakness of top-down and bottom-up modelling approach; which are the two traditional modelling approach for modelling domestic rural load profiles, was also reviewed. Furthermore, classification of bottom-up modelling approach; in terms of the load profile resolution, into high-resolution and low-resolution bottom-up modelling approaches was also presented.

Section 3.8 presents the literature review of some of the several economic and technical indicators used to assess the suitability of a hybrid energy system design. While the different hybrid energy system design and simulation optimization techniques; which are classified broadly into computer software tools, classical techniques, artificial intelligent (modern) techniques, is presented in Section 3.9

Chapter 4 HYBRID ENERGY SYSTEM DESIGN METHODOLOGY

In this chapter theoretical methods used for modelling the hybrid energy system components, community households' energy consumption patterns, and simulating the optimal design of the hybrid renewable energy systems are presented. As earlier reported in Section 3.2, because of the ability of hybrid-coupled energy system configurations to increase the energy efficiency of hybrid energy systems in comparison to either DC or AC coupled energy system configuration options [166], [167], it is selected here. Fig. 4.1 presents the hybrid-coupled topology applied in this study to guarantee reliable supply of clean electricity energy at minimal cost.

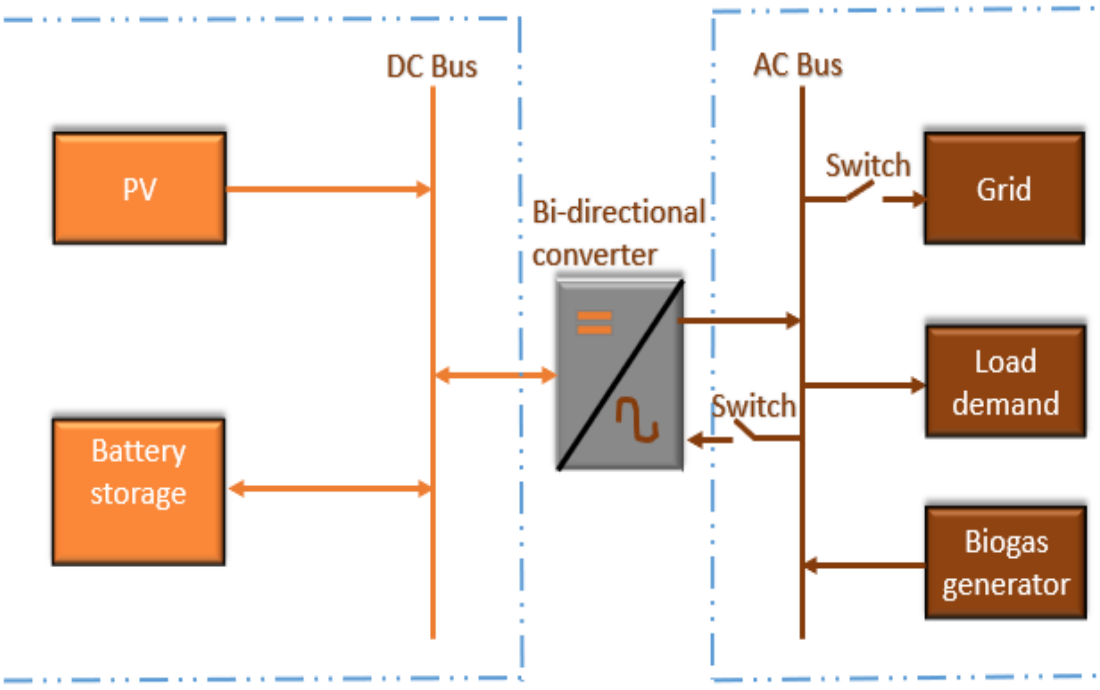

Fig. 4.1. Hybrid-coupled energy systems configuration

The DC bus connects the photovoltaic and the battery storage system, while the AC bus connects the biogas generator and the AC loads. Also, the DC bus is linked to the AC bus by the bi-directional converter. Charger controller is part of the PV system. To demonstrate the energy supply strategy, 2 switches were included in Fig. 4.1. For a biogas generator operating under full-loading condition, electricity is first supply to the load, and if the supplied energy from the biogas generator exceed the load

demand, the battery is charged, and when the battery is charged the excess is sold to the grid. Meanwhile, a rural community connected to an un-reliable grid was considered here because the possibility to accurately determine households' energy consumption behaviour is higher when a community is connected to an un-reliable grid than when the community is un-electrified, However, the un-reliable grid does not supply the community because its electricity availability cannot be predicted.

4.1 Load profile modelling methodology

As mentioned in Section 3.7, because of the lack of extensive rural energy consumption data from the energy utilities or the national statistical office, a bottom-up modelling approach is used for generating a stochastic rural household(s) load profile. This achieved by the collection and processing of household occupancy-based survey, and the stochastic modelling of the survey outcomes. For the credibility of the household consumption survey to be guaranteed, the survey questionnaire should be a representation of household(s) energy consumption parameters such as household consumption behaviour, and households' appliance characteristics [380]. The design questionnaire can mirror surveyed households' energy consumption because Section 3.7.1 explains that questions from the questionnaire can be used to acquire important data that can generate occupants' activity schedule. Then, household's occupancy behaviour is modelled from generated occupants' activity schedule because an household's energy consumption is highly dependent on its occupancy behaviour [324], [325].

Apart from modelling households load profile based on energy survey data, sometimes load profile modelling input data might be acquired from energy monitoring electronic devices [381]–[383]. Meanwhile, because of the variability in occupancy energy consumption patterns, to guarantee credible measurement, the energy monitoring device should continuously measure energy consumptions for several number of days [384]. In Nigeria, it is unlikely for grid-connected communities to have electricity continuous for 24 hours. So, the use of energy monitoring devices for measuring domestic consumption patterns is less applicable here. However, this does not suggest that energy monitoring devices cannot be used

when there is improved electricity availability or in similar studies with better electricity availability.

4.1.1 Survey data collection

The use of surveys for acquiring households' energy consumption data is generally acceptable whenever there is paucity of information and the perception, awareness, and acceptance end user are required [385]. Therefore, the survey questionnaire has been designed to collate data on household demographics, occupants' activity schedule, appliance ownership, and for in-direct validation of the model. To ensure consistency during the collection and analysis of survey data, occupants' activity schedule were restricted to hourly time steps.

The sample size of a survey is an important parameter that influence the accuracy of a survey, and its calculation is dependent on the survey population, the margin of error and the confidence level. The margin of error or confidence intervals is defined as the acceptable positive and negative deviation between the true population and a sample estimate of the true population. Therefore, the margin of error explains how truly the survey results reflect the views of the overall population. The confidence level is defined as the percentage of the population that lies within the boundaries of the margin of error. Mathematically, a survey sample size is defined as [386], [387]:

$$N_{ss} = \frac{\left(Z_{score}{}^2 \times p \times (1-p)\right)/e^2}{1 + \frac{\left(\left(Z_{score}{}^2 \times p \times (1-p)\right)/e^2\right) - 1}{N_{pop}}} \tag{4.1}$$

where N_{ss} is the survey sample size, Z_{score} the value of the confidence level on a $Z-$ table, p is the proportion of the expected outcome, e is the margin of error, and N_{pop} is the population size.

The population size is estimated based on power holding company of Nigeria (PHCN) data on the number of residential customers in the survey location rather than national population and housing census data because PHCN identify a residential customer (household) as a physical structure(s) with a single electric

meter or an assigned electricity bill rather than on the family-tie of the occupants of the physical structure. Esan north-east local government area (LGA) in the south-southern region of Nigeria is selected as the survey location. This is because south-southern region of Nigeria is reported to have the lowest solar energy potential in the country [48], [84]. Therefore, the survey location is suitable for studying the effect of integrating HRES in locations with lower solar radiation potential.

Esan north-east LGA is located on latitude 6.7297°N and longitude 6.3439°E, and it has an area of 255.744 km^2. Accord to 2006 (the most recent) Nigerian national population and housing census report, Esan north-east LGA has a household (family) population of 24,532 [388], and the household population is distributed amongst 26 residential communities. Electricity supplied to the survey location is predominantly consumed by residential customers and a few low energy consumption business (commercial) customers. PHCN records shows that 7881 electricity bill paying residential customer are connected to Esan north-east LGA distribution network. However, not all the residential customers in the distribution network are currently captured by PHCN.

It is reported that 36% of PHCN's dispatched electricity is unaccounted for due to electricity collection losses such as un-captured customers and the non-payment of electricity bills [43]. One of PHCN major challenges is to reduce the high number of un-captured residential customers (households) connected to its distribution network. Therefore, it is assumed here that the number un-captured residential customers (households) account for the electricity collection losses. By scaling PHCN captured residential customers by 36%, the estimated number of residential customers (household population size) in the survey location is 10,718. Meanwhile, for a household population of 10,718 and by selecting a confidence level and a margin of error of 95% and 5% respectively, the survey sample size calculated from Eq. (4.1) is 371. So, 380 questionnaires were administered to the surveyed community residential customers, but only 297 was received. Of the 297 questionnaires received, 24 of the questionnaires were discarded because they were not thoroughly filled, leaving 273 fully completed questionnaires to be used for data analysis.

4.1.2 Load profile modelling scheme

The input data used by the developed stochastic demand model can be categorized into utility company data, national population and housing census data, and survey data. The utility company data is used to estimate the survey location household population. National population and housing census data is used as the criterion for distributing the housing unit of the survey location into different household classes, while survey data are used to determine occupants' consumption behaviour, appliance ownership, and appliance time use. Based on the physical structure of the survey households, they are grouped into four household classes:

- Household class I: Traditional or hut structure, informal or improvised dwelling
- Household class II: Rooms let in house
- Household class III: Detached and semi-detached house
- Household class IV: Flat in block of flats

Simulation of the load profile of the community is performed by aggregating the simulated load profile of the surveyed households weighted by the household classes [309]. The assigned weighs to the four household classes were derived from Nigerian national population and housing census report on the studied location. An illustration of how the developed modelling scheme uses data outcomes from the surveyed households to simulates a household load profile, or a community load profile is present in Fig. 4.2.

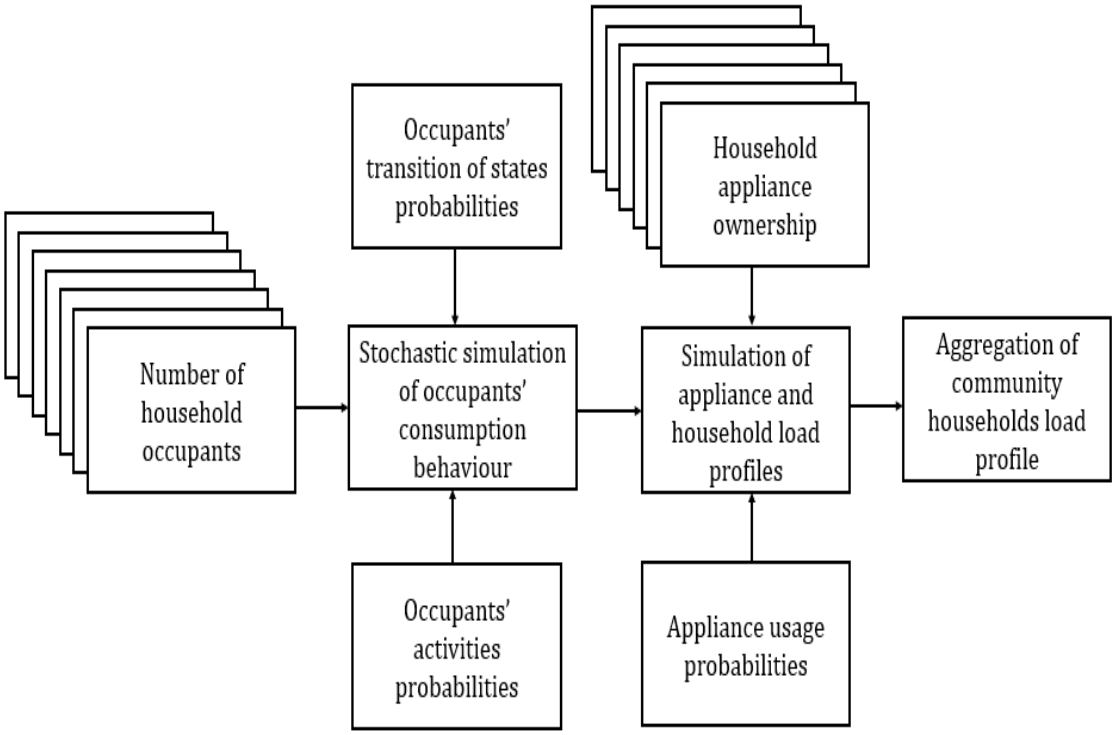

Fig. 4.2. Demand model implementation scheme

The demand model scheme in Fig. 4.2 is used to perform hourly stochastic simulation of occupants' consumption behaviour while simulation of appliance, household, and community load profiles are performed minutely. To simulate occupants' consumption behaviour, Markov chain technique is used to generate an occupancy state matrix that contains the number of household occupant(s) present/absent per occupancy state for each simulation time step. Then, from the occupancy state matrix, an active occupancy vector that represent the number of active occupant(s) in each time step is generated. To capture how the time when active occupants perform their activities affect occupants' consumption behaviour, the active occupancy vector and the occupants' activities probabilities are combined to generate an active occupants' activity matrix for each time step.

The usage of all household appliances is not influenced by occupants' consumption behaviour. So, if a unit step function $U(t)_{occ}$ represent the effect of occupants' consumption behaviour on an appliance usage, the value of $U(t)_{occ} = 1$ whenever occupants' consumption behaviour affects an appliance usage, else the value of $U(t)_{occ} = 0$. If $U(t)_{act\_occ}$ represent the present or absent of an active occupant(s),

the value of $U(t)_{act\_occ} = 1$ whenever an active occupant is present at a time t, else the value of $U(t)_{act\_occ} = 0$. Similarly, if $U(t)_{activity}$ represent the present or absent of active occupant(s) in a household activity (i.e., cooking, cleaning or leisure activity), the value of $U(t)_{activity} = 1$ whenever an active occupant is engaged in a household activity at time t, else the value of $U(t)_{activity} = 0$. Furthermore, if $U(t)_{non\_act\_occ}$ represent the unit step function of an appliance such as a refrigerator, whose usage is not affected by the absence of active occupants, for all time step, the value of $U(t)_{non\_act\_occ} = 1$. Therefore, the effect of occupants' consumption behaviour on appliance usage ($U(t)_{occ}$) is defined by:

$$U(t)_{occ} = \begin{cases} U(t)_{act\_occ} & \text{for all active occupant(s) dependent appliance} \\ U(t)_{activity} & \text{for all household activity dependent appliance} \\ 1 & \text{for all non} - \text{active occupant(s) dependent appliance} \end{cases} \quad (4.2)$$

where $U(t)_{act\_occ}$ is a unit step function that represent the present or absent of an active occupant(s) and $U(t)_{activity}$ is a unit step function that represent the present or absent of an active occupant(s) in a household activity.

An appliance type (j) actual time of use $\left(U(t)_{app\_usage,j}\right)$ is calculated by combining the value of $U(t)_{occ}$ with the appliance usage probability $\left(U(t)_{app,j}\right)$. Therefore, for each time step, $U(t)_{app\_usage,j}$ is defined by [278], [309]:

$$U(t)_{app\_usage,j} = U(t)_{occ} \times U(t)_{app,j} \quad (4.3)$$

The energy consumption of an appliance ($E_{app,j}$) is defined by [278], [279], [309]:

$$E_{app,j} = P_{app,j} \times N_{app,j} \times U(t)_{app\_usage,j} \quad (4.4)$$

where $P_{app,j}$ is power rating of the appliance, $N_{app,j}$ is the quantity of an appliance in a household and $U(t)_{app\_usage,j}$ in Eq. (4.4) was defined in Eq. (4.3).

The operating duration of household appliances are classified into short and long operating duration. Short operating duration appliances are appliances such as food

blender, electric iron and bedroom bulb whose operating duration is less than an hour. Long operating duration appliance are appliances whose operating duration is at least 1 hour. Meanwhile, because the model generates load profiles in minutely time step, the energy consumption patterns of short operating duration appliances are captured.

A Markov process is a random process X(t) whereby the transition from the present time t_o into the future t, (i.e. $\{X(t);\ t_0 < t\}$), is only dependent on its past $\{X(k);\ k \leq t_0\}$ through the present value $X(t_0)$ [389], [390]. So, a limited amount of memory suffices is required to produce a great diversity of behaviours. Therefore, a random process does have a Markov property or memoryless property, if the process has conditional independence attributes or properties such that probabilistic dependence on the past is only through the present state [390], [391]. Meanwhile, although there are alternative stochastic methods to Markov chain process, and these stochastic methods include: Gibbs fields [392], constrained random paths mode [393], self-avoiding walks [394], levy processes [395], [396], and multimodal nested sampling [397], but in comparison to Markov chain process, many of these methods are considerably more difficult stochastic method to study.

Application of Markov process is relevant modelling energy consumption behaviour of households in this study, because when the present value $X(t_0)$ is known, the future value of X(t) can be determined without prior knowledge on how the present value $X(t_0)$ was reached. If $X = \{X_1, X_2, X_3, \dots, X_t\}$ is a random process in the discrete time space E, and the transition between the states, say from X_i to X_j occurs with a probability $\mathbb{P}_{ij}(t)$ that satisfy the Markov property, then, the set of state X is called a Markov Chain [389], [390]. $\mathbb{P}_{ij}(t)$ is called the transitional probability, that is, the conditional probability that the process is in a state X_j at time t, given that it is in state X_i at time $t - 1$. So, the conditional probability X_j given X_i, which is denoted by $\mathbb{P}[X_j|X_i]$ is defined by [389], [390]:

$$\mathbb{P}[X_j|X_i] = \frac{\mathbb{P}[X_j \cap X_i]}{\mathbb{P}[X_i]} \qquad \mathbb{P}[X_i] > 0 \tag{4.5}$$

Similarly, the Markov property can be expressed mathematically as [389], [390]:

$$\mathbb{P}(X_{t+1}|X_1, X_2, \dots, X_{t-1}, X_t) = \mathbb{P}(X_{t+1}|X_t) \tag{4.6}$$

where for every sequence $X_1, \dots, X_t, X_{t+1}$ of elements of E and for every $t \geq 1$, the left hand side of Eq. (4.6) defines the conditional probability of an event that is one step into the future while the right-hand side of Eq. (4.6) defines the conditional probability of an event in the future when the present value is known. The transitional probability matrix (TPM) is expressed as [389], [390]:

$$\text{TPM} = \begin{bmatrix} \mathbb{P}_{00} & \mathbb{P}_{01} & \cdots & \mathbb{P}_{0X} \\ \mathbb{P}_{10} & \mathbb{P}_{11} & \cdots & \mathbb{P}_{1X} \\ \mathbb{P}_{20} & \mathbb{P}_{21} & \cdots & \mathbb{P}_{2X} \\ \vdots & \vdots & \vdots & \vdots \\ \mathbb{P}_{X1} & \mathbb{P}_{X2} & \cdots & \mathbb{P}_{XX} \end{bmatrix} \tag{4.7}$$

If each row represents all the transitional probabilities from a single initial state, the sum of the probabilities will be equal to 1. Also, if a Markov chain has y states and an initial condition vector v_0, then the transition probability matrix after z steps is expressed as [390]:

$$v_0 \mathbb{P}_{ij}^{z} = \sum_{w=1}^{y} v_0 \left(\mathbb{P}_{iw}^{z} \mathbb{P}_{wj} \right) \tag{4.8}$$

In summary, when household's occupancy behaviour is modelled in Chapter 5, these Markov chain process equations, i.e., Eqs. (4.5) - (4.8) are used to process data on occupants' activity schedule, so that, a stochastic hourly occupancy state matrix that represent household's occupancy behaviour can be generated.

4.2 Modelling of energy subsystem

This section presents the theoretical methods used for modelling biogas generation subsystem, battery subsystem, charge controller subsystem, converter subsystem, and photovoltaic generation subsystem.

4.2.1 Biomass energy system modelling

As earlier mention in Section 3.5, the operation of a biogas generation at full-loading condition is necessary for optimum biogas use and for healthy engine operation [231]–[233], therefore, biogas generator hourly electricity generation (E_{Bio}) is defined as:

$$E_{Bio} = P_{Bio} \times \Delta t \tag{4.9}$$

where P_{Bio} is the biogas generator rated capacity, Δt is the change in time. Biogas generator hourly electricity generation (E_{Bio}) can also be defined in terms of the biogas fuel consumption as [236]:

$$E_{Bio} = \frac{Y_{biogas} \times bmc \times \eta_{bio} \times H_{LHV}}{f_{energy}} \tag{4.10}$$

where Y_{biogas} (m^3) is the biogas generator hourly biogas consumption at full-loading condition, η_{bio} is the biogas generator electrical conversion efficiency [1]; and η_{bio} for a biogas powered generator is between 25% - 40% [336], H_{LHV} ($MJ\ m^{-3}$) is low heating value. H_{LHV} for methane gas is 37 MJm^{-3} [236], [237], f_{energy} ($MJ\ kWh^{-1}$) is mechanical to electrical energy conversion factor. Therefore, f_{energy} is 3.6 $MJ\ kWh^{-1}$. bmc (%) is the biogas methane content of a bio-waste. The bmc of many bio-waste is usually between 50% to 70% [398], [399]. So, an average bmc value of 60% is selected here. Based on the assumption that the biogas generator always operate at full-loading condition, biogas generator hourly biogas consumption (Y_{biogas}) can be defined by [236], [237]:

$$Y_{biogas} = \frac{E_{Bio} \times f_{energy}}{bmc \times \eta_{bio} \times H_{LHV}} = k_o \times P_{Bio} \times \Delta t \tag{4.11}$$

[1] This is because most of the energy from the biogas will be lost as heat as well as other mechanical losses in the biogas powered generator.

where k_o is the energy to biogas conversion factor ($m^3\ kWh^{-1}$).

Digester (reactor) working volume (Vol_w) in m^3, is defined by [238], [239], [251]:

$$Vol_W = HRT \times Q_{rate} \tag{4.12}$$

HRT (day) is the hydraulic retention time and Q_{rate} ($m^3\ day^{-1}$) is the substrate influent flow rate. The substrate influent flow rate (Q_{rate}) can be defined as [158]:

$$Q_{rate} = \frac{(\sum_{t=1}^{8760} Y_{Bio})}{365 \times S_{biogas} \times \rho \times C_i} \tag{4.13}$$

where C_i $(kg\_VS\ kg^{-1}_{wet\_weight})$ is the influent volatile solids (VS) content. A feedstock influent volatile solids (VS) content is calculated by multiplying its total solid (TS) content and its volatile solid (VS) content. TS and VS content of a feedstock are measured in terms of the percentage (%) of energy content in a wet weight Also, S_{biogas} ($m^3\ kg\_VS^{-1}$) is the specific biogas production, and ρ_s ($kg\ m^{-3}$) is the density of the substrate. Daily bio-waste quantity or mass (M_{waste}) in kg, can be calculated by multiplying the substrate influent flow rate (Q_{rate}) and the substrate density (ρ_s).

Digester (reactor) actual volume (Vol_{actual}) is calculated as the sum of the digester working volume (m^3) and the digester non-working volume (m^3). The digester non-working volume (u) is required for improving he digester metabolic activities [158], and it is defined as a fractional or percentage (u) of the digester working volume. Therefore, digesters actual volume (m^3) is defined by [158]:

$$Vol_{actual} = Vol_W \times (1 + u) \tag{4.14}$$

For the optimal design of the digester volume, a value of $u = 10\%$ is required [158].

In summary, biomass energy system methodology presented in this section shows how Eqs. (4.9) – (4.14) are used in Chapter 7 for calculating biogas generator hourly electricity generation, daily bio-waste demand and anaerobic digester volume.

4.2.2 Battery energy system modelling

The battery energy storage is used to ensure reliable supply of electricity to the electrical load whenever the PV system and biogas generator are either not supplying electricity or can only supply apart of the energy demand. Despite the continuous fall in the price of battery energy storage over the years, they are still expensive [267], [271], [273]. Therefore, the optimal sizing of the battery storage system is required to ensure optimal sizing of an energy system. To avoid oversizing of the battery storage system, the optimal size the battery energy storage is calculated by using power pinch analysis to optimize the maximum cumulative net energy drawn from the battery energy storage [171], [361], [362], [400]–[405].

To model battery energy storage system, operational properties such as self-discharge rate, depth of discharge, and round-trip efficiency are considered. In Fig. 4.1, the battery storage system is connected to the DC bus, so the DC bus periodic net energy $\left(E_{DC\_net}(t)\right)$ is used to determine the size and the state of charge (SOC) of the battery energy storage. Meanwhile, the net energy surplus in the DC bus does not directly determine the optimal size of the battery, rather it is used to charge the battery, and when the battery is fully charged, the remaining net energy surplus (excess net energy) in the DC bus is sold to the grid. At the start of the battery storage simulation, it is assumed that battery storage system is completely charged, so energy is only drawn from the battery energy storage. But for subsequent periods, the DC bus net energy can be supplied to or drawn from the battery energy storage. The amount of DC bus net energy surplus $\left(E_{DC\_net}(t) > 0\right)$ used for charging the battery energy storage is dependent on its state of charge. Consequently, the battery energy storage state of charge is modelled with the charging energy and discharging energy of battery energy storage.

During the battery charging operation, energy discharged due to the battery self-discharge (E_{BSD}) is supplied by the DC bus net energy surplus $\left(E_{DC\_net}(t) > 0\right)$. But during the battery discharging operation, the total energy discharge from the battery is equal to the sum of the battery self-discharge and the DC bus net energy deficit $\left(E_{DC\_net}(t) < 0\right)$. Furthermore, when sizing the battery energy storage, the

state of charge of the battery energy ($E_{B/SOC}$) is constrained, so that it does not exceed zero (i.e. a non-positive value) [171], [400]. Hence, this sizing technique can be referred to as a non-positive battery state of charge technique. Battery self-discharge (kWh) can be defined in term of the battery state of charge as [366], [400]:

$$E_{BSD}(t) = \text{abs}\left(\left(E_{B/SOC}(t)\right) \times R_{BSD}\right) \tag{4.15}$$

where E_{BSS} is the battery storage capacity in kWh, and R_{BSD} is the battery self-discharge rate in %/h.

The battery charging energy (kWh) can be defined in terms of the battery self-discharge and DC bus net energy as [366], [400]:

$$E_{B/charging}(t) = -E_{BSD}(t-1) + \left[E_{DC\_net}(t) \geq 0\right] \times \eta_{rt} \tag{4.16}$$

where $E_{BSD}(t-1)$ is the previous time step battery self-discharge, E_{DC_net} is the DC bus net energy surplus and η_{rt} is the battery energy storage round trip efficiency.

Similarly, the battery discharging energy (kWh) can be defined in terms of the battery self-discharge and DC bus net energy as [366], [400]:

$$E_{B/discharging}(t) = -E_{BSD}(t-1) + \left[E_{DC\_net}(t) < 0\right] \tag{4.17}$$

$E_{BSD}(t-1)$ and E_{DC_net} in Eq.(4.17) were defined in Eq. (4.16)

The battery state of charge (kWh) is dependent on the battery charging and discharging energy and can be defined as [366], [400], [403]:

$$E_{B/SOC}(t) = \begin{cases} E_{B/SOC}(t-1) + E_{B/charging}(t) & \text{if } E_{DC\_net}(t) \geq 0 \\ & \text{and } E_{B/SOC}(t) < 0 \\ E_{B/SOC}(t-1) + E_{B/charging}(t) = 0 & \text{if } E_{DC\_net}(t) > 0 \\ & \text{and } E_{B/SOC}(t) > 0 \\ E_{B/SOC}(t-1) + E_{B/discharging}(t) & \text{if } E_{DC\_net}(t) < 0 \end{cases} \tag{4.18}$$

DC bus excess energy $\left(E_{DC\_excess}\right)$ or the unused DC bus net energy surplus is defined by:

$$E_{DC\_excess}(t) = \left(E_{DC\_net}(t) > 0\right) - E_{B/charging}(t) \tag{4.19}$$

To determine the battery storage size (E_{BSS}) or capacity, the non-positive battery state of charge technique is used to determine the minimum state of charge of the battery. Therefore, battery storage size (E_{BSS}) is defined as [171], [366], [400], [403]:

$$E_{BSS} = \frac{abs\left(E_{B/SOC\_min}\right)}{DOD} \tag{4.20}$$

where abs mean absolute value, E_{B/SOC_min} is the state of charge minimum value, and DOD is the battery storage system depth of discharge.

For each time step, an iterative check is performed in order to determine if the estimated battery energy storage capacity in the previous time step should be re-estimated. Furthermore, power pinch analysis technique is applied in the developed battery energy storage model, so that a battery state of charge at the start and end of the simulation are equal $\left(\text{i.e.}, E_{BSS_{start}} = E_{BSS_{end}}\right)$. A scheme that illustrates how Eqs. (4.15) - (4.20) are applied to calculate the optimal battery capacity is presented in Fig. 4.3.

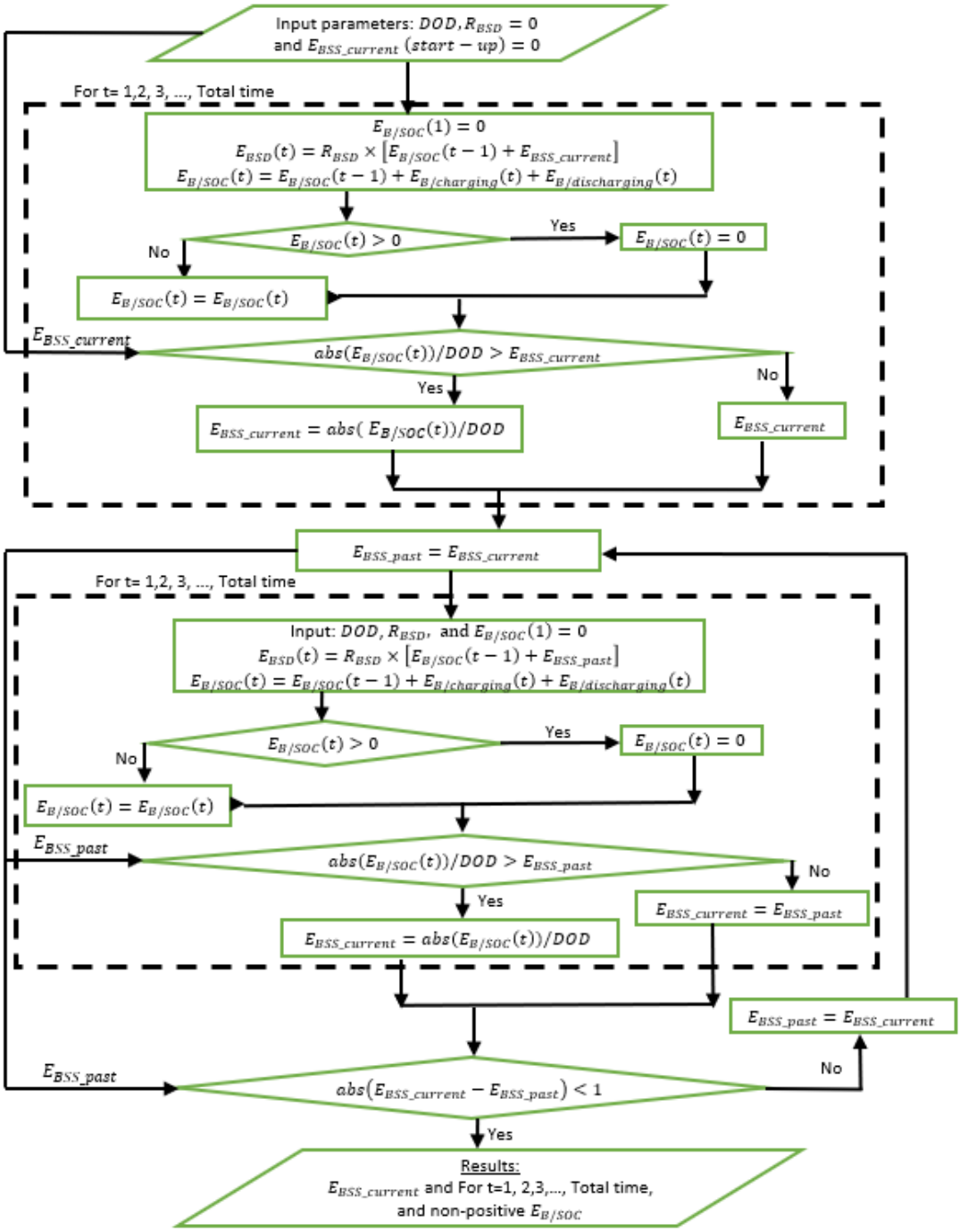

Fig. 4.3. Battery energy storage modelling scheme

In summary, the battery energy system methodology presented in this section shows that for different combinations of PV and biogas generator in the HRES design space in Chapter 7, Eqs. (4.15) - (4.20) calculates the optimal size of the battery capacity by evaluating the maximum cumulative energy deficit between the energy generated and the load profile.

4.2.3 Converter system modelling

The converter in a hybrid-coupled topology is designed to allow a bidirectional flow of power. This is because the converter serves as the interface between the AC bus and the DC bus. Therefore, the converter is used as an inverter whenever the energy generated from the photovoltaic system or discharged from the battery is supplied to the load (i.e. transforming DC to AC power), and as a rectifier whenever the excess energy generated from the biomass generator is used to charge the battery storage system (i.e. transforming AC to DC power). Typically, the capacity of the converter is often designed with respect to the peak demand of the AC load. However, due to the choice of hybrid-coupled configuration option, the optimal size of the converter is determined by the maximum AC/DC net energy (E_{AC/DC_net}) surplus/deficit. Furthermore, for optimal design of the converter, the estimated converter size is increased by a factor of 20% [406], to account for transient rise in load demand conditions that might arise during power system operations as well as to account for the reactive power component flowing through the network. Therefore, the size of the converter (P_{Conv}) is defined by [406]:

$$P_{Conv} = 1.2 \times \left(\frac{\max\left(\text{abs}\left(E_{AC/DC\_net}\right)\right)}{\eta_{Conv}} \right) \tag{4.21}$$

4.2.4 Photovoltaic energy system modelling

As stated in Section 3.3.1, the output of a photovoltaic (PV) module is dependent on several parameters such as the type of material, the PV design cell temperature, and the intensity of solar irradiation that falls on the surface of the module. Therefore, the PV installation hourly electricity generation (E_{PV}) can be expressed as [407]–[410]:

$$E_{PV}(t) = DF_{PV} \times \eta_{PV} \times A_{PV} \times I_g \times \Delta t \tag{4.22}$$

where in Eq. (4.22), DF_{PV} is the PV installation derating factor. DF_{PV} accounts for the PV power reduction due to dust accumulation on the panels, shading, aging and

wiring losses [409]. Also, in Eq. (4.22), η_{PV} is PV panel electrical efficiency, A_{PV} (m^2) is effective collection area of a PV installation and Δt is a measure of the change in time. I_g (Wm^{-2}) is hourly instantaneous irradiance and this value is location dependent. Hourly instantaneous irradiance is not measured by Nigerian meteorological agency (NiMet) weather stations. Therefore, a theoretical method is used in this study to estimate the hourly instantaneous irradiance of the studied location. Meanwhile, an established model for estimating η_{PV} is [189], [407]:

$$\eta_{PV} = \eta_{ref}\left[1 - k_{temp}(T_{PV} - T_{ref}) + \gamma_o \log I_g\right] \quad (4.23)$$

η_{ref} is PV panel manufacturer's reference efficiency under standard test conditions (i.e. at a reference solar irradiance (I_{STC}) of 1000 Wm^{-2} and reference temperature (T_{STC}) of 25°C). k_{temp} ($\%°C^{-1}$) is the temperature power correction coefficient, and its value is dependent on the PV panel material. For example, k_{temp} value range from -0.25%°C^{-1} for CdTe panels to -0.45%°C^{-1} for Multi-c-Si panels. γ_o is irradiance level correction coefficient and it is also dependent on the material used for making the panel. The explicit irradiance term $\gamma_o \log I_g$ in Eq. (4.23) can be neglected [189], [407], [411], [412] because PV temperature (T_{PV}) implicitly account for the irradiance effect. Therefore, when η_{PV} is calculated in Eq. (4.23), the removal of $\gamma_o \log I$ will have insignificant impact on its accuracy [189], [407].

T_{PV} (°C) is defined explicitly as [185], [413]–[415]:

$$T_{PV} = T_a + k_\alpha I_g \quad (4.24)$$

where T_a (°C) is ambient temperature, I_g is hourly irradiance and k_α (°C m^2W^{-1}) is the Ross coefficient, that relates solar radiation with the PV temperature. Because the PV system considered here is a free standing installation, the PV system will have a better ventilation/heat dissipation in comparison to a roof integrated systems and its estimated Ross coefficient (k_α) is 0.02 °C m^2W^{-1} [185], [408], [414].

PV installation peak power or rated capacity (P_{PV}) is calculated by multiplying the peak power of a meter squared PV panel ($P_{PV,1m^2}$) and the effective area of the PV

installation (A_{PV}) [413]. Therefore, the calculated value of P_{PV} can be substituted for A_{PV} in Eq. (4.22) to estimate the periodic energy generated from a PV installation (E_{PV}). Furthermore, the total number of PV modules in a PV installation (N_{PV}) is calculated as [84], [403]:

$$N_{PV} = \frac{A_{PV}}{A_{mod}} \tag{4.25}$$

where A_{mod} (m^2) in Eq. (4.25) the effective area of a PV module, and this value is found in the manufacturer data sheet.

In summary, photovoltaic energy system methodology presented in this section shows how Eqs.(4.22) - (4.25) utilize the studied location hourly global solar radiation and ambient temperature data in Chapter 7 to calculate the hourly electricity generation and the effective area of the PV installation.

4.2.5 Estimation of global solar radiation

Typically, accurate prediction of the instantaneous global solar radiation for a given design location is vital for evaluating the techno-economic feasibility of the solar energy project. This is because the estimated global solar radiation data provide useful information on the estimated solar energy yield from the given location. Meanwhile, the position of the PV panel in relation to the sun's position is one of the factors that influence the eventual estimated energy yield from the PV system. This is because the orientation of the solar panel surface can substantially influence the solar energy yield from a solar panel [416]. A common approach used in literature for estimating global solar radiation is the use of empirical techniques to determine the trends in long-term daily local meteorological data for a given location, so as to accurately predict the global solar radiation of future years [194], [417]–[419]. During the estimation of global solar radiation, evaluation of long-term measurement of local/ground meteorological data is preferred for achieving accurate estimation in comparison to data collected from satellite observation because more site-specific characteristics of a location are measured by local meteorological stations [219].

Because there is no meteorological station within the rural area, long-term measured meteorological data from the nearest Nigerian meteorological agency (NiMet) weather station (Benin weather station), will be used to estimate the hourly horizontal and inclined surfaces global solar radiation in the location. The use of Benin weather station data is suitable for this research because the different load centres that will be considered in Chapter 7 during the power flow study will be in Edo state, Nigeria. Furthermore, only daily measured horizontal surface global solar radiation data is available in the few NiMet's weather station that measured global solar radiation.

4.2.5.1 Estimation of daily horizontal surface global solar radiation

In this study, for accurate estimation of daily horizontal surface global solar radiation, several empirical modelling approaches will be evaluated, in order to ascertain the most accurate empirical model that gives the best representation of NiMet's long-term measured data for the location. In this research, 15 different models are evaluated based on the classification of empirical models provided by Besharat [194].Therefore, the 15 selected solar radiation estimation models in this research comprises of 5 sunshine-based model (Angstrom-Prescott model and its variations), 5 temperature-based model (Hargreaves and Sammani model and its variations), and 5 hybrid parameter-based model. The mathematical expressions for the 15 selected solar radiation estimation models are presented in Table 1 to Table 3.

Angstrom-Prescott model

The general form of Angstrom-Prescott model is expressed by [198], [420]:

$$\frac{H_g}{H_o} = a + b\frac{S}{S_o} \tag{4.26}$$

where $\frac{H_g}{H_o}$ is the clearness index (K_T) and it measures the degree of clearness of the sky, H_g (Wm^{-2}) is the average daily global solar radiation on a horizontal surface, 'a and b' are constant (Angstrom constants), S in hour is the daily average sunshine

duration, S_0 in hour is the maximum sunshine duration or day length, and H_0 (Wm^{-2}) is the daily extra-terrestrial solar radiation on a horizontal surface.

Meteorological stations in Nigeria records average daily global solar radiation on a horizontal surface (H_g) in MJ m^{-2} day^{-1}. The daily extra-terrestrial solar radiation (H_0) on a horizontal surface in MJ m^{-2} day^{-1} can be defined by [192], [196], [219], [421], [422]:

$$H_0 = \frac{24 \times 3600 \times G_{SC}}{\pi}\left[1 + 0.033\cos\left(\frac{360 \times N_{day}}{365}\right)\right] \times \left[\cos\phi\cos\delta\sin\omega_S + \left(\frac{\pi\omega_S}{180}\right)\sin\phi\sin\delta\right] \quad (4.27)$$

where G_{SC} (kWm^{-2}) is the solar constant 1.367 (kWm^{-2}), N_{day} is the day number of a year ($N_{day} = 1$ for 1^{st} January and $N_{day} = 365$ for 31^{st} December), ϕ (°) is the location latitude, δ (°) is the sun declination angle, and ω_S (hour) is the mean sunrise hour angle for the given location. The solar declination angle (δ) can be estimated with the approximate equation of Cooper [423] or with the approximate equation of Spencer [424]. The approximate equation of Spencer [424] is more accurate [117], [118]. In this study, Spencer [424] approximate equation is used for estimating the solar declination angle (δ). And it is defined as [117], [230], [424]:

$$\delta = \left(\frac{180}{\pi}\right)(0.00692 - 0.399912\cos\Gamma + 0.070257\sin\Gamma - 0.006758\cos 2\Gamma + 0.000907\sin 2\Gamma - 0.002697\cos 3\Gamma + 0.00148\sin 3\Gamma) \quad (4.28)$$

where the day angle (Γ) in Eq. (4.28) is defined by [117], [230], [424]:

$$\Gamma = (N_{day} - 1)\frac{360}{365} \quad (4.29)$$

N_{day} in Eq. (4.29) is the day of the year

For a location, the sunrise angle (ω_S) is a function of the solar declination and the latitude and it is defined by [192], [218], [219], [421], [422], [425]:

$$\omega_S = \cos^{-1}(-\tan(\phi)\tan(\delta)) \tag{4.30}$$

Because the daily solar declination angle and the latitude for a location are constant, the value of ω_S for a day is constant. Meanwhile, because the sunrise hour angle is the negative value of the sunset hour angle, so, the hourly rotation of the earth about its axis is approximately 15°. Therefore, the number of daylight hours (S_0) is defined as [192], [196], [421], [425], [426]:

$$S_0 = \left(\frac{2}{15}\right) \times \omega_S \tag{4.31}$$

Table 4.1 presents the mathematical expression for the 5 selected Angstrom-Prescott empirical model and its variations.

Table 4.1. Angstrom-Prescott model and its variations

Model	Model type	Model equation
I	Linear [198], [420]	$\frac{H_g}{H_0} = a + b\left(\frac{S}{S_0}\right)$ (Angstrom-Prescott model)
II	Quadratic [427]	$\frac{H_g}{H_0} = a + b\left(\frac{S}{S_0}\right) + c\left(\frac{S}{S_0}\right)^2$
III	Cubic [428]	$\frac{H_g}{H_0} = a + b\left(\frac{S}{S_0}\right) + c\left(\frac{S}{S_0}\right)^2 + d\left(\frac{S}{S_0}\right)^3$
IV	Exponential [418]	$\frac{H_g}{H_0} = ae^{b\left(\frac{S}{S_0}\right)}$
V	Logarithmic [418]	$\frac{H_g}{H_0} = a + b\log\left(\frac{S}{S_0}\right)$

From Table 4.1, H_g (Wm^{-2}) is the average daily global solar radiation on a horizontal surface, 'a, b, c, and d' are regression constant (Angstrom constants), S (hour) is the daily average sunshine duration in hour, S_0 (hour) is the maximum sunshine duration or day length, and H_0 (Wm^{-2}) is the daily extraterrestrial solar radiation on a horizontal surface.

Hargreaves and Sammani model

Hargreaves and Sammani empirical model do not require weather data on the sunshine hour to estimate horizontal surface global solar radiation. However, Hargreaves and Sammani empirical model is a function of the clearness index and the square root of the difference between the maximum and minimum temperature values. Hargreaves and Sammani empirical model is defined by [209]:

$$\frac{H_g}{H_0} = a + b\sqrt{\Delta T} \tag{4.32}$$

where ΔT in Eq. (4.32) is the difference between the values of maximum temperature (T_{max}) and minimum temperature (T_{min}). Table 4.2 presents the mathematical expression for the 5 selected Hargreaves and Sammani empirical model and its variations.

Table 4.2. Hargreaves and Sammani model and its variations

Model	Model type	Model equation
VI	Linear [209]	$\frac{H_g}{H_0} = a + b\left(\sqrt{\Delta T}\right)$ (Hargreaves and Samani model)
VII	Quadratic [429]	$\frac{H_g}{H_0} = a + b\left(\sqrt{\Delta T}\right) + c(\Delta T)$
VIII	Cubic	$\frac{H_g}{H_0} = a + b\left(\sqrt{\Delta T}\right) + c(\Delta T) + d(\Delta T)^{\frac{3}{2}}$
IX	Exponential	$\frac{H_g}{H_0} = a + e^{b\left(\sqrt{\Delta T}\right)}$
X	Logarithmic	$\frac{H_g}{H_0} = a + b\log\left(\sqrt{\Delta T}\right)$

From Table 4.2, ΔT is the difference between the values of maximum temperature (T_{max}) and minimum temperature (T_{min}), and 'a, b, c, and d' are regression constants.

Hybrid Models

Similarly, Table 4.3 presents the mathematical expression for the 5 selected variations of the hybrid empirical model.

Table 4.3. Variations of hybrid empirical model

Model	Model type	Model equation
XI	Integration of S_R, T_{min}, and P [430]	$\frac{H_g}{H_0} = a + b\left(\frac{S}{S_0}\right) + c(T_{min}) + d(P)$
XII	Integration of ΔT, RH, S_0, and T_R [431]	$\frac{H_g}{H_0} = a + b\left(\sqrt{\frac{\Delta T + RH}{S_0}}\right) + c\left(\frac{T_{min}}{T_{max}}\right)$
XIII	Integration of S_R, $T_R = \frac{T_{min}}{T_{max}}$, T_{max}, and C_R [417]	$\frac{H_g}{H_0} = a + b\left(\frac{S}{S_0}\right) + c\left(\frac{T_{min}}{T_{max}}\right) + d(T_{max}) + e(C_R)$
XIV	Integration of S_R, C_R, T_{max}, and RH [432]	$\frac{H_g}{H_0} = a + b\left(\frac{S}{S_0}\right) + c(C_R) + d(T_{max}) + e\left(\frac{RH}{100}\right)$
XV	Integration of $\cos\phi$, $\cos N_{day}$, T_{max}, S_R, RH, and $\cos^2 N_{day}$ [212]	$\frac{H_g}{H_0} = a + b(\cos\phi) + c(\cos N_{day}) + d(T_{max}) + e\left(\frac{S}{S_0}\right) + f\left(\frac{T_{max}}{RH}\right) + g(RH) + h[(\cos\phi) \times (\cos N_{day})] + i\left(\frac{T_{max}}{\cos\phi}\right) + j\left(\frac{T_{max}}{RH}\right)^2 + k\left(\frac{S}{S_0}\right)^2 + l(\cos^2 N_{day})$

From Table 4.3, P is precipitation, RH is relative humidity, N_{day} is the day number in the year, C_R is cloudiness index, ϕ is the latitude of the location, and 'a, b, c, d, e, f, g, h, I, j, k, and l' are regression constants (Angstrom constants).

4.2.5.2 Empirical model's performance evaluation

Evaluation of the performance of the selected empirical models will be performed by analysing how best selected prediction models fit the measured data. The essence of performance evaluation of the selected models is to assess how NiMet long-term measured meteorological data influences the accuracy of the selected models. So that the most accurate prediction model is used to determine a horizontal surface annual daily global solar radiation.

To evaluate the estimation capability of the 15 selected models, 9 widely used performance test indicators are selected [196], [197], [418], [419], [422]. The 9 selected test indicators are: mean absolute error (MAE), root mean square error (RMSE), mean percentage error (MPE), mean absolute relative error (MARE), relative root mean square error (RRMSE), root mean square relative error (RMSRE), maximum absolute relative error (erMAX), uncertainty at 95% (U_{95}), and

coefficient of determination R^2). Mathematical expression for the 9 selected test indicators and their preferred values are presented in Table 4.4.

Table 4.4. Test indicators mathematical expression [196], [197], [422]

S/N	Statistical tools	Formula	Preferred value
1	Mean absolute error (MAE)	$MAE = \frac{1}{n} \times \sum_{i=1}^{n} \left(\left| H_{pred}(i) - H_{meas}(i) \right| \right)$	0
2	Root mean square error (RMSE)	$RMSE = \sqrt{\frac{1}{n} \times \sum_{i=1}^{n} \left(H_{pred}(i) - H_{meas}(i) \right)^2}$	0
3	Mean percentage error (MPE)	$MPE = \frac{100}{n} \times \sum_{i=1}^{n} \left(\frac{H_{meas}(i) - H_{pred}(i)}{H_{meas}(i)} \right)$	0
4	Mean absolute relative error (MARE)	$MARE = \frac{1}{n} \times \sum_{i=1}^{n} \left(\left| \frac{H_{meas}(i) - H_{pred}(i)}{H_{meas}(i)} \right| \right)$	0
5	Relative root mean square error (RRMSE)	$RRMSE = \frac{\sqrt{\frac{1}{n} \times \sum_{i=1}^{n} \left(H_{meas}(i) - H_{pred}(i) \right)^2}}{\sum_{i=1}^{n} \left(H_{meas}(i) \right)}$	0
6	Root mean square relative error (RMSRE)	$RMSRE = \sqrt{\frac{1}{n} \times \sum_{i=1}^{n} \left(\frac{H_{meas}(i) - H_{pred}(i)}{H_{meas}(i)} \right)^2}$	
7	Maximum absolute relative error (erMAX)	$erMAX = \max \left(\left| \frac{H_{meas}(i) - H_{pred}(i)}{H_{meas}(i)} \right| \right)$	0
8	Uncertainty at 95% (U_{95})	$U_{95} = 1.96 \times \sqrt{(SD^2 - RMSE^2)}$	0
9	Coefficient of determination (R^2)	$R^2 = 1 - \left[\frac{\sum_{i=1}^{n} \left(H_{meas}(i) - H_{pred}(i) \right)^2}{\sum_{i=1}^{n} \left(H_{meas}(i) - H_{avg_{meas}} \right)^2} \right]$	1

4.2.5.3 Estimation of horizontal surface hourly global solar radiation

Many authors have developed models for estimating the hourly global solar radiation of a horizontal surface (I_g) [433]–[440]. One of the widely used model for estimating long-term hourly global solar radiation is Collares-Pereira and Rabl [438] model. Unlike in some other estimation models such as Whillier [433] model

and Liu and Jordan [439] model whereby atmospheric effect on global solar radiation is assumed as constant, in Collares-Pereira and Rabl (CPR) [438] model, atmospheric effect on global solar radiation is dependent on the hour angle (ω). Collares-Pereira and Rabl [438] accounted for atmospheric effect on global solar radiation by multiplying Liu and Jordan [439] hourly global solar radiation estimation model by a hour angle based empirical expression $(a + b\cos\omega)$. Therefore, Collares-Pereira and Rabl (CPR) [438] model for estimating horizontal surface hourly global solar radiation ($kWm^{-2}h^{-1}$) from horizontal surface daily global solar radiation ($kWm^{-2}h^{-1}$) is defined as [438]:

$$\frac{I_g}{H_g} = (a + b\cos\omega) \times \frac{\pi}{24} \times \left[\frac{(\cos\omega - \cos\omega_s)}{\sin\omega_s - \frac{\pi\omega_s}{180}\cos\omega_s}\right] = (a + b\cos\omega) \times r_o \qquad (4.33)$$

where ω_s included in Eq. (4.33) was defined in Eq. (4.30). While a and b are linear functions of $\omega_s - 60^\circ$ and are defined by [438]:

$$\left.\begin{aligned} a &= 0.4090 + 0.5016\sin(\omega_s - 60^\circ) \\ b &= 0.6609 + 0.4767\sin(\omega_s - 60^\circ) \end{aligned}\right\} \qquad (4.34)$$

The hour angle (ω) in Eq. (4.34) is an angular measure of time and unlike ω_s that remain constant in a day, ω changes depending on the hour of the day [219], [416]. Based on the rotation of the earth on its axis, ω is defined by the angular displacement of the sun east or west of the local meridian due to rotation of the earth on its axis at 15° per hour [192], [219], [230], [425]. So, the hour angle varies from -180° to $+180^\circ$; and the usual convention is to measuring the hour angle from noon, that is, morning being negative degrees and afternoon positive angles [117], [219]. Therefore, the hour angle is defined by [192], [219], [230], [425]:

$$\omega = 15^\circ \times [12 - T_S] \qquad (4.35)$$

where T_S in Eq. (4.35) is the solar time.

The solar time is also known as local apparent time, and it is dependent on the apparent angular motion of the sun across the sky. The solar time of a given location is estimated by the difference between the location's longitude and the meridian of its time zone, and the yearly perturbations in the rate of rotation of the earth around the sun [117], [219], [416], [425]. Because of the yearly perturbation in the rate of rotation of the earth around the sun, the solar time for a location does not coincide with the standard or local clock time (T_{st}) [117], [192], [416], [425]. So, the relationship between solar time and standard time is defined by [168], [192], [219], [416], [425], [426]:

$$T_S = T_{st} \pm 4(L_{st} - L_{loc}) + E_t \tag{4.36}$$

Positive/negative sign ($\pm$) is applied in Eq. (4.36) because a negative sign is applicable for the eastern hemisphere, while positive sign is applicable for the western hemisphere [219]. For Nigeria, a negative sign is used because the country is in the eastern hemisphere (i.e. east of the prime meridian). Also, in Eq. (4.36), L_{st} is the standard meridian for the local time zone, L_{loc} is the longitude of the location, and E is the equation of time (in minutes). Equation of time (E_t) is defined by [117], [118], [192], [219], [425]:

$$\begin{aligned} E_t = 229.18 \times (&0.000075 + 0.001868\cos\Gamma - 0.032077\sin\Gamma \\ &- 0.014615\cos 2\Gamma - 0.04089\sin 2\Gamma) \end{aligned} \tag{4.37}$$

Where day angle (Γ) included in Eq. (4.37) is defined in Eq. (4.29).

Gueymard [440] slightly modified Collares-Pereira and Rabl [438] model in Eq. (4.33), by incorporating a normalising factor (f_n) to improve the correction of atmospheric effect of global solar radiation suggested. So, the modified Eq. (4.33) is defined as [440]:

$$\frac{I_g}{H_g} = \frac{(a + b\cos\omega) \times r_0}{f_n} \tag{4.38}$$

where f_n parameters in Eq. (4.38) is defined as follow [440]:

$$f_n = a + 0.5b\left[\frac{\left(\frac{\pi\omega_s}{180} - \sin\omega_s\cos\omega_s\right)}{\sin\omega_s - \frac{\pi\omega_s}{180}\cos\omega_s}\right] \quad (4.39)$$

In this study, Gueymard [440] modified Collares-Pereira and Rabl [438] (GCPR) model is used for estimating hourly global solar radiation on a horizontal surface. This is because the model is reported as amongst the top performing models for estimating the hourly global solar radiation of a horizontal surface [416], [441].

4.2.5.4 Estimation of global solar radiation on inclined surfaces

Most of the models for estimating inclined surface global solar radiation requires the disintegration of global solar radiation into direct and diffuse solar radiation [220]–[228]. But because Nigerian meteorological agency weather stations do not measure diffuse solar radiation, Olmo et al. [229] estimation model which does require diffuse solar radiation data to estimate inclined surface global solar radiation is used. As earlier mentioned in Chapter 3, an alternative approach is to estimate the diffuse solar radiation of the location but most of the diffuse solar radiation estimation models include numerical definitions with numerous coefficients that are mainly valid for a location [230]. However, the alternative approach is less desirable in this study because it is a more complex approach and it requires the use of measured diffuse solar radiation data; which is un-available for the location, to derive the modelling coefficients and to evaluate the most suitable diffuse solar radiation estimation model for the location. Therefore, after the evaluation of the top performing model for estimating the location horizontal surface daily global solar radiation and subsequent estimation of the hourly global solar radiation with GCPR model, Olmo et al. [229] estimation model is used to estimate the hourly global solar radiation of an inclined surface. Olmo et al. [229] estimation model is defined by [229]:

$$I_\gamma = I_g\psi_o f_c \quad (4.40)$$

The parameter I_g included in Eq. (4.40) has been defined in Eq. (4.38), while the function ψ_o is the function that converts horizontal surface global solar radiation into the tilted surface global solar radiation. ψ_o is defined by [229]:

$$\psi_o = \exp\left(-K_t\left[\left(\frac{\pi\theta}{180}\right)^2 - \left(\frac{\pi\theta_z}{180}\right)^2\right]\right) \tag{4.41}$$

where K_t in Eq. (4.41) is the clearness index and it is calculated by dividing the estimated hourly global solar radiation (I_g) by the hourly extra-terrestrial global solar radiation (I_o). The expression for calculating hourly extra-terrestrial global solar radiation (I_o) is [117], [219], [416], [425]:

$$I_0 = 3600 \times G_{SC}\left[1 + 0.033\cos\left(\frac{360 \times N_{day}}{365}\right)\right] \times [\sin\phi\sin\delta + \cos\phi\cos\delta\cos\omega] \tag{4.42}$$

where the parameters G_{SC}, N_{day}, and ϕ in Eq. (4.42) are symbol for solar constant, day of the year, and the latitude of the location. While δ and ω in Eq. (4.42) are symbol declination angle, and hour angle respectively. Expressions for calculating δ and ω have been defined in Eq. (4.28) and Eq. (4.35) respectively. Also, θ in Eq. (4.41) is the solar incidence angle. θ for a surface oriented in any direction is expressed as follow [117], [118], [218], [230]:

$$\cos\theta = \sin\delta\sin\phi\cos\beta - \sin\delta\cos\phi\sin\beta\cos\gamma + \cos\delta\cos\phi\cos\beta\cos\omega + \cos\delta\sin\phi\sin\beta\cos\gamma\cos\omega + \cos\delta\sin\beta\sin\gamma\sin\omega \tag{4.43}$$

where the parameters β and γ in Eq. (4.43) are the symbol for the tilt angle and the surface azimuth angle. Nigeria is in the northern hemisphere, and for a surface in the northern hemisphere facing south, the surface azimuth angle (γ) is 0° [117], [218], [219]. So, Eq. (4.43) is simplified as:

$$\theta = \cos^{-1}([\sin\delta\sin(\phi - \beta)] + [\cos\delta\cos(\phi - \beta)\cos\omega]) \tag{4.44}$$

For a horizontal surface, the tilt angle (β) is 0°, while the angle of incidence (θ) is equal to the solar zenith angle (θ_z). Substituting $\beta = 0^{\circ}$ into Eq. (4.44), the solar zenith angle (θ_z) is defined by [117], [218], [219], [230], [425]:

$$\theta_z = \cos^{-1}([\sin\delta \sin(\phi)] + [\cos\delta \cos(\phi) \cos\omega]) \tag{4.45}$$

Meanwhile, the multiplying factor (f_c) included in Eq. (4.40) is used to account for the effect of anisotropic reflection and it is dependent on the solar incidence angle (θ) and on the reflectivity (albedo) of the collector's surrounding (ρ_r). So, the multiplying factor (f_c) is defined as [229]:

$$f_c = 1 + \rho_r \left[\sin^2\left(\frac{\theta}{2}\right)\right] \tag{4.46}$$

The reflectivity or ground albedo is defined as the ratio of the reflected/scattered radiation to the incident radiation and it can be estimated by subtracting the emissivity of the location surface from one [425]. So, ground albedo is dependent on several factors, such as deviations from Lambert's law of isotropy and variations in ground properties [230]. The value of ground albedo commonly used are $\rho_r = 0.2$ for hot and humid tropical location [118], [230], [442], $\rho_r = 0.55$ for old snow-covered ground [442], $\rho_r = 0.85$ for fresh snow-covered ground [442]. In Nigeria where the presence of snow cover is unlikely, the ground albedo of the collector's surrounding is expected to be low. So, a ground albedo of 0.2 is selected in this study.

4.3 Hybrid energy system design model

The primary objective of performing an optimal sizing of the hybrid energy system is to ensure that energy demands are supplied reliably and at the lowest possible cost. To achieve reliable supply, more electricity generation will be required, and there will be a potential increase in energy system cost. However, the potential high system cost of achieving a reliable supply of electricity can be reduced if the hybrid system energy losses/wastage is minimized. So, the objective function (OF) for the optimal sizing problem is defined by:

$$\text{minimize: OF} = \begin{cases} f(\text{LPSP}) \\ f(C_{ann,tot}) \end{cases} \tag{4.47}$$

where LPSP is the loss of power supply probability, $C_{ann,tot}$ is total annualized system cost. The LPSP is the ratio between the total unmet load and the total load within the period under consideration, therefore, it is defined by [190], [337]:

$$\text{LPSP} = \frac{\sum_{t=1}^{T} E_{deficit}(t)}{\sum_{t=1}^{T} E_{load}(t)} \tag{4.48}$$

where $E_{deficit}$ is the energy deficit, and E_{load} is electrical load

A search of the optimal combination of system components is required for the optimal sizing of the hybrid energy system, the optimal sizing problem can be referred to as a search space problem. Therefore, minimization of the objective function is performed with a graphical construction technique called design space modelling technique. This modelling technique is selected because it is a quick and precise optimization technique and it can be easily understood and replicated [338], [365], [403]. The search space simulation is performed by initially separating the feasible regions from the non-feasible regions, before a search for the optimal point (i.e. point of least cost) in the feasible region of the design search space is determined. Poddar and Polley [443] is credited with the concept of design space optimization technique [361]. By searching the feasible region of a chemical process plant, Poddar and Polley [443] applied design space technique to optimize the design of a heat exchanger.

Currently, design space optimization is not restricted to the optimization of the design of heat exchangers, but also to other fields where the concept can be applied to a search space problem. For example, in a power system, it has been used for energy system components optimal sizing [338]–[340]. In this study, two axes (x-axis and y-axis) search is carried out within the feasible region of the design search space to determine the optimal size of the photovoltaic (P_{PV}) and biogas generator (P_{Bio}) that should be installed. The feasible region, in this case, is defined by the

portion of the design space, whereby selected sizes or combinations of the PV system, biogas generator, and battery energy storage system can be used to achieve a minimal LPSP. The flowchart that describes the operations of the design space optimization modelling technique is presented in Fig. 4.4.

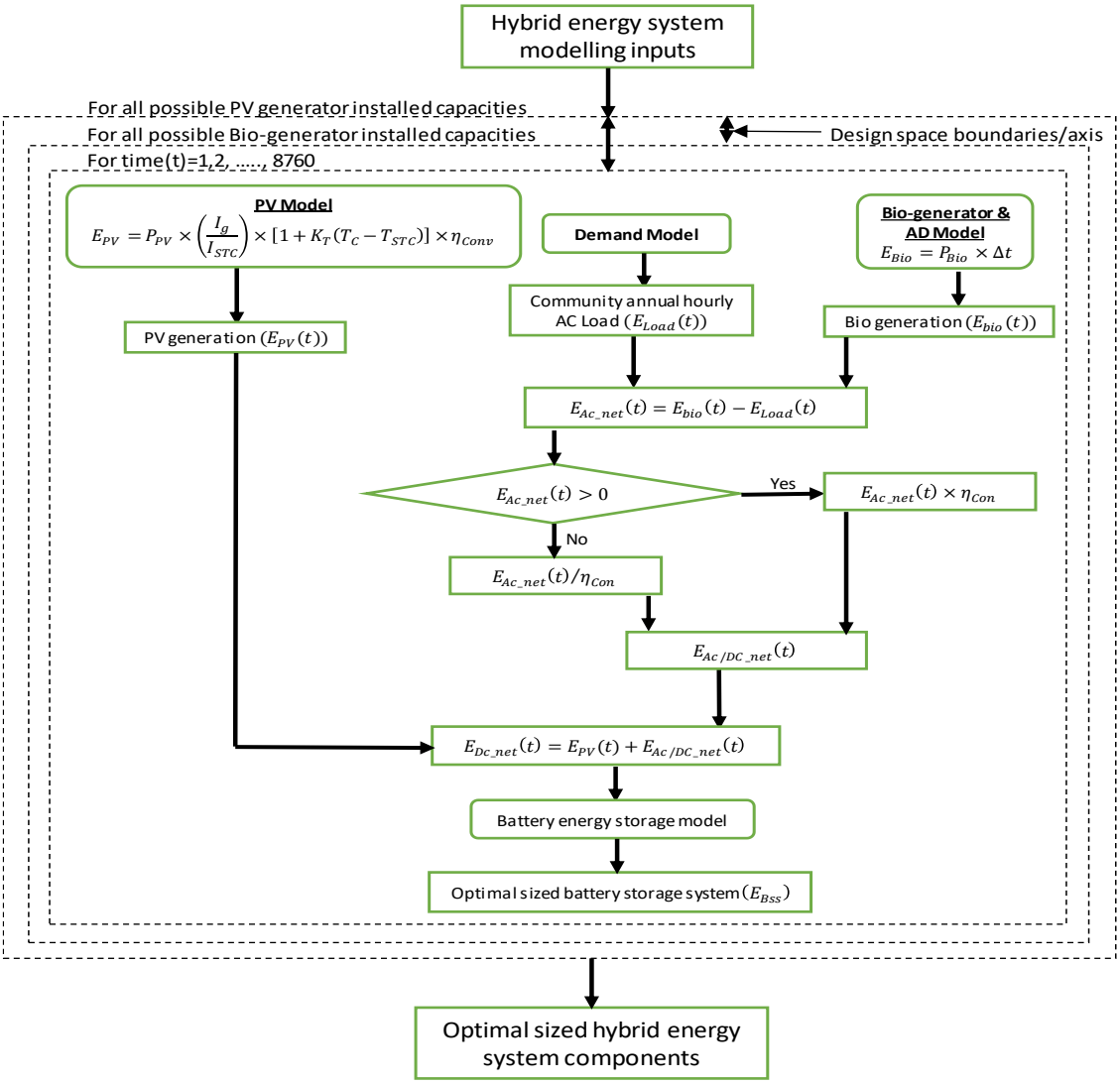

Fig. 4.4. Design space optimization technique

The sequence of energy balancing presented in Fig. 4.4 represents the technical strategy of the hybrid energy system design model. Meanwhile, because Fig. 4.4 will be used to simulate the optimal size of system components, the technical design strategy illustrated in Fig. 4.4 is linked with the technical strategy for the regional-grid power distribution as well as the economic strategy for the optimal sizing of the hybrid energy system.

4.3.1 Technical design strategy

The technical design strategies applied here is categorized into two strategies. The first technical design strategies are used to minimize the un-met load within the hybrid energy system presented in Fig. 4.1. The second technical design strategy emanates from the desire to aggregate electrical load, since load aggregation leads to peak demand shaving (lower load diversity factor) [444]. Hence, resulting in the reduction of the generator capacity. So, renewable energy system scalability advantage [46], [445], [446], can be explore to study if it is a better operating strategy to centralize or distribute generators and energy storage when community grids are integrated into a regional-grid, in order to minimise the power losses in the network.

4.3.1.1 Hybrid energy system technical design strategy

In this section the technical design strategies are used to minimize the un-met load. These technical design strategies are applied to carried out the design space optimization presented in Fig. 4.4. The technical design strategy adopted to minimize the hybrid energy system conversion losses is such that the AC load in the AC bus of the hybrid-coupled topology in Fig. 3.3 is supplied first by the AC generator, before the net AC energy (surplus/deficit) is transferred to the DC bus through the energy converter. So, the hybrid energy system net AC energy (E_{AC_net}) can be defined as [366], [400], [401]:

$$E_{AC\_net}(t) = E_{Bio}(t) - E_{Load}(t) \tag{4.49}$$

where E_{Bio} is the energy supplied by the biogas generator and E_{Load} is the electrical load.

When the hybrid energy system net AC energy is surplus, the excess AC energy is sold to the national grid rather than been used to charge the battery in order to minimise energy conversion losses. But when the net AC energy is deficit, the un-met load will be supplied by the PV system or the battery energy storage connected to the DC bus in Fig. 3.3. The supplied energy from the DC bus are transformed from

DC to AC by the energy converter in Fig. 3.3. So, the net transformed energy surplus/deficit (E_{AC/DC_net}) can be defined as [171], [366], [400], [401], [403]:

$$E_{AC/DC\_net}(t) = \begin{cases} E_{AC\_net}(t)/\eta_{con} & E_{AC\_net}(t) < 0 \\ E_{AC\_net}(t) \times \eta_{con} & E_{AC\_net}(t) \geq 0 \end{cases} \quad (4.50)$$

where $E_{AC\_net}(t)$ included in Eq. (4.50) was defined in Eq. (4.49), while η_{con} is the converter efficiency and η_{con} is used to accounts for the energy transformation losses. Similarly, the net energy surplus or deficit within the DC bus (E_{DC_net}) of the hybrid-coupled topology in Fig. 4.1 can be defined as [366], [400], [403]:

$$E_{DC\_net}(t) = E_{PV}(t) + E_{AC/DC\_net}(t) \quad (4.51)$$

where E_{AC/DC_net} included in Eq. (4.51) was defined in Eq. (4.50), while E_{PV} is the energy supplied by the photovoltaic system. The calculation of E_{DC_net} is vital because it is required for the optimal sizing the battery energy storage system, so that un-met load can be supplied.

4.3.1.2 Technical design strategy for regional-grid power distribution

To determine the preferred technical design strategy for power distribution with a regional-grid, a power flow study will be used to investigate if it is a better operating strategy to centralize or distribute generators and energy storage when power is distributed in a regional-grid. The power flow study is useful because the resultant power losses that emanates from centralizing or distributing generators and energy storage in different load buses within the regional-grid distribution network can be evaluated. Also, power flow analysis is concerned with the healthy operation of the electrical network; thus, enabling potential economic saving in the long run.

Execution of the power flow study begins with the initialization of assigned power network parameters (electrical loads, generation specification and constraints), and the subsequent calculation of relevant parameters such as bus admittance matrix, bus conductance matrix, and bus susceptance matrix of the power network. The next procedure is the use of a mathematical technique (i.e. Newton-Raphson method

which was proposed in Section 3.4.8) to simulate the power flow in the network. Meanwhile, during the power flow study, simulation of the voltage profiles, power flows, and power losses of the power network are performed by ensuring pre-defined constraints are not violated. A schematic diagram that can be adopted to carry out a power flow analysis is presented in Fig. 4.5.

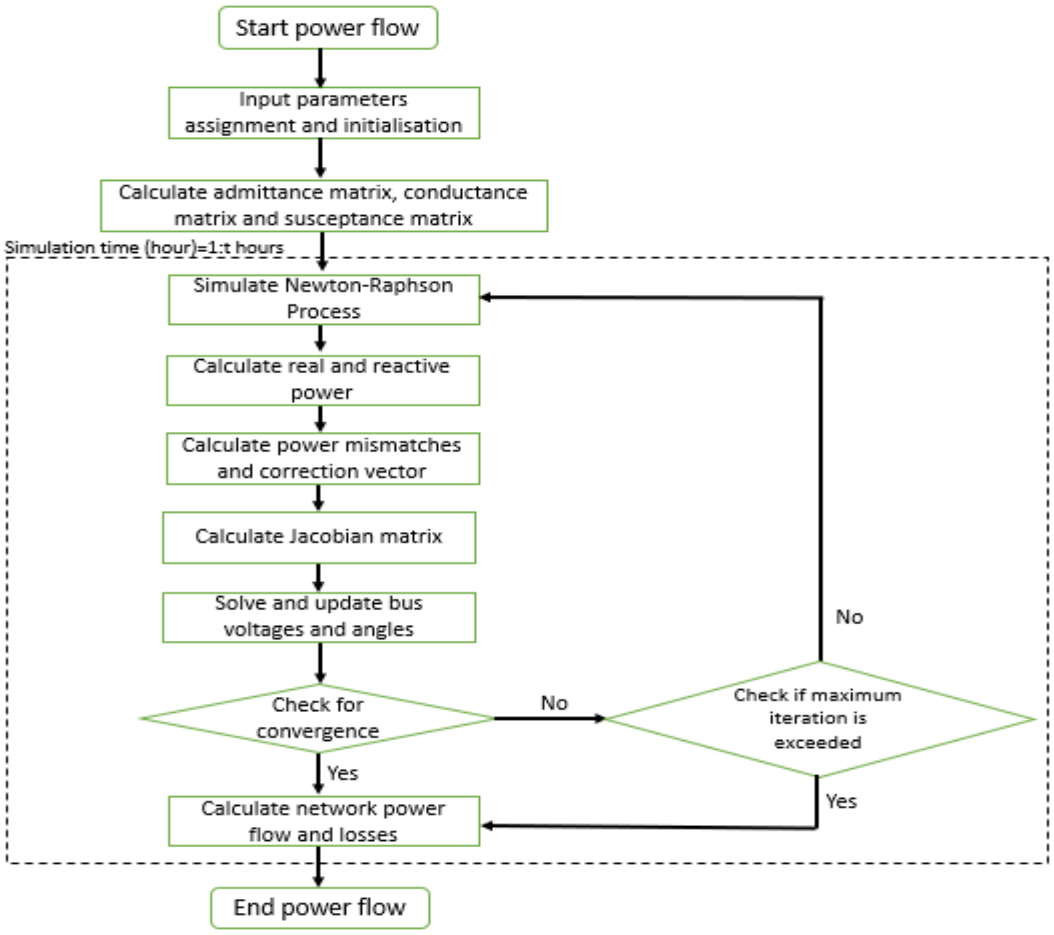

Fig. 4.5. Power flow study modelling scheme

In executing the power flow study, the underlying electrical circuit is analysed with the use of nodal analysis. Therefore, for a power system with several buses, the nodal equations that define the admittance (Y), the current (I), and the voltage (V), is given by [349], [350], [352]:

$$\begin{bmatrix} I_1 \\ I_2 \\ I_3 \\ \vdots \\ I_N \end{bmatrix} = \begin{bmatrix} Y_{11} & Y_{12} & Y_{13} & \cdots & Y_{1N} \\ Y_{21} & Y_{22} & Y_{23} & \cdots & Y_{2N} \\ Y_{31} & Y_{32} & Y_{33} & \cdots & Y_{3N} \\ \vdots & \vdots & \vdots & & \vdots \\ Y_{N1} & Y_{N2} & Y_{N3} & \cdots & Y_{NN} \end{bmatrix} \begin{bmatrix} V_1 \\ V_2 \\ V_3 \\ \vdots \\ V_N \end{bmatrix} \tag{4.52}$$

where N in Eq. (4.52) is the number of buses. By using matrix notation, the several buses nodal equation in Eq. (4.52) can be expressed in a compact form by:

$$I = Y_{bus} \times V \tag{4.53}$$

From Eq. (4.53), I is the N column vector of source currents injected into each bus, V is the N column vector of bus voltages, and Y_{bus} is the bus admittance. One of the advantages of representing power flow problems with nodal equations is that from the specified parameters of the power system buses, computer programs can be used to calculate the required power flow variables. The diagonal element (Y_{mm}) of the bus admittance matrix (Y_{bus}) is also known as self-admittance or driving point admittance, while the off-diagonal element (Y_{mn}) of the bus admittance matrix (Y_{bus}) also known as mutual admittance or transfer admittance. The bus admittance matrix (Y_{bus}) is symmetrical (i. e. $Y_{mn} = Y_{nm}$). The diagonal and the off-diagonal elements of the bus admittance matrix (Y_{bus}) can be defined by [350]:

$$\begin{aligned} Y_{mm} &= \text{sum of admittances connected to bus m, for } (m = 1,2,\cdots,N) \\ Y_{mn} &= -(\text{sum of admittances connected to bus m}), \text{for } (m \neq n) \end{aligned} \tag{4.54}$$

By substituting Y_{bus} in Eq. (4.53) with Eq. (4.54), the current entering a bus m (I_m) is defined by:

$$I_m = Y_{m1}V_1 + Y_{m2}V_2 + \cdots + Y_{mn}V_n = \sum_{n=1}^{N} Y_{mn}V_n \tag{4.55}$$

In practice, for a network bus m, the apparent power (S_m) is specified, while the bus current (I_m) is not specified. Therefore, the apparent power entering into a network and its complex conjugate is defined by [350]:

$$S_m = P_m + jQ_m = V_m I_m^*$$
$$S_m^* = P_m - jQ_m = V_m^* I_m \tag{4.56}$$

By substituting (I_m) from Eq. (4.55) into the apparent power complex conjugate equation in Eq. (4.56), the apparent power complex conjugate (S_m^*) is defined by:

$$S_m^* = P_m - jQ_m = V_m^* \left[\sum_{n=1}^{N} Y_{mn} V_n\right] \qquad \text{for } m = 1,2,\cdots,N \tag{4.57}$$

The voltages and the admittance elements in Eq. (4.57) are complex quantities, and their corresponding polar and complex notations is defined by:

$$\begin{aligned} V_m^* &= |V_m| \angle -\delta^\circ_m = |V_m|(\cos\delta^\circ_m - j\sin\delta^\circ_m) \\ V_n &= |V_n| \angle \delta^\circ_n = |V_n|(\cos\delta^\circ_n + j\sin\delta^\circ_n) \\ Y_{mn} &= |Y_{mn}| \angle \theta_{mn} = |Y_{mn}|\cos\theta_{mn} + |Y_{mn}|\sin\theta_{mn} = G_{mn} + jB_{mn} \end{aligned} \tag{4.58}$$

where G is the conductance and B is the susceptance in Eq. (4.58). By substituting the mutual admittance (Y_{mn}) and the complex conjugate of voltage (V_m^*) of Eq. (4.58) into Eq. (4.57), the complex conjugate of the apparent power becomes:

$$\begin{aligned} P_m - jQ_m = \sum_{n=1}^{N} |V_m||V_n|(&G_{mn}\cos(\delta^\circ_m - \delta^\circ_n) + jB_{mn}\cos(\delta^\circ_m - \delta^\circ_n) \\ &- jG_{mn}\sin(\delta^\circ_m - \delta^\circ_n) + B_{mn}\sin(\delta^\circ_m - \delta^\circ_n)) \end{aligned} \tag{4.59}$$

Also, by separating the real part of Eq. (4.59) from the imaginary part of the equation, the amount of active power (P_m) and reactive power (Q_m) flowing into the m_{th} bus is defined by:

$$\begin{aligned} P_m &= \textstyle\sum_{n=1}^{N} |V_m||V_n|G_{mn}\cos(\delta^\circ_m - \delta^\circ_n) + |V_m||V_n|B_{mn}\sin(\delta^\circ_m - \delta^\circ_n) \\ Q_m &= \textstyle\sum_{n=1}^{N} -|V_m||V_n|B_{mn}\cos(\delta^\circ_m - \delta^\circ_n) + |V_m||V_n|G_{mn}\sin(\delta^\circ_m - \delta^\circ_n) \end{aligned} \tag{4.60}$$

P_m and Q_m are non-linear functions with several unknowns. Thus, a numerical (iteration) method are required for calculating P_m and Q_m.

Newton–Raphson method is applied to analyse the power flow problem. Newton–Raphson method is selected because it gives more accurate results within less converge time than many other methods such as Gauss-Siedel method and Jacobi methods [350], [352], [353]. Newton-Raphson method is developed based on Taylor's series expansion of a function, and it is used for finding successively better approximations to the solutions (roots) of a function [350], [351]. Therefore, a function is optimized when the difference between the calculated and the scheduled values become close to zero. The generalized form of the Newton–Raphson method is given by the expression [350]–[352]:

$$x^{p+1} = x^{p} - \frac{f(x^{p})}{f^{1}(x^{p})} \tag{4.61}$$

For multi-equations function, Eq. (4.61) becomes [350]:

$$X^{p+1} = X^{(p)} - J^{-1}(X^{p})f(X^{p}) \tag{4.62}$$

where x and f are column vectors, and $J(X^{p})$ is a matrix known as the Jacobian matrix or partial differentiation matrix. When Newton-Raphson's method is used in power flow study, the real and reactive power mismatch between the scheduled and calculated power is set at a value close to zero [350]. So, the real power and reactive power mismatch are defined by [349], [350]:

$$\begin{aligned} \Delta P &= P_{Sch} - P_{calc} \approx 0 \\ \Delta Q &= Q_{Sch} - Q_{calc} \approx 0 \end{aligned} \tag{4.63}$$

The x and f column vectors are expressed as follow [350]:

$$x = \begin{bmatrix} \delta^{\circ} \\ V \end{bmatrix} = \begin{bmatrix} \delta^{\circ}_{2} \\ \vdots \\ \delta^{\circ}_{N} \\ V_2 \\ \vdots \\ V_N \end{bmatrix}$$
$$f = \begin{bmatrix} P \\ Q \end{bmatrix} = \begin{bmatrix} P_2 \\ \vdots \\ P_N \\ Q_2 \\ \vdots \\ Q_N \end{bmatrix} \tag{4.64}$$

The slack bus variables δ°_{1} and V_1 are omitted in the column vectors in Eq. (4.64) because they are pre-defined in a slack bus. So, if Newton-Raphson's method is applied to a N-bus power system, the linearized relationship between changes in voltage phase angle ($\Delta\delta^{\circ}$) and voltage magnitude (ΔV) to changes in real power (ΔP) and reactive power (ΔQ), is can be represented by Jacobian matrix as follow [349], [350]:

$$\begin{bmatrix} \Delta\delta^{\circ}_{2} \\ \vdots \\ \Delta\delta^{\circ}_{N} \\ \hline \Delta V_2 \\ \vdots \\ \Delta V_N \end{bmatrix}^{(0)} = \left[\begin{array}{ccc|ccc} \frac{\partial P_2}{\partial\delta^{\circ}_{2}} & \cdots & \frac{\partial P_2}{\partial\delta^{\circ}_{N}} & \frac{\partial P_2}{\partial V_2} & \cdots & \frac{\partial P_2}{\partial V_N} \\ \vdots & J_{11} & & \vdots & J_{12} & \\ \frac{\partial P_N}{\partial\delta^{\circ}_{2}} & \cdots & \frac{\partial P_N}{\partial\delta^{\circ}_{N}} & \frac{\partial P_N}{\partial V_2} & \cdots & \frac{\partial P_N}{\partial V_N} \\ \hline \frac{\partial Q_2}{\partial\delta^{\circ}_{2}} & \cdots & \frac{\partial Q_2}{\partial\delta^{\circ}_{N}} & \frac{\partial Q_2}{\partial V_2} & \cdots & \frac{\partial Q_2}{\partial V_N} \\ \vdots & J_{21} & & \vdots & J_{22} & \\ \frac{\partial Q_N}{\partial\delta^{\circ}_{2}} & \cdots & \frac{\partial Q_N}{\partial\delta^{\circ}_{N}} & \frac{\partial Q_N}{\partial V_2} & \cdots & \frac{\partial Q_N}{\partial V_N} \end{array}\right]^{(0)}{}^{-1} \begin{bmatrix} \Delta P_2 \\ \vdots \\ \Delta P_N \\ \hline \Delta Q_2 \\ \vdots \\ \Delta Q_N \end{bmatrix}^{(0)} \tag{4.65}$$

The elements of the Jacobian sub-matrix are calculated by carrying out a partial differentiation of the real and reactive power equations defined in Eq. (4.60), with respect to the voltage magnitude and the voltage phase angle. A summary of the partial derivatives for the Jacobian sub-matrix diagonal and off-diagonal elements are presented in Table 4.5.

Table 4.5. Diagonal and off-diagonal elements of Jacobian sub-matrix [349], [350]

Sub-matrix	Partial derivative for the diagonal elements $(m = n)$	Partial derivative for the off-diagonal elements $(m \neq n)$
J_{11}	$\frac{\partial P_m}{\partial \delta^\circ_m} = -Q_m - \lvert V_m\rvert\lvert V_m\rvert B_{mm}\cos(\delta^\circ_m - \delta^\circ_m) = -Q_m - \lvert V_m\rvert^2 B_{mm}$	$\frac{\partial P_m}{\partial \delta^\circ_n} = \lvert V_m\rvert\lvert V_n\rvert G_{mn}\cos(\delta^\circ_m - \delta^\circ_n) + \lvert V_m\rvert\lvert V_n\rvert B_{mn}\sin(\delta^\circ_m - \delta^\circ_n)$
J_{12}	$\frac{\partial P_m}{\partial \lvert V_m\rvert} = \frac{1}{\lvert V_m\rvert} \times (P_m - \lvert V_m\rvert^2 G_{mm}) + 2\lvert V_m\rvert G_{mm} = \frac{P_m}{\lvert V_m\rvert} + \lvert V_m\rvert G_{mm}$	$\frac{\partial P_m}{\partial \lvert V_n\rvert} = \lvert V_m\rvert G_{mn}\cos(\delta^\circ_m - \delta^\circ_n) + \lvert V_m\rvert B_{mn}\sin(\delta^\circ_m - \delta^\circ_n) = -\lvert V_n\rvert \frac{\partial Q_m}{\partial \delta^\circ_n}$
J_{21}	$\frac{\partial Q_m}{\partial \delta^\circ_m} = P_m - \lvert V_m\rvert\lvert V_m\rvert G_{mm}\cos(\delta^\circ_m - \delta^\circ_m) = P_m - \lvert V_m\rvert^2 G_{mm}$	$\frac{\partial Q_m}{\partial \delta^\circ_n} = -\lvert V_m\rvert\lvert V_n\rvert B_{mn}\sin(\delta^\circ_m - \delta^\circ_n) - \lvert V_m\rvert\lvert V_n\rvert G_{mn}\cos(\delta^\circ_m - \delta^\circ_n)$
J_{22}	$\frac{\partial Q_m}{\partial \lvert V_m\rvert} = -\frac{1}{\lvert V_m\rvert} \times (-Q_m - \lvert V_m\rvert^2 B_{mm}) - 2\lvert V_m\rvert B_{mm} = \frac{Q_m}{\lvert V_m\rvert} - \lvert V_m\rvert B_{mm}$	$\frac{\partial Q_m}{\partial \lvert V_n\rvert} = -\lvert V_m\rvert B_{mn}\cos(\delta^\circ_m - \delta^\circ_n) + \lvert V_m\rvert G_{mn}\sin(\delta^\circ_m - \delta^\circ_n)$

4.3.2 Hybrid energy system economic strategy

The total system cost of an energy project comprises of initial investment or capital cost $(C_{ann,cap})$, subsequent investment or replacement cost $(C_{ann,rep})$, operation and maintenance cost $(C_{ann,O\&M})$, and fuel cost $(C_{ann,fuel})$ [170]. The different sub-total system costs of an energy project often occur at different stages of the energy project lifetime. For example, capital cost occurs at the start of the energy project, while replacement cost, operation and maintenance cost, and fuel cost occur at later stages of the hybrid energy system project. In this study, fuel cost is associated with the amount of biowaste purchased from outside the studied community. So, the total annualised system cost of the hybrid energy system is optimized with respect to the annualized capital cost, the annualized replacement cost, and the annualized operation and maintenance cost, and the annualized fuel cost. Therefore, the hybrid energy system total annualized system cost $(C_{ann,tot})$ is minimized by:

$$\text{Minimize: } \sum_{1}^{m} C_{ann,tot} = \sum_{1}^{m} \left(C_{ann,cap} + C_{ann,rep} + C_{ann,O\&M} + C_{ann,fuel}\right) \quad (4.66)$$

where $C_{ann,cap}$ is the annualized capital cost, $C_{ann,rep}$ is the annualized replacement cost, $C_{ann,O\&M}$ is the annualized maintenance cost, $C_{ann,fuel}$ is the annualized fuel cost, and m is the number of system components. Photovoltaic system, biogas system (i.e., biogas generator and AD system), battery storage system, and converter system, are the four core system components in the hybrid energy system in Fig. 4.1. So, the equivalent total annualized cost for each of the four system components are aggregated to calculate the total annualized system cost of the hybrid energy system. The annualized capital cost $\left(C_{ann,tot}\right)$ is defined as [168]:

$$C_{ann,tot} = C_{cap} \times CRF(ir, n) \quad (4.67)$$

where C_{cap} is the initial capital cost of system components, $CRF(ir, n)$ is the capital recovery factor or annuity factor. Capital recovery factor is defined by [170]:

$$CRF(ir, n) = \frac{i \times (1 + ir)^n}{(1 + ir)^n - 1} \quad (4.68)$$

where n is the useful lifetime of project and ir is the real interest rate. Nigeria real interest rate is influenced by the country high inflation rate [119]. So, Fisher's expression is used here to determine Nigeria real interest rate. Fisher's real interest rate (ir) is defined as [119], [170], [191]:

$$ir = \frac{ir_{nom} - f_r}{1 + f_r} \quad (4.69)$$

where ir_{nom} is the nominal interest rate and f_r is the inflation rate. To calculate the annualized replacement cost $\left(C_{arep}\right)$, the present worth of replacing the system component and the capital recovery factor required. So, the annualized replacement cost $\left(C_{ann,rep}\right)$ is defined as [168]:

$$C_{ann,rep} = C_{cap} \times \sum_{k=q,r,\ldots,v}^{n} \left(\frac{1}{1+ir}\right)^{k} \times CRF(ir,n) \tag{4.70}$$

where $k = q, r, \ldots, v$ are the different system components expected year of replacement. Meanwhile, because the initial capital cost of system and the capital recovery factor are both functions of the annualized capital cost and the annualized replacement cost in Eqs. (4.67) – (4.70) respectively, therefore, the sum of Eq. (4.67) and Eq. (4.70) can be re-written in terms of a single payment present worth factor as:

$$C_{ann,cap} + C_{ann,rep} = C_{cap} \times \left[1 + \sum_{k=q,r,\ldots,v}^{n} \frac{1}{(1+ir)^{k}}\right] \times CRF(ir,n) \tag{4.71}$$

Furthermore, if the annualized operation maintenance cost and annualized fuel cost for the system components can be estimated, then, the hybrid energy system annualised total cost of system is defined as:

$$C_{ann,tot} = \sum_{1}^{m} \left(C_{cap} \times CRF(ir,n) \times \left[1 + \sum_{k=q,r,\ldots,v}^{n} \frac{1}{(1+ir)^{k}}\right] + C_{ann,O\&M} + C_{ann,fuel} \right) \tag{4.72}$$

The levelized cost of energy (LCOE) and the net present cost (NPC), which are convenient means of comparing different hybrid energy system configuration are also used in this research. The levelized cost of energy (LCOE) of an energy project is defined as [335], [356]:

$$LCOE = \frac{C_{ann,tot}}{E_{supplied}} \tag{4.73}$$

where $C_{ann,tot}$ is the total annualized system cost and E_{load} is the total electrical energy supplied.

Whilst, the net present cost (NPC) of an energy project is defined by [85], [170], [177], [334]–[336]:

$$\mathrm{NPC} = \frac{C_{ann,tot}}{\mathrm{CRF}(ir, n)} \tag{4.74}$$

In summary, economy strategy methodology presented in this section shows how the annualized system cost, the net present cost and the levelized cost of energy, are calculated with Eq. (4.72), Eq. (4.73) and Eq. (4.74) respectively. In the feasible region of the HRES design space, decision on the optimal combinations of system components in Chapter 7 is based on their annualized system cost. While net present cost and levelized cost of energy are used to evaluate the impact that different loss of power supply probabilities (LPSP) have on the HRES cost.

4.4 Chapter summary

The methodology chapter can be divided into 3 sections. Section 4.1 presents the approach used in collecting household energy consumption survey data as well as the methodology applied to model a stochastic household occupancy-based load profile for a developing country household and rural residential community. Specifically, the relevance of residential customers survey data, Nigerian national population and housing census data and the electricity utility company data for the development of the stochastic household occupancy-based model was also highlighted. Furthermore, illustration of Markov chain process and its usage during the modelling of household(s) energy consumption behaviour was also presented in this section.

Section 4.2 presents the methodologies and boundary conditions adopted in modelling the different energy sub-systems of the hybrid energy system. These methodologies include the operation and sizing techniques of the biogas generator and anaerobic digester, battery energy storage, converter, and PV system. Furthermore, because hourly measured solar irradiation data is not available for many locations in developing countries like Nigeria, theoretical methods that can be used to estimate the hourly global solar irradiation of a horizontal and an inclined

surface was presented. Finally, the last section of the methodology chapter presents the design model of the hybrid energy system, the technical strategies adopted to perform the optimal sizing of hybrid energy system, the technical strategies applied to study if it is a better operating strategy to centralize or distribute generators and energy storage when community grids are integrated into a regional-grid, and the economic strategies adopted to ensure that electrical demands of the hybrid energy system are supplied at minimal cost.

Chapter 5 HOUSEHOLD ENERGY CONSUMPTION SURVEY AND STOCHASTIC MODELLING OF RESIDENTIAL LOAD PROFILE

To assess the electricity consumption patterns in Nigerian rural communities, modelling of households' load profile is carried out here. The scope of this chapter is to develop a stochastic occupancy-based model that can be used to simulate the load profile of a household or a community (aggregated households) in a developing country. In Chapter 7, the simulated load profile of the studied rural community is used as an input for the design and analysis of a hybrid energy system. Esan North-East local government area (LGA) in the south-southern region of Nigeria is selected as the survey location. The south-southern region is one of the six geo-political zones in Nigeria and the region is reported to have the lowest solar energy potential in the country [48], [84]. So, the selected rural residential community can serve as an ideal location for carrying out a worst-case solar energy assessment in Chapter 6 as well as studying the possibility of using integrated PV, biogas and battery energy storage system for rural electrification.

5.1 Household survey questionnaire design

The questions of the household survey questionnaire were grouped into 5 questionnaire sections or headings. In the household characteristic section, household class question will be used to group the surveyed households into the four household classes presented in Section 4.1.2. The question on the head of household occupation will be used to evaluate if there are links between the head of a household and a household energy consumption. While questions on the number of bedrooms in the house and the number of occupants will be used to determine the dwelling size and the household population respectively.

As earlier mentioned in Section 3.7.1, household occupants' behaviour section and the household activities section of the questionnaire are used to collate data relating to occupants' activity schedule. Therefore, from these sections, household activity-based questions such as household occupants' bedtime, time for work, waking up time, leisure time, cooking time and cleaning time will be used to determine the

transitions of occupants from one state to another and how active occupants perform different household activities.

In the energy usage and power availability section, questions on the difference in weekdays and weekends energy consumption, average daily electricity availability and average monthly electricity bill will be used to determine define some of the modelling assumptions and validation because existing data to validate the developed load profile model are limited. Finally, the list of household appliances tabulated in the last section of the questionnaire is used to acquire data on household appliance ownership. Due to the survey location insecurity challenges, question on appliance wattage was avoid because some survey participant might consider this question as too personal. Therefore, a market survey of household appliance stores was carried out to determine the power rating of commonly purchase appliances in the survey location.

5.2 Time use survey and stochastic modelling assumptions

- The lifestyle of households' occupants in the survey location is modelled with survey data on occupants' activity schedule because the survey sample size is a statistical representation of the survey location household population.
- Household occupants' daily engagements are grouped into inactive home (asleep) state, active home state, away from home state. In the morning, household occupants' transit from asleep state to active home state, then from active home state to away from home state. While in the evening, household occupants' transit from away from away from home state to active home state, then from active home state to asleep state.
- The power rating and time of use for an appliance type is assume as the same if a household has multiple quantities. Therefore, if there is a bulb in each of the 3 bedrooms of a household, the power rating and time of use of these bedroom bulbs are the same.

5.3 Time use survey outcomes

Outcomes from the time use survey are presented in this section of the thesis. The occupations of surveyed head of household are captured by a pie-chart in Fig. 5.1.

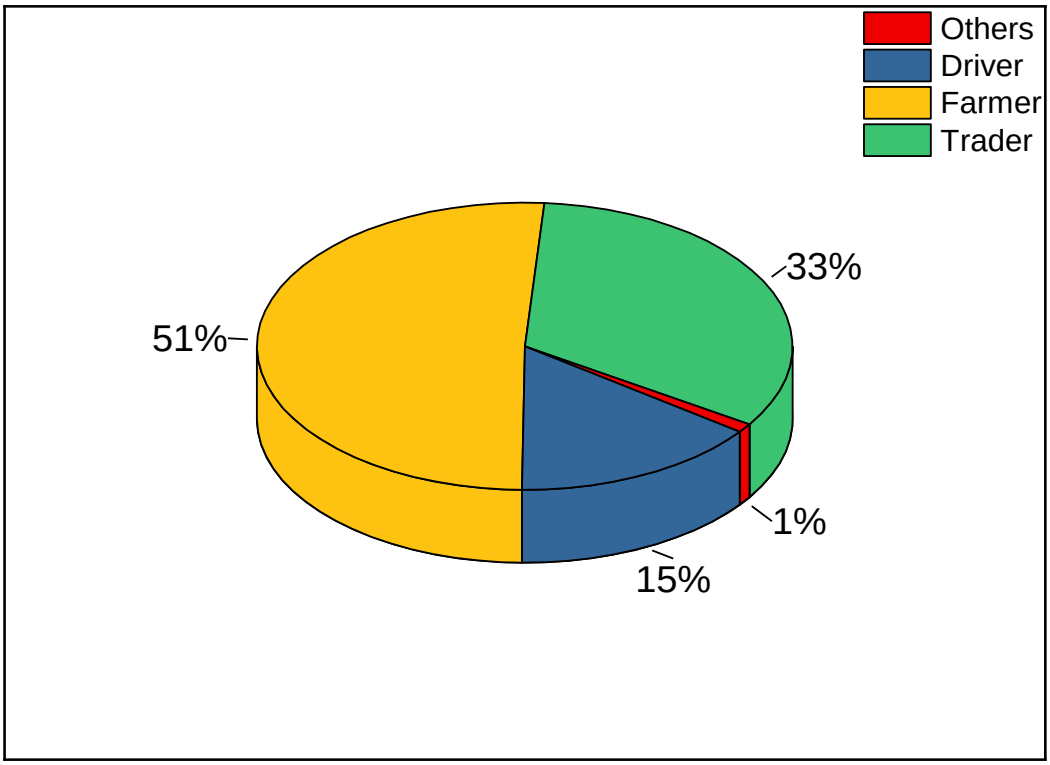

Fig. 5.1. Head of household occupation in the survey area

Fig. 5.1 reveals that 99% of the head of the surveyed households were either farmers, traders, or drivers. These main head of households' occupations are directly and indirectly linked with farming activities. This is because farmers work directly on the farm, while traders that sell farm products in the market and drivers that transport the farms' products to the market are indirectly linked to the farm. A bar-chart showing the percentage share of different household sizes in the survey area is present in Fig. 5.2.

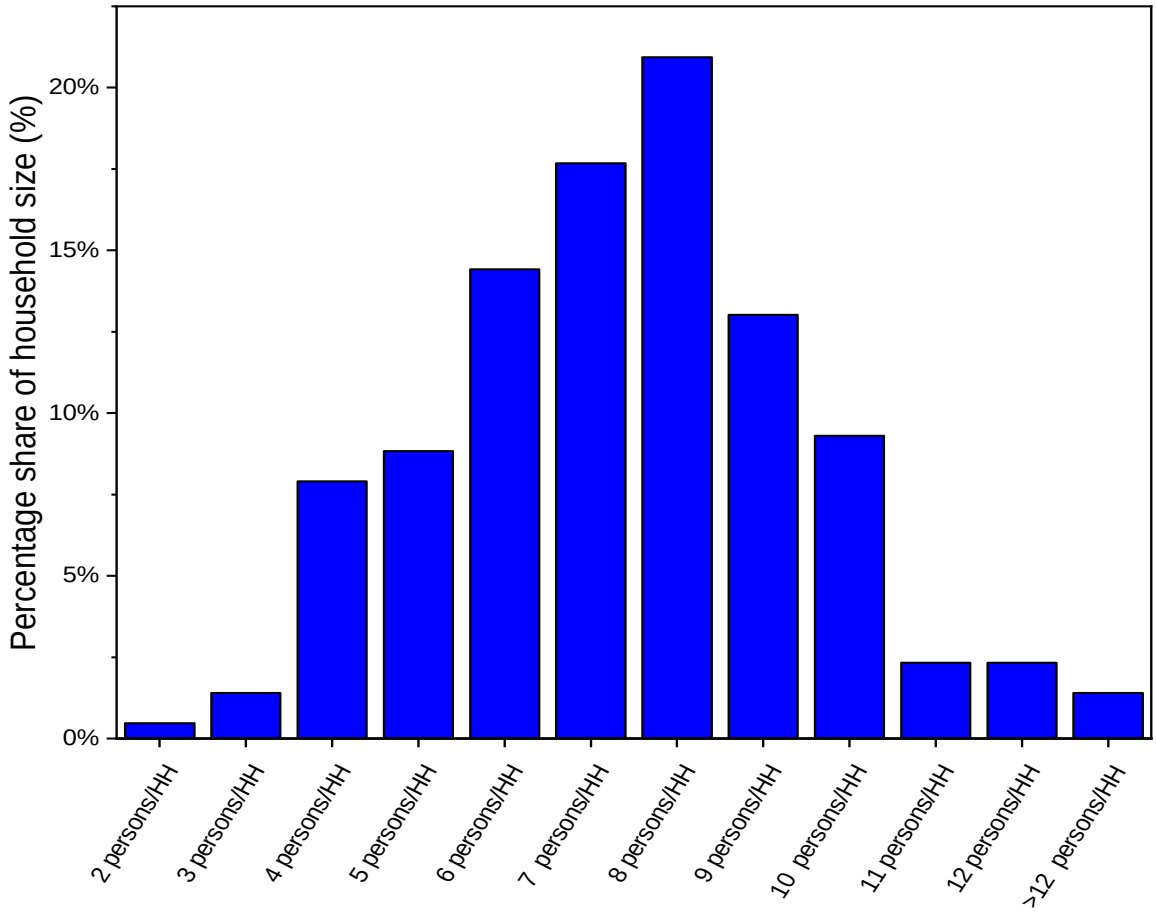

Fig. 5.2. Percentage share of household (HH) size in the survey area

Fig. 5.2 shows that 67% of the surveyed households had between 4 and 9 occupants per household, while 92.1% of the surveyed households had a minimum of 4 persons per household and a maximum of 10 persons per households. The absent of a 1 occupant household size in Fig. 5.2 is expected in this study because a household has been classified based on the number of individuals or families with the same electric bill or metering.

With respect to the number of bedrooms per household, the pie-chart in Fig. 5.3 reveals that 59% of the surveyed households had 3 to 4 bedrooms per households, while 99% of the surveyed households had a minimum of 2 bedrooms and a maximum of 6 bedrooms per households. This is similar to what was reported for Esan North-East LGA in 2006 national population and housing census report [388].

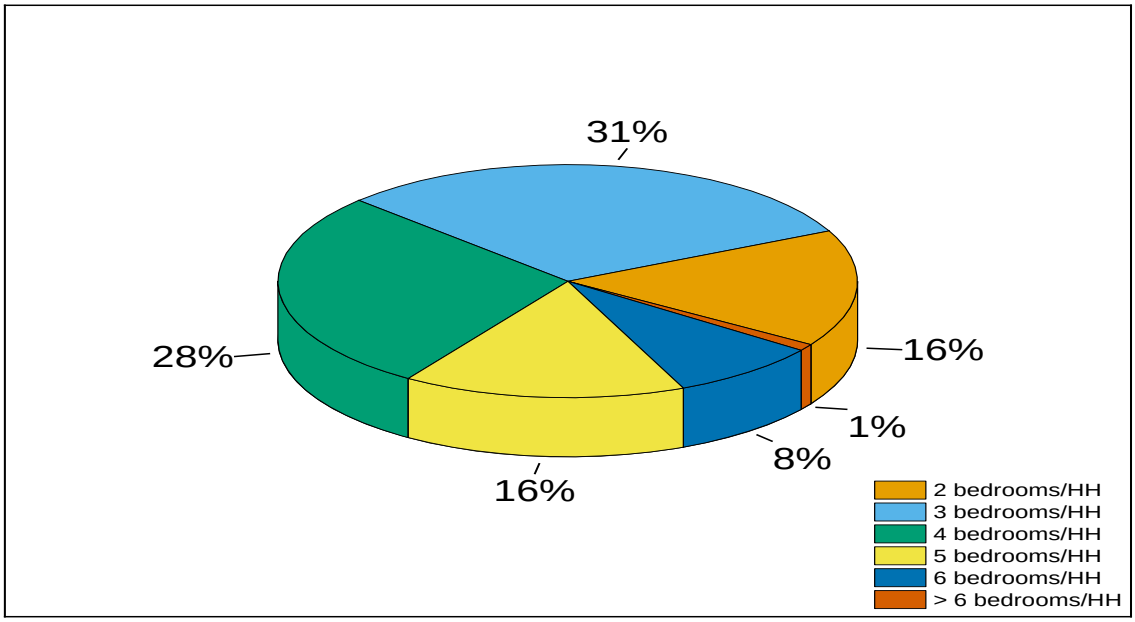

Fig. 5.3. Percentage share of bedrooms per household

Because the number of survey households is a statistical representation of the community household population, collated survey data that define occupants' activity schedule are used to model the lifestyle of household occupants in the community. To model the behaviour of household occupants, the three occupancy states mentioned in Section 5.2, are used to describe the daily engagement of household occupants. The possible hourly transition of an occupant in any of three occupancy states is captured in Fig. 5.4.

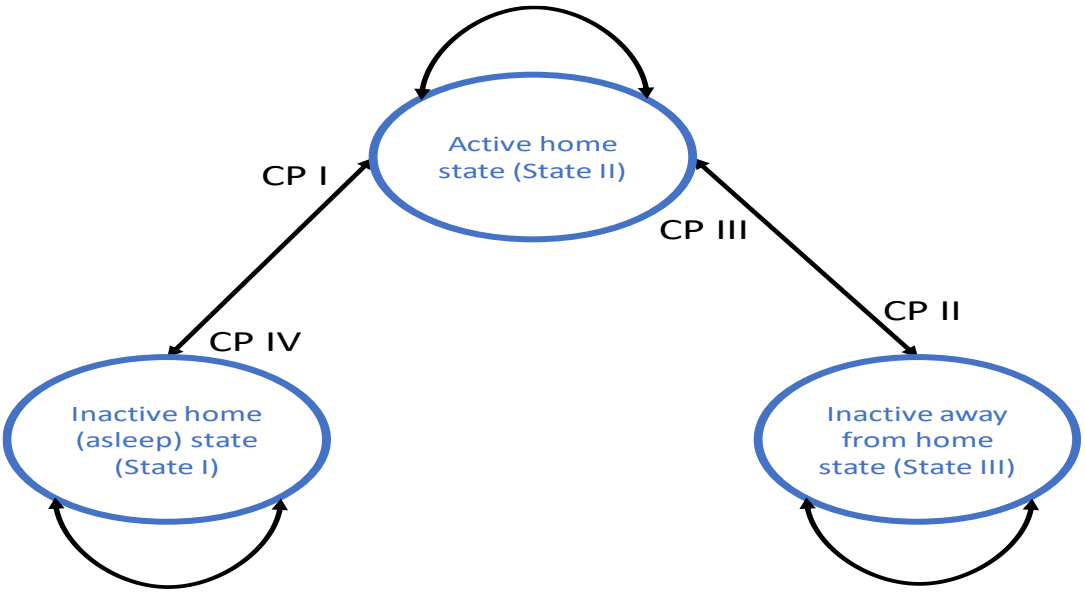

Fig. 5.4. Household occupants' states transition pathway

The black directional arrows in Fig. 5.4 show that an occupant in any of the three occupancy states either remains in his/her current state or transit to another state. There are 4 transition pathways amongst the three occupancy states. The number of occupants that transit through these 4 transition pathways every hour is dependent on the hourly conditional probabilities (CP) of CPI, CPII, CPIII and CPIV in Fig. 5.4. CPI, CPII, CPIII and CPIV are defined as the conditional probability of getting up in the morning given that the occupant is asleep, the conditional probability of going to work given that the occupant is awake at home, the conditional probability of coming home given that the occupant is away from home and the conditional probability of going to sleep given that the occupant is awake at home respectively. During load profile modelling, the conditional probabilities of CPI, CPII, CPIII and CPIV used to simulate daily engagement of household occupants, are calculated with survey data collated from household occupants' behaviour section of the questionnaire.

Over a 24 hours' time step, Table 5.1 illustrates how the conditional probabilities (CP_{ST}) for the household occupants' states transitions are calculated. A time step of 5:00 – 6:00 hour was selected for this illustration because during this time step, there is the possibility that the occupants of a household might occupy all the three occupancy states.

Table 5.1. Illustration of the calculation of survey area state transition

Primary State	Transition amongst states		Transition pathway	Survey-based transition	Conditional probabilities
	05:00 hours	06:00 hours			
State I	State I	State I	No transition	15	15/67 = 0.224
	State I	State II	CP_{ST} I	52	52/67 = 0.776
State II	State II	State I	CP_{ST} IV	0	0/206 = 0.000
	State II	State II	No transition	177	177/206 = 0.859
	State II	State III	CP_{ST} II	29	29/206 = 0.141
State III	State III	State II	CP_{ST} III	0	0/0 = 0.000
	State III	State III	No transition	0	0/0 = 0.000

Evaluation of Table 5.1 shows that the calculated conditional probabilities derived from the survey data are acceptable. For instance, the sum of the survey-based

transitions in Table 5.1 was equal to the survey sample size (273), and the calculated conditional probabilities within a state was equal to zero or one. Based on the time use survey data, the calculated hourly conditional probabilities for the states transition (i.e., CP_{ST} I, CP_{ST} II, CP_{ST} III, CP_{ST} IV) are presented in Table 5.2. Similarly, the probabilities for occupants' activities and appliance time use were also calculated from the collated survey data. The hourly probabilities calculated for cleaning, cooking, and leisure activities as well as for appliance time use are presented in Table 5.3 and Table 5.4 respectively. Amongst the available electrical appliances in the surveyed households, refrigerator/cold appliance and mobile phone charger time use were not presented in Table 5.4.

Refrigerators time use was not presented because its continuous operation is not dependent on the presence of an active occupant. Although mobile phone charger time use is dependent on the presence (active or inactive at home) of a household occupant, its specific time use could not be predicted by most survey participants because the charging of a mobile phone is usually performed when its battery is fully or partially discharged. Hence, it is assumed that mobile phone batteries are only charged at home and that it takes similar time to fully charge and fully discharge a mobile phone battery. Therefore, the average time for complete charging and discharging of a mobile phone battery are used as part of the parameters for modelling the load profile of mobile phone chargers.

Table 5.2. State transition pathway

Time slot		00hr	01hr	02hr	03hr	04hr	05hr	06hr	07hr	08hr	09hr	10hr	11hr	12hr	13hr	14hr	15hr	16hr	17hr	18hr	19hr	20hr	21hr	22hr	23hr
States transition pathway	CP_{ST} I	0.000	0.000	0.000	0.000	0.042	0.746	0.774	1.000	0.000	0.000	0.000	0.000	0.000	0.000	0.000	0.000	0.000	0.000	0.000	0.000	0.000	0.000	0.000	0.000
	CP_{ST} II	0.000	0.000	0.000	0.000	0.000	0.000	0.142	0.794	0.959	1.000	0.000	0.000	0.000	0.000	0.000	0.000	0.000	0.000	0.000	0.000	0.000	0.000	0.000	0.000
	CP_{ST} III	0.000	0.000	0.000	0.000	0.000	0.000	0.000	0.000	0.000	0.000	0.000	0.000	0.000	0.000	0.000	0.144	0.179	0.589	0.677	0.700	1.000	0.000	0.000	0.000
	CP_{ST} IV	0.000	0.000	0.000	0.000	0.000	0.000	0.000	0.000	0.000	0.000	0.000	0.000	0.000	0.000	0.000	0.000	0.000	0.000	0.000	0.000	0.067	0.224	0.583	1.000

Table 5.3. Occupants activity time use

Time slot		00hr	01hr	02hr	03hr	04hr	05hr	06hr	07hr	08hr	09hr	10hr	11hr	12hr	13hr	14hr	15hr	16hr	17hr	18hr	19hr	20hr	21hr	22hr	23hr
Activity	Cleaning	0.000	0.000	0.000	0.000	0.005	0.028	0.390	0.310	0.080	0.000	0.000	0.000	0.000	0.000	0.000	0.000	0.010	0.020	0.020	0.020	0.020	0.010	0.000	0.000
	Cooking	0.000	0.000	0.000	0.000	0.040	0.210	0.530	0.130	0.040	0.000	0.000	0.000	0.000	0.000	0.000	0.050	0.160	0.660	0.880	0.240	0.080	0.020	0.000	0.000
	Leisure	0.020	0.000	0.000	0.000	0.030	0.310	0.570	0.430	0.170	0.000	0.000	0.000	0.000	0.000	0.000	0.070	0.130	0.312	0.840	0.920	0.860	0.560	0.090	0.000

Table 5.4. Appliance time use

Time slot	00hr	01hr	02hr	03hr	04hr	05hr	06hr	07hr	08hr	09hr	10hr	11hr	12hr	13hr	14hr	15hr	16hr	17hr	18hr	19hr	20hr	21hr	22hr	23hr
Food blender	0.000	0.000	0.000	0.000	0.000	0.000	0.125	0.000	0.000	0.000	0.000	0.000	0.000	0.000	0.000	0.000	0.000	0.125	0.625	0.125	0.000	0.000	0.000	0.000
Electric iron	0.000	0.000	0.000	0.000	0.000	0.120	0.188	0.070	0.020	0.000	0.000	0.000	0.000	0.000	0.000	0.000	0.000	0.063	0.250	0.406	0.344	0.125	0.094	0.000
Television	0.000	0.000	0.000	0.000	0.000	0.054	0.101	0.048	0.012	0.000	0.000	0.000	0.000	0.000	0.000	0.000	0.031	0.204	0.431	0.850	0.898	0.862	0.725	0.050
DVD player	0.000	0.000	0.000	0.000	0.000	0.030	0.050	0.010	0.000	0.000	0.000	0.000	0.000	0.000	0.000	0.000	0.000	0.142	0.299	0.634	0.806	0.806	0.097	0.000
Electric iron	0.001	0.001	0.001	0.001	0.070	0.320	0.430	0.340	0.080	0.000	0.000	0.000	0.000	0.000	0.000	0:000	0.050	0.137	0.484	0.536	0.412	0.130	0.030	0.000
Bedroom fan	0.050	0.030	0.030	0.030	0.100	0.450	0.100	0.010	0.000	0.000	0.000	0.000	0.000	0.000	0.000	0.000	0.000	0.000	0.000	0.000	0.230	0.650	0.930	0.320
Sitting room fan	0.000	0.000	0.000	0.000	0.000	0.075	0.080	0.031	0.012	0.000	0.000	0.000	0.000	0.000	0.000	0.000	0.000	0.000	0.528	0.882	0.981	0.920	0.170	0.020
Bedroom bulb	0.000	0.000	0.000	0.000	0.120	0.460	0.010	0.000	0.000	0.000	0.000	0.000	0.000	0.000	0.000	0.000	0.000	0.000	0.000	0.000	0.060	0.840	0.350	0.015
Sitting room bulb	0.000	0.000	0.000	0.000	0.031	0.230	0.000	0.000	0.000	0.000	0.000	0.000	0.000	0.000	0.000	0.000	0.000	0.000	0.030	1.000	0.920	0.670	0.170	0.020
Security bulb	1.000	1.000	1.000	1.000	1.000	0.725	0.001	0.000	0.000	0.000	0.000	0.000	0.000	0.000	0.000	0.000	0.000	0.000	0.020	1.000	1.000	1.000	1.000	1.000

96% of the survey households stated that there is no obvious difference between weekdays and weekends in their daily time use of electricity. This survey outcome can be linked with earlier findings in Fig. 5.2 since 99% of the head of households' occupations were directly and indirectly associated with farming activities. Thus, the head of household's activities is expected to be similar. Due to the relevance of the difference between weekdays and weekends daily electricity time use, statistical verification was performed by collecting 3 months (January 2019 to March 2019) hourly daily electricity dispatch data from Uromi service unit and sorting the data into weekdays and weekends before a statistical test for the level of significance was performed.

Daily electricity dispatch data is used for the verification because an electrical load is defined as any device that draws electricity from an electrical network [447]. Thus, daily electricity dispatch data will substantially mirror the community energy consumption time use. d-bar analysis was used to test if there is a significant difference between the hourly weekend and weekday data, for a selected critical value or level of significance of 5%. The test statistic is calculated by [448].

$$T_d = \frac{\hat{d}}{\left(STDV/\sqrt{n}\right)} \tag{5.1}$$

where $\hat{d}$ and STDV are respectively the mean and standard deviation of the hourly difference between the weekend and weekday data, while n is the data size (24 hours). From Eq. (5.1), the calculated T_d is 2.154. Based on the degree of freedom (df) of the data size, the calculated value of T_d was checked on a t-table, in order to determine the corresponding level of significant. Calculation df is by subtracting one from the data size (i.e., $df = n - 1$). Consequently, for a df of 23 and a T_d value of 2.154, the corresponding level of significance from a t-table was 2.1% (0.021). This value (0.021) is less than the selected critical value ($P<0.05$) for rejecting the hypothesis. Therefore, the difference between weekdays and weekends daily time use of electricity is minimal since the difference between their hourly data were statistically insignificant. Hence, it is assumed in this research that the daily time use for weekdays and weekends are the same.

For the daily electricity availability in the community, 91% of the surveyed households reported that their daily electricity availability was unpredictable. The reason for the unpredictability of daily electricity availability is traceable to the practice of load shedding within the national power grid transmission and distribution network. The typical average daily electricity availability of the surveyed households is presented in Fig. 5.5.

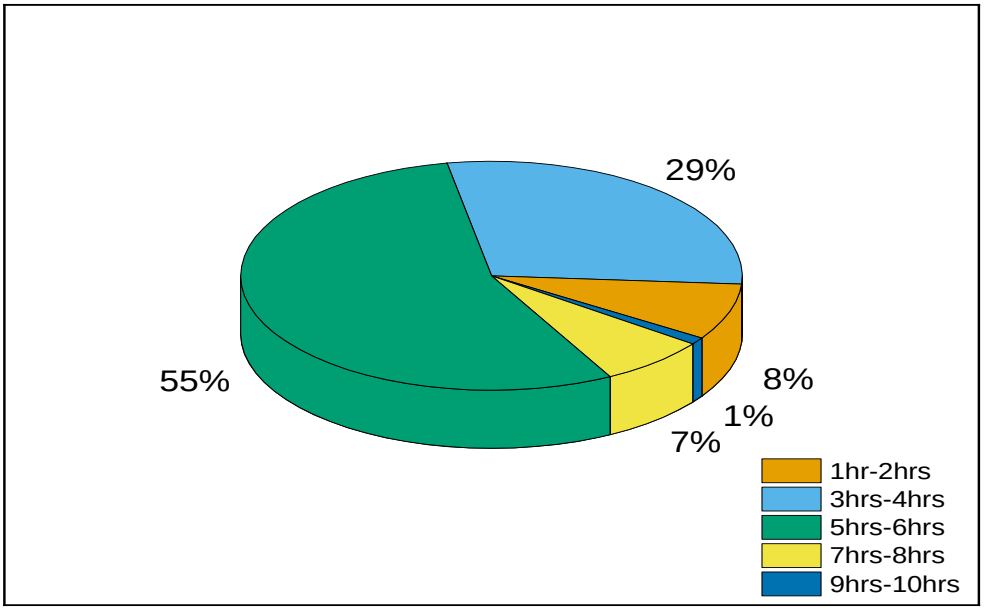

Fig. 5.5. Typical daily electricity availability in the survey area

The pie-chart in Fig. 5.5 shows that only 8% of the survey area households had more than 6 hours daily access to electricity, while 84% of the households had daily access to electricity in the range of 3 to 6 hours. But, the surveyed households' average daily access to electricity was 6 hours. Daily power availability survey data was also verified with the use of 3 months hourly daily electricity dispatch data collected from Uromi service unit. Over the 90 days period, the time and total hours of daily electricity dispatched was unpredictable. Also, analysis of the electricity dispatch data revealed that there was no electricity dispatch for a total of 9 days within the 90 days period. Furthermore, the maximum hours of electricity dispatch within a day was 9 hours, and this occurred once within the 90 days period. The average daily electricity dispatch to the survey area feeders is presented in Fig. 5.6.

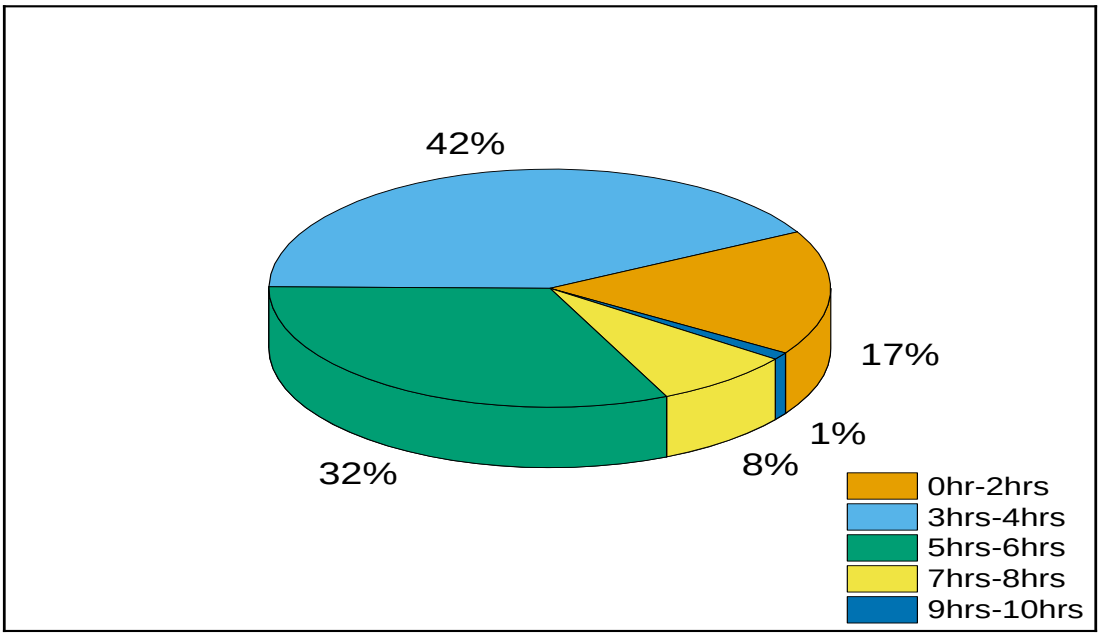

Fig. 5.6. Daily total electricity dispatch in the survey area

There are noticeable similarities between Fig. 5.5 and Fig. 5.6, for instance, the percentage share for daily electricity availability/dispatch for a total duration of 9-10 hours was 1% in both pie-charts. While the percentage share for daily electricity availability and electricity dispatch for more than a minimum of 6 hours were 8% and 9% respectively. However, the total duration of daily electricity availability in Fig. 5.5 was slightly over-estimated, because Fig. 5.6 shows that there is a lesser chance of having daily electricity dispatched to the community for a total duration of 6 hours. In fact, the average daily electricity dispatched over the 90 days period was 4 hours. However, the reason for the difference is perhaps because the energy consumption survey was carried out about a year before the electricity dispatch data was measured.

Pre-paid, post-paid, and community contribution are the three residential billing systems operated in the survey location. The average monthly electricity bill in Naira[1] of households in the survey area is presented in Fig. 5.7.

[1] Naira (₦) is Nigeria's currency. 1 U.S dollar is equivalent to ₦ 360

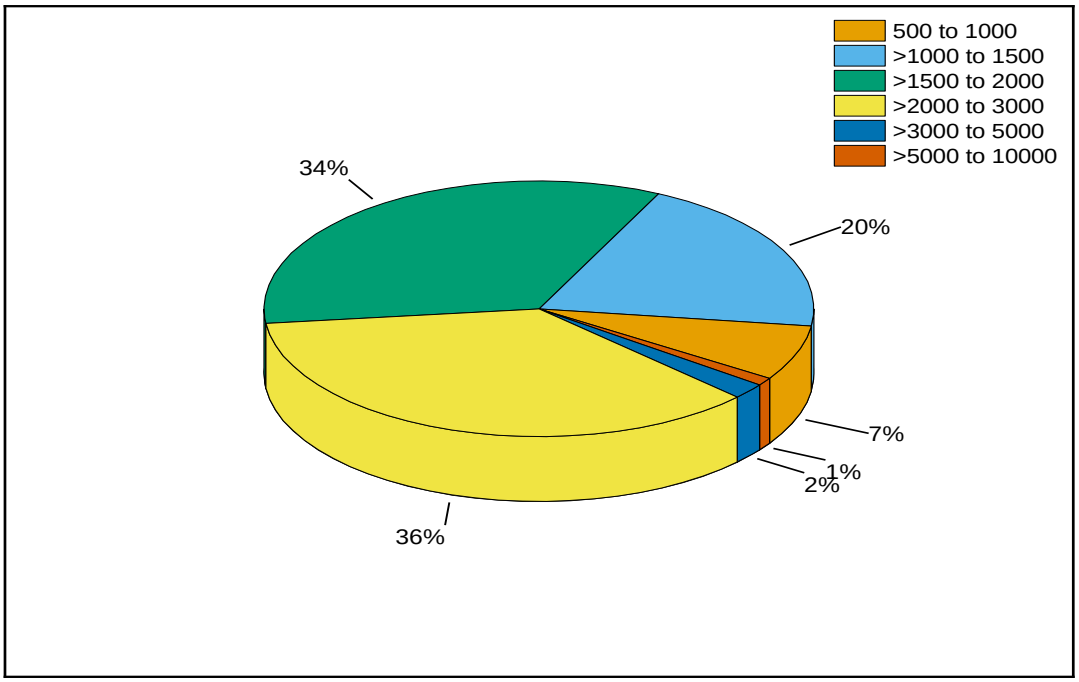

Fig. 5.7. Average monthly electricity bill in the survey area

The pie-chart in Fig. 5.7 shows that 90% of the survey households pay an average of about 1000 to 3000 Naira monthly, while 70% of the survey households pay an average of about 1500 to 3000 Naira monthly. The relationship between the different types of billing systems and the average monthly electricity bill of households was carried out. However, no direct link can currently be established between the different types of billing systems and the average monthly electricity bill of households.

Community household appliance time use has already been presented in Table 5.4, while the percentage share of appliances ownership within the survey area is presented in Fig. 5.8.

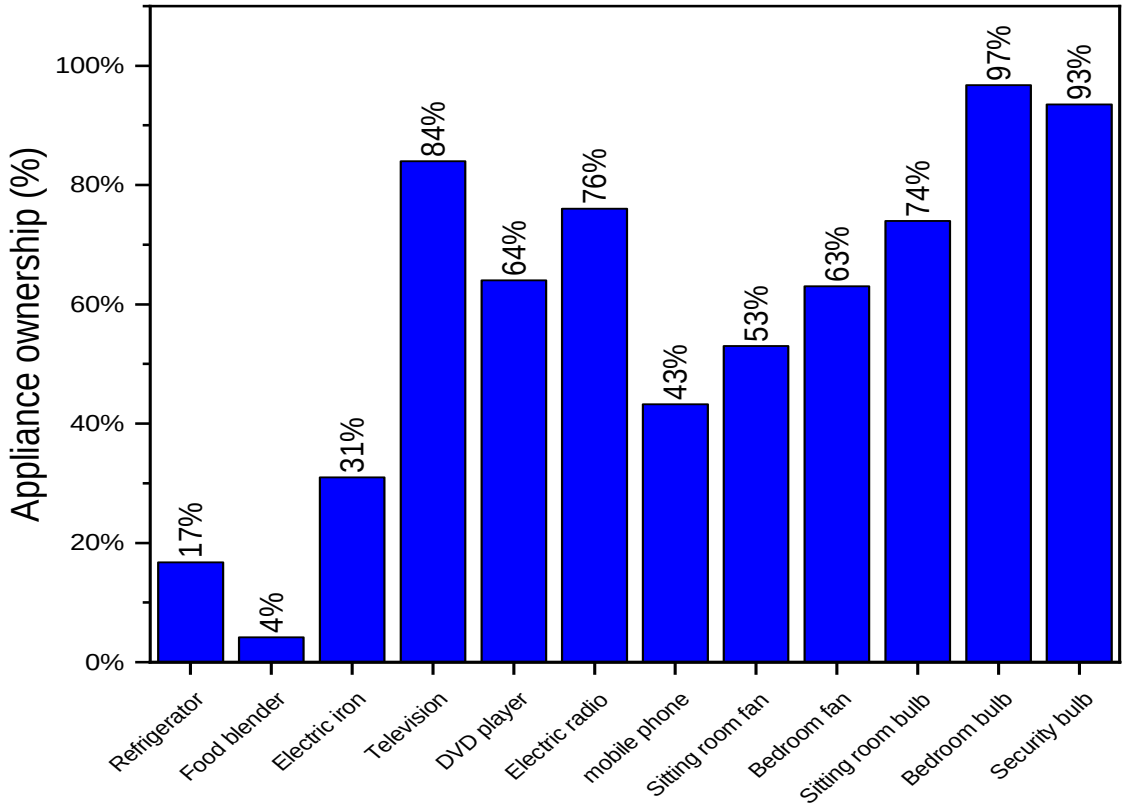

Fig. 5.8. Appliance ownership in the survey area

The percentage share of each appliance in Fig. 5.8 was calculated based on the number of surveyed households that have at least one of the appliance types. Furthermore, with respect to households' ownership of fans, survey outcomes show that about 85% of the surveyed household had at least a sitting room fan or a bedroom fan, while with respect to households' ownership of bulbs, the survey showed that all the surveyed households had at least a sitting room bulb, a bedroom bulb or an external bulb. Similarly, analysis of the electric bulbs revealed that over 96% of the total surveyed households had at least one incandescent bulb while only about 9% of the total surveyed households had at least one energy saving bulbs. Based on the four different household classification described in Section 4.1.2, the percentage share of appliance ownership in each of the four different household classes is presented in Fig. 5.9.

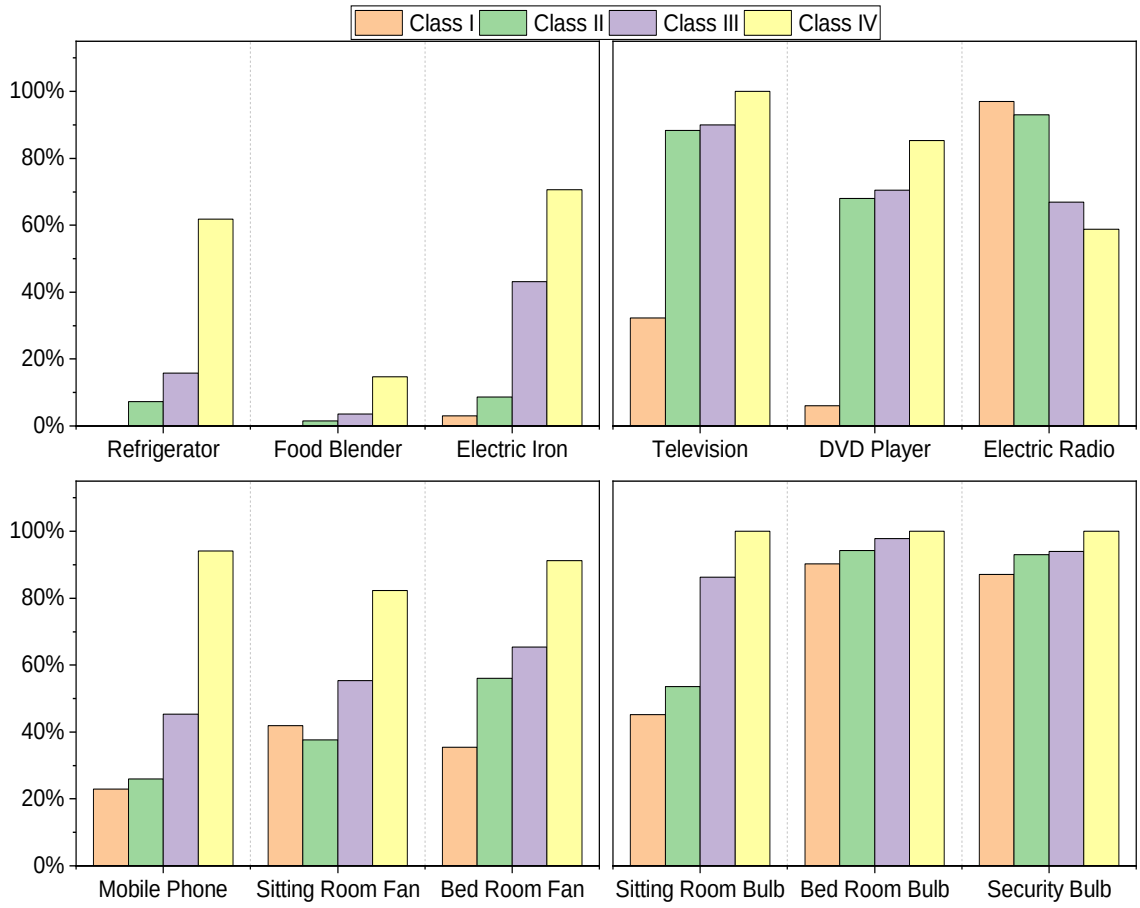

Fig. 5.9. Household class appliance ownership in the survey area

The percentage share of most of the appliances in Fig. 5.9 increases from household class I to household class IV, that is, household class I and household IV have the lowest and highest percentage share respectively. The reason for this trend is perhaps due to the social class difference between the occupants of the different household class. For example, building structures for household class IV are mostly well-planned and built within the community. Also, it is more expensive to rent a flat than to rent a room in a house. For the sitting room fan, the change in the expect increasing order between household class I and household class II, might be because households in household class II do not always have a dedicated sitting room in the house. Similarly, with respect to the electric radio, the reason for the change in the expected order might also be connected to social class difference amongst occupants of the different household class. For instance, there are perhaps lesser need for electric radio by households with higher income. While for a household with low

income, it is cheaper to buy an electric radio than to buy a television. In addition, the operating duration of household appliances can be categorised into two groups:

Short operating duration appliances: These are appliances that often operates continuous for less than an hour.
Long operating duration appliances: These are appliances that often operates continuous for more than an hour

For instance, it unlikely for food blender and electric iron to operate continuously for an hour, thus, the daily load profile for food blender and electric iron are modelled based on their average operating duration within an hour. Outcomes from the survey reveal that the operating duration for food blender and electric iron with an hour averages at 5 minutes and 10 minutes respectively. A market survey of 8 electronic stores around the surveyed community revealed that for each household appliance, some appliance makes, or models were more purchased than others. The sellers attributed the reason for the preference for an appliance model to the cost, and the durability of an appliance than on the brand name or quality. However, they emphasized that the cost of an appliance was a more dominant factor that influences the purchase of an appliance model. Furthermore, with respect to data acquired from the market survey, appliance power rating used in this study are presented in Table 5.5.

Table 5.5. Household appliance power rating

Appliance type	Appliance power rating (Watts)
Refrigerator	140
Food blender	250
Electric Iron	1000
Television	50
DVD	15
Electric radio	10
Mobile phone charger	5
Electric fan	70
Incandescent bulb	60

5.4 Occupancy model output

Based on the bottom-up modelling steps presented in Fig. 4.2 as well as the survey-based probabilities presented in Table 5.2 and Table 5.3, modelling outcomes on household occupants' transitions or behavioural patterns are presented in this section. An eight occupant's household will be used to illustrate the transitions of household occupants in this section because Fig. 5.2 shows that an eight-occupant household was the most common household size in the community.

5.4.1 Household occupants state transition

Over a 24 hours period, the transitions or behavioural patterns of household occupants in asleep (inactive home) state, active home state, or absent (away from home) state are presented in Fig. 5.10.

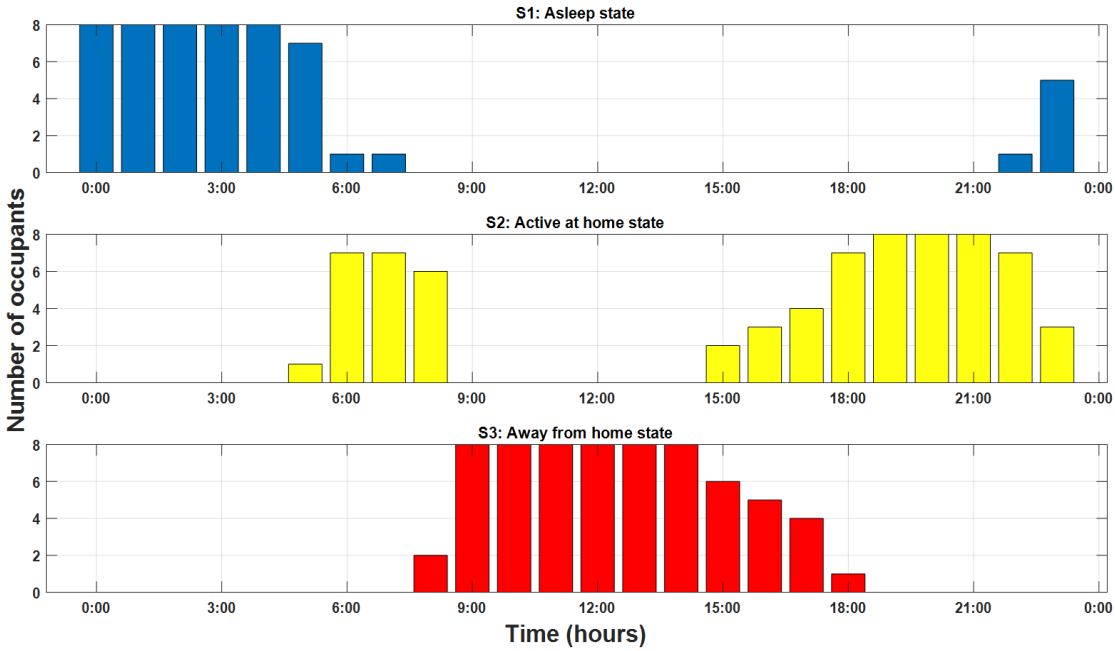

Fig. 5.10. Simulated household occupants states

The bars in Fig. 5.10 show the number of household occupants in the different state at each time step. As expected, it is evident in Fig. 5.10 that for each time step, the sum of household occupants in the three states was equal to the total number of household occupants.

5.4.2 Active occupants' activities

Over a 24 hours period, the number of active occupants performing either cleaning, cooking, or leisure activities is presented in Fig. 5.11.

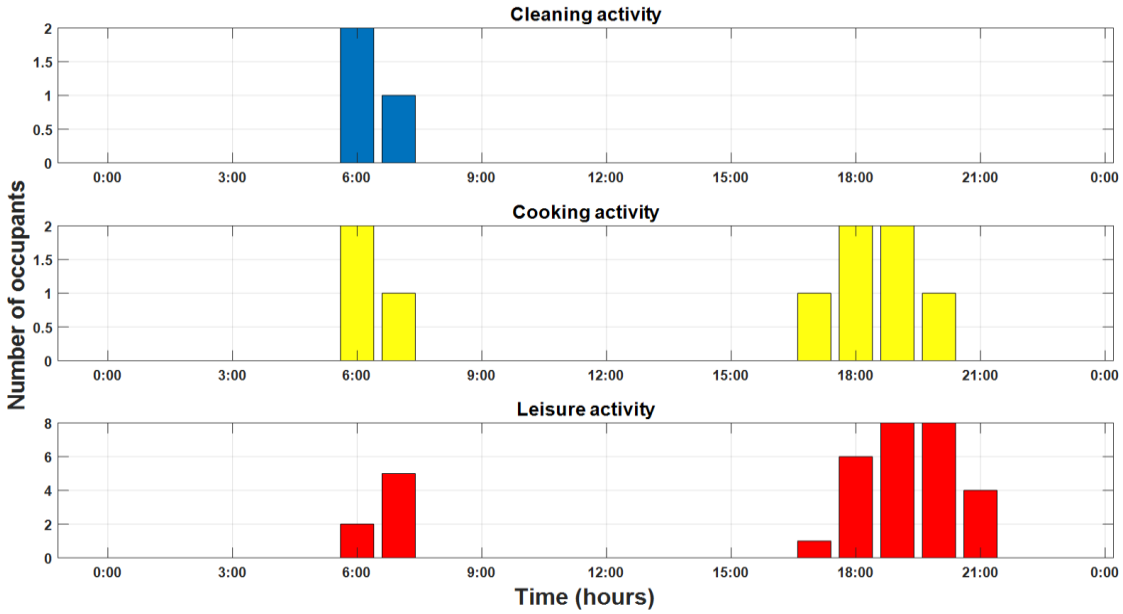

Fig. 5.11. Simulated activities of active occupants.

It is evident from Fig. 5.10 and Fig. 5.11 that the possibility of performing cleaning, cooking, or leisure activities within a time step is dependent on the presence of at least an active occupant as well as on occupant's activity time use presented in Table 5.3. Meanwhile, because an occupant can be involved in more than one activity at a time, therefore, for each time step, the sum of the number of occupants engaged in the three activities can be greater than the number of active household occupants. This is exemplified in time step 19:00 and 20:00 of Fig. 5.11, whereby the sum of household occupants engaged in cooking and leisure activities were 2 occupants and 1 occupant more than the total number of active household occupants.

5.5 Appliance energy consumption model

Appliance load profiles are modelled by converting the states of operation of appliances with their rated power presented in Table 5.5. This is similar to the approach used in [279], [308]. The operating states of appliances are simulated based on the energy consumption survey time use outcomes presented in Table 5.2,

Table 5.3, and Table 5.4. Meanwhile, to ensure that the load profile of short operating duration appliances is well captured, the load profiles of all appliances are synthesized in minutely time step.

5.5.1 Refrigerator model

Modelling of the load profile of a refrigerator is not limited to the present or absent of an active occupant, therefore, survey data on occupants' consumption behaviour cannot be used to determine the proclivity of using the refrigerator. To capture the on-time and off-time of the refrigerator, mean and standard deviation values for its on and off operation are calculated from measured data. Then, a normal distribution of the refrigerator on and off operation is simulated from the calculated mean and standard deviation values. Based on refrigerator measured data presented in [449], it is evident that the mean and standard deviation values during the refrigerator on operation were 12 minutes and 3 minutes respectively, while during off operation, mean and standard deviation values were 24 minutes and 8 minutes respectively. Over a 24-hour period, an example of a simulated refrigerator load profile is presented in Fig. 5.12.

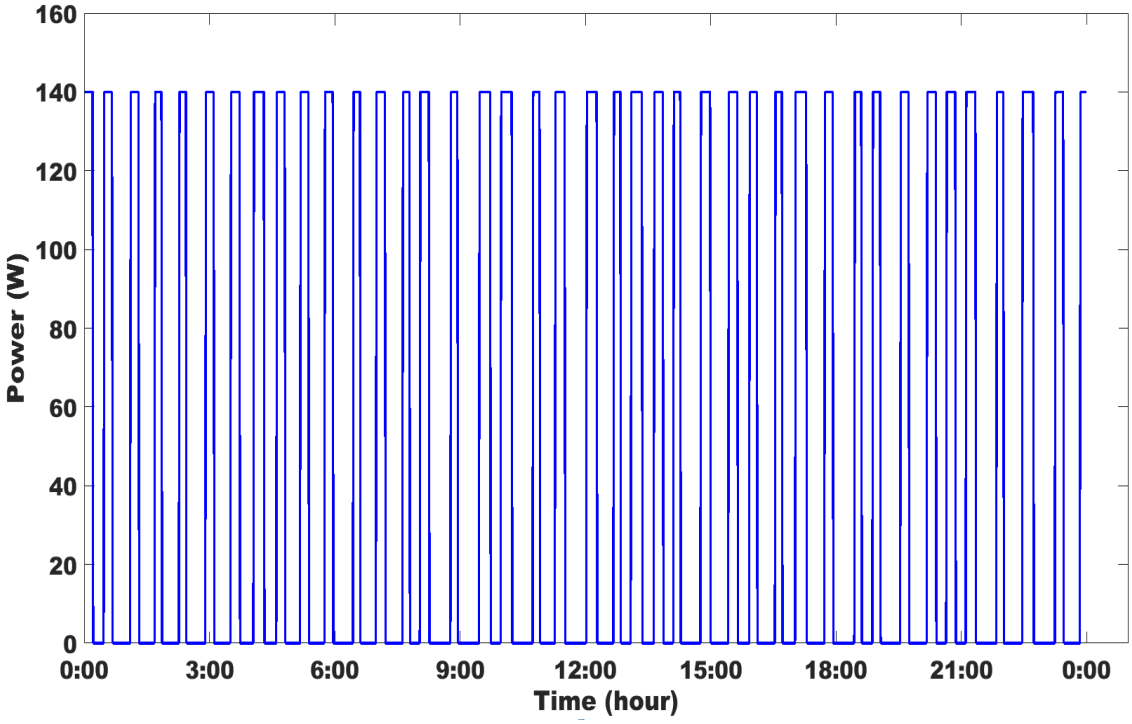

Fig. 5.12. Simulated load profile for refrigerator

5.5.2 Food blender model

Modelling of the energy consumption of food blender is based on the presence of at least an active occupant engaging in cooking activity as well as on food blender time use presented in Table 5.4. Meanwhile, because food blender is amongst short operating duration appliance, it is unlikely that it will be used continuously for an hour. Therefore, its short operating duration is considered during its modelling. Since evidence from the energy consumption survey reveals that food blender usage within an hour average at 5 minutes, during the modelling of the food blender energy consumption, it is assumed that food blender is used for 5 minutes within an hour. An example of a simulated load profile for food blender is presented in Fig. 5.13.

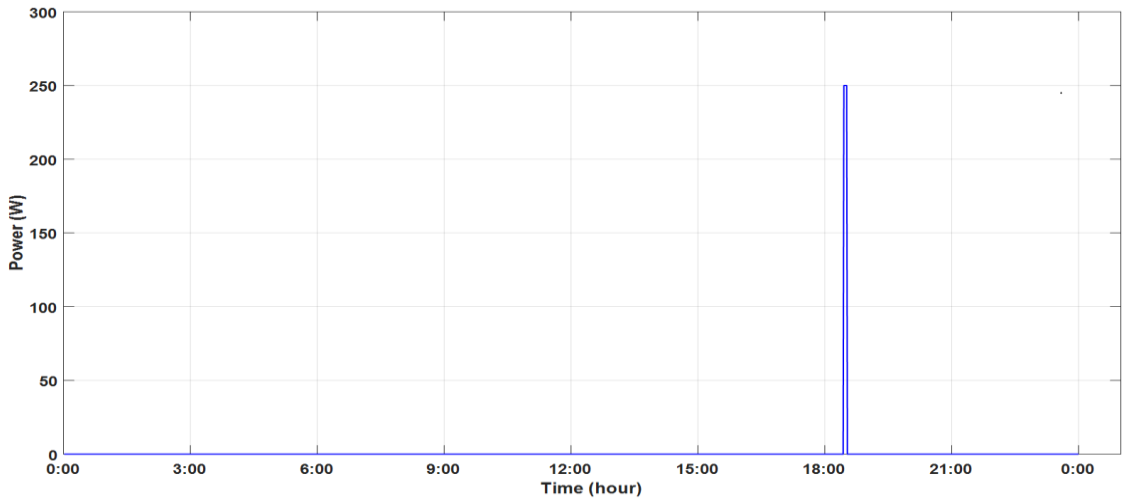

Fig. 5.13. Simulated load profile for food blender

5.5.3 Electric iron model

Modelling of the energy consumption of electric iron is based on the presence of at least an active occupant engaging in cleaning activity as well as on electric iron time use presented in Table 5.4. Just like food blender, electric iron is amongst short operating duration appliance. Thus, it is unlikely that it will be used continuously for an hour. Hence, its short operating duration is considered during its modelling. Since evidence from the energy consumption survey reveals that electric iron usage within an hour average at 10 minutes, therefore, during the modelling of electric iron energy consumption, it is assumed that electric iron operates for 10 minutes

within an hour. An example of a simulated load profile for electric iron is presented in Fig. 5.14.

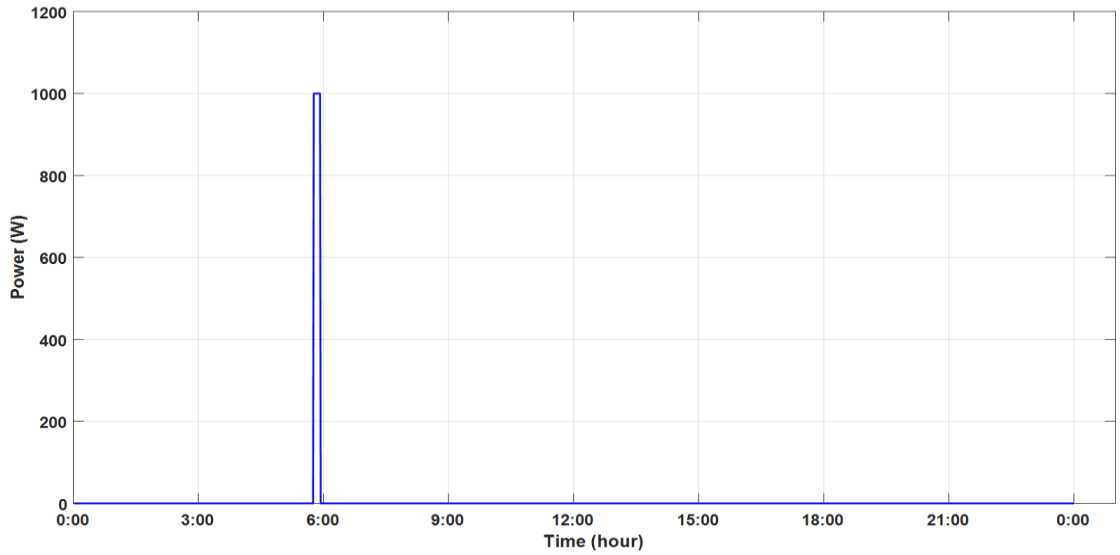

Fig. 5.14. Simulated load profile for electric iron

5.5.4 Television model

Evidence from the energy consumption survey reveals that the operation of television is not limited to the presence of an active occupant in leisure activity but rather on the presence of an active household occupant. Therefore, modelling of the energy consumption of television is based on the presence of an active occupant as well as on television time use presented in Table 5.4. An example of a simulated load profile for television is presented in Fig. 5.15.

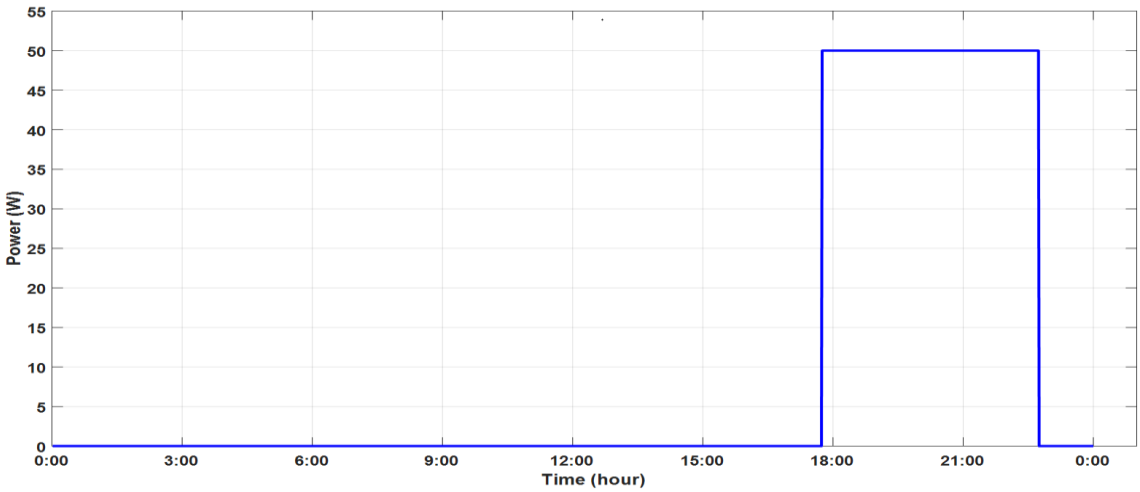

Fig. 5.15. Simulated load profile for television

5.5.5 Digital video/versatile disc (DVD) model

Evidence from the energy consumption survey reveals that the operation of DVD is dependent on the presence of an active household occupant in leisure activity. Therefore, modelling of the energy consumption of DVD is based on the presence of an active household occupant in leisure activity as well as on DVD time use presented in Table 5.4. An example of a simulated load profile for DVD is presented in Fig. 5.16.

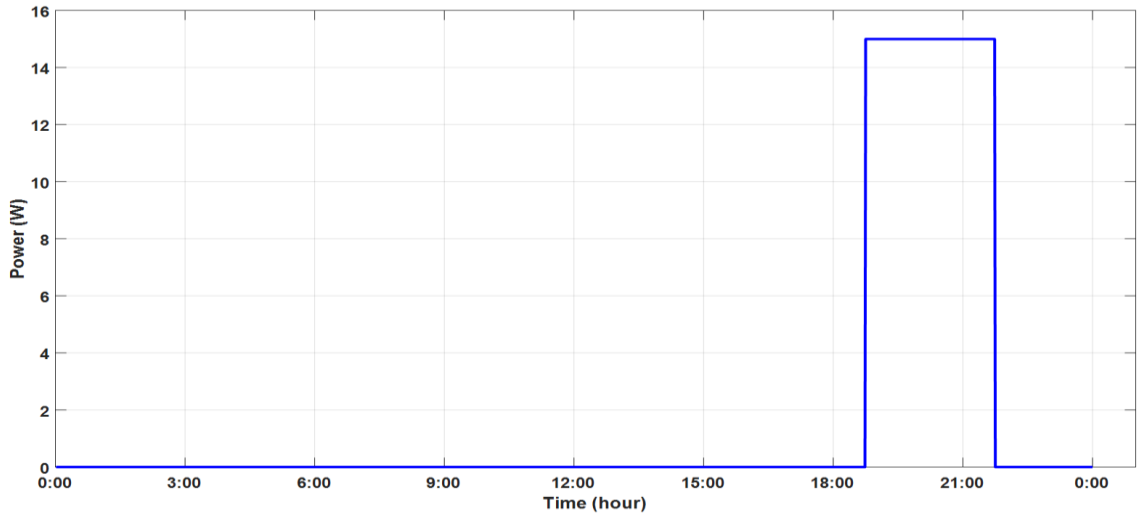

Fig. 5.16. Simulated load profile for DVD

5.5.6 Electric radio model

Just like the television, evidence from the energy consumption survey reveals that the usage of electric radio is dependent on the presence of an active household occupant at home. Therefore, modelling of the energy consumption of electric radio is based on the presence of at least an active occupant as well as on electric radio time use presented in Table 5.4. An example of a simulated load profile for electric radio is presented in Fig. 5.17.

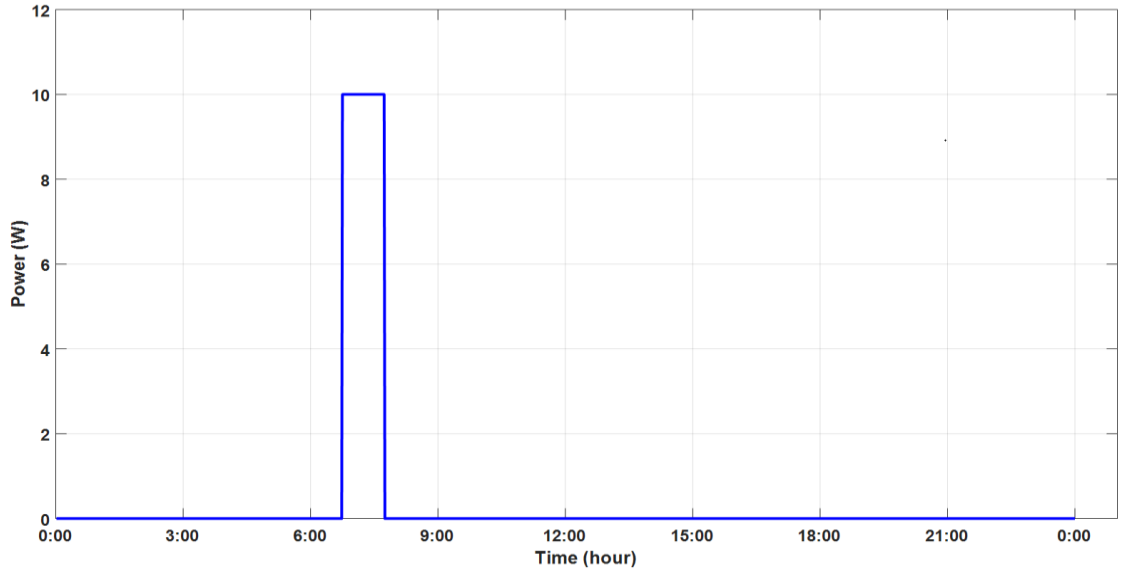

Fig. 5.17. Simulated load profile for electric radio

5.5.7 Mobile phone charger model

Mobile phones can be charged whenever there is the presence of an active occupant. It is evident from the survey that the average time to fully charge a mobile phone battery that was completely discharged is 2 hours. If mobile phones are only charged at home, then, whenever there is an active occupant, mobile phone charger daily operating duration is randomly selected for 2 hours. Therefore, the load profile of mobile phone charger load is calculated from its power rating, its quantity, and its daily operating duration. An example of a simulated load profile for a mobile phone charger is presented in Fig. 5.18.

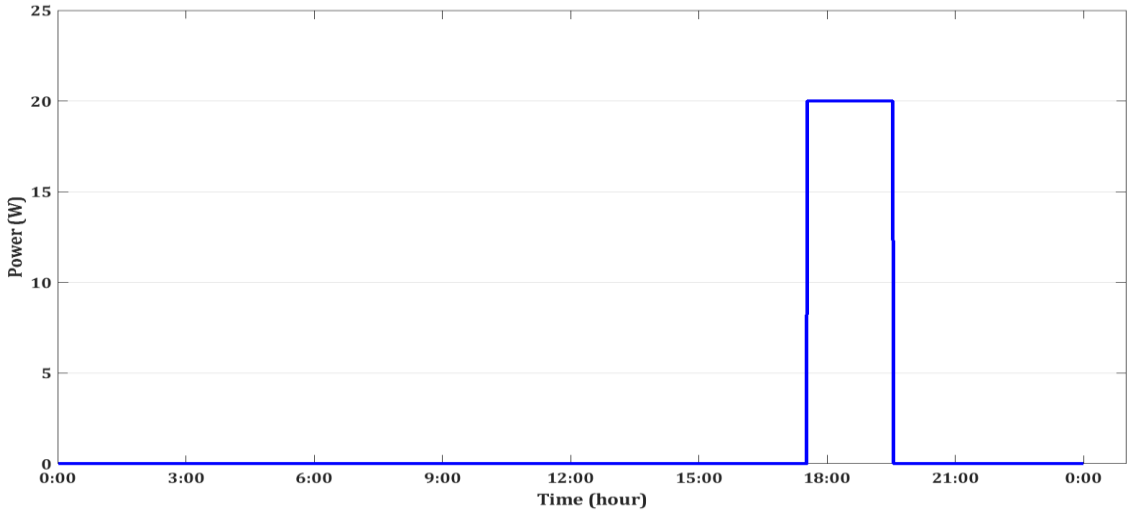

Fig. 5.18. Simulated load profile for mobile phone charger

5.5.8 Fan model

A household fan in this study is classified into sitting room fan and bedroom fan. For the sitting room fan, evidence from the energy consumption survey reveals that sitting room fan energy usage is dependent on the time that active household occupants perform leisure activities. Therefore, modelling of the energy consumption of sitting room fan is based on the presence of an active household occupant in leisure activity as well as on sitting room fan time use presented in Table 5.4. An example of a simulated load profile for sitting room fan is presented in Fig. 5.19.

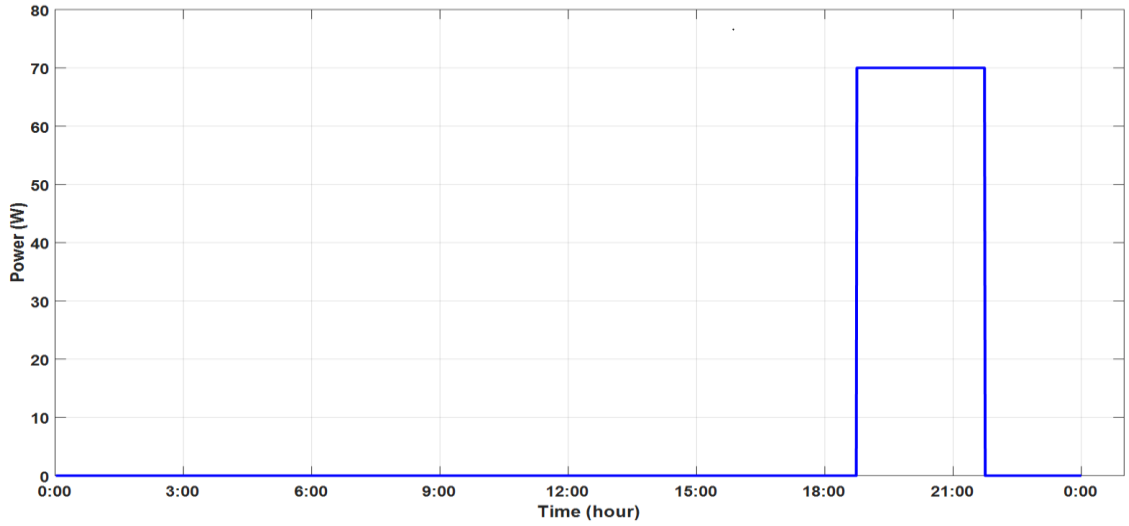

Fig. 5.19. Simulated load profile for sitting room fan

For the bedroom fan, evidence from the energy consumption survey reveals that bedroom fan energy usage is dependent on the time that household occupants' transit to asleep state. Therefore, modelling of the energy consumption of bedroom fan is based on the presence of a household occupant in an asleep state as well as on bedroom fan time use presented in Table 5.4. An example of a simulated load profile for bedroom fan is presented in Fig. 5.20.

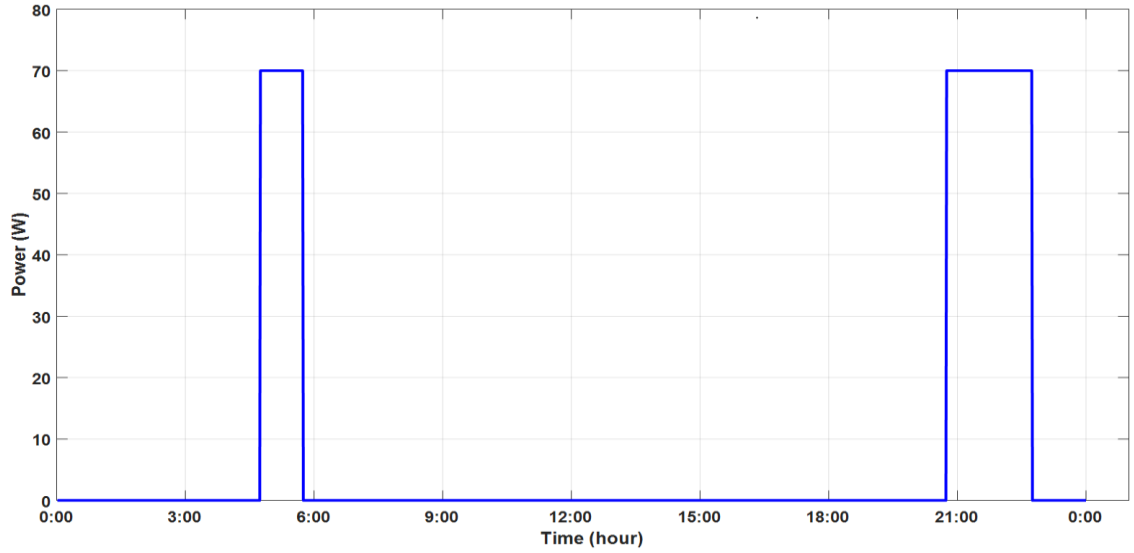

Fig. 5.20. Simulated load profile for bedroom fan

The simulated bedroom fan load profile in Fig. 5.20 shows the ability of the developed bottom-up model to capture the possibility of using an appliance at different time steps in a day.

5.5.9 Lighting model

Household lighting bulbs are classified in this study into sitting room bulb, bedroom bulb, and security bulbs. In modelling lighting bulb energy consumption, human perception to natural light level from the sun is considered by the lighting bulb end-use model. This approach has been previously used in [308], [310]. Due to human perception to natural light level from the sun, lighting energy usage is affected by seasonal and diurnal variation [310], [329], [332]. To account for natural light level for the survey location, Eqs. (4.28) – (4.31) are used to calculate the annual daily sunrise and sunset time (in minutes) for the survey area. Furthermore, because it is unlikely that household occupants will always switch-on their lighting bulbs exactly by sunset or dusk and switch-off their lighting bulbs exactly by dawn or sunrise, civil twilight[1] is used in this study to provide an off-set between dawn and sunrise in the morning and an off-set between sunset and dusk in the evening. Over a period of a

[1]Civil twilight is the point in time when the centre of the sun is 6° below the horizon.

year, the expected daily time for dawn, sunrise, sunrise, and dusk calculated with Eqs. (4.28) – (4.31) for the survey area are presented in Table 5.6.

Table 5.6. Daily time range for dawn, sunrise, sunset, and dusk

Period	Earliest Time (hour)	Latest time (hour)	Average time (hour)
Dawn	05:25	05:47	05:36
Sunrise	05:49	06:11	06:00
Sunset	17:49	18:11	18:00
Dusk	18:13	18:35	18:24

Comparison between the survey-based time use for sitting room bulb, bedroom bulb, and security bulb in Table 5.4 and the calculated time ranges in Table 5.6, shows that there are similarities between the time of switching-on of the lighting bulbs in the evening and the time of switching-off of the lighting bulbs in the morning. For the sitting room bulb model, since evidence from the energy consumption survey reveals that sitting room bulb energy consumption is also dependent on the presence of at least an active household occupant in leisure activity, modelling of the energy consumption of sitting room bulb is based on human perception to natural light level from the sun, the presence of an active household occupant in leisure activity, as well as on sitting room bulb time use presented in Table 5.4. An example of a simulated load profile for the sitting room bulb is presented in Fig. 5.21.

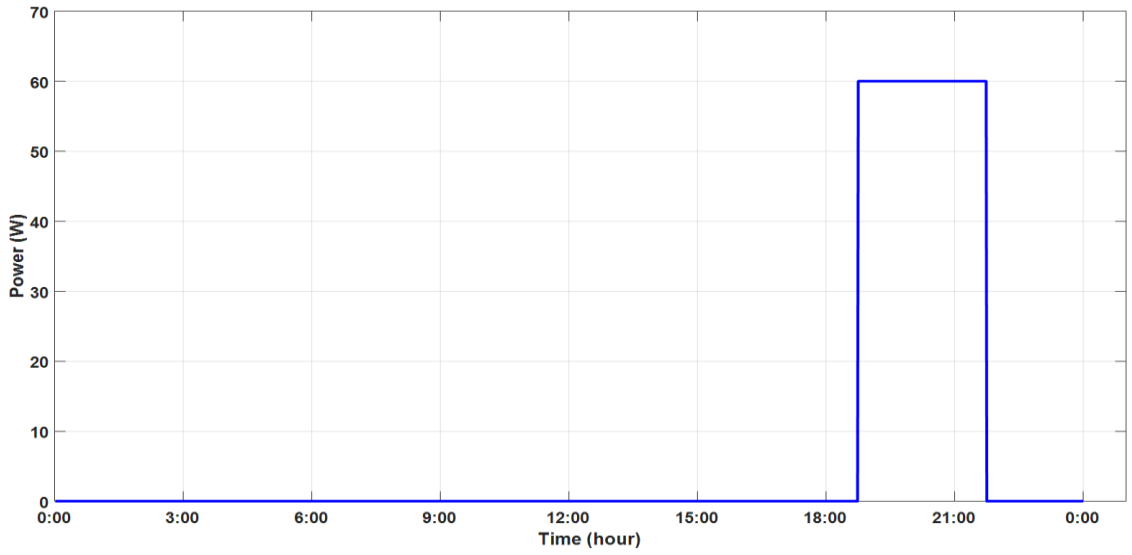

Fig. 5.21. Simulated load profile for sitting room bulb

For the bedroom bulb model, evidence from the energy consumption survey reveals that bedroom bulb energy consumption is dependent on the time that household occupants' transit to asleep state, and it is often used for short duration, that is, an average duration of use of 10 minutes per hour. So, modelling of the energy consumption of bed room bulb is based on human perception to natural light level from the sun, the presence of at least an occupant in asleep state, as well as on bedroom bulb time use presented in Table 5.4. To demonstrate the ability of the load model to capture multiple quantities of an appliance type, an example of a simulated load profile of a household with four bedroom bulbs is presented in Fig. 5.22.

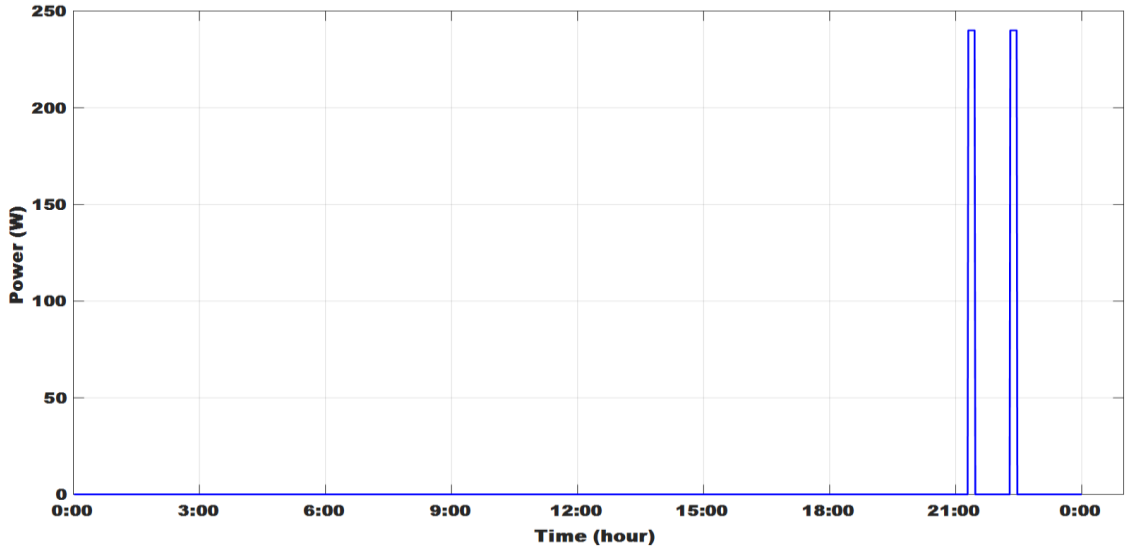

Fig. 5.22. Simulated load profile for bedroom bulb

Modelling of security bulb energy consumption is based on household occupants' response towards the level of natural light from the sun. So, households' occupants will switch-on their security bulbs at any time between sunset and dusk (twilight), while they switch-off their security lighting bulbs at any time between dawn and sunrise (twilight) bulbs in response to the level of natural light from the sun. The choice of this modelling approach is because of the similarity between security bulb time use in Table 5.4 and the calculated natural light levels time ranges in Table 5.6. For example, the number of hourly time steps between zeros conditional probabilities (switch-off states) and the ones conditional probability (switching-on states) is similar to the number of average hourly time steps between sunrise and sunset in Table 5.6. Furthermore, another motivation for using only human

perception to natural light level from the sun to model security bulb time use is because the potential switching-on and switching-off of security bulbs are calculated in minutely time steps. An example of a simulated load profile of a household with four security bulbs is presented in Fig. 5.23.

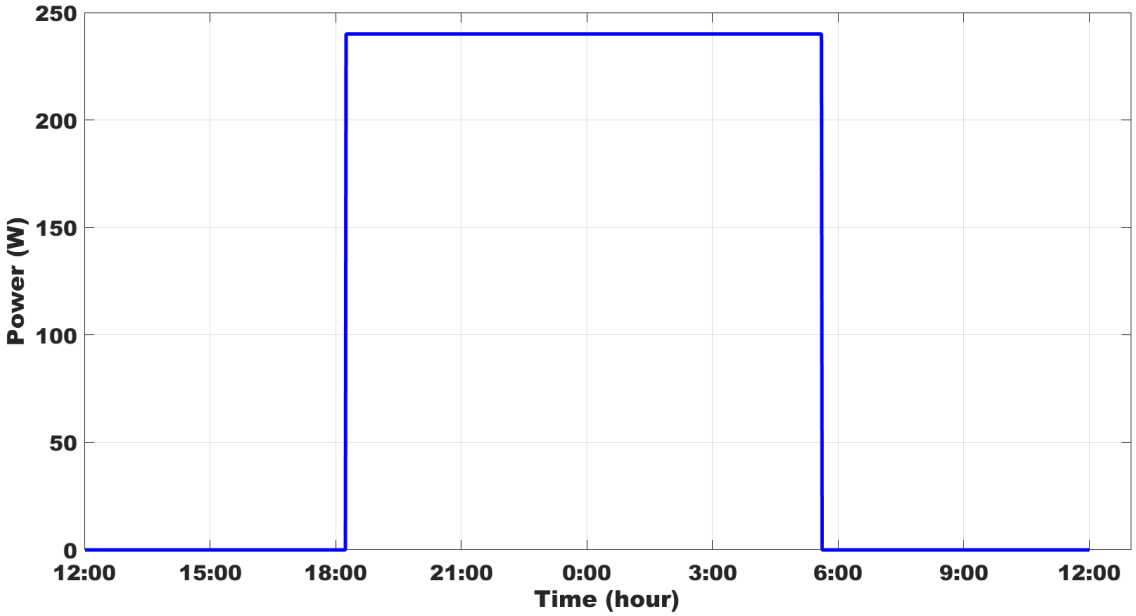

Fig. 5.23. Simulated load profile for security bulb

In comparison to the time axis of other simulated appliance plots in Fig. 5.13 to Fig. 5.22, the time axis of Fig. 5.23, has been adjusted to start from 12:00 to 12:00 in order to clearly capture the operating time of security bulb. Simulation of the security bulb operation revealed that the security bulbs were switched-on by 5:46 and switched-off by 18:06 on a simulated day.

5.5.10 Simulation of household load profile

As showed in the load profile implementation scheme in Fig. 4.2, a household load profile is synthesized from the aggregation of all the appliance load profiles within a household. An example of a simulated load profile for a household with refrigerator, food blender, electric iron, television, DVD, electric radio, mobile phone, sitting room fan, bedroom fan, sitting room bulb, bedroom bulb, and security bulb is presented in Fig. 5.24.

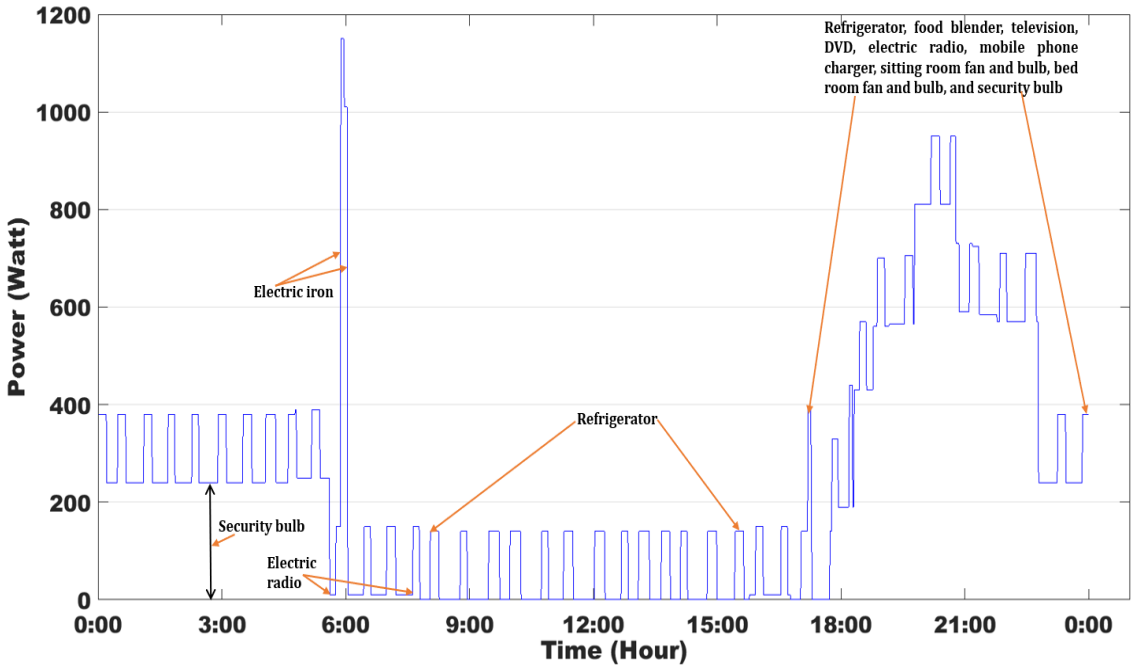

Fig. 5.24. Simulated load profile for a household

It is observed the household load profile in Fig. 5.24 has a high energy consumption in the night. Simulation result show that the annual energy consumption for the household in Fig. 5.24 is 2385 kWh. The household incandescent bulbs which comprise of a sitting room bulb, 4 bed bedroom bulbs, and 4 security bulbs, account for 1108 kWh (46.5%) of the annual energy consumption. If each of the 60-watt incandescent bulbs with a brightness level of 500 – 700 lumen were replaced by compact fluorescent lamp (CFL) and light emitting diode (LED) lamp of similar brightness level, that is, by either a CFL of 11-watt or a LED lamp of 7-watt, the annual energy consumption for the household will be reduced to 1480 kWh or 1406 kWh respectively.

To investigate the impact that this study major energy consumption drivers, i.e., occupants' consumption behaviour, number of bedrooms and number of occupants, have on household's energy consumption patterns, 10 surveyed households load profiles are presented in Fig. 5.25.

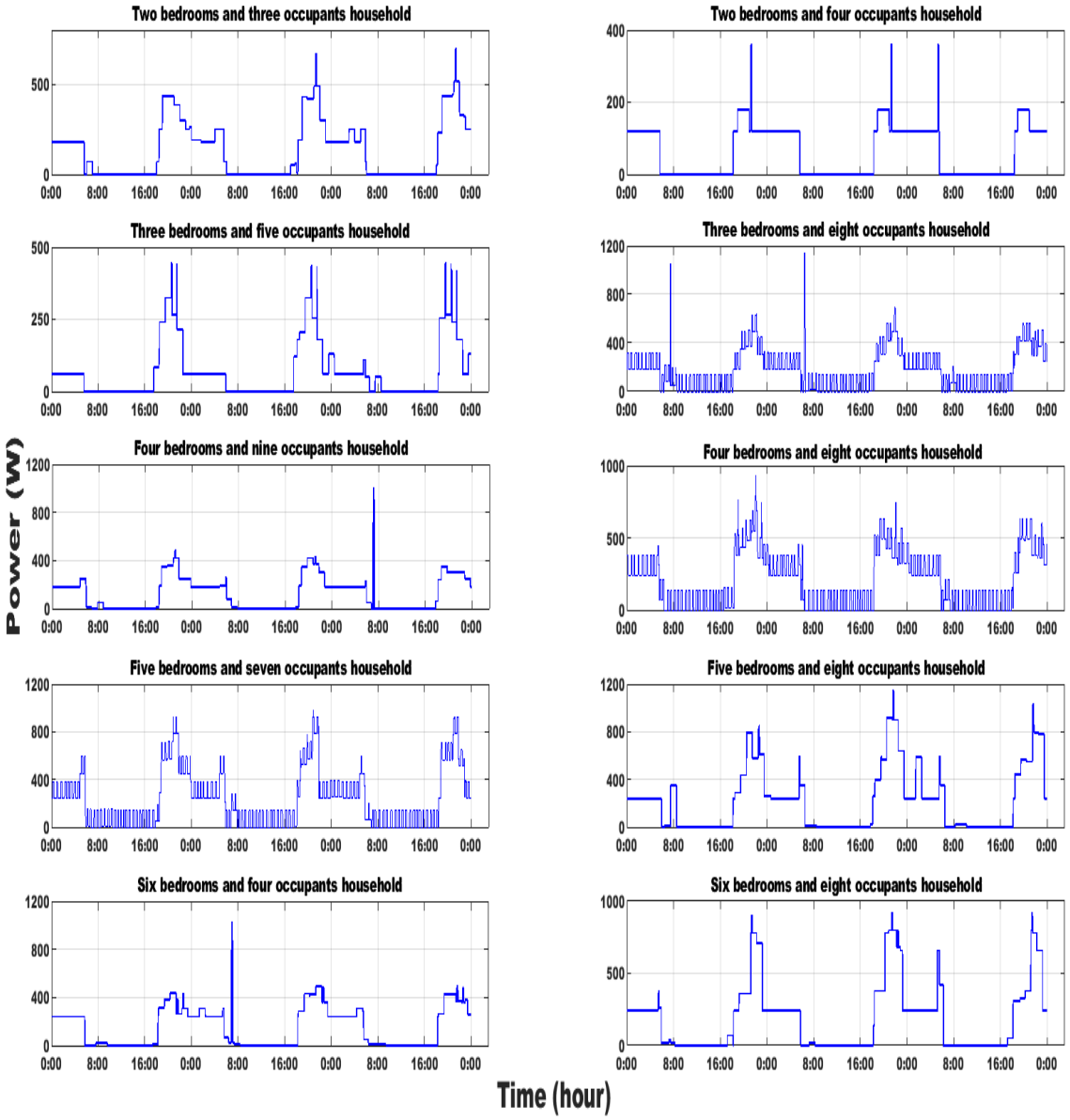

Fig. 5.25. Energy consumption pattern of 10 surveyed households

In Fig. 5.25, all the 10 household load profiles had characteristic morning and evening peaks, as well as noticeable daily variations in their energy consumption patterns. The observed daily variations in load profile were directly linked to occupants' consumption behaviour and appliance ownership in a household. Furthermore, comparison of households shows that some households with more bedrooms had increase energy consumption because they had more quantity of some appliances, while some households with more occupants had increase energy consumption because they had higher chances of having an active occupant at home

daily. This suggest that the number of bedroom and the number of occupants in a household have limited influence on energy consumption because their impact on household energy consumption is not representative of all households. Therefore, occupants' consumption behaviour and appliance ownership are the major energy consumption driver that influence load profile modelling in this study.

To check if load profile simulated by the developed model is a true representation of the questionnaire collated data, the relationship between the annual energy consumption of an appliance when it is calculated directly from the questionnaire collated data and when it is simulated by the developed load profile model is evaluated. For a household, an appliance annual energy consumption is calculated from questionnaire collated data by multiplying its power rating, its quantity, and its usage duration. For the 273 surveyed households, an appliance total annual energy consumption is calculated by aggregating its annual energy consumption in each household. Simulated and calculated total annual energy consumption per household appliance are presented in Table 5.7.

Table 5.7. Simulated and calculated total annual appliance consumption

Appliance	Simulated total annual energy consumption		Calculated total annual energy consumption	
	kWh	%	kWh	%
Refrigerator	20273	6.80	20236	6.79
Food blender	133	0.04	106	0.04
Electric Iron	1263	0.42	1281	0.43
Television	17833	5.98	17829	5.98
Digital video disc	2936	0.98	2895	0.97
Electric radio	2470	0.83	2462	0.83
Mobile phone charger	1078	0.36	1037	0.35
Sitting room fan	16109	5.40	16068	5.39
Bedroom fan	26932	9.03	26950	9.05
Sitting rood bulb	21037	7.06	21051	7.07
Bedroom bulb	4829	1.62	4814	1.62
Security bulb	183248	61.47	183214	61.49
Total annual consumption	298121	100.00	221708	100.00

From Table 5.7, appliance simulated and calculated total annual energy consumption per household is 1092 kWh and 1091 kWh respectively. Despite the closeness of these annual energy consumption values, the drawback with calculating annual energy consumption directly from questionnaire collate data is that this method cannot capture the daily variation in energy consumption. Meanwhile, to evaluate the difference between appliance simulated and calculated total annual energy consumption, a d-bar analysis was carried here. 5% is selected as for the significance level for rejecting the null hypothesis, and the null hypothesis (H_0) and alternative hypothesis (H_a) are defined as follow:

H_0: There is significant different between appliance simulated and calculated total annual energy consumption.

H_a: There is no significant different between appliance simulated and calculated total annual energy consumption.

When a d-bar analysis of the appliance simulated and calculated total annual energy consumption data presented in Table 5.7 was performed, the significant level calculated was 2.6%. The calculated significant level is less than the selected critical value of 5%, therefore, the null hypothesis is rejected. This implies that the difference between appliance simulated and calculated total annual energy consumption is statistically insignificant.

5.6 Simulation of community load profile

In modelling the community load profile, a total of 409 households was selected. The selected number of households within the community was calculated by dividing the estimated number of residential customers connected to the low voltage distribution network in the survey location (10,639) by the number of communities in the survey location (26). The number of households (409) required for simulating the community load profile is more than the number of completely surveyed households (273). To limit simulation bias during the aggregation of households' load profiles, the selection of households from amongst the four residential household classes is determined by the ratio in which the housing population was distribution amongst the four residential household classes in the survey location.

According to national population and housing census data, Esan North-East LGA housing population distribution ratio between household Class I, Class II, Class III, and Class IV is 0.114:0.253:0.508:0.125 respectively [388]. Therefore, out of the 409 households load profiles required for simulating the community load profile, 208 households load profiles should be simulated from within household class III. An illustration of a simulated load profile for the surveyed community is present in Fig. 5.26.

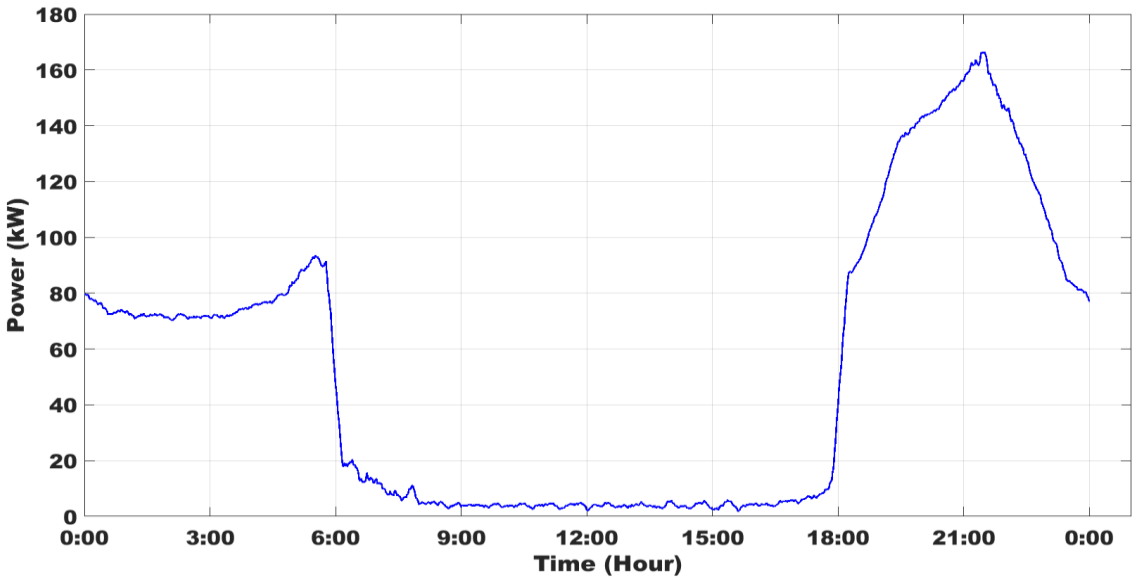

Fig. 5.26. Simulated community load profile for the survey area

Fig. 5.26 shows that a peak power of about 94 kW and 166 kW were drawn in the morning and evening respectively, by the community households. When the bottom-up model was run for a year, an annual energy of 467858 kWh was consumed by the 409 community households. So, the average annual (daily) energy consumption per household in the community is 1144 kWh (3.13 kWh). The household load profile (Fig. 5.24) and the community load profile (Fig. 5.26) are associated with morning and evening peaks. For Fig. 5.24, there was a higher power peak in the morning than in the evening (unusual). This was because of the power drawn by the electric iron. While for Fig. 5.26, there was an expected higher peak in the evening than in the evening. This is because the aggregation of households' load profiles allows for the averaging of appliance usage. Typically, more variability in household energy consumption; which can lead to power network stability issues or the need for more robust network protection [447], [450], is expected from a household load profile

than from a community load profile. In fact, the lower variability in community load profiles in comparison to household load profiles is one of the benefits of a community grid system over a single household or standalone energy system.

Furthermore, the high energy consumption household in Fig. 5.24, has an annual energy consumption value (2385 kWh) that is much higher value than the average annual energy consumption per household in the community (1144 kWh). The wide difference in annual energy consumption can serve as one of the motivations why community households with higher appliance ownership should combine their resources and/or partner with governmental and non-governmental institutions in establishing a community grid system.

With respect to household's monthly electricity bill presented in Fig. 5.7, an indirect verification of the survey outcome is carried out with the average annual energy consumption per household (1144 kWh). Based on the information provided by Uromi service unit, a single-phase line is mainly used to supply electricity to households within the survey area. The unit electricity rate (₦/kWh) for the sales of 1kWh of electricity to residential customers connected to a single-phase line is ₦ 31.26 [451]. Because the average monthly energy consumption per household in the survey area is 95 kWh, the equivalent monthly electricity bill for a single-phase household with a daily average electricity availability of 4 hours (based on the average daily electricity dispatch to the survey area by the utility company) is ₦ 495, but if the daily average electricity availability is 6 hours (based on the survey area average daily electricity availability that was evaluated from the time use survey), the equivalent monthly electricity bill for the single-phase household is ₦ 742. So, the monthly electricity bill for households with a daily electricity availability of either 4 or 6 hours (i.e. ₦ 495 and ₦ 742 respectively) is less than the amount paid for electricity consumption by 90% of the surveyed households (see Fig. 5.7).

The reason for the difference is perhaps associated with the existing accusation by residential customers that they are made to pay more for the energy they consume, when estimated billing system are used by energy providers [153]. If permission is granted by the utility company to access the monthly generated electricity bills for

households in the survey area and the hourly electricity dispatch to the survey area, more detailed verification will be performed in future studies. Meanwhile, based on the survey outcomes on appliance ownership and the proclivity for appliance use presented in Fig. 5.8 and Table 5.4 respectively, the annual energy consumption for the different appliances, and the effect of replacing the commonly used incandescent bulb in the survey area with either CFL or LED bulb is presented in Table 5.8.

Table 5.8. Energy saving bulbs influence on total energy consumption

Appliance	Incandescent bulb		CFL		LED bulb	
	kWh	%	kWh	%	kWh	%
Refrigerator	63823	13.64	63823	28.79	63823	31.66
Food blender	177	0.04	177	0.08	177	0.09
Electric Iron	2091	0.45	2091	0.94	2091	1.04
Television	26908	5.75	26908	12.14	26908	13.35
Digital video disc	3971	0.85	3971	1.79	3971	1.97
Electric radio	3084	0.66	3084	1.39	3084	1.53
Mobile phone charger	1722	0.37	1722	0.78	1722	0.85
Sitting room fan	23514	5.03	23514	10.61	23514	11.66
Bedroom fan	41161	8.80	41161	18.57	41161	20.42
Sitting rood bulb	28429	6.08	5212	2.35	3317	1.65
Bedroom bulb	5286	1.13	969	0.44	617	0.31
Security bulb	267692	57.22	49077	22.14	31231	15.49
Total annual consumption	467858	100.00	221708	100.00	201615	100.00

As shown in Table 5.8, when incandescent bulbs are used, 64% of the annual energy consumption was for lighting. However, if incandescent bulbs are replaced by CFL or LED bulbs, there is an annual reduction in the community energy consumption by 53% and 57% respectively. Furthermore, the percentage of annual energy consumption that is used for lighting was reduced to 25% and 17% when CFL or LED bulbs are used respectively. Despite the enormous reduction in residential energy consumption by using energy saving bulbs, it is surprising that there is low usage of energy saving bulbs. This challenge is not limited to the surveyed community, rather it is a national problem [281], [452]. For the community, the

relationship between household classes annual energy consumption and number of bedrooms is presented in Fig. 5.27.

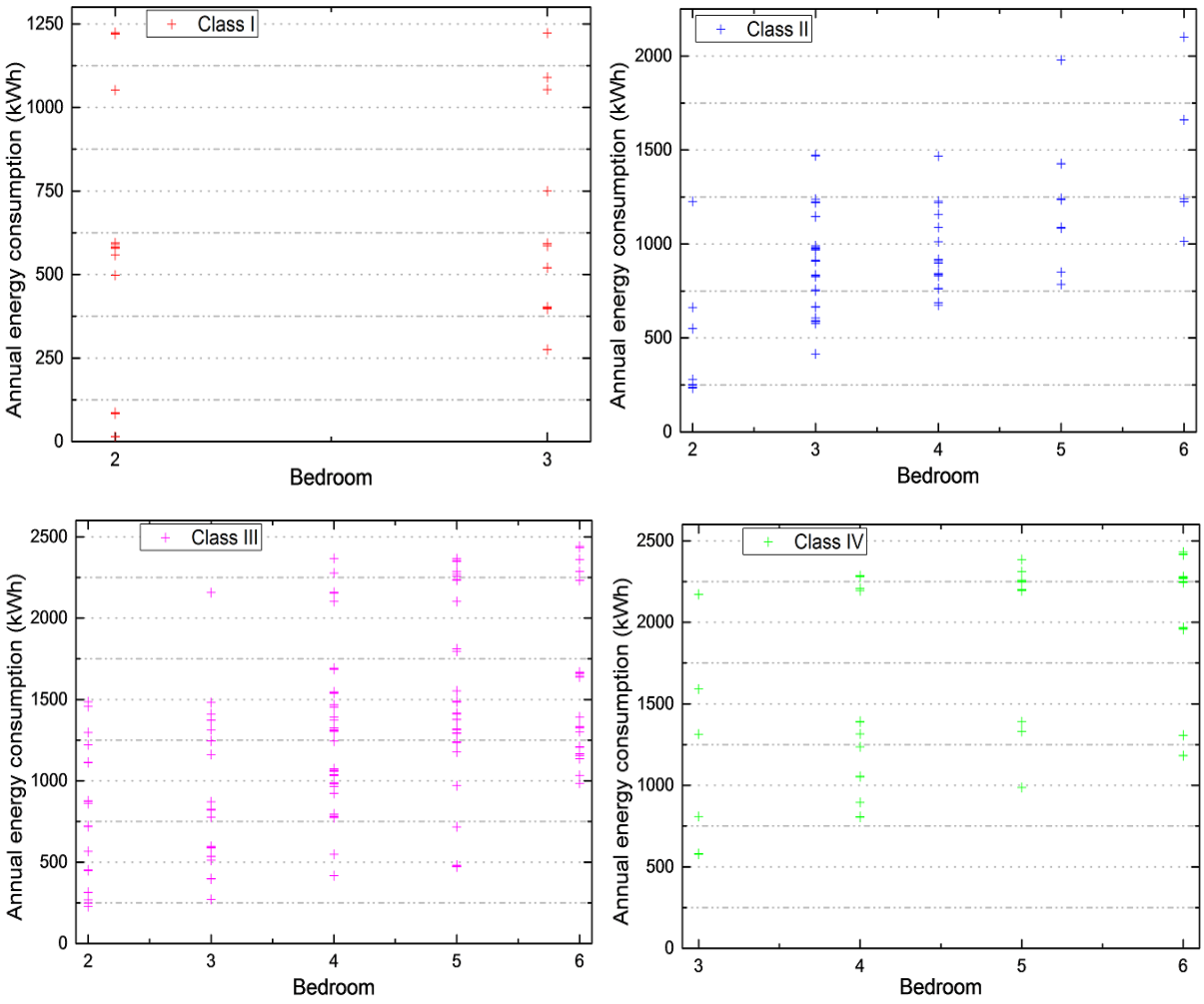

Fig. 5.27. Relationship between households' annual energy consumption and their number of bedrooms for each of the household classes

It is evident from Fig. 5.27 that For the community, the relationship between household classes annual energy consumption and number of bedrooms is presented in (see Fig. 5.9shows that these households had low appliance ownership. Also, because these households are traditional and informal housing structures, the maximum number of bedrooms was 3. Household classes percentage distribution for different range of annual energy consumption values is presented in Fig. 5.28.

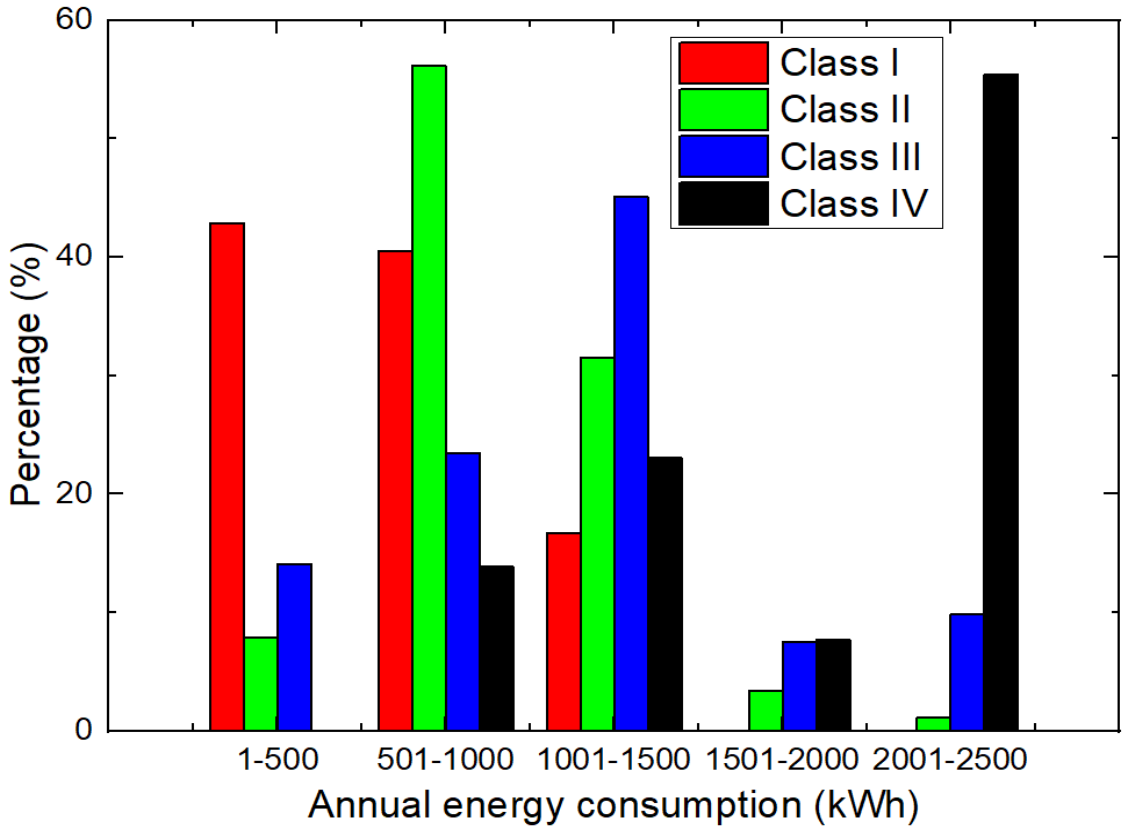

Fig. 5.28. Household classes percentage distribution for different range of annual energy consumption values

In general, Fig. 5.28 shows that for the different energy consumption range of values, each of the 4 household classes had substantial percentage of their households' annual energy consumption within the 501 - 1000 kWh and 1001 - 1500 kWh range of values. Meanwhile, household Class I, Class II, Class III and Class IV had their households' annual energy consumption distributed mostly in 1 - 500 kWh, 501 - 1000, 1001 - 1500, and 2001 - 2500 range of values respectively. Descriptive statistical analysis of the distribution of households' energy consumption in the 4 household classes is presented in Table 5.9.

Table 5.9. Analysis of simulated household class energy consumption

Indicators	Class I	Class II	Class III	Class IV
Household population	42	89	213	65
Sum (kWh)	22783	82459	246494	116122
Maximum (kWh)	1224	2101	2442	2431
Minimum (kWh)	14	234	150	576
Mean (kWh)	542	927	1157	1786
Standard deviation (kWh)	338	361	522	601
Skewness	0.57	0.52	0.50	-0.72
Coefficient of variation (%)	62.41	38.99	45.13	33.66

In Table 5.9, the coefficient of variation shows that there was high relative variability in annual energy consumption for all the household classes. Household Class I had the highest coefficient of variation value because many of its households' low annual energy consumption are not clustered, therefore, its standard deviation value was high when it is compared with its mean value. Household Class IV had the lowest coefficient of variation value because many of its households' high annual energy consumption values are clustered, therefore, its standard deviation value was low when it is compared with its mean value. Similarly, household Class II coefficient of variation was lower than that of household Class III because households Class III comprises of many high energy consumption households as well as many low energy consumption households than in household Class II.

5.7 Developed load profile model verification

An indirect approach was used to validate the developed demand model because the injection sub-station is the closest point that PHCN measures hourly electricity dispatch to residential customers. Therefore, residential customers population and hourly electricity dispatch data for the survey location collected from PHCN was used to perform the indirect validation of the demand model. Because of data protection policy, permission for data collection was granted for only three months (January 2019 to March 2019). In the survey location, energy consumption during weekend and weekdays are alike, and electricity is daily dispatch for an average of

4 hours. Furthermore, the residential customer population is 7881 and the monthly average electricity dispatch is 345839. Therefore, calculation of average annual electricity consumption per residential customer is presented in Table 5.10.

Table 5.10. Average annual electricity consumption per residential customer

Energy Allocation	kWh
Monthly average electricity dispatch	345839[a]
Equivalent monthly electricity dispatch for 24 hours daily availability	2075034[b]
Monthly electricity dispatch to electricity bills paying customers	1016767[c]
Monthly electricity dispatch to electricity bills paying residential customer	833749[d]
Monthly average electricity consumption per residential customer	106[e]
Annual (daily) average electricity consumption per residential customer	1270 (3.48)

[a] this value correspond to a daily average electricity availability of 4 hours, [b] for 24 hours (steady) electricity supply, [c] this value was calculated by subtracting the total estimated energy loss of 51%, that is, 15% due to transmission and distribution losses and 36% due to collection losses [43]. [d] this value was calculated by multiplying electricity dispatch to bills paying customers by the percentage of residential customers in the survey location. According to PHCN, 82% of the customers in the survey location are residential customers, [e] this value is calculated by dividing [d] by the residential customer population.

In Table 5.10, the value of 3.48 kWh calculated as residential customers daily average energy consumption is close to the simulated value of 3.13 kWh. It is hoped that the difference between the calculated and simulated values will reduced if energy consumption data were measured more closer to residential customers loads. Meanwhile, from a survey on the energy consumption of 480 rural households in south-west Nigeria, it was reported that the daily average energy consumption of households was 2.32 kWh [59]. Even though the effect of household-occupancy behaviour on appliance usage was not considered during the survey in [59], and both surveys (i.e., the survey here and the survey in [59]) were performed in different region of the country, the difference in daily average energy consumption

per household is perhaps link to the rapid growth in electricity demand in developing economies [1], [3]. This is because different household energy consumption surveys were carried out 17 years apart.

5.8 Model availability

The stochastic occupancy-based demand model was developed with the aid of MATLAB. The MATLAB code for the developed demand model is presented in appendix C of this thesis. Analysed market and household energy consumption survey data used for simulating the load profiles in this study can also be shared, provided necessary acknowledgement of this thesis is guaranteed.

5.9 Chapter conclusion

A stochastic load model was developed here to generate the load profile of households in a developing country. This model combines surveyed households' occupancy behaviour and appliance ownership with census-based household classes proportion data and use Markov-chain technique to continuously synthesize data that represent household occupants' activity pattern. Therefore, realistic load profiles that can capture diversity between households or group of households, the effect of load coincidence, annual and diurnal variation, and short time-scale fluctuations is generated by the stochastic model.

Evaluation of the simulated community load profile shows that incandescent bulbs accounts for 64% of the community's annual energy consumption. But when the commonly used incandescent bulbs were replace with CFL and LED bulbs, an annual energy savings of 53% (with CFL) or 57% (with LED bulbs) was achieved. Therefore, it is recommended that policies and regulations that would encourage the use of energy saving bulbs should be implemented because substantial energy savings in household energy consumption can be achieved by using energy saving bulbs.

In-direct validation of the developed stochastic model with utility measured data shows that households' average daily consumption calculated from utility measured energy dispatch is 3.48 kWh day^{-1} and from the developed model, it is 3.13

kWh day^{-1}. It is hoped that the difference between the measured and simulated values can be reduced if energy consumption data were measured more closer to residential customers loads. Therefore, in developing countries without national measured time use data, this developed modelling approach can be applied to model the load profiles of households and communities.

Chapter 6 ESTIMATION OF GLOBAL SOLAR RADIATION FOR PHOTOVOLTAIC APPLICATION

Global solar radiation is a measure of the amount of solar energy received by the earth's surface. During the planning of a solar energy project, global solar radiation data are used for energy projection and economic viability studies. The amount solar energy received is location dependent [212], [213], [417], and due to solar energy stochastic natural, there is substantial variation in diurnal and seasonal global solar radiation. So, when a solar energy project is evaluated, high-resolution solar radiation data should be used because minutely or hourly global solar radiation data will guarantee better design accuracy than daily or monthly global solar radiation data [230], [441], [453]. Furthermore, load profiles are characterised by daily varying energy consumption patterns and peak load (see Fig. 5.25). So, for optimal design of a solar energy project, high-resolution global solar radiation data is required to carry out an extensive study of the relationship between the solar energy supplied and the energy demand. Consequently, hourly solar radiation data is used in this study for techno-economic analysis of the solar system in Chapter 7.

Long-term solar radiation data is required to capture solar radiation seasonal variation, but the cost of purchasing long-term hourly solar radiation is expensive. An alternative approach is to calculate long-term hourly solar radiation from weather station long-term measured daily solar radiation data. In Nigeria, solar radiation is measured by only few Nigerian meteorological agency (NiMet) weather stations, and amongst the few NiMet weather stations that measures solar radiation, only daily global solar radiation received on a horizontal surface is measured.

In locations without measured solar radiation data, long-term daily measurement of other related meteorological parameters can be used to estimate daily horizontal surface global solar radiation. In literature, authors have used NiMet's long-term daily measured meteorological parameters such as temperature, sunshine hours, relative humidity, cloud cover, and precipitation data to derive solar radiation estimation models [212], [417], [418], [427], [431], [454]. Amongst the derived

solar radiation estimation models, there are noticeable variations in the model's mathematical formation/expression as well as in the choice of the meteorological parameter(s) used for estimating daily horizontal surface global solar radiation. Therefore, it is difficult to ascertain the most suitable model as well as the most dominant NiMet's meteorological parameter(s) that can estimate daily horizontal surface global solar radiation. Also, the minimum time span that modern data should be collected to achieve substantial accuracy during the estimation of daily horizontal surface solar radiation is unknown. Due to seasonal variation that arises from the revolution of earth round the sun, estimated horizontal surface solar radiation will not represent the optimal solar energy yield of a location. Therefore, to estimate the hourly optimal solar energy yield of the studied location (Esan North-East LGA in Nigeria), the following research work are performed in this chapter:

1. Performance evaluation of different global solar radiation models as well as evaluation of dominant meteorological parameter(s) that influences the estimation of daily global solar radiation.

2. Determination of the minimum time span that modern data should be collected to achieve substantial accuracy in estimating the solar radiation of the studied location.

3. Estimation of hourly horizontal global solar radiation from the estimated daily horizontal global solar radiation of Esan North-East LGA.

4. Evaluation of the optimal monthly, quarterly or annual global solar radiation produced from a PV panel that is positioned on an angled surface.

6.1 Meteorological data collection and performance evaluation of global solar radiation estimation models

In this study, ground measured NiMet's meteorological parameters are acquired. The acquired NiMet's measured meteorological parameters serve as input parameters for evaluating the performance of global solar radiation estimation models as well as evaluating if there are dominant meteorological parameter(s) that influences the estimation of daily global solar radiation. 15 global solar radiation estimation models are selected for this study. The selected models comprise of

linear, polynomial, exponential, logarithmic, and hybrid models. These selected global solar radiation estimation models were presented in Table 4.1 to Table 4.3 of Chapter 4.

The top-performing model amongst the selected estimation models is used to model the daily global solar radiation of the studied rural community (Esan North-East local government area, Edo state, Nigeria) and evaluate the location solar energy potential. So, daily recorded meteorological data collected from the nearest NIMet's weather station (Benin weather station) are used for the performance evaluation of the selected global solar radiation estimation models. A map showing the location of NiMet Benin weather station and Esan North-East local government area, Edo state, Nigeria (studied location) is presented in Fig. 6.1.

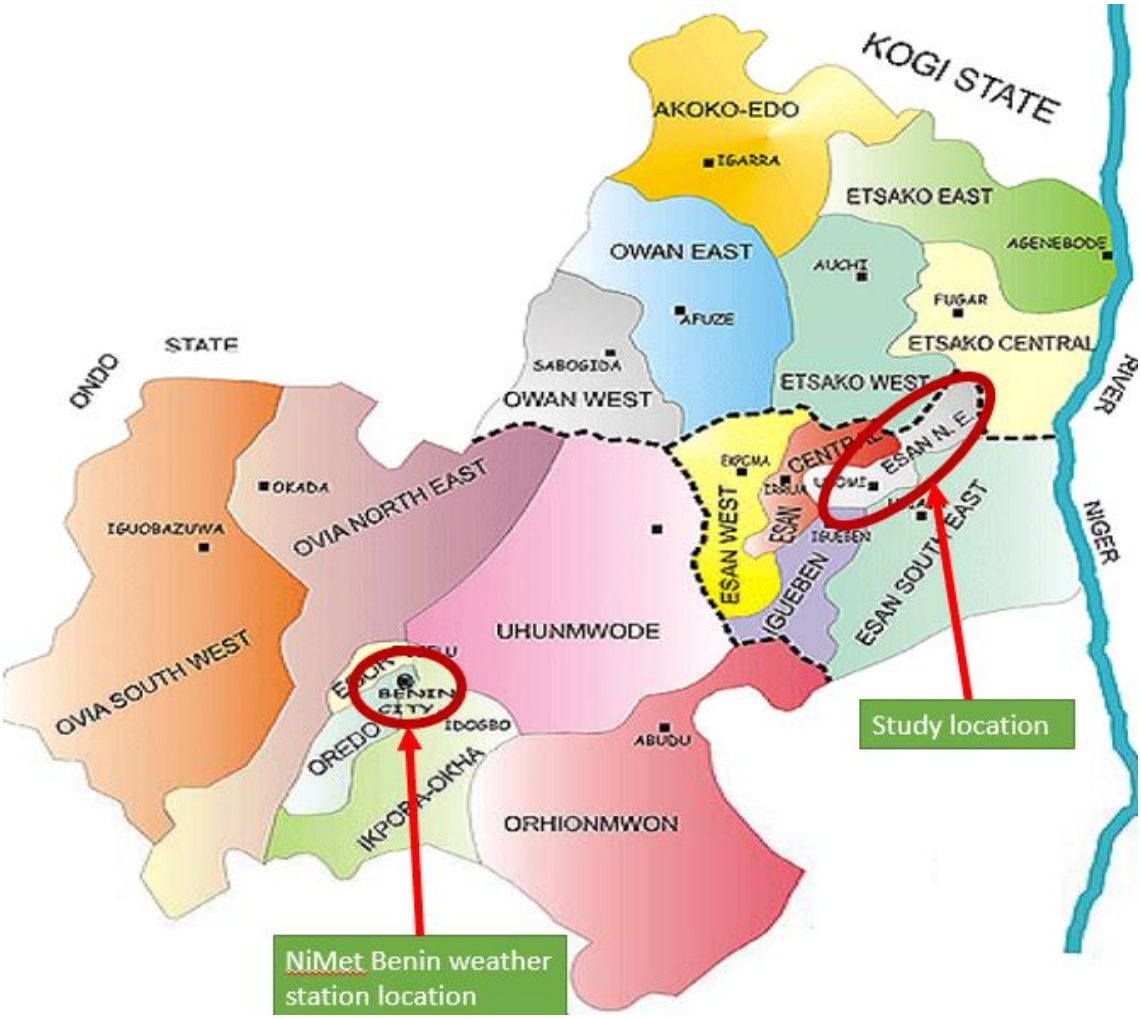

Fig. 6.1. Map of Edo state, Nigeria [455]

6.2 Data collection and regression analysis

The data collected from NiMet's Benin weather station were input meteorological parameters that are required by the 15 selected global solar radiation estimation models. Meanwhile, because the estimation error of a global solar radiation estimation model is reduced when long-term measured meteorological parameter(s) are employed [192], 26 years (1993-2018) daily measured meteorological parameter(s) for the 15 selected global solar radiation estimation models were acquired from the database of NiMet's Benin weather station.

The acquired daily measured NiMet data were checked to ensure that there was no day without records of measured meteorological data. If there is a day without a measure meteorological data, then the missing meteorological data will be interpolated. To use the 26 years long-term measured daily meteorological data sets for the design as well as for the performance evaluation of the 15 selected estimation models, the acquired and checked meteorological data is divided into two sub-datasets. This approach has been previously employed in studies such as [194], [417]. Furthermore, to generate the daily mean values across a year for both sub-datasets, the yearly average daily measured meteorological data can be averaged by using the same date in every year [117].

The first sub-dataset used for designing the estimation model comprises of 21-years (1993-2003) measured daily meteorological data. Therefore, the estimation models' meteorological parameters were derived by averaging the first sub-dataset daily values. To calculate the estimation models' regression coefficients (Angstrom coefficients), regression analysis between the models' average daily clearness index and the models' average daily meteorological parameters inputs, was performed. The calculated Angstrom coefficients for the estimation models are presented in Table 6.1.

Table 6.1. Estimation models Angstrom coefficients

Model	Angstrom coefficients											
	a	b	c	d	e	f	g	h	i	j	k	l
Model I	0.2668	0.5985	0.0000	0.0000	0.0000	0.0000	0.0000	0.0000	0.0000	0.0000	0.0000	0.0000
Model II	0.0950	1.5172	-1.1747	0.0000	0.0000	0.0000	0.0000	0.0000	0.0000	0.0000	0.0000	0.0000
Model III	0.5329	-2.1219	8.4991	-8.2610	0.0000	0.0000	0.0000	0.0000	0.0000	0.0000	0.0000	0.0000
Model IV	-0.0905	0.3987	0.0000	0.0000	0.0000	0.0000	0.0000	0.0000	0.0000	0.0000	0.0000	0.0000
Model V	0.7174	0.5183	0.0000	0.0000	0.0000	0.0000	0.0000	0.0000	0.0000	0.0000	0.0000	0.0000
Model VI	-0.1822	0.2377	0.0000	0.0000	0.0000	0.0000	0.0000	0.0000	0.0000	0.0000	0.0000	0.0000
Model VII	0.2822	-0.0961	0.0593	0.0000	0.0000	0.0000	0.0000	0.0000	0.0000	0.0000	0.0000	0.0000
Model VIII	3.6383	-3.7381	1.3664	-0.1550	0.0000	0.0000	0.0000	0.0000	0.0000	0.0000	0.0000	0.0000
Model IX	0.2485	0.0137	0.0000	0.0000	0.0000	0.0000	0.0000	0.0000	0.0000	0.0000	0.0000	0.0000
Model X	-0.1916	1.5182	0.0000	0.0000	0.0000	0.0000	0.0000	0.0000	0.0000	0.0000	0.0000	0.0000
Model XI	0.2968	0.3367	0.0053	-0.0080	0.0000	0.0000	0.0000	0.0000	0.0000	0.0000	0.0000	0.0000
Model XII	1.8436	0.0438	-1.9709	0.0000	0.0000	0.0000	0.0000	0.0000	0.0000	0.0000	0.0000	0.0000
Model XIII	1.4715	0.0783	-1.3593	0.0073	-0.3251	0.0000	0.0000	0.0000	0.0000	0.0000	0.0000	0.0000
Model XIV	0.6142	0.1373	-0.6485	0.0158	-0.2893	0.0000	0.0000	0.0000	0.0000	0.0000	0.0000	0.0000
Model XV	-0.5222	0.0000	0.0571	0.0000	0.3358	2.5061	0.0032	0.0000	-0.0002	-1.9435	-0.3660	0.0180

The second sub-dataset used for evaluating the performance of the estimation models comprises of 5-years (2014-2018) measured daily meteorological data. Similarly, the meteorological parameters annual average daily values were derived by averaging the second sub-dataset daily values.

6.2.1 Statistical evaluation of models

To evaluate the estimation models' performance, statistical test indicators were employed. Nine widely used statistical test indicators in the literature have been selected in this study and were presented in Table 4.4. As shown in Table 4.4, except for the coefficient of determination (R^2) value, the closer an estimation model statistical test indicator's value is to zero, the more the accuracy of the estimation model. So, whenever an estimation model R^2 value is close to one, there is a perfect linear relationship between the measured value and estimated value or there is little or no variability between the measured value and the estimated value. While, whenever an estimation model R^2 value is close to zero, there is no linear relationship between the measured value and the estimated value. Based on the comparison between the 15 selected empirical models daily estimated global solar radiation values and the measured daily global solar radiation values, the statistical performance of the 15 selected estimation models are presented in Table 6.2.

Table 6.2. Evaluation of the solar radiation estimation models

Model	Model Type	MAE	RMSE	MPE	MARE	RRMSE	RMSRE	erMAX	U_{95}	R^2
Model I	Linear (L)	1.596383	1.902967	1.178311	0.090771	0.000292	0.108589	0.299573	2.165561	0.250062
Model II	Quadratic (Q)	1.568139	1.878276	1.135425	0.089452	0.000241	0.108335	0.318671	3.025632	0.269396
Model III	Cubic (C)	1.521178	1.858152	1.110823	0.086422	0.000285	0.106228	0.324872	2.310232	0.284968
Model IV	Exponential (E)	1.612274	1.919019	1.210885	0.091682	0.000295	0.109438	0.294479	2.110443	0.237356
Model V	Logarithmic (Log)	1.584995	1.889323	1.154886	0.090380	0.000290	0.108806	0.311344	2.210978	0.260777
Model VI	Linear (L)	0.603285	0.732081	0.149558	0.001496	0.000112	0.042135	0.135010	4.067222	0.889011
Model VII	Quadratic (Q)	0.575126	0.705140	0.157087	0.032360	0.000108	0.039661	0.128724	4.085467	0.897029
Model VIII	Cubic (C)	0.571913	0.695850	0.151119	0.032225	0.000107	0.039237	0.136351	4.091582	0.899725
Model IX	Exponential (E)	0.590957	0.729468	0.189291	0.033131	0.000112	0.040593	0.120044	4.069025	0.889802
Model X	Logarithmic (Log)	0.638790	0.778714	0.158982	0.036885	0.000120	0.045578	0.140475	4.033812	0.874420
Model XI	Hybrid (H)/L	1.138720	1.424071	0.668024	0.066148	0.000219	0.085469	0.351611	3.287931	0.580022
Model XII	Hybrid (H)/L	0.607070	0.746493	0.170272	0.034626	0.000115	0.042961	0.159585	4.057146	0.884598
Model XIII	Hybrid (H)/L	0.556310	0.692212	0.135310	0.031975	0.000106	0.040221	0.139355	4.093952	0.900770
Model XIV	Hybrid (H)/L	0.716613	0.877302	0.243664	0.040316	0.000135	0.049219	0.128480	3.955307	0.840610
Model XV	Hybrid (H)/L & Q	0.318679	0.410424	0.368167	0.018039	0.000063	0.023188	0.077788	4.237224	0.965116

From Table 6.2 it is observed that Model XV had the highest coefficient of determination (R^2) value of 0.965, while 8 out of the remaining 14 estimation models also had an excellent R^2 value that was above 0.84. Based on the coefficient of determination values in Table 6.2, most of the estimation models had excellent performance. However, it is misleading to judge the statistical performance of the estimation model on only a single statistical test indicator value [196], [197], [422]. Therefore, in relation to the other eight selected statistical test indicators, it is vital to assess the performance of the estimation models.

With respect to the MAE test indicator in Table 6.2, Model XV with the least MAE value (0.319 MJ m^{-2} day^{-1} or 0.089 kWh m^{-2} day^{-1}) amongst the solar radiation estimation models, is the top-performing estimation model. Apart from R^2 and MAE statistical test indicators, whereby Model XV was the most accurate estimation model amongst the selected estimation models, Model XV with RMSE=0.410 MJ m^{-2} day^{-1}, RRMSE=0.00006, RMSRE=0.023, and erMAX=0.078 was also the top-performing estimation model for these four statistical test indicators.

Although Model XV was the top performing model in 6 out of the 9 selected statistical test indicators in Table 6.2, with respect to MARE and MPE statistical test indicators, Model XV performance was ranked the 2nd and the 9th position respectively. Also, with respect to U_{95} statistical test indicators, Model XV was the least performing model. With respect to the top-performing models for MARE, MPE, and U_{95} statistical test indicators, Model VI, Model XIII, and Model XI with a value of 0.0015, 0.135%, and 2.11 MJ m^{-2} day^{-1} respectively, are the top performing models for these statistical test indicators. Meanwhile, it is difficult to predict from Table 6.2 the extent of closeness between the models' statistical test indicators values. Therefore, the boxplot presented in Fig. 6.2 is used to capture the variations amongst models in each of the selected statistical test indicators.

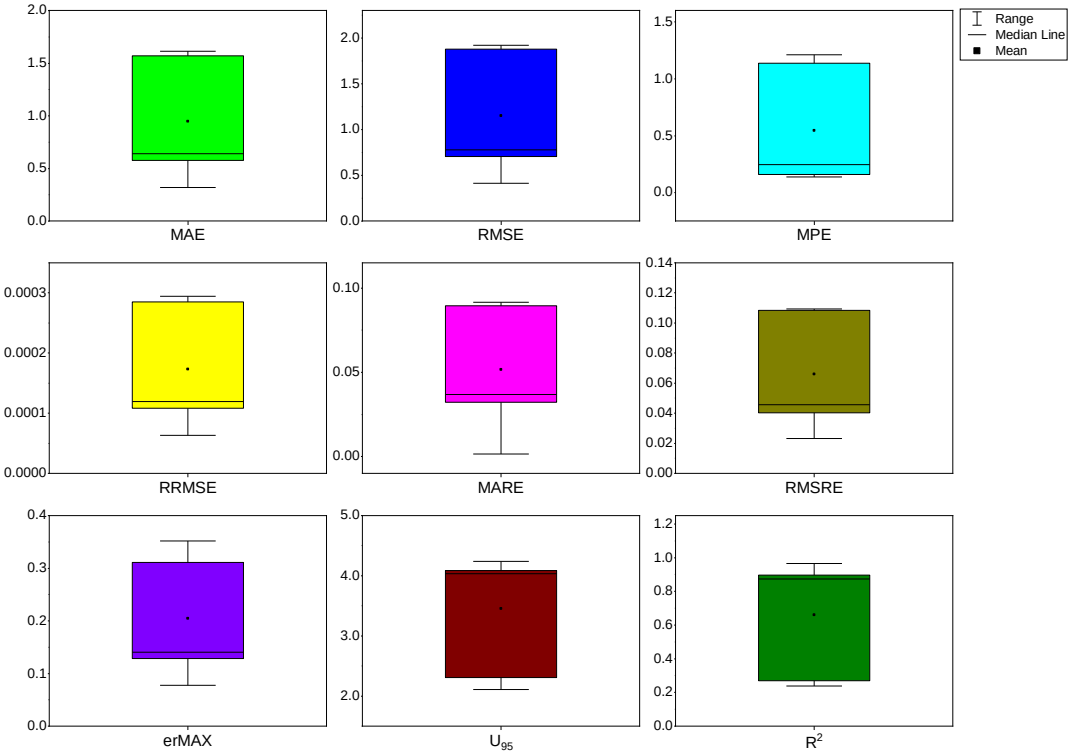

Fig. 6.2. Statistical test indicators boxplots

From Fig. 6.2, the top and bottom tails of the boxplots represent the maximum and minimum values of the estimation models, the top and bottom edge of the boxplot represent the first and third quartile, and the line across the rectangle is the median line. Therefore, the performance of a model in comparison to the general performance of other models can easily be inferred from the boxplots. By comparing the different boxplots, no obvious relationship between the different boxplots' first and third quartile rectangle, median line, or range tails was identified, but the estimation models' performance values within a boxplot were generally close to each other.

In summary, from Table 6.2, none of the selected solar radiation estimation models achieved top performance for all the 9 statistical test indicators. In terms of the individual performance of the selected estimation models, Model XV was the top performing model in 6 out of the 9 selected test indicators but with respect to U_{95} statistical test indicator, Model XV was the worst performing model. Meanwhile, Model VI and Model XIII were individually the top performing model once but with respect to the 9 statistical test indicators performance evaluation, these models

were never the worst performing models. Consequently, it might be misleading to automatically rank the Model XV as the best performing model or rank any other estimation models has the best performing model since an obvious lead by an estimation model in all the 9 selected statistical test indicators could not be established. Therefore, a combined ranking of the 15 selected estimation models is required. For the combined ranking of the statistical performance of the selected estimation models, global performance indicator (GPI) is employed.

6.2.2 Global performance indicator and ranking of the models

In recent studies, global performance indicator (GPI) presented by Despotovic et al. [196] is a statistical procedure that has been widely used to evaluate the combined performance of an estimation model. One of the advantages of using GPI is that the evaluation of the combined performance of a model is unbiased because the calculation of the combined performance of a model is not based on the product of the individual statistical test indicators [196]. Therefore, in cases whereby the value of one or more statistical test indicators is equal to zero, the combined performance of the model does not equate to zero. The global performance indicator steps used for evaluating the combined statistical performance of the selected solar radiation estimation models are explained in detail below:

The first step for calculating the estimation models global performance indicator values is to scale/normalize the statistical test indicators values between of 0 and 1 (y_{ij}) [197], [422]. So, since the least statistical test indicator value is 0 and the highest statistical test indicator value is 1, the other statistical test indicator values are interpolating between 0 and 1. Based on the MAE statistical test indicator, since the lowest value and highest value is 0.319 and 1.596 MJ m^{-2} day^{-1}respectively, the scaled or interpolated MAE value that corresponds to Model I is 0.988. The next step is to obtain the difference $(y_j - y_{ij})$ by subtracting the scaled values of the statistical test indicators (y_{ij}) from their scaled median value (y_j). Finally, the values obtained from $(y_j - y_{ij})$ are multiplied by a suitable weighted factor (α_j) to obtain the selected estimation models GPI values. Therefore, the expression for calculating an ith estimation model GPI value is defined by [196], [197]:

$$GPI_i = \sum_{j=1}^{9} \alpha_j (\tilde{y}_j - y_{ij}) \tag{6.1}$$

where from Eq. (6.1), $\tilde{y}_j$ is the median value of the scaled statistical test indicator j, y_{ij} is the value of the scaled statistical test indicator j for the estimation model i, and α_j is the weighted factor of the scaled statistical test indicator j. For all statistical test indicators, the value (magnitude) of α_j is 1, but the sign of α_j is dependent on the selected statistical test indicators [196]. Based on the selected statistical test indicators in this study, α_j is defined as:

$$\alpha_j = \begin{cases} -1, & \text{for the coefficient of determination } (R^2) \\ +1, & \text{for the other selected performance indicator} \end{cases} \tag{6.2}$$

Based on the estimation models calculated GPI values, the ranking of the estimation models is performed. The order of ranking the estimation models is such that estimation models with higher GPI values (better performing estimation models) are ranked higher than estimation models with lower GPI values. Therefore, the model with the maximum GPI value is ranked top-most amongst the selected estimation models, while other estimation models are ranked accordingly based on their calculated GPI values. Estimation models statistical test indicators scaled values, estimation models GPI values and ranking of the estimation models are presented in Table 6.3.

Table 6.3. Estimation models scaled statistical test indicators values as well as their GPI values and ranking

Model	Model Type	MAE	RMSE	MPE	MARE	RRMSE	RMSRE	erMAX	U95	R^2	GPI	Rank
Model I	L	-0.7403	-0.7452	-0.8690	-0.5975	-0.7452	-0.0630	-0.5810	0.8784	-0.8579	-4.3207	13
Model II	Q	-0.7184	-0.7289	-0.8291	-0.5829	-0.5233	-0.0628	-0.6508	0.4740	-0.8314	-4.4534	15
Model III	C	-0.6821	-0.7155	-0.8062	-0.5493	-0.7155	-0.0607	-0.6734	0.8104	-0.8100	-4.2023	11
Model IV	E	-0.7525	-0.7559	-0.8993	-0.6076	-0.7559	-0.0639	-0.5624	0.9044	-0.8754	-4.3684	14
Model V	Log	-0.7315	-0.7362	-0.8472	-0.5932	-0.7362	-0.0632	-0.6240	0.8571	-0.8432	-4.3175	12
Model VI	L	0.0275	0.0309	0.0875	0.3924	0.0309	0.0034	0.0200	-0.0157	0.0201	0.5969	2
Model VII	Q	0.0492	0.0488	0.0805	0.0502	0.0488	0.0059	0.0429	-0.0243	0.0311	0.3330	4
Model VIII	C	0.0517	0.0549	0.0860	0.0517	0.0549	0.0063	0.0151	-0.0272	0.0348	0.3283	5
Model IX	E	0.0370	0.0326	0.0506	0.0416	0.0326	0.0050	0.0746	-0.0166	0.0211	0.2786	6
Model X	Log	0.0000	0.0000	0.0787	0.0000	0.0000	0.0000	0.0000	0.0000	0.0000	0.0787	8
Model XI	H/L	-0.3865	-0.4278	-0.3945	-0.3245	-0.4278	-0.0399	-0.7711	0.3507	-0.4045	-2.8258	10
Model XII	H/L	0.0245	0.0214	0.0682	0.0250	0.0214	0.0026	-0.0698	-0.0110	0.0140	0.0964	7
Model XIII	H/L	0.0638	0.0573	0.1007	0.0544	0.0573	0.0054	0.0041	-0.0283	0.0362	0.3510	3
Model XIV	H/L	-0.0602	-0.0654	0.0000	-0.0380	-0.0654	-0.0036	0.0438	0.0369	-0.0465	-0.1983	9
Model XV	H/L & Q	0.2475	0.2441	-0.1158	0.2090	0.2441	0.0224	0.2289	-0.0956	0.1246	1.1092	1

From Table 6.3, Model XV with the highest GPI value of 1.1092 is the 1st ranked model (best ranked), while Model II with the lowest GPI value of -4.4534 is the 15th ranked model (least ranked). Furthermore, based on the result outcomes in Table 6.3, the following conclusions have been reached:

- Although the top-most ranked model (Model XV) in Table 6.3 is a hybrid (linear and quadratic type) estimation model, there is no substantial evidence from the ranking of the estimation models to suggest that the hybrid estimation model type or any other model type is the top performing model type for estimating the global solar radiation of the studied location.
- Assessment of the dominant meteorological parameters that influence the performance of the models shows that all the top 10 ranked estimation models in Table 6.3 had temperature as one of their meteorological parameters, but the least performing models were without temperature. This suggests that temperature is the most dominant meteorological parameter for estimating the global solar radiation of the studied location.
- The assertion that temperature is a dominant meteorological parameter for estimating the global solar radiation of the studied location is supported by the fact that the simple linear and temperature only estimation model (Model VI) was the top-most ranked model in Table 6.3 after Model XV. Therefore, for Benin or any other location with similar climate conditions, Model VI can be used to estimate the global solar radiation whenever there are scarce financial resources to purchase NiMet meteorological data. This is because Model VI only requires measured temperature to estimate global solar radiation and the measurement of temperature is one of the cheapest and widely measured meteorological parameter.

In summary, the performance evaluation of some of the widely recommended models for estimating global solar radiation in Nigeria revealed that there is no substantial evidence to suggest that the estimation model types influence the performance of an estimation model, however, temperature was found to be a dominant meteorological parameter that influences the studied location estimated horizontal surface global solar radiation. Meanwhile, since all the input

meteorological parameters used for the performance evaluation of the 15 selected estimation models were NiMet's ground measured long-term data, the highest ranked solar radiation estimation model (Model XV) in Table 6.3 is used here and in Chapter 8 to estimate daily global solar radiation of a horizontal surface. Furthermore, because Esan North-East LGA have similar climatic conditions as NiMet Benin weather station, the best performing empirical model that can be used for estimating Esan North-East LGA daily global solar radiation on a horizontal surface is:

$$\frac{H_g}{H_0} = -0.5222 + 0.0571(\cos N_{day}) + 0.3358\left(\frac{S}{S_0}\right) + 2.5061\left(\frac{T_{max}}{RH}\right) + 0.0032(RH) - 0.0002\left(\frac{T_{max}}{\cos\phi}\right) - 1.944\left(\frac{T_{max}}{RH}\right)^2 - 0.366\left(\frac{S}{S_0}\right)^2 + 0.018(\cos^2 N_{day})$$

where N_{day} is the day of the year, S is the average daily sunshine duration in hours, S_0 is the maximum sunshine duration or day length, T_{max} is the maximum temperature, RH is the relative humidity, and ϕ is the latitude.

6.3 Assessment of the minimum duration of measured data

As earlier mentioned, NiMet's long-term solar radiation dataset is unavailable for many weather stations and is expensive when available. Long-term measured solar radiation dataset is now reconstructed to determine the minimum time span of recent data required for the calculation. A pyranometer can be installed at an existing weather station to collect the recent short-term solar radiation dataset. The most recent 10 years of data is used to calculate regression coefficients using periods of the full 10 years, 5 years, 2 years, 1 year, 6 months, 3 months, and 1 month measured global solar radiation data. Durations less than a year were included to investigate seasonal effects and seasonal variation. Solar radiation is then reconstructed over the earlier 16 years period from meteorological parameters other than solar radiation, and R^2 values calculated for reconstructed solar radiation data against measured data. The R^2 values using Model XV are shown in Fig. 6.3.

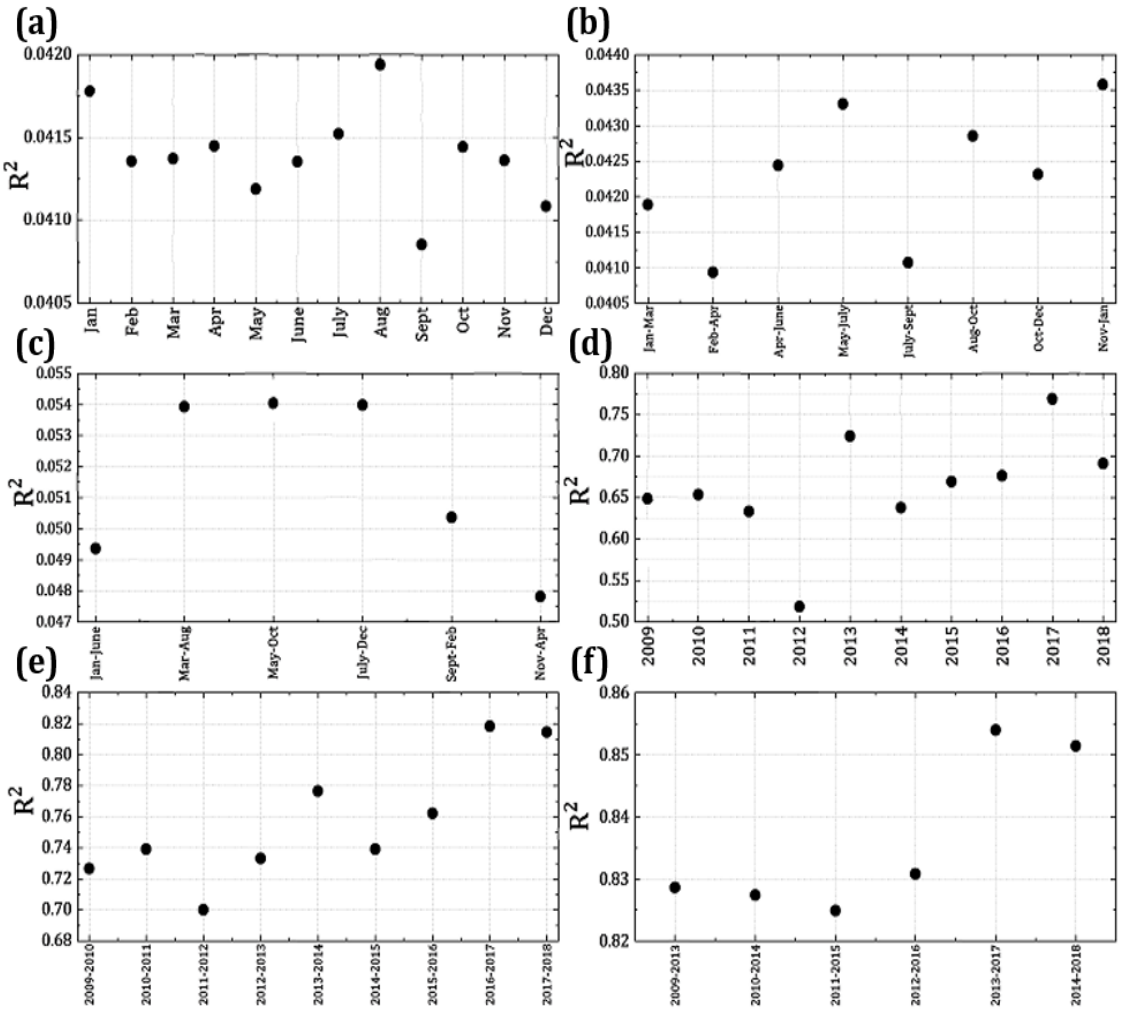

Fig. 6.3. R^2 for reconstructed against measured solar radiation using regression durations of (a) 1 month, (b) 3 months, (c) 6 months, (d) 1 year, (e) 2 years, and (f) 5 years.

It is evident from Fig. 6.3 that R^2 values increase as the measured solar radiation regression duration increases. A weak positive correlation is seen in Fig. 2e and Fig. 2f, which is likely caused by long-term climate variation or climate change. No seasonal effects are evident. A plot of average R^2 values for regression duration of 1 month, 3 months, 6 months, 1 year, 2 years, 5 years, and 10 years, is presented in Fig. 6.4.

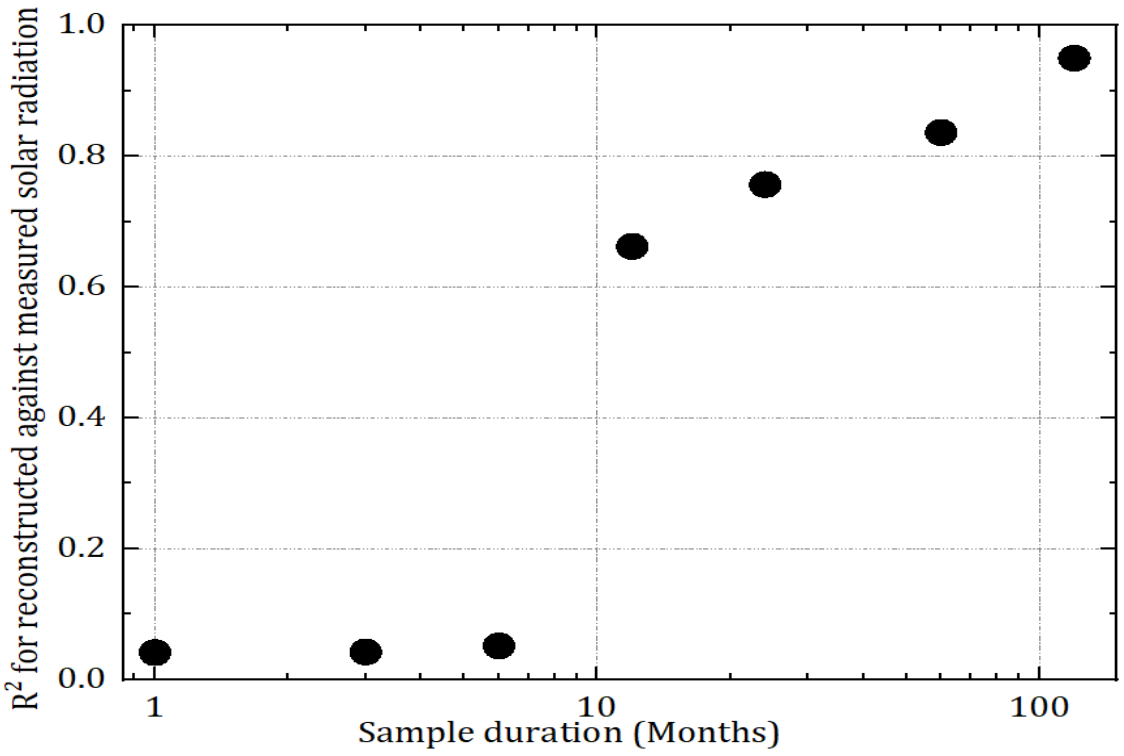

Fig. 6.4. R^2 values for different sample durations of measured data

To achieve accurate estimation of the studied location solar radiation, Fig. 6.4 shows that at least 2 years measured solar radiation or meteorological dataset is required to achieve a coefficient of determination greater than 0.75 and at least 4 years of measured solar radiation or meteorological dataset is required to achieve a coefficient of determination greater than 0.9.

6.4 Estimation of hourly global solar radiation

As earlier mentioned in this chapter, hourly global solar radiation (I_g) data will be used here to carry out techno-economic analysis of the solar energy system in Chapter 7. Therefore, hourly global solar radiation (I_g) data is derived from Model XV estimated daily horizontal surface global solar radiation (H_g). So, Gueymard [440] modified Collares-Pereira and Rabl [438] model (also known as CPRG model) that was presented in Section 4.2.6.3 is used to estimate the hourly horizontal surface global solar radiation of Esan North-East LGA. Meanwhile, in the literature, studies have shown that the CPRG model is usually the top performing model for estimating hourly horizontal surface global solar radiation [416], [441]. An

illustration of the modelling details of CPRG model was presented in Section 4.2.6.3 by Eqs. (4.33) – (4.39). The main input parameters of CPRG model is the studied location daily horizontal surface global solar radiation. Monthly average hourly global solar radiation generated by CPRD model is presented in Fig. 6.5.

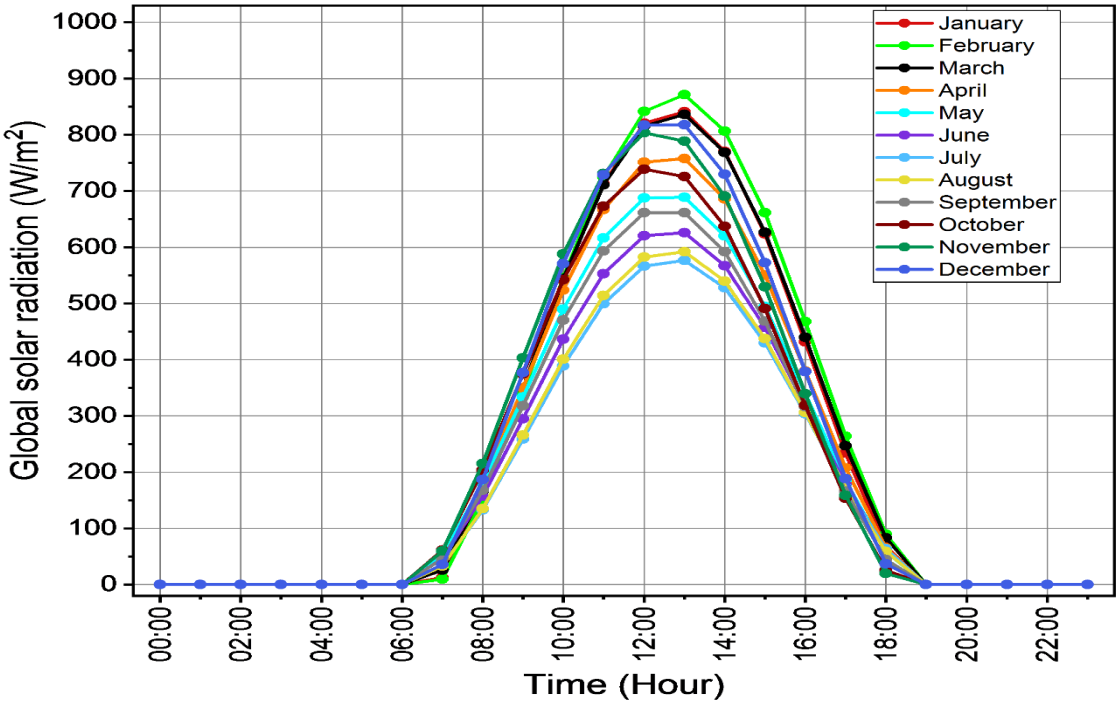

Fig. 6.5. Horizontal surface monthly average hourly global solar radiation for Esan North-East LGA

From Fig. 6.5, there are noticeable variations amongst the different monthly average hourly global solar radiation plots, especially during the hours of peak global solar radiation. It is observed that peak hourly global solar radiation occurred at 12:00 noon for the month of September to December, while for the month of January to August, peak hourly global solar radiation occurred at 13:00. Furthermore, over a year, Fig. 6.5 showed that the month of February had the highest peak average hourly solar irradiance of 871.10 Wm^{-2}, while the month of July had the lowest peak average hourly solar irradiance of 576.75 Wm^{-2}.

To in-directly evaluate the performance of CPRG model in estimating horizontal surface hourly global solar radiation, graphical and statistical analytical tests is performed here. Graphical analytical test is performed by calculating the percentage

deviation between the CPRG model estimated hourly global solar radiation (I_g) and the daily global solar radiation (H_g) that was used for estimating the hourly global solar radiation. An illustration of the graphical relationship between monthly average daily I_g values and monthly average H_g values for Esan North-East LGA is presented in Fig. 6.6.

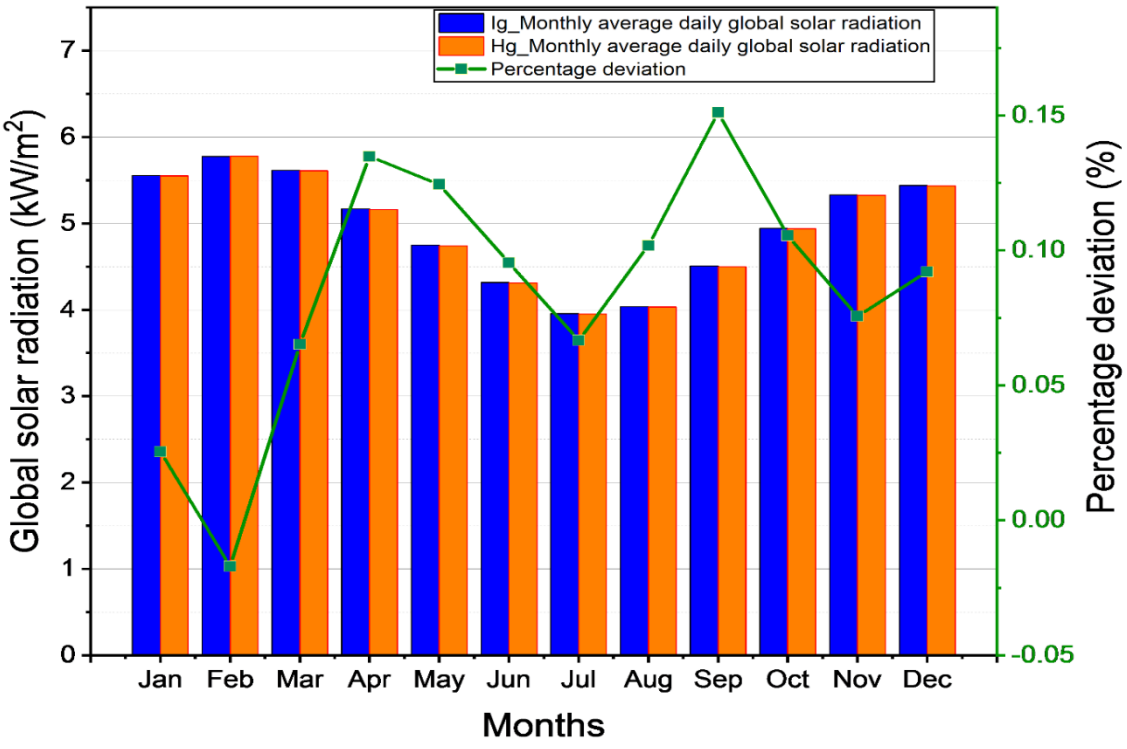

Fig. 6.6. Monthly relationship between daily average I_g and H_g

From Fig. 6.6, a close similarity exists between the daily average hourly global solar radiation (I_g) plot and the daily global solar radiation (H_g) plot. Furthermore, the maximum and the minimum monthly percentage deviation between the daily average hourly global solar radiation values and the daily global solar radiation values were 0.15% and 0.02%, respectively. Comparison between the daily average I_g values and the H_g values shows that apart from February, whereby the CPRG model estimated hourly global solar radiation values were slightly underestimated (negative monthly average daily percentage deviation), the CPRG model estimated hourly global solar radiation values for other months were slightly overestimated (positive monthly average daily percentage deviation).

Meanwhile, statistical analysis to evaluate the performance of CPRG model in estimating horizontal surface hourly global solar radiation is performed with the use of d-bar analysis. The d-bar analysis is a statistical procedure, and it will be used to evaluate how significant is the effect of the monthly percentage deviation between the daily average hourly global solar radiation values and the daily global solar radiation values. Typically, whenever statistical decisions are made to either accept or reject the null hypothesis, a critical value or level of significance of 5% is widely. So, a critical value of 5% is selected here. For the hypothesis test, the null hypothesis (H_0) and the alternative hypothesis (H_a) are defined as follow:

H_0: There is a significant difference between the daily average hourly global solar radiation values and the daily global solar radiation values.
H_a: There is no significant difference between the daily average hourly global solar radiation values and the daily global solar radiation values.

Based on the equation for calculating the test statistic (T_d) presented in Eq. (5.1), the calculated T_d is 6.24. Meanwhile, because the data size is 12, the degree of freedom (df) is 11. Consequently, for a df of 11 and a T_d value of 6.24, the corresponding level of significance from a t-table is 0.00317% (0.0000317). Because the calculated t-table value (0.0000317) is less than the selected critical value ($P<0.05$), and the null hypothesis should be rejected. Therefore, the difference between the daily average hourly global solar radiation values and the daily global solar radiation values is statistically insignificant.

In summary, because a close graphical similarity exists between the daily average hourly global solar radiation and the daily global solar radiation plots, and the monthly percentage deviation between the daily average hourly global solar radiation and the daily global solar radiation values is statistically insignificant, so, the CPRG model is therefore a suitable approach for estimating Esan North-East LGA horizontal surface hourly global solar radiation.

6.5 Estimation of global solar radiation on inclined surfaces

To evaluate the annual optimal hourly global solar radiation received by a PV panel in a location, the amount of global solar radiation received by a PV panel when it is

positioned (facing south since the studied location is in the Northern hemisphere) at different angles that ranges from 0° to 90° is assessed. Data on the amount of global solar radiation received on inclined surfaces are rarely available in developing countries like Nigeria. For example, NiMet's weather stations do not measure the global solar radiation received on an inclined surface. There are several models derived in the literature for estimating inclined surfaces global solar radiation. Most of these derived models requires measured diffuse solar radiation data to estimate inclined surfaces global solar radiation of a location. Diffuse solar radiation is not measured by NiMet's weather station. So, Olmo et al. [229] estimation model (described by Eqs. (4.40) – (4.46)) which does not require disintegrated global solar radiation (direct and diffuse solar radiation) data before estimating the global solar radiation of inclined surfaces is used for estimating hourly global solar radiation of inclined surfaces in Esan North-East LGA.

Olmo et al. [229] model is a simple model because the main input parameters required by Olmo et al. [229] model to estimate inclined surfaces global solar radiation are horizontal surface global solar radiation, sun's zenith angle, and sun's incident angle. Furthermore, amongst these required input parameters, only horizontal surface global solar radiation is measured. Therefore, to maximize the annual global solar radiation received by a PV panel in Esan North-East LGA, numerical simulation of Olmo et al. [229] model is performed to evaluate the required optimal tilt angle to maximize the annual global solar radiation received in Esan North-East LGA.

Based on the assumption that the PV panel is inclined at a fixed angle throughout the year, the required optimal tilt angle to maximize the annual of global solar received in Esan North-East LGA is 11.6°. If an annual tilt angle of 11.6° is selected for Esan North-East LGA, February 5th is the date with the highest peak hourly global solar radiation (948 W m^{-2}) and the highest daily global solar radiation (6340 W m^{-2} day^{-1}) in a year. To study the hourly global solar radiation received at different tilt angles in Esan North-East LGA, an illustration of the hourly global solar radiation received on the 5th of February in Esan North-East LGA at some selected annual tilt angles are presented in Fig. 6.7.

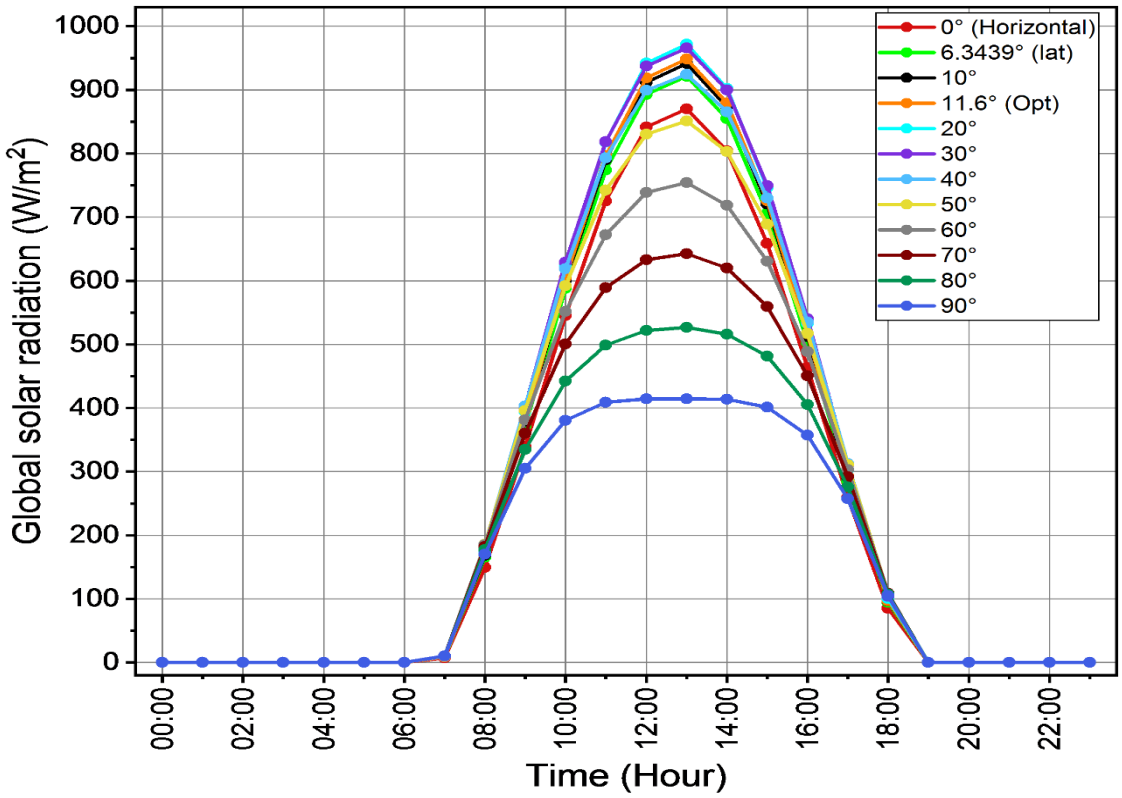

Fig. 6.7. Hourly global solar radiation received on the 5th of February in Esan North-East LGA at different annual tilt angles

Fig. 6.7 shows that on the 5th of February in Esan North-East LGA, a PV panel positioned at a tilt angles of 20° or 30° with a peak hourly global solar radiation of 972 W m^{-2} and 966 W m^{-2} respectively and a daily global solar radiation of 6518 Wh m^{-2} and 6548 Wh m^{-2} respectively, received higher peak hourly global solar radiation and higher daily global solar radiation than PV panel positioned at a tilt angle of 11.6°. So, it is evident from Fig. 6.7 that the hourly global solar radiation for Esan North-East LGA can be optimized if the tilt angle of a PV panel is adequately adjusted seasonally (monthly or quarterly) to its optimal tilt angle. For an illustration, the monthly global solar radiation received in Esan North-East LGA by a PV panel positioned at the selected tilt angles in Fig. 6.7 are presented in Table 6.4.

Table 6.4. Esan North-East LGA monthly global solar radiation for different tilt angles

	Global solar radiation (kWh m^{-2})											
Month	0°(Hor)	6.34° (lat)	10°	11.6° (Opt)	20°	30°	40°	50°	60°0	70°	80°	90°
January	176.8	186.6	191.4	193.3	200.9	204.5	201.9	193.4	179.9	162.5	142.8	122.2
February	165.4	171.4	173.9	174.8	177.5	175.9	169.3	158.3	143.9	127.2	109.6	92.2
March	177.4	179.2	179.3	179.2	176.5	169.1	157.7	143.3	127.0	109.8	92.9	77.1
April	157.9	155.9	154.1	153.1	146.7	136.3	123.6	109.5	94.9	80.5	67.1	55.1
May	150.1	146.0	143.0	141.6	133.1	121.0	107.5	93.5	79.6	66.6	54.7	44.5
June	132.2	127.9	125.0	123.6	115.6	104.6	92.7	80.5	68.5	57.3	47.3	38.6
July	125.2	121.8	119.5	118.3	111.8	102.6	92.3	81.6	70.8	60.5	51.0	42.4
August	127.6	125.5	123.9	123.1	118.1	110.4	101.3	91.2	80.7	70.2	60.2	50.9
September	137.7	137.7	137.1	136.7	133.6	127.5	119.1	109.0	97.8	86.1	74.4	63.3
October	156.5	159.9	161.1	161.5	161.9	158.7	151.9	141.9	129.5	115.5	100.8	86.2
November	164.0	171.6	175.2	176.6	181.8	183.4	179.8	171.4	158.9	143.4	126.1	108.1
December	173.5	184.0	189.3	191.4	200.2	205.3	204.2	197.0	184.5	167.8	148.3	127.6
Annual (kWh m^{-2})	1844.4	1867.4	1872.8	1873.3	1857.7	1799.4	1701.5	1570.7	1416.0	1247.4	1075.1	908.1

Table 6.4 shows that for the different months, tilt angle 11.6° was never the optimal tilt angle for maximizing the amount of monthly global solar radiation received in Esan North-East LGA, but a higher annual global solar radiation was received at tilt angle 11.6°. Furthermore, it was observed that the tilt angles with maximum monthly global solar radiation were influenced by the time of the year. For instance, between April and September, maximum monthly global solar radiation was received at 0° (low tilt angle), while between November and January, maximum global solar radiation was received at 30° (high tilt angle).

There are two weather seasons (dry and rainy season) in Esan North-East LGA. Typically, the core dry season months are from November to February, and the rainy season months are from March to October. Therefore, based on the outcomes from Table 6.4, higher tilt angles (of about 30°) are suitable for the dry season months while lower tilt angles are generally for the rainy season months. Because the simulated tilt angle for maximizing the monthly global solar radiation was affected by the weather seasons, it is necessary to also analyse the received monthly global solar radiation at different tilt angles. However, since the number of days in each month is not the same, the monthly evaluation of the global solar radiation received at the different tilt angles will be misleading. Therefore, monthly average daily global solar radiation received in Esan North-East LGA at the selected tilt angles are presented in Fig. 6.8.

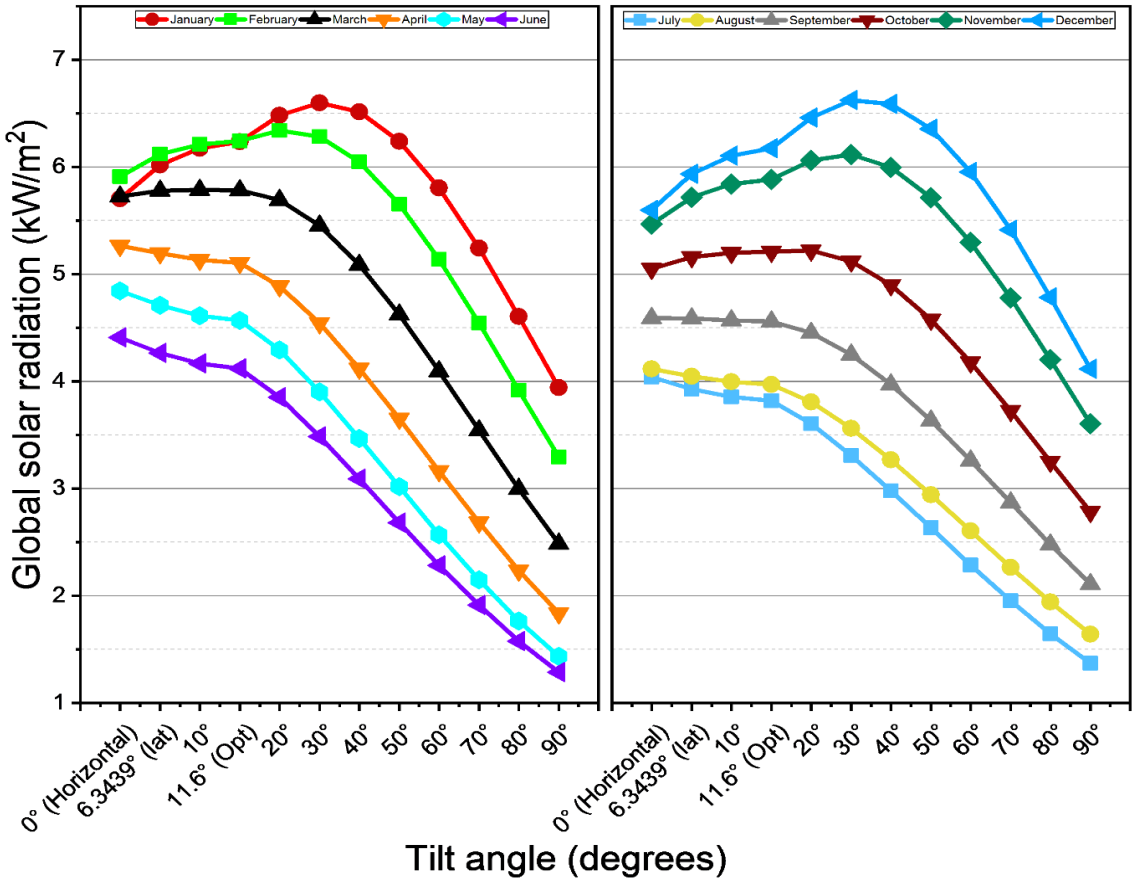

Fig. 6.8. Tilt angles monthly average daily global solar radiation

Noticeable trends can be identified from Fig. 6.8 when the received monthly average daily global solar radiation at different tilt angles are compared based on the weather seasons of Esan North-East LGA. So, it is observed from Fig. 6.8 that the monthly average daily global solar radiation received on a PV panel during the dry season months is generally increase from the horizontal tilt angle position (0°) to a certain angle of inclination, then after, subsequent increment in the PV panel angle of inclination results in the reduction of the monthly daily average global solar radiation. But during the rainy season months, Fig. 6.8 shows that the monthly average daily global solar radiation received on a PV panel generally decreases as the angle of inclination increases from the horizontal tilt angle position (0°) to the vertical tilt angle position (90°).

Meanwhile, because the selection of the optimal tilt angle is influenced by the weather season, therefore, simulation of the PV panel optimal monthly, seasonal (quarterly), and annual tilt angles is vital. The optimal tilt angles simulation was

made to start from November (beginning of the core dry season months) in order to capture the different weather seasons. Therefore, starting from November, the quarterly optimal tilt angle values are calculated by assessing the tilt angle that produces the maximum global solar radiation within each quarter (3 months). A plot of the simulated optimal monthly, quarterly, and annual tilt angles against the day of the year is presented in Fig. 6.9.

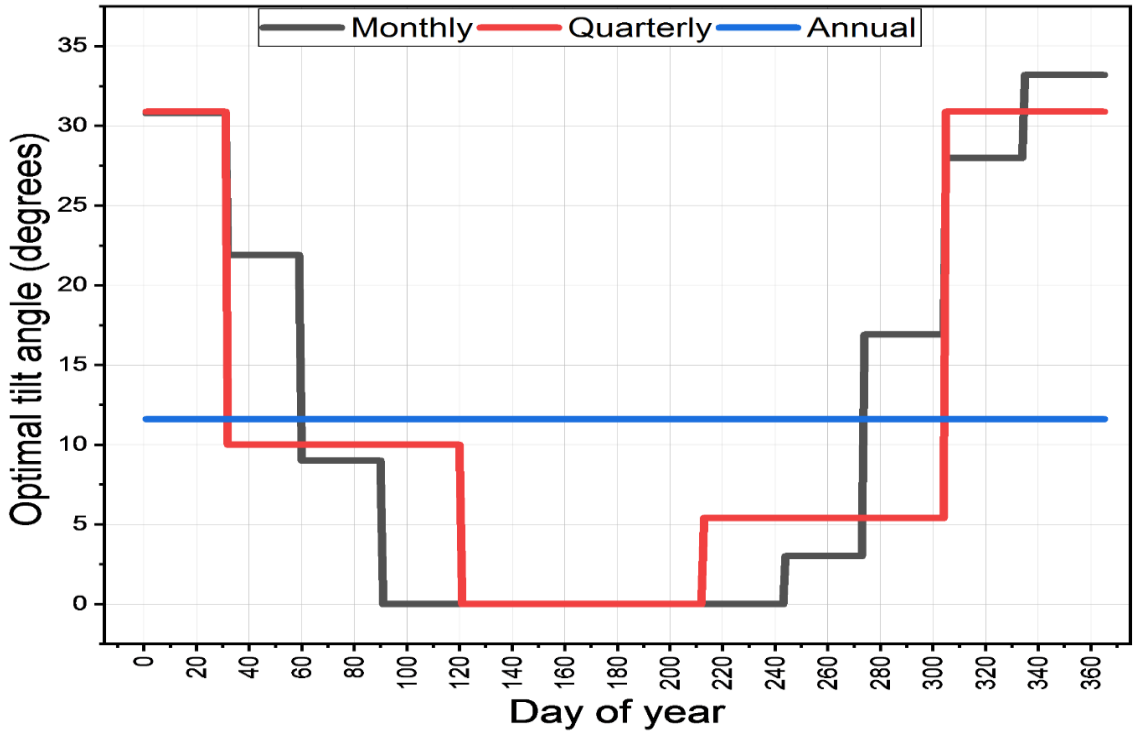

Fig. 6.9. Variations of monthly, seasonal, and annual optimum tilt angle for Esan North-East LGA

Fig. 6.9 shows that the 1st quarter (November to January) had the highest quarterly tilt angle, while the 3rd quarter (May to July) had the lowest quarterly tilt angle. Furthermore, December (mid-dry season month) had the highest optimal monthly tilt angle value of 33.2°, while the month of April to August, had the lowest optimal monthly tilt angle value of 0°. Meanwhile, the monthly average daily global solar radiation received by a PV Panel in Esan North-East LGA when the PV panel is positioned horizontally or inclined based on the studied location simulated monthly, quarterly, and annual optimal tilt angles, are presented in Table 6.5.

Table 6.5. Esan North-East LGA estimated monthly daily average global solar radiation at monthly, quarterly, and annual optimal tilt angles

Month	Season type	Daily average global solar radiation ($kWh\ m^{-2}$)			
		βopt_horizontal	βopt_month	βopt_quarter	βopt_ann
January	Dry	5.705	6.598	6.598	6.235
February	Dry	5.908	6.344	6.212	6.245
March	Rainy	5.723	5.786	5.785	5.781
April	Rainy	5.263	5.263	5.135	5.104
May	Rainy	4.843	4.843	4.843	4.567
June	Rainy	4.408	4.408	4.408	4.120
July	Rainy	4.038	4.038	4.038	3.818
August	Rainy	4.115	4.115	4.061	3.972
September	Rainy	4.590	4.594	4.591	4.558
October	Rainy	5.050	5.228	5.145	5.211
November	Dry	5.466	6.118	6.111	5.886
December	Dry	5.597	6.634	6.629	6.174
Annual yield ($kWh\ m^{-2}$)		1844.43	1943.70	1931.40	1873.34
Annual percentage gain		-	5.38%	4.72%	1.57%

Table 6.5 shows that whether a PV panel in Esan North-East LGA is fixed or adjusted periodically based on its optimal tilt angles, the lowest monthly average daily global solar radiation was received in July (mid-rainy season month). Also, Table 6.5 shows that when a PV panel is positioned horizontally or fixed at its annual optimal tilt angle, the highest monthly average daily global solar radiation was received in January, but when the PV panel is adjusted periodically at its monthly, or quarterly optimal tilt angles, the highest monthly average daily global solar radiation was received in February. Furthermore, the calculated amount of annual global solar radiation received when a PV panel is either positioned horizontally $\left(G_\gamma\big|_{\beta=0}\right)$ or inclined at its optimal monthly, quarterly, or annual tilt angles $\left(G_\gamma\big|_{\beta=\beta_{opt_i}}\right)$ were also presented in Table 6.5. So, the global solar radiation percentage gain $(\%_{gain})$ when a PV panel is positioned at either its optimal monthly, quarterly, or annual tilt angles in comparison to when it is positioned horizontally, is expressed as:

$$\%_{gain} = \left(\frac{G_\gamma|_{\beta=\beta_{opt_i}}}{G_\gamma|_{\beta=0}} - 1 \right) \times 100 \qquad (6.3)$$

where β_{opt_i} in Eq. (6.3) is either the monthly, seasonal (quarterly), or annual optimal tilt angles, while $\beta = 0$ means the PV panel is positioned horizontally.

Based on Eq. (6.3), the annual global solar radiation percentage gained when a PV panel is inclined at its monthly, quarterly, or annual optimum tilt angles in comparison to when the PV panel is positioned horizontally in Esan North-East LGA is 5.38%, 4.72%, or 1.57% respectively. Therefore, there are noticeable annual global solar radiation percentage gained when a PV panel is inclined at its monthly, quarterly, or annual optimum tilt angles than when it is positioned horizontally in Esan North-East LGA. Meanwhile, the annual global solar radiation percentage loss ($\%_{loss}$) that would arise from the quarterly or the annual adjustment of PV panels rather than the monthly adjustment of PV panels is defined by:

$$\%_{loss} = \left(1 - \frac{G_\gamma|_{\beta=\beta_{opt_j}}}{G_\gamma|_{\beta_{opt}(monthly)}} \right) \times 100 \qquad (6.4)$$

where β_{opt_j} in Eq. (6.4) is either the quarterly or annual optimal tilt angles.

Based on Eq. (6.4), the percentage loss in annual global solar radiation when a PV panel is inclined at its monthly optimal tilt angles in comparison to when the PV panel is inclined at its quarterly or annual optimal tilt angles is 0.63% or 3.62% respectively. Therefore, the percentage loss in in annual global solar radiation is more obvious when the PV panel is inclined at its annual optimal tilt angle than when it is inclined at its quarterly optimal tilt angles.

6.6 Chapter Summary

Information on the amount of global solar radiation that can be received by a solar energy project is vital for the solar energy project design and operation. However, the suitability of available global solar radiation data is location dependent. For many locations in developing locations like Nigeria, measured global solar radiation data is unavailable, while for locations with measured global solar radiation data, it is expensive to purchase the measured data. Therefore, several researchers have derived estimation models that utilize long-term measured meteorological parameter(s) to estimated global solar radiation, but the rationale for including, and the influence that the various meteorological parameter(s) have on the estimation models is often unclear.

In this study, 15 global solar radiation estimation models were selected in this study. Long-term measured data (1993-2018) on the required meteorological parameters of the 15 selected solar radiation estimation models were sourced from Benin weather station NiMet's archive. To avoid misleading conclusion during the performance evaluation of the 15 selected solar radiation estimation models, 9 statistical test indicators were selected, and the overall performance of the solar radiation estimation models were assessed by ranking the performance of the solar radiation estimation models based on their global performance indicator (GPI) values. Outcome from the study shows that Model XV (hybrid- linear and quadratic type- model) with a GPI value of 1.1092, was the best performing model while Model II with a GPI value of -4.4534, was the worst performing model. Furthermore, the study showed that temperature is a dominant meteorological parameter for estimating the global solar radiation of the studied location, but there was no substantial evidence to suggest that the hybrid estimation model type (i.e. the model type of the best ranked model) or any other model type was the top performing model type for estimating the global solar radiation of the studied location.

To determine the minimum duration of measured data required to calculated past solar radiation data, recent long-term measured data were reconstructed. Investigation of seasonal effects and seasonal variation that was performed by reconstructing less than a year duration of measured data show that seasonal

variation has no influence on the calculation of past solar radiation data. A minimum of 2 years of recent data should be measured with a pyranometer or purchased from a NiMet weather station in order to achieve R^2 greater than 0.75, and more than 5 years of recent solar radiation data is required to achieve R^2 greater than 0.9.

To estimate the hourly global solar radiation that is required for optimal design of the HRES, Gueymard modified Collares-Pereira and Rabl model (CPRG model) was used. In-direct graphical and statistical analytical test of the suitability of using CPRG model to estimate the studied location hourly global solar radiation was performed. Outcomes from the graphical analytical test shows that the maximum monthly overestimation and underestimation by the CPRG model were 0.15% and 0.02%, respectively. While outcomes from the statistical analytical test shows that when CPRG model was used, the level of significance from a t-table was 0.0000317. This value was less than the selected critical value of 0.05; which is required for the CPRG model estimated hourly global solar radiation to be inaccurate (rejected). Therefore, CPRG model is suitable for estimating the studied location hourly global solar radiation because the deviation or errors observed from the graphical and statistical analytical test was insignificant.

Diffused solar radiation data is usually required by most estimation models to determine the optimal inclined angle to position a PV panel in a studied location. But because weather stations in Nigeria that measure solar radiation data rarely measure diffused solar radiation data, so, the common practice (which might be less optimal solution) is to position PV panel based on the studied location latitude. Olmo et al. [229] estimation model; which is one of the few models that does not require disintegrated global solar radiation (direct and diffuse solar radiation) data before estimating the optimal inclined angle to position a PV panel was used here.

With respect to Nigeria's two weather seasons (dry and rainy season), it was found that during the dry season, maximum global solar radiation was received in the studied location at an inclined angle of 30°, while during the rainy season when the sun is mostly over cast, maximum global solar radiation was received in the studied location at an inclined angle of 0°. Furthermore, there was an increase in the annual

global solar radiation received when a PV panel was adjusted monthly to its optimal angle than when it was adjusted quarterly or positioned annually at its optimal angle. Similarly, more global solar radiation was received annually when a PV panel was adjusted quarterly to its optimal angle than when it was positioned annually at its optimal angle. However, because of the economics and technicalities of adjusting PV panels periodically (i.e., monthly or quarterly), it is perhaps a better option to annually position PV panels at its optimal angle when there is scarcity of financial resources and/or lack of technical expertise. Therefore, the global solar radiation received when a PV panel in the studied location is positioned annually at its optimal angle of 11.6° is used in Chapter 7 for the optimal sizing of hybrid energy system.

Chapter 7 DESIGN AND ANALYSIS OF HYBRID ENERGY SYSTEM

Electricity is vital for improving human's standard of living. In rural communities of developing countries like Nigeria, many people have no access to electricity, while others are connected to an un-reliable grid. As earlier presented in Chapter 1, communal-grid system; which allows for the aggregation of community loads, is a viable approach that can be used to supply reliable electricity to these rural communities. Therefore, a techno-economic communal grid model that comprises of PV, biogas generator, and battery energy storage is developed here to evaluate the cost of using communal grid system to supply reliable electricity to a community that is either un-electrified or whose electrical loads are connected to an unreliable grid. The developed community load profile model in Chapter 5 and the hourly solar radiation data estimated in Chapter 6 are some of the input parameters used by the techno-economic model to optimally size the hybrid energy system components, in order to guarantee reliable supply of electricity at minimal cost.

Meanwhile, it is profitable to aggregate several communal or regional electrical loads in a regional-grid, but when the aggregated regional loads are not close to each other, there will be substantial power losses in the regional-grid. Therefore, a power flow study is also carried out in this chapter to determine the benefit of regional load aggregation and to evaluate if centralised or distributed generation is the best approach to supply electricity to the load buses of a regional-grid in order to minimise the power losses in the network and to guarantee the healthy operation of the regional-grid.

7.1 Simulation of the hybrid energy system

As earlier mentioned in Chapter 4, a quick, and simplified optimization approach called design space optimization approach is used for simulating the optimal size of the hybrid energy system components in this study. This is because design space optimization approach is a useful approach for providing optimal solution to search space problem [338]–[340]. And a search space problem will arise from the

selection of the best combination of energy system components that minimize the total annualized cost of system and the amount of un-met load. Although, the proposed hybrid system configuration was presented in Fig. 4.1, the modelling architecture of the bottom-up demand model and battery energy storage were presented in Fig. 4.2 and Fig 4.3 respectively, and the design space modelling scheme was presented in Fig. 4.4, a simplified one-line diagram of the operating methodology of the hybrid energy system is presented in Fig. 7.1.

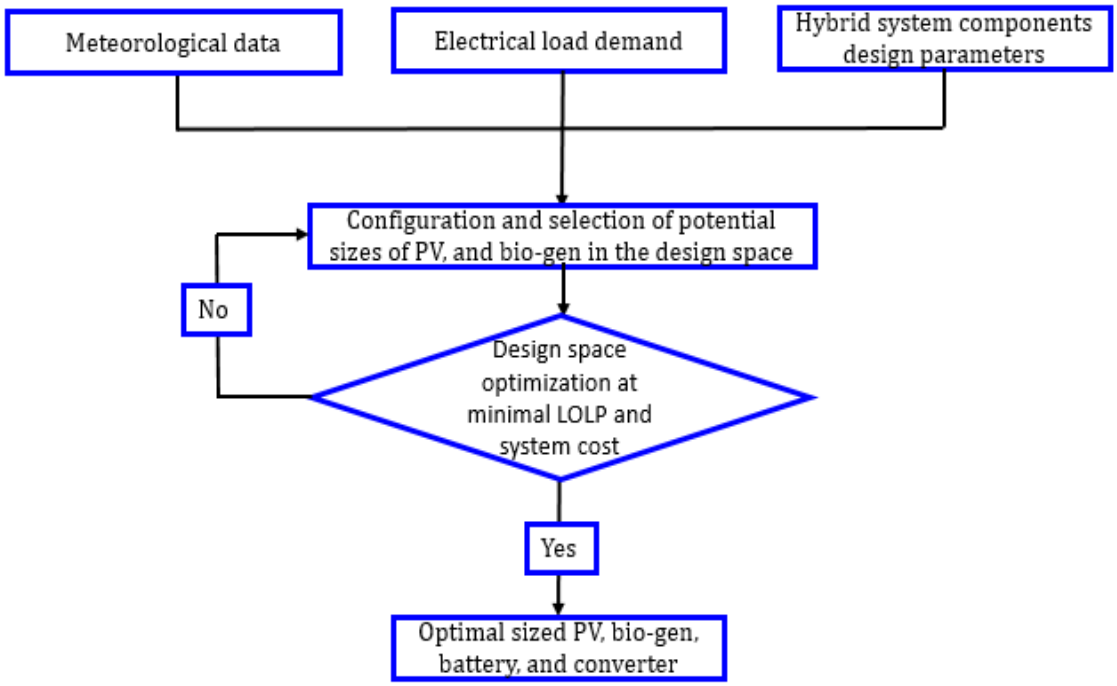

Fig. 7.1. One-line diagram of design space optimization approach

Fig. 7.1 shows that the optimal size of system components is selected by a search of the design space for the best combination of PV and biogas generator, and battery storage that will guarantee minimal loss of power supply probability (LPSP) is achieved at minimal total annualized cost of system. The intermittency in solar radiation and the variability in the community load profile is captured by the hourly time step simulation performed here. Also, because the community load demand is characterized by morning and evening peak power (see Fig. 5.25), to avoid over-sizing of the PV and biogas generator, and ensure optimal energy balance between energy demand and supply at minimal cost of system, the battery energy storage is sized with power pinch analysis technique [338]–[340].

The operation of a biogas generator at full-loading condition is vital for the optimal operation of the biogas generator [231]–[233] as well as to guarantee healthy engine operation and long engine life. This is because the operation of a generator at lower load ratio over a long duration of time can lead to exhaust manifold slobber or wet stacking [234]. So, the biogas generator here is designed not to operate when the load demand is below the selected minimum load ratio[1]. In this study, a 50% minimum load ratio is selected for the biogas generator because this is the lowest recommended load ratio for a gas generator [234], [404]. Furthermore, to ensure optimal supply and usage of the energy generated from the biogas generator at full load, whenever the energy generated exceed the load demand, the excess generated energy is sold to the grid, when the battery is fully charged. Therefore, in periods when the community electrical load demand is low and the biogas generator is switch-off, un-met load will be supplied by the PV generator and the stored energy in the battery storage.

7.2 Hybrid energy system modelling inputs and design parameters

To implement the design space optimization approach in Fig. 7.1, the modelling inputs and design parameters used for the optimal sizing of the hybrid energy system components are presented in this section. A list of the financial inputs and some of the design parameters used for modelling the hybrid energy system is presented in Table 7.1.

[1] Generator minimum load ratio is the minimum allowable load on the generator, and it is defined as a percentage of the generator rated capacity.

Table 7.1. System components cost and performance characteristics

Parameters	Values	Parameters	Values
Project lifetime (years)	20	Nominal interest rate (%)	13.5 [456]
Real interest rate (%)	2.2	Inflation rate (%)	11.1 [457]
Photovoltaic system			
Capital cost ($\$\ kW_P^{-1}$)	1260 [ab]	Operation and maintenance cost ($\$\ kW_P^{-1}year^{-1}$)	0.01 [b]
Replacement cost ($\$\ kW_P^{-1}$)	0	Module efficiency (%)	17.44 [c]
Biogas generator			
Capital cost ($\$\ kW^{-1}$)	280 [b]	Replacement cost ($\$\ kW^{-1}$)	280 [b]
Operation and maintenance cost ($\$\ kW^{-1}year^{-1}$)	0.05 [b]	Biogas methane content (%)	60 [398], [399]
Biogas heating value ($MJ\ kWh^{-1}$)	37 [236], [237]	Biogas efficiency (%)	26 [236], [237]
Lifetime (years)	5 [c]		
Anaerobic digester			
Capital cost ($\$\ m^{-3}$)	470 [b] [458]	Total solid (%)	10.2 [459]
Cost of dry cow dung ($\$\ kg^{-1}$)	0.056 [b]	Influent volatile solid ($kgVS\ kg_{wet\_weight}^{-1}$)	0.078 [459]
Feedstock density ($kg\ m^{-3}$)	1040 [158]	Replacement cost ($\$\ m^{-3}$)	0
Specific biogas production ($m^3 kg\_VS^{-1}$)	0.35 [158]	Hydraulic retention time (days)	42.5 [158]
Lithium-ion Battery			
Capital cost ($\$\ kWh^{-1}$)	530 [b]	Depth of discharge (%)	80 [c]
Replacement cost ($\$kWh^{-1}$)	530 [b]	Charging efficiency (%)	99 [c]
Self-discharge rate ($\%day^{-1}$)	0.2 [b]	Lifetime (years)	5 [c]
Converter			
Capital cost ($\$\ kW^{-1}$)	350 [b]	Lifetime (years)	10 [c]
Replacement cost ($\$\ kW^{-1}$)	350 [b]	Efficiency (%)	90 [c]

[a] Local market capital cost (including the balance of system cost) for a CS6U-340P Canadian solar module.
[b] Information are acquired locally or country-specific
[c] Information from datasheet or professional recommendations

The lithium ion battery cost and performance characteristics presented in Table 7.1 are for a lithium iron phosphate ($LiFePO_4$) battery. LiFePO4 is a safe battery

technology because of its good chemical and thermal stability. In comparison to lithium cobalt dioxide ($LiCoO_2$) battery, that may suffer thermal runaway and heats up faster under charging conditions, $LiFePO_4$ are stable under overcharging or short circuit conditions (i.e., they don't get overheated or catch fire) and can withstand high temperature without decomposing. Unlike the cathode of $LiCoO_2$ battery, that is hazardous in nature, the cathode of the $LiFePO_4$ battery is a nontoxic material, therefore, there is no concern with the disposal of $LiFePO_4$ battery. Furthermore, they are about 2 times cheaper than lithium titanium battery [87]

7.2.1 Electrical load demand

Bottom-up modelling of a minutely time step load profile for the studied rural community was presented in Chapter 5. However, because of computational convenience, an hourly time step simulation of the hybrid energy system is performed here. So, the minutely time step simulated load profile is averaged hourly. The average hourly time step load profile for the studied rural community is presented in Fig. 7.2.

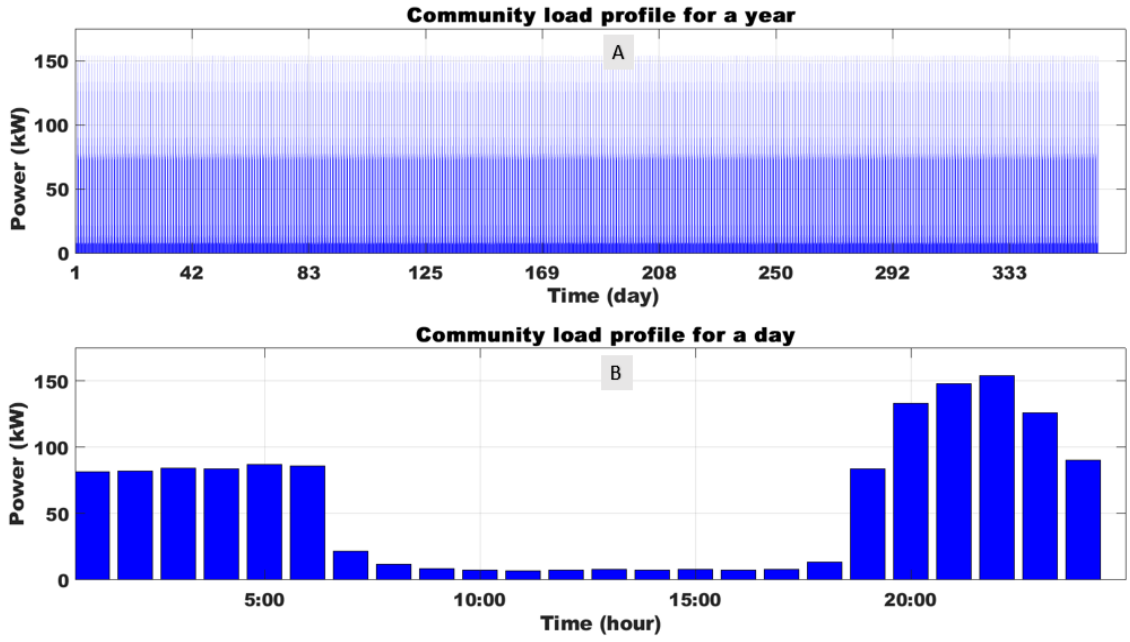

Fig. 7.2. Hourly time step load profile for the studied rural community

In comparison to the minutely simulated load profile (see Fig. 5.25), the morning peak is less evident as shown in Fig. 7.2B. This is because amongst the electrical

appliances used in the morning, some of the appliances operating duration in an hour is low (e.g. electric iron), hence, their effect is averaged over an hour, while some other appliances with relatively high operating duration, their percentage ownership within the community (see Fig. 5.8) is low (e.g. refrigerator). Therefore, the security/outside incandescent bulbs in the community is responsible for most of the energy consumption in the morning.

7.2.2 PV energy system

The approach employed for estimating the hourly solar insolation of a PV panel that is positioned annually at its optimal tilt angle is presented in Chapter 6. So, the meteorological data for simulating the PV generated energy are the hourly estimated solar insolation at an annual tilt angle of 11.6° (i.e. the studied location annual optimal tilt angle) and Benin city measured ambient temperature by national centre for energy and environment (NCEE). The Benin city measured ambient temperature is used in this study because there is no annual measured ambient temperature for the studied location, and the ambient temperature of both locations are expected to be alike. A plot of the studied location hourly estimated solar insolation at optimal annual tilt angle is presented in Fig. 7.3.

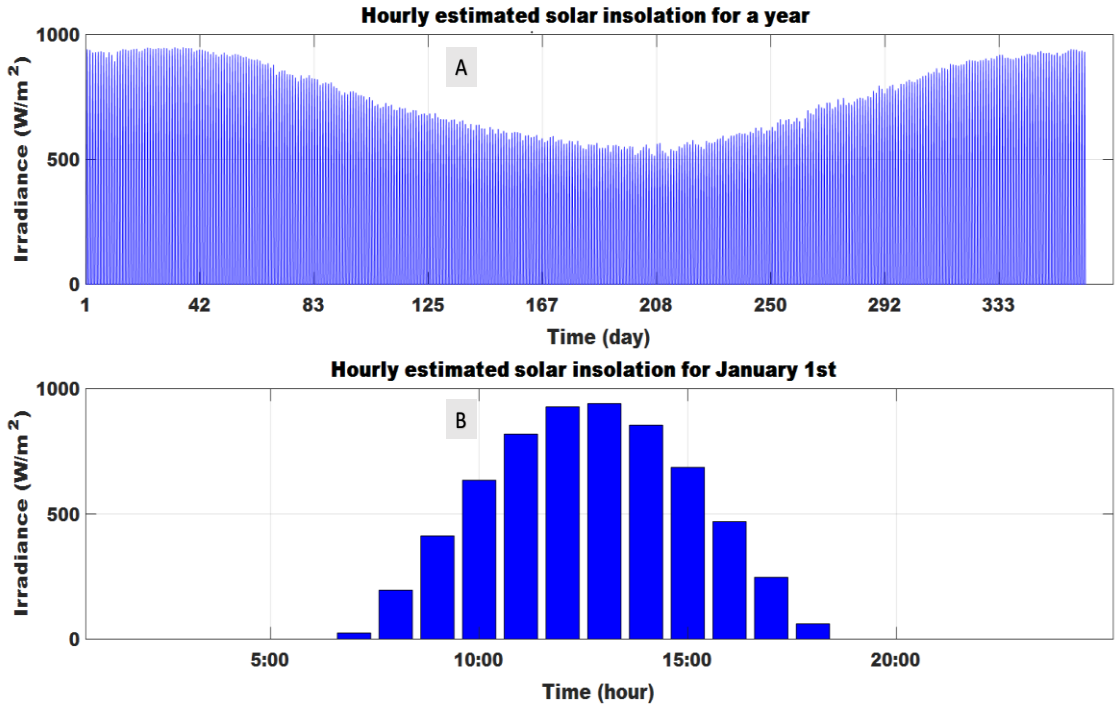

Fig. 7.3. Hourly estimated solar insolation at optimal annual tilt angle

Cloudy weather conditions experienced during rainy season months (i.e. between March and October) that causes the PV panel to be over-cast is responsible for the noticeable dip in the values of the estimated solar insolation in Fig. 7.3A. Detailed evaluation of the amount of solar insolation received in the studied location at different time of the year as well as when the PV panel is placed horizontally or inclined at different angular positions has already been presented in Chapter 6. National centre for energy and environment (NCEE) measured ambient temperature for Benin, Nigeria, is measured every 5-minutes. But because hourly simulation is performed here, hourly average of the measured ambient temperature is presented in Fig. 7.4.

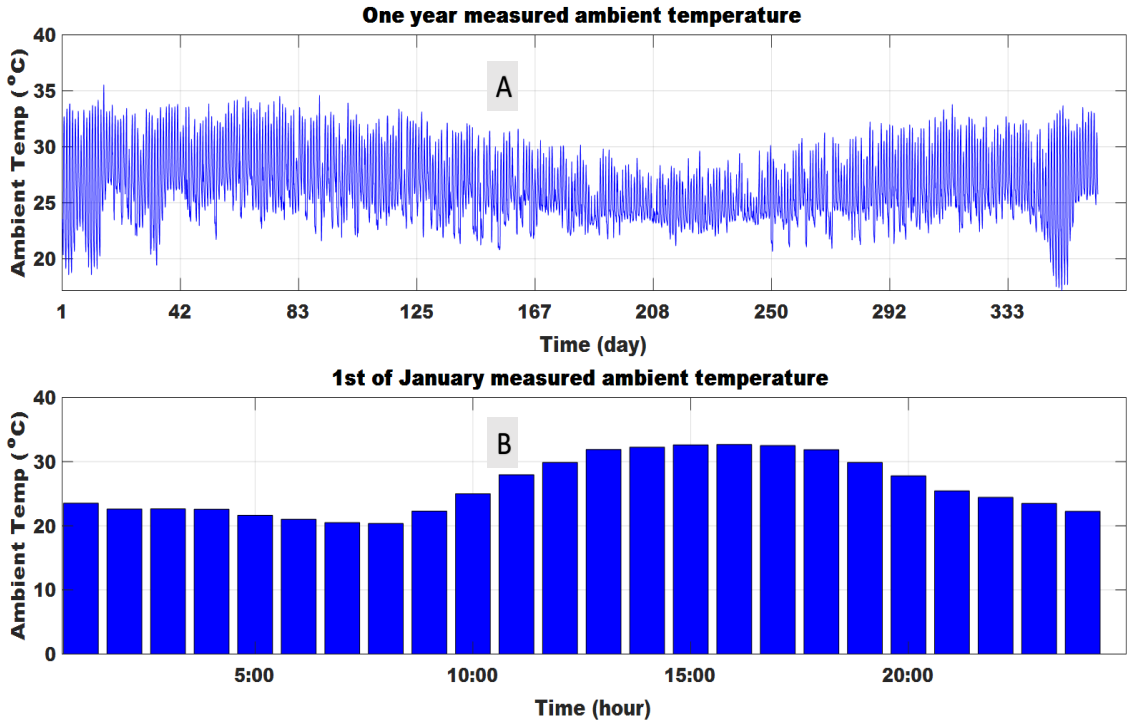

Fig. 7.4. Annual measured ambient temperature for Benin, Nigeria

Over a year, Fig. 7.4A shows that the measured ambient temperature had its lowest peak values during the rainy seasons, while over a day, Fig. 7.4B show that the measured ambient temperature had its lowest values at night and during the early hours of the morning and its higher values in the afternoon and the early hours of the evening. Meanwhile, PV panel design parameters are available in the datasheet of PV modules. In this study, the design parameters obtained from the datasheet of

Canadian solar manufactured CS6U-340 poly crystalline silicon module are used for the simulation. Some important data from

Table 7.2. CS6U-340P design parameters for a 340 W_P module [187]

Module efficiency (η_{ref})	17.49%
Maximum power temperature coefficient (K_{temp})	$-0.39\ \%°C^{-1}$
Nominal operating cell temperature (NOCT)	43°C
Derating factor over 25 years (DF_{PV})	85 %
340 W_P module effective area	1960x992 mm^2

7.2.3 Biomass energy system

The generated biogas energy is dependent on the rated capacity of the biogas generator and the daily biogas production from the bio-digester/reactor. As earlier mentioned in Chapter 7.1, under the biogas generator operating condition, the biogas generator operate at full-loading condition (i.e. its rated capacity) and when the electrical load demand is lesser 50% (minimum load ratio), the biogas generator is turn-off. Bio-waste availability and the size of the bio-digester are amongst the main external factors that influence daily biogas production. Bio-waste can either be gotten locality or outsourced (purchased) from another location. Estimation of the bio-waste availability of a studied location is challenging. Therefore, some assumptions are made here in estimating the bio-waste availability in the community.

Assumptions for estimating the bio-waste availability in the community:

- Although co-digestion will likely result in higher biogas yield than a single feedstock digestion process [238], [247], [262], but the combinational proportion between the co-digested feedstocks must be maintained for optimal biogas production to be guaranteed [96], [238], [259]. So, this will result in an increase in the complexity of the anaerobic digestion process and the need for an expert for the digester operation. But, because the required expertise for the day to day operation of an installed anaerobic digester might not be guaranteed

in a rural community of a developing country like Nigeria, it is assumed here that the selected feedstock in the community are digested individually.

- Here, the available AD feedstock in the studied community are only from animal and household wastes because crop waste serves as animal feeds, and the balance are spread crop waste across the farmland as a crude way of improving the soil quality ahead of a new planting season. Also, it is assumed that digester waste is supply to the community farmland in order to augment the crop waste that were used as animal feeds.
- In the literature, Ogwueleka [68] reported that the average bio-waste generated by a rural dweller in Nigeria is 0.44 $kgcap^{-1}day^{-1}$ or $kghead^{-1}day^{-1}$. Meanwhile, Nigeria population increase from 140.4 million in 2006 [388] to 195.9 million in 2018 [6], i.e., 1.4 times the population of 2006. So, it is assumed that the population of every region in 2018 have increased by 1.4 times their population number of 2006. Because the population of Esan North-East local government area was 121989 in 2006 [388], then, the population of the area is 170785 in 2018. The average number of persons in each of the 26 communities in Esan North-East LGA is 6569. Assuming that 60% of the daily generated household waste were recovered [66], then, the total amount of daily waste generated in the community is 1734 kg. Furthermore, the daily specific biogas yield per kg of household waste is 0.02740 $m^3\ kg^{-1}day^{-1}$ [108], therefore, the daily estimated biogas production from household waste in the community is 47.51 m^3.
- 2016 animal population data (see Fig. 2.2) reported by FAO [90], are assumed to be equally distributed amongst Nigeria 774 local government area (LGA). Also, animal population in each LGA are also assumed to be equally distributed amongst the communities of an LGA. Therefore, estimated amount of biogas that can be generated from animal and human waste in the studied community are presented in Table 7.3

Table 7.3. Animals and human potential biogas production in the studied community

Animal species	Average population [a, b]	Dry dung output (kg/head /day) [c, d]	Dry dung (kg /day)	Biogas yield			
				Available fraction collected [d, e]	Total solid (kg /day)	Specific yield (m^3/ kg total solid) [d]	Biogas yield (m^3/ day)
Cattle	159 [a]	1.8 [c]	286.2	0.3 [d]	85.86	0.2	17.17
Goat	1251 [a]	0.4 [c]	500.4	0.4 [d]	200.16	0.25	50.04
Sheep	852 [a]	0.4 [c]	340.8	0.3 [d]	102.24	0.25	25.56
Pig	305 [a]	0.8 [c]	244	0.8 [d]	195.2	0.56	109.31
Chicken	10551 [a]	0.06 [c]	633.06	0.8 [d]	506.45	0.28	141.81
Humans	6569 [b]	0.09 [d]	591.21	0.125 [e]	73.90	0.45	33.26
Total							377.15

Source: [a][90], [b][6], [388], [c][67], [d] [66], [e] [460].

Therefore, the annual estimated biogas production from household and animal waste in the studied community is 155001 m^3. In terms of the cost of purchasing cow dung, market survey from 5 sellers of cow dung reveals that the equivalent cost of cow dung that can product 1 m^3 of biogas is $0.28. Meanwhile. the total size of the bio-digester is dependent on the daily amount of feedstock (i.e. gotten locality and/or purchased) fed into the digester.

By applying Eqs. (4.9) – (4.14) in Section 4.2.1 to model the biogas energy system, the annual biogas consumption and the anaerobic digester volume of the system can be calculated with respect to the size of biogas generator. Therefore, for different selected sizes of biogas generators that operate all through a year at full-loading condition, the calculated values for annual biogas consumption and anaerobic digester volume is presented in Fig. 7.5.

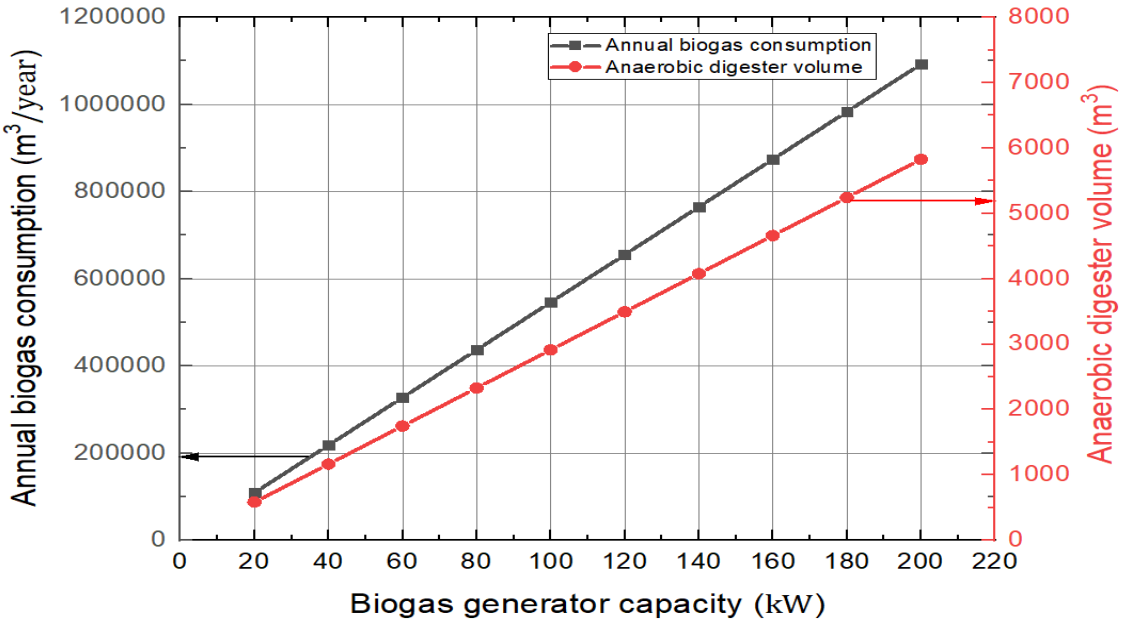

Fig. 7.5. Annual biogas consumption and anaerobic digester volume required by different biogas generator capacities.

The biogas energy system modelling outcomes in Fig. 7.5 can be used to make important decision during the project planning of a biomass energy system. For example, if a 100kW biogas generator is installed in the studied community and it is operated continuously throughout the year, the studied community annual biogas production of 155001m^3 can only supply 28.4% of the biogas consumed by the 100kW biogas generator. But if the 100kW biogas generator total usage in a year is 6 months, the studied community annual biogas production can supply 56.8% of the biogas consumed by the 100kW biogas generator. Consequently, biogas generator should only be used during periods of high energy consumption because continuous usage of biogas generator result in excessive demand for bio-waste beyond the studied location bio-waste generation capability estimated and anaerobic digester volume also increase with continuous biogas generator usage

7.2.4 Battery energy system

Section 3.3 explains that the HRES battery is used to supply energy to the load whenever selected combinations of PV and biogas generator capacities in the feasible region of the HRES design space cannot supply the entire load. By the

application of Eqs. (4.15) - (4.20), the battery energy system used here is modelled. To supply reliable energy to the surveyed community annual load profile in Fig. 7.2, the optimal size of battery capacity that should be integrated with different combinations of PV and biogas generator capacities is studied in this section. The biogas generator capacities selected here, only operate daily at full-load condition from 19:00 in the evening to 6:00 in the morning because about 94% of the daily energy demand of the community are consumed during this period and continuous operation of biogas generator can increase bio-waste demand beyond the community waste generation capacity. Based on this, the optimal size of battery capacity that should be integrated with different combinations of PV and biogas generator capacities in order to supply reliable energy surveyed community load is presented in Fig. 7.6.

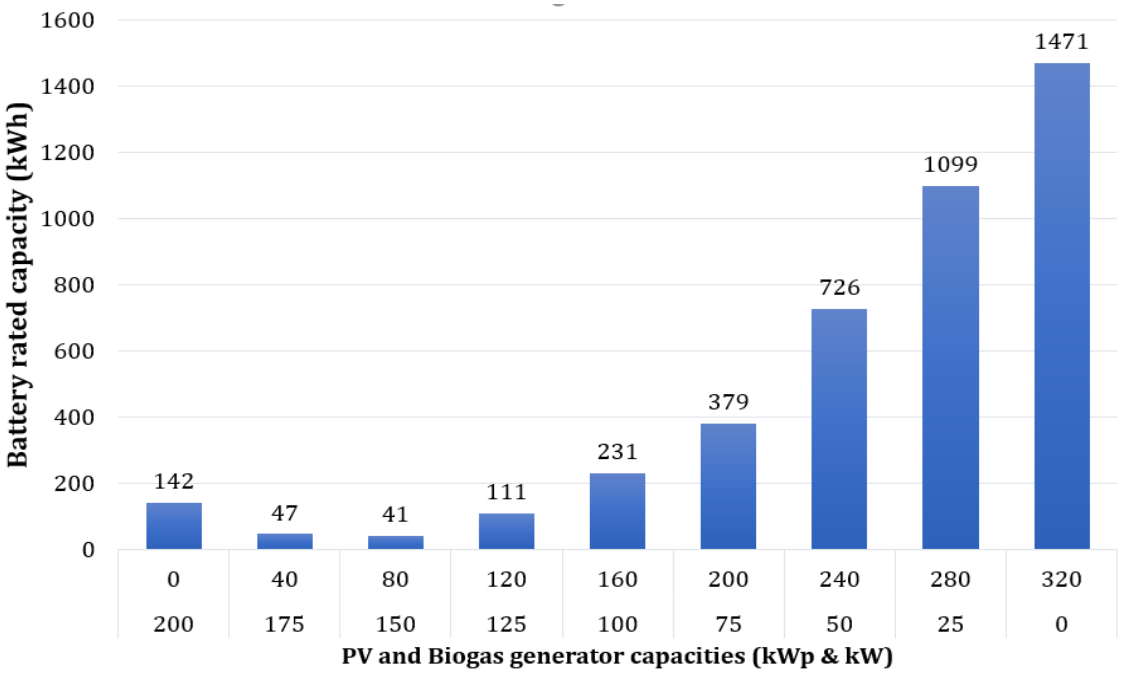

Fig. 7.6. Optimal battery capacity for different combinations of PV and Biogas generator capacities

On the x-axis of Fig. 7.6, the rated capacities 0 to 320 kW_P and 0 to 200 kW show selected capacities of PV and biogas generators respectively. It is evident from Fig. 7.6 that in the feasible region of HRES design space, there is more demand for battery when only PV is selected electricity generation than when only biogas generator is selected. Fig. 7.6 also shows that when PV and biogas generator

capacities were optimally combined, the required battery capacity is much lower than when only biogas generator or only PV is selected for electricity generation.

7.3 Hybrid energy system techno-economic analysis

In this section, the cost of HRES components is considered when calculating the optimal combinations of HRES component that will supply reliable energy to the load profile in Fig. 7.2. Outcomes from the optimization process is presented and discussed. Sensitivity analysis on how different sizing decision criteria affect the optimum combination of hybrid system components is also presented. Accurate hybrid energy system modelling was ensured by carrying out annual hourly simulations. This is because seasonal inputs such as solar radiation and ambient temperature vary seasonally over a year. The electrical load demand data presented in Fig. 7.2 and meteorological data (hourly solar insolation and ambient temperature data) presented in Fig. 7.3 and in Fig. 7.4, and other system component design parameters in Table 7.1 are used as the inputs for simulating the optimize of hybrid energy system components. A contour plot of annualized system costs that were calculated from different combinations of PV and biogas generator capacities in the design space is presented in Fig. 7.7.

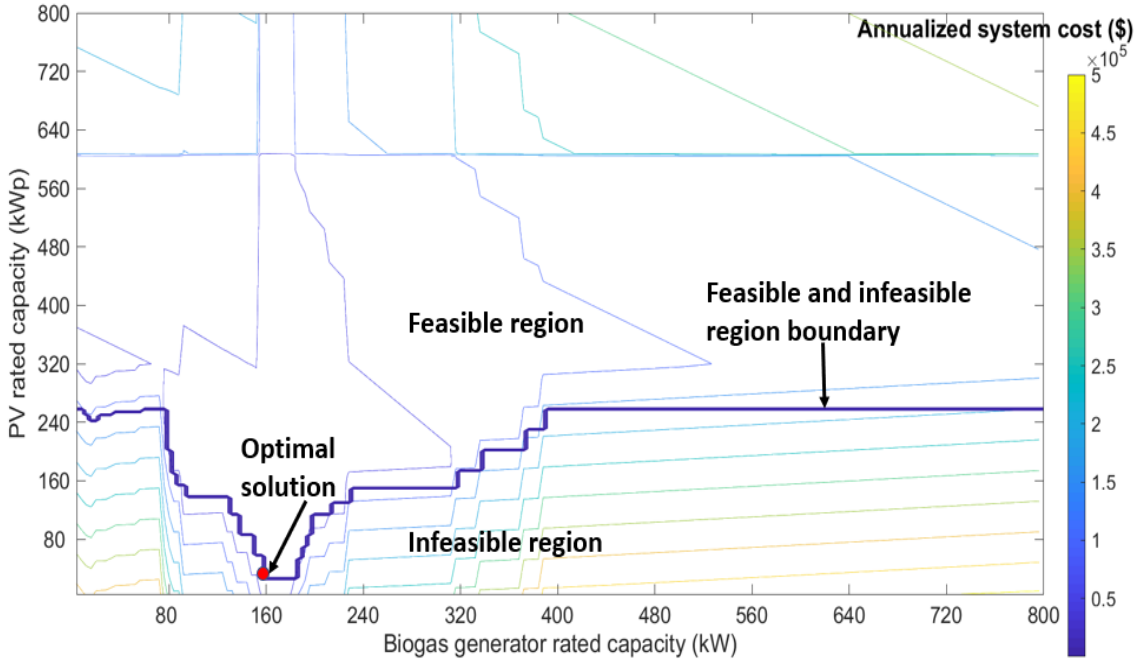

Fig. 7.7. Design space search of optimal solution

To ensure that there is no un-met load (0% loss of load probability), Fig. 7.7 shows that the feasible region is separated from the infeasible region by the feasible and infeasible region boundary. The variations in the feasible and infeasible region boundary is an indication of how the use of battery energy storage for balancing energy mismatch in the hybrid energy system influence the selection of PV and biogas generator capacities in the feasible region of the design space. Meanwhile, in the feasible region of the design space, the point of optimal solution is the point whereby the combination of PV, biogas generator, and battery energy storage results in the lowest possible system cost (i.e., optimization of system cost).

Even though the infeasible region is not a useful region in the design space, the high system cost at the bottom of the infeasible region is an indication of the impact of a high increase in the size of battery energy storage on the system cost, when the rated capacity of PV and/or biogas generator is low. Furthermore, the high system cost at the bottom right corner of Fig. 7.7 (infeasible region), despite the increase rated capacity of biogas generator, is because the biogas generator is not used to supply electricity to the community load whenever the load demand is lower than 50% of the size of the biogas generator rated. Consequently, a high battery energy storage capacity (that result in an increase in system cost) is required to supply electricity to the load since the PV rated capacity was low.

At the point of optimal solution (i.e., the minimum hybrid energy system annualized total cost that guarantees 0% loss of power supply probability), the rated capacity of PV system, biogas generator, battery energy storage, and converter system were 40 kW_P, 160 kW, 32 kWh, and 24 kW respectively. The hybrid energy system annualized total cost at the point of optimal solution in the design space was \$78708. Furthermore, the hybrid energy system levelized unit cost of energy (LCOE) and net present cost (NPC) was \$0.1657/kWh and $\$1.2634 \times 10^6$ respectively. A breakdown of the hybrid energy system annualized total cost ($C_{ann,tot}$) into the PV system annualized cost, biogas system annualized cost, battery system annualized cost, and converter system annualized cost is presented in Fig. 7.8.

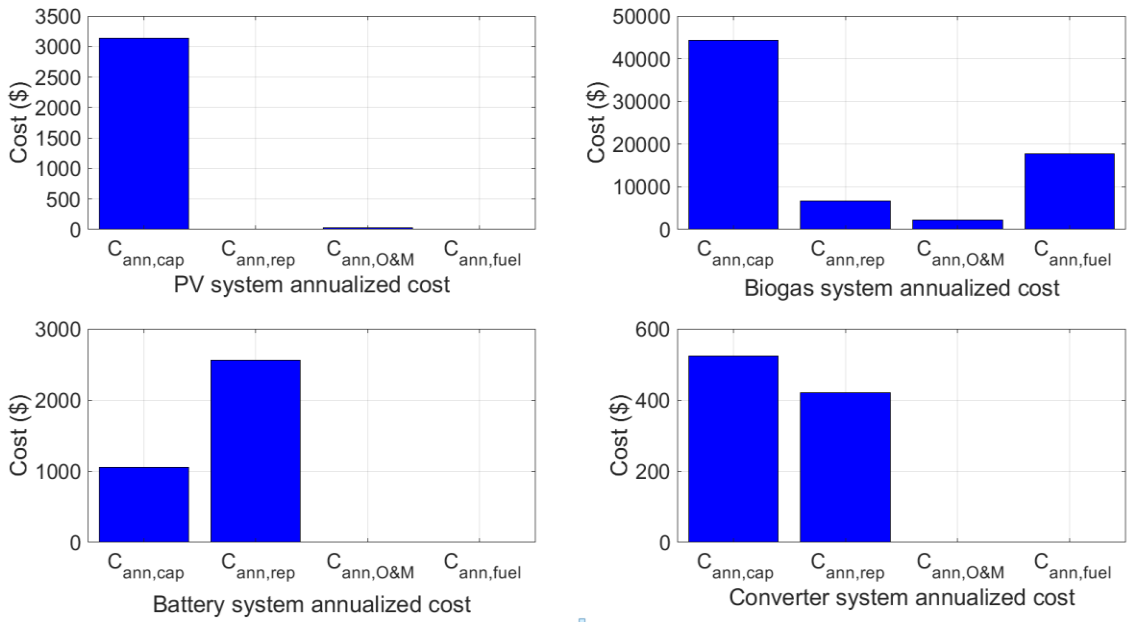

Fig. 7.8. Hybrid energy system components annualized cost distribution

The total annualized capital ($C_{ann,cap}$), total annualized replacement cost ($C_{ann,rep}$), total annualized operation and maintenance cost ($C_{ann,O\&M}$), and total annualized fuel cost ($C_{ann,fuel}$) in Fig. 7.8, account for 62%, 12%, 3%, and 23% respectively of the hybrid energy system annualized total cost of $78708. Furthermore, Fig. 7.8 shows that PV system, biogas system, battery energy storage system, and converter system accounted for 4%, 90%, 5%, and 1% respectively, of the hybrid energy system annualized total cost. The design of the converter in terms of the maximum power flow between the DC bus and AC bus in Section 4.2.3 rather than on the peak load is the reason why the optimal size and annualized total cost of the converter is 24kW and $944 respectively. The biogas system annualized cost (i.e., a combination of the annualized cost of the biogas generator, the anaerobic digester, and the fuel cost) account for most of the hybrid energy system annualized total cost because when the biogas generator is used (i.e., when the load demand is at least 50% of the peak load demand), it supplies most of the community residential load demands (see Fig. 7.2). Also, for healthy operation of the biogas generator, it operates under full load condition.

By operating the biogas generator under full load conditon, only 31% of the biogas generator supplied electricity was consumed by the community while the rest was

sold to the grid. The amount of biogas required to operate the biogas generator annually under full load conditon was 4.526×10^5 m^3 $year^{-1}$, while the anaerobic digester volume that is needed to generate the required amount of biogas is 2.5177×10^3 m^3. From Section 7.2.3, the amount of biogas that can be generated annually from the community waste was 1.610×10^5 m^3 $year^{-1}$ (i.e., 36% of the total required biogas). So, the balance amount of biogas (2.916×10^5 m^3) is generated from purchased cow dung. Consequently, the quantity of cow dung to be purchased annually is 1.458×10^6 kg $year^{-1}$, while the annual cost of purchasing the cow dung is $81648. However, a total of $63847 will be generated by selling the excess electricity supplied by the biogas generator to the grid. Therefore, the cost of purchasing cow dung (biogas system annualized fuel cost) was reduced to $17801 as shown in Fig. 7.8.

To illustrate the supply-demand energy balance (i.e. 0% loss of power supply probability) of the hybrid energy system, the hourly relationship between the energy demanded and the energy supplied on the 1st of August (i.e. day of the year in the community with the least daily solar irradiation) is presented in Fig. 7.9.

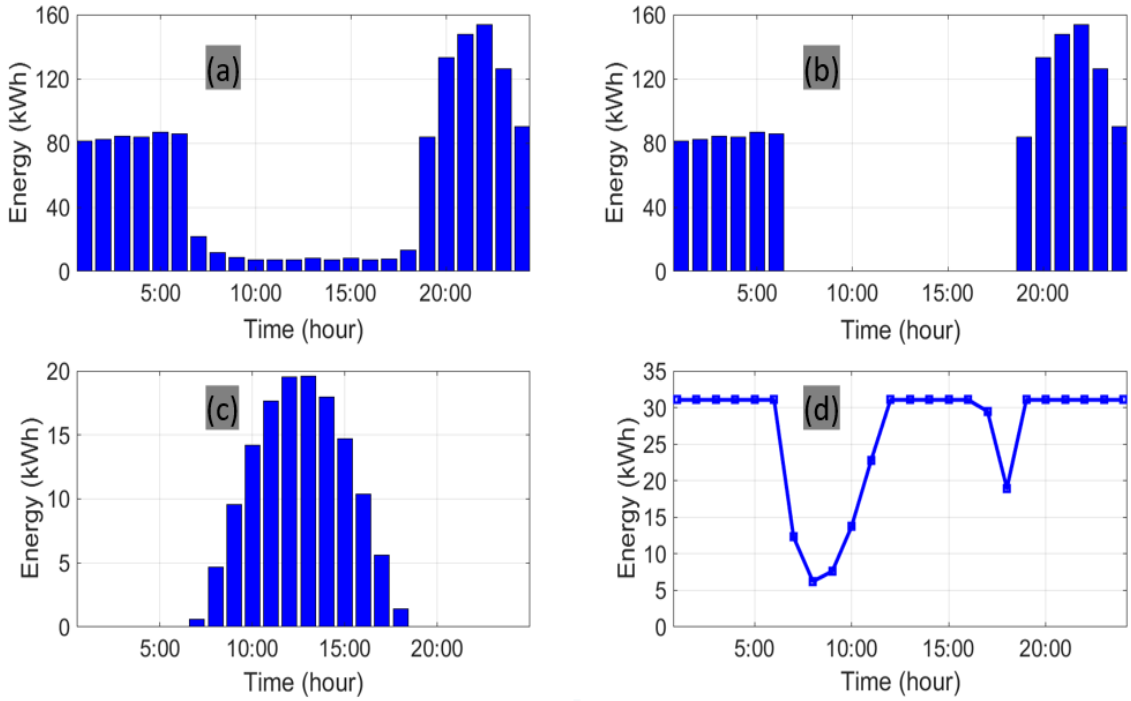

Fig. 7.9. Hybrid energy system balance relationship. (a) Community households' electrical load, (b) Bio-energy generation, (c) PV generation, (d) Battery state of charge

Fig. 7.9 shows that the energy mismatch between the generators supplied electricity and the community load demand was met by the battery energy storage. Specifically, Fig. 7.9b shows that the biogas generator operated under full-loading condition, and it supplied the community electrical load whenever the community electrical load was up to 50% of its rated capacity. Whilst, Fig. 7.9d shows that from 6:00 – 8:00 hours and from 16:00 – 18:00 hours, the battery energy storage supplied either the entire or part of the community electrical load. The battery state of charge in Fig. 7.9d also shows that the battery energy storage was constrained not to discharge energy beyond its depth of discharge (DOD). Meanwhile, because the community households' electrical load are non-critical loads, part or the entire community households' electrical load supplied by the battery energy storage in Fig. 7.9d can be shifted to the first and last operating hours (i.e., 18:00 and 5:00 hours respectively) of the biogas generator, without increasing the rated capacity of the biogas generator.

During demand side management, load shifting techniques can be applied to a load profile in order to reduce the optimal size of generators and/or energy storage [366], [400], [402], [461]–[463]. With respect to Fig. 7.9, if the community households' electrical load supplied by the battery energy storage at 6:00 hour is shifted to 5:00 hour, the battery energy storage capacity is reduced by 51% to 15 kWh. Also, if the community households' electrical load supplied by the battery energy storage at 6:00 and 17:00 hours are shifted to 5:00 and 18:00 hours respectively, the battery energy storage capacity is reduced by 79% to 8 kWh. Furthermore, the use of battery energy storage can be avoided by shifting the community households' electrical load supplied by the battery energy storage from 6:00 – 8:00 hours and from 16:00 – 18:00 hours to 5:00 and 18:00 hours respectively. Research on the development of a suitable model that can encourage load shifting of the community peak load demand is necessary in future study because biogas generator optimal sizing, and the anaerobic digester volume, and the biogas fuel consumption is influenced by the peak load demand of the community.

Meanwhile, assuming that the life style of the community household occupants does not support the shifting of the community households' electrical load, but it is

possible to slightly increase the hybrid energy system 0% loss of power supply probability (LPSP), then, the hybrid energy system annual LSPS when the capacity of the battery energy storage is reduced to 15 kWh, 8 kWh and 0 kWh (i.e., no battery energy storage), is 1.7%, 2.3%, and 3.7% respectively. Therefore, the effect of an increase in the loss of power supply probability of the hybrid energy system (i.e., from 0% LSPS to 1.7% LSPS, 2.3% LSPS, or 3.7% LSPS) on the net present cost (NPC) and levelized cost of energy (LCOE) is presented in Fig. 7.10.

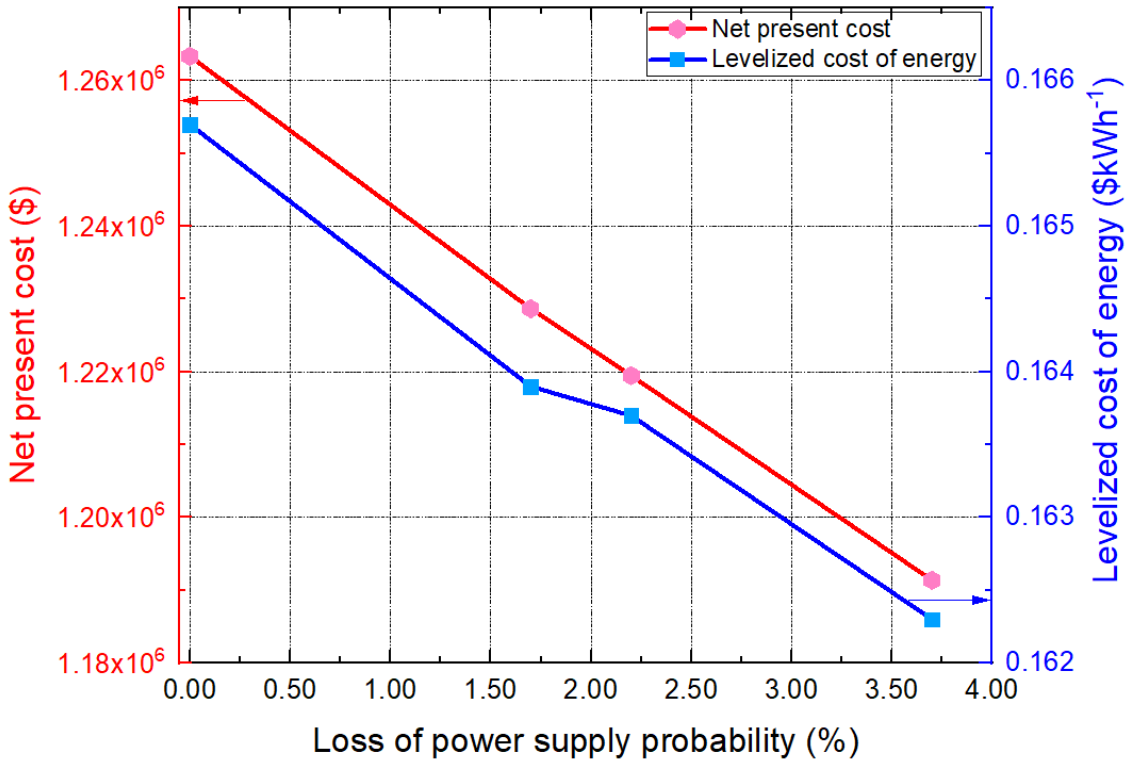

Fig. 7.10. Effect of selected LPSP on NPC and LCOE of the HRES

Fig. 7.10 shows that when the loss of power supply probability (LPSP) of the hybrid energy system was increased in order to reduce the battery energy storage annualized system cost, the net present cost (NPC) and the levelized cost of energy (LCOE) were reduced. For example, when the hybrid energy system LPSP was increased from 0% to 3.7%, the hybrid energy system NPC and LCOE were reduced by 5.7% and 2.1% respectively. Therefore, the complete removal of the battery energy storage from the hybrid energy system is perhaps the most preferred option because despite the increase in the hybrid energy system LPSP, there is the

noticeable reduction in NPC and LCOE as well as in the complexity of the hybrid energy system. Furthermore, because of the load profile of the community, the complete removal of the battery energy storage also takes away the concern that part of the battery might easily be stolen, the concern that there might be a need for an early battery replacement because its cycle lifetime is limited. Also, an inverter and not a bi-directional converter will be required by the hybrid energy system.

The HRES LCOE presented in Fig. 7.10 can compete with the LCOE of a diesel alone energy system and the LCOE of the national grid. For example, at 0% LPSP, LCOE for this study HRES was $0.1657/kWh, but the LCOE for a diesel alone energy system was $0.62/kWh [85]. Despite the national grid unreliability (see Fig. 5.6), the studied location 2019 residential customers reflective tariff (i.e., a tariff without subsidizes) was $0.164/kWh [451]. Furthermore, if the HRES LPSP is increased to 3.7%, its LCOE is reduced to $0.1623/kWh. So, for a LPSP of 3.7%, the HRES LCOE is less than the rural area residential customers tariff. Meanwhile, more reduction in the hybrid energy system LCOE can be achieved by the development of an energy scheme for peak load shifting of the community load profile or by aggregating communities' residential load profiles in a regional grid. Research on the development of an energy scheme for peak load shifting of the community load profile will be performed in future studies, but a study on the effect of communities' residential load profile aggregation on a regional grid is performed in the next section of this chapter.

7.4 Study of the effect of load aggregation on a regional grid

The aggregation of regional loads in a regional-grid leads to peak demand shaving (lower load diversity factor or coincidence factor) [444]. For example, in Chapter 5, comparison between a single household load profile in Fig. 5.24 and a community load profile in Fig. 5.26 shows that the higher the number of residential customers

(electrical loads) connected to an electrical network, the lower the load diversity[1] factor and the estimated size of generators are reduced. When regional electrical loads (load bus) are aggregated in a regional grid, it will cost less to supply reliable electricity to more people. Meanwhile, if the regional loads (load buses) in a regional grid are not close to each other, there will be substantial power losses in the network [346]–[349]. Therefore, a power flow study is performed here to evaluate if it is a better operating strategy to centralize or distribute generators in order to minimise the power losses in the network and to guarantee the healthy operation of the regional grid. The modelling approach (flow chart) used in carrying out the power flow study is presented in Fig. 4.5, while more detailed explanations on how Fig. 4.5 sub-system simulations are performed are presented in Eqs. (4.51) – (4.64).

7.4.1 Estimation of power flow study input parameters

To perform this study, a regional grid that comprises of 5 interconnected loads centres is investigated here. Typically, the first step to study a power network problem is to convert the power network into a one-line diagram representation, so that a simplified power flow study can be performed. This is necessary because power flow study input parameters, such as, bus data, transmission line data and transformer data can easily be defined/represented in a one-line diagram, hence, unusual network conditions, such as low voltage and excessive load on the transmission line, can be identified on the one-line diagram and corrected before it escalates into a major network problem [350]. Therefore, a one-line diagram representation of the regional-grid is presented in Fig. 7.11.

[1] Load diversity is defined as the total expected power drawn from a power source by a device or system of devices during peak period.

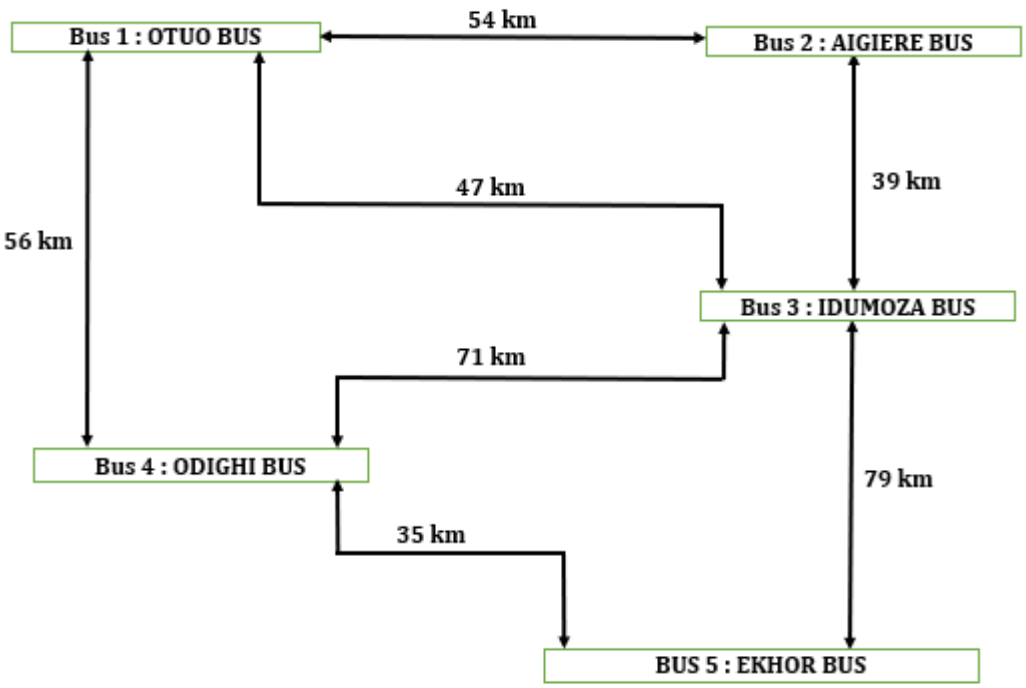

Fig. 7.11. One-line diagram of a distributed power network

The 5 load buses in Fig. 7.11 were selected from the 3 senatorial districts in Edo state (i.e., Odighi and Ekhor load buses are in Edo south senatorial district, Otuo and Aigiere load buses are in Edo north senatorial district, while Idumoza load bus is in Edo central senatorial district), so that continuous grid expansion can be achieved. Also, Otuo load bus, Aigiere load bus, Idumoza load bus, Odighi load bus, and Ekhor load bus are located in Owan East LGA, Etsako East LGA, Esan North-East LGA, Ovia North-East LGA, and Uhunmwonde LGA respectively. Furthermore, to guarantee energy security, the selected load centres are interconnected by 7 transmission lines, that is, each load centre is connected to a minimum of 2 transmission lines. As shown in Fig. 4.5, the actual power flow simulation begins with the initialization of assigned power network parameters (i.e., electrical loads, generation specifications and constraints), then, the subsequent parameters such as bus admittance matrix, bus conductance matrix, and bus susceptance matrix of the power network are calculated before Newton Raphson method (a mathematical technique) is used to simulate the power flow in the power network.

To determine the electrical load parameters in the 5 load buses, it is assumed that each of the 5 load buses in Fig. 7.11 are connected to all the residential electrical

loads in their respective local government areas. So, the aggregated residential electrical loads in a selected local government area (load bus) is referred to as a regional load. Because there are 26 communities in Esan North-East LGA, and the studied community had 409 residential customers (see Chapter 5), the total residential customers connected to Idumoza bus is 10634. Furthermore, because the 5 selected local government areas are in the same states in Nigeria, it is assumed that household occupants' consumption behaviour and appliance ownership in the five selected local government areas are alike. Therefore, population and housing census data were used to scale the number of residential customers that are connected to the other four load buses.

Based on population and housing census data, the ratio of the number of households in Esan North-East LGA to the number of households in Ovia North-East LGA, Uhunmwonde LGA, Owan East LGA, and Etsako East LGA is 1:1.13, 1:1.04, 1:1.31, and 1:1.22 respectively [388]. So, the estimated number of residential customers in Ovia North-East LGA, Uhunmwonde LGA, Owan East LGA, and Etsako East LGA is 12016, 11059, 13931, and 12973 respectively. Meanwhile, because the 5 load centres in Fig. 7.11 are interconnected and it is assumed that their household occupants' consumption behaviour and appliance ownership are alike, the aggregated number of residential customers in the regional-grid is 60613. The developed stochastic load model in Chapter 5 is used to simulate the regional-grid annual load profile. Simulation of the regional-grid annual load profile shows that the peak load for the regional-grid is 17.7 MW. A 23% reduction in peak load was achieved when compared with the expected peak load if the peak load of 156kW for 409 residential customers was scaled to represent the peak load of the 60613 residential customers in the regional grid. The reduction in the regional-grid peak load is associated with the higher number of residential customers in the regional-grid; which leads to a lower load diversity factor [444].

Consequently, the load profile of the 5 load buses in Fig. 7.11 were estimated by using the ratio between the number of households in the 5 local government areas to scaled the simulated regional-grid load profile. Therefore, the estimated real power drawn at peak load from Otuo bus, Aigiere bus, Idumoza bus, Odighi bus, and

Ekhor bus is 4.07 MW, 3.79 MW, 3.10 MW, 3.51 MW, and 3.23 MW respectively. Meanwhile, because excess generated energy can be sold to the grid, Nigeria grid recommended power factor value of 0.86 is used here to estimate the reactive power and the apparent power of the power network. For example, based on the estimated real power drawn from the 5 selected buses at peak load, the equivalent reactive power drawn at peak load from Otuo bus, Aigiere bus, Idumoza bus, Odighi bus, and Ekhor bus is 2.41 MV_{ar}, 2.25 MV_{ar}, 1.84 MV_{ar}, 2.08 MV_{ar}, and 1.92 MV_{ar} respectively, while the equivalent apparent power drawn at peak load from Otuo bus, Aigiere bus, Idumoza bus, Odighi bus, and Ekhor bus is 4.73 MVA, 4.41 MVA, 3.61 MVA, 4.08 MVA, and 3.76 MVA respectively.

The developed design space optimization technique presented in Fig. 4.4 and Fig. 7.1 is used to optimally size the PV, biogas generator, and battery storage. So, with the assumption that the meteorological characteristics of the regional-grid are similar, and the use of the simulated regional-grid annual load profile, the optimal size of the PV, biogas generator, and battery energy storage that is required to supply electricity to the regional-grid loads is 2.78 MW_P, 17.7 MW (20.58 MVA), and 1.83 MWh respectively. However, because the removal of the battery energy storage will only slightly increase the regional grid LSPS but will lead to reduction of the net present cost and levelized cost of energy of the regional grid, it is removed from the power flow study.

Meanwhile, because transmission line apparent power losses benchmark for developing countries is 2 – 6 % [43], the simulated values from the optimal sizing of PV, and biogas generator is scaled by 6% to 2.95 MW_P, 18.76 MW (21.82 MVA) respectively. The optimally sized PV, and biogas generators can either be distributed or centralized because renewable generators are scalable [46], [445], [446]. In practice, most biogas generator are designed to operate with natural gas, while Edo state (study location) is one of the locations in Nigeria with large natural gas deposit, therefore, challenges with the purchase of the desired amount of bio-waste or the construction of large anaerobic digester volume that can affect the reliable supply of biogas to the biogas generator can be resolved by the use natural gas, despite its less environmental friendly nature.

With respect to the transmission lines modelling input parameters, because 79 km is the maximum length of all the transmission lines in Fig. 7.11, and the maximum length of a short transmission line is 80 km [352], therefore, the characteristics of a short transmission line is used to estimate the impedance of the 7 transmission lines in the regional-grid. For a regional-grid with short transmission lines, and a transmission voltage level of 33 kV is recommended for the transmission of electricity amongst load buses of the network [352], [464]. Typically, in Nigeria, the conductor size of a 33 kV transmission lines is 150 mm^2. Based on the design standards of international electrotechnical commission (IEC), the resistance and inductive reactance per kilometre for a 33 kV transmission line with a conductor size of 150 mm^2, is 0.27 $\Omega\ km^{-1}$ and 0.12 $\Omega\ km^{-1}$ [464]. So, the impedance of the 79 km transmission line between Idumoza bus and Ekhor bus is $(21.33 + j9.48)\ \Omega$. Note that for a short transmission line, the capacitive reactance is negligible [465].

To estimate the transformer input modelling parameters, the maximum apparent power that can be drawn from the regional grid is used. So, with the assumption that the PV, and biogas generator are centralized, all the regional-grid loads will be directly or in-directly connected to the load bus with the centralized PV and biogas generators. Also, because the maximum apparent power that can be drawn from the regional-grid is a function of the maximum apparent power drawn from the regional-grid at peak load and the total apparent power losses in the network, the maximum apparent power that can be drawn from the regional-grid can be estimated by scaling the apparent power drawn from the regional-grid at peak load (20.58 MVA) by 6% (i.e., the maximum benchmark for developing countries transmission line apparent power losses). Therefore, a transformer rating of 25 MVA and 11 kV/33 kV is selected here for each of the 5 load buses. Meanwhile, for transformers with rated capacity between 6.3 MVA and 25 MVA, the impedance of the transformer is estimated by a reactive reactance of 8% [466]. So, reactance of the transformers in the regional-grid 5 load buses is 8%.

As a result of the one-line diagram representation of the power network, the transformer reactive reactance of 8% is added to the transmission line impedance during the calculation of the power losses in the network. So, the transmission lines

estimated power losses are dependent on the transmission lines impedance and the transformer impedance. Typically, simulation of power flow studies are performed in terms of per-unit (PU) values [346], [347], [349]. Therefore, the per-unit values of transmission line impedance and the transformer impedance in power flow model are combined. Meanwhile, because the maximum estimated apparent power that can be drawn from the regional-grid is 21.82 MVA, and a voltage level of 33 kV is selected for the short transmission line network, a base apparent power (S_{base}) and a base voltage (V_{base}) of 25 MVA and 33 kV respectively are used for calculating the per-unit values of the power flow model input parameters. Whilst, the base impedance (Z_{base}) is defined in terms of the base apparent power and the base voltage as [347], [349]:

$$Z_{base} = \frac{(V_{base})^2}{S_{base}} = \frac{(kV)^2}{MVA} = 43.59\ \Omega \tag{7.1}$$

So, the per-unit value for the transmission line impedance is defined by [347], [349]:

$$Z_{TX-PU} = \frac{\text{Actual value}}{\text{Base value}} = \frac{Z_{TX-actual}}{Z_{base}} \tag{7.2}$$

The per-unit values for the impedance of the 7 transmission lines in the regional-grid is presented in Table 7.4.

Table 7.4. Transmission lines impedance per-unit values

Sending Bus		Receiving Bus		Transmission line impedance	
Bus Name	Bus No.	Bus Name	Bus No.	Resistance (Ω)	Reactance (Ω)
OTUO	1	AIGIERE	2	0.335	0.149
OTUO	1	IDUMOZA	3	0.292	0.130
OTUO	1	ODIGHI	4	0.346	0.154
AIGIERE	2	IDUMOZA	3	0.240	0.107
IDUMOZA	3	ODIGHI	4	0.440	0.196
ODIGHI	3	EKHOR	5	0.489	0.217
ODIGHI	4	EKHOR	5	0.216	0.096

7.4.2 Evaluation of the best approach to supply electricity in a regional grid

To minimise the transmission losses in the regional-grid, the power flow model calculated per-unit or normalized values of the input parameters were used to evaluate if centralised or distributed generation is the best approach to supply electricity to the load buses in a regional-grid. To carry out the power flow evaluation, three different cases were considered.

- Case 1: Centralization of the generators in the regional grid
- Case 2: Even distribution of the generators across the 5 load buses of the regional grid.
- Case 3: Distribution of the generators in the terms of the amount of apparent power drawn by each load bus of the regional grid. For example, because the ratio of apparent power drawn at peak load from Otuo in comparison to Odumoza is 1.33:1, the distribution ratio of generators between Otuo and Odumoza is 1.31:1.

Based on the power flow analysis, an illustration of the power flowing in and out of the load buses and the transmission line losses in the regional-grid is presented in Fig. 7.12. For this illustration, the regional-grid generators were centralized. Also, for this illustration, peak load is drawn from the regional-grid, and the PV system is not supplying electricity through the inverter to the regional-grid.

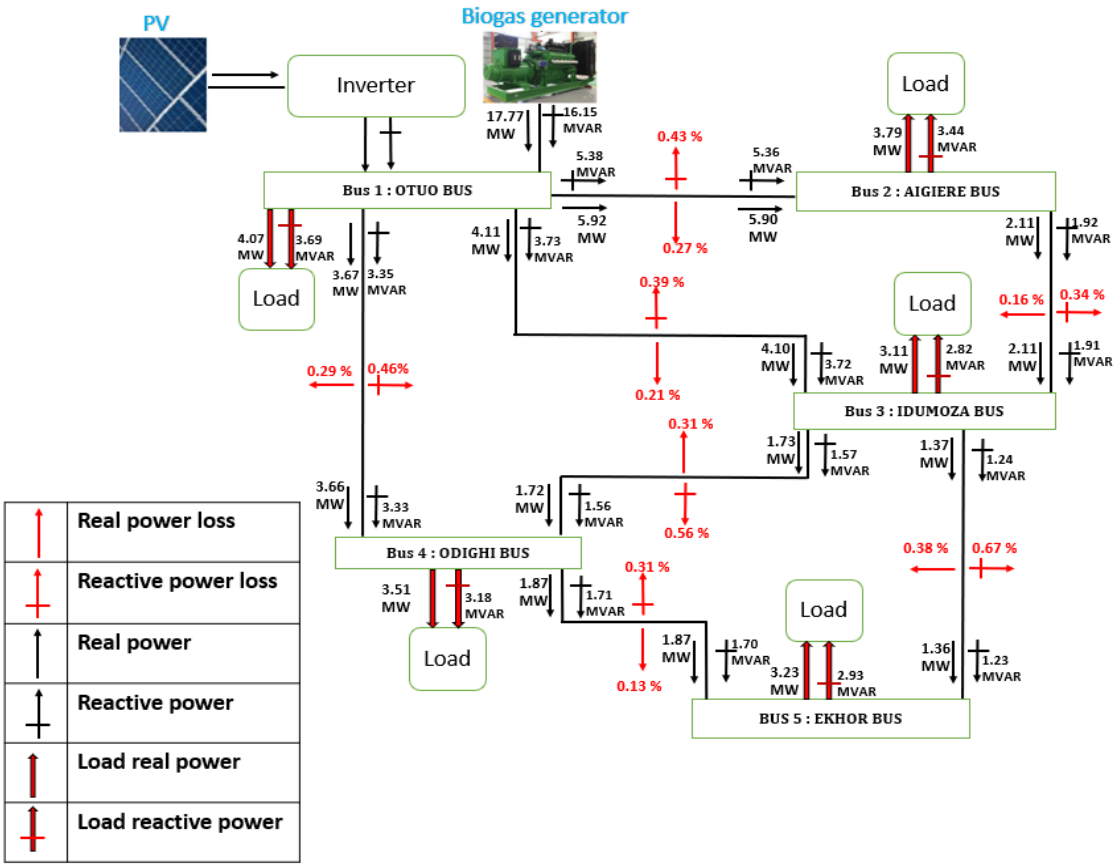

Fig. 7.12. Illustration of power flow simulation outcome

The simulated outcomes in Fig. 7.12 shows that the sum of the real power entering and leaving a load bus is the same (i.e., the algebraic sum of real power in a load bus is zero). Similarly, the algebraic sum of reactive power entering and leaving a load bus is zero. Also, Fig. 7.12 shows that the real and reactive power losses in the transmission line is affected by the length of the transmission line. The total real power losses, reactive power losses, and apparent losses in Fig. 7.12 is 0.40%, 0.57%, and 0.44% respectively, and these values are equivalent to a power of 70.8 kW, 59.9 kV_{ar}, 90.6 kVA. Furthermore, because the maximum benchmark for developing countries transmission losses was used to scale the size of the biogas generator, the regional-grid peak load and transmission line power losses were supplied by operating the biogas generator at 94.6% loading condition. Meanwhile, during the simulation period, the 5 load buses per-unit voltage and angle values are presented in Table 7.5.

Table 7.5. Voltage and angle parameters

Bus name	Voltage (Per unit)	Angle (radian)
OTUO	1	0
AIGERIE	0.9929	-0.3282
IDUMOZA	0.9963	-0.4320
ODIGHI	0.9904	-0.0229
EKHOR	0.9867	-0.2682

Table 7.5 shows that the maximum voltage deviation from Otuo (slack) bus was 1.33%, and the maximum voltage deviation value here is less than voltage deviation acceptable limit of 5% [352]. For the three cases considered, based on hourly power flow simulation of the regional-grid, the maximum percentage apparent power losses in the regional-grid is presented in Fig. 7.13.

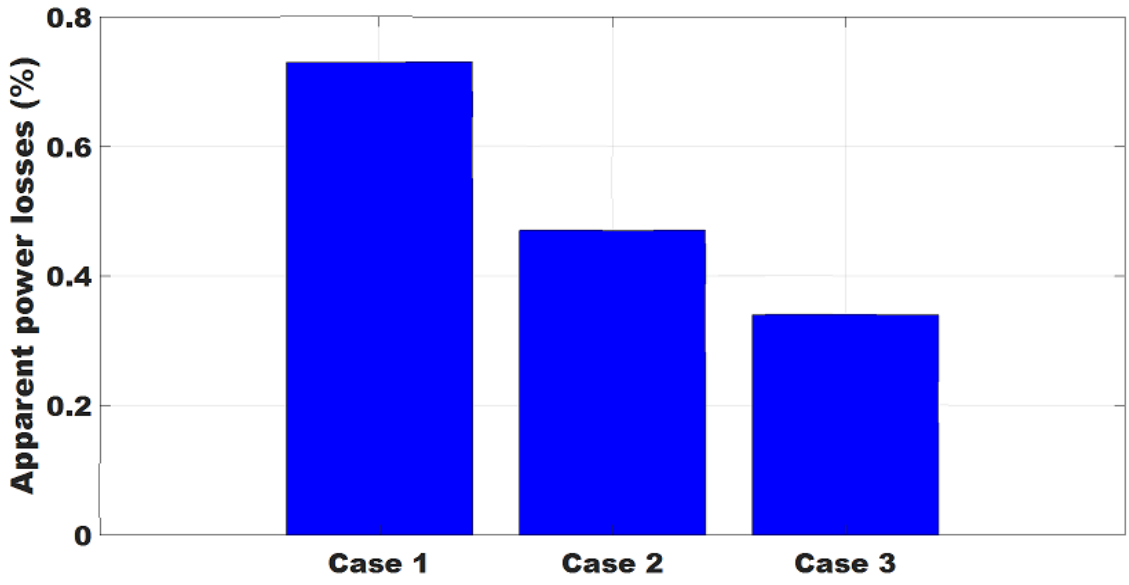

Fig. 7.13. Regional-grid maximum percentage of apparent power losses for the cases considered

Fig. 7.13 shows that the maximum percentage of apparent power losses for Case 1, Case 2, and Case 3 is 0.73%, 0.47%, and 0.34% respectively. Therefore, Case 3 is the best approach to supply electricity to the load buses in the regional grid. Although, Case 1 is the least favourable approach to supply electricity to the load buses in the

regional-grid, the maximum percentage apparent power losses for Case 1 is still lesser than the minimum transmission line benchmark of 2% that is acceptable for developing countries [43]. For the 3 cases considered, the maximum percentage of apparent power losses in the regional grid occurred during periods when the load demands were met by the PV system. This is perhaps because there are additional losses from the use of the inverter to convert the PV system DC energy to AC energy. Note that the regional-grid percentage apparent power losses for Case 1, Case 2, and Case 3 is equivalent to an apparent power of 18.92 kVA, 12.18 kVA, and 8.81 kVA respectively.

Comparison of the regional grid apparent power percentage loss at peak load to the regional-grid maximum apparent power percentage loss, shows that if the maximum apparent power percentage loss does not occur at the time of peak load, the use of the maximum apparent power percentage loss to estimate the actual amount of apparent power losses in the regional-grid can be misleading. For example, hourly power flow simulation of Case 1, show that regional-grid apparent power percentage loss at peak load is 0.44%, and this value the is less than 0.74% (which is the maximum apparent power percentage loss), but the regional-grid actual apparent power loss at peak load is 90 kVA, while for maximum apparent power percentage loss, the regional-grid actual apparent power loss is 18.92 kVA.

In summary, the power flow study performed here shows that the distribution of generators in the terms of the amount of apparent power drawn by each load bus of the regional-grid (Case 3) is the best approach to supply electricity to the regional-grid load buses. Hourly simulation of the power flow in a regional-grid is necessary for assessing the maximum apparent power loss in a regional-grid. Also, it is preferable to assess the regional-grid maximum apparent power losses in terms of its actual value (kVA) rather than its percentage values because the estimated value for maximum apparent power percentage loss might be misleading if it does not occur during the period of peak load.

7.5 Conclusion

Communal/regional grid electrification of rural residential electrical load can serve as a viable alternative to national grid electrification because it supports the aggregation of electrical loads, as well as serve as a quicker means of electrifying communities without electricity access or a means of supplying reliable electricity to communities that are connected to an un-reliable national grid. Two studies; techno-economic study and power flow study, were carried out in this chapter in order to evaluate the unit cost of using a hybrid PV and biogas generator to supply reliable electricity to a community residential loads, as well as to study the effect of load aggregation on a regional grid. A quick, and simplified optimization technique called design space optimization technique was used to optimally size the hybrid energy system components, while Newton Raphson method was used to perform the power flow study.

Biomass availability assessment shows that the quantity of recoverable household and animal bio-waste in the studied location is limited. To reduce the quantity of outsourced bio-waste and minimize anaerobic digester volume, biogas generator is only used when energy demand is greater than 50% of its rated capacity. Study on how different combinations of PV, biogas generator and battery systems affect the optimal sizing of battery shows that an optimally designed HRES requires a much smaller battery capacity than when a biogas generator and battery or a PV and battery are integrated for rural electrification in the studied location. Outcomes from the techno-economic study shows that the optimal size of PV system, biogas generator, battery energy storage, and converter system that guaranteed 0% loss of power supply probability (LPSP) at minimal hybrid energy system annualized total cost were 40 kW_P, 160 kW, 32 kWh, and 24 kW respectively. When the hybrid energy system supplies reliable electricity to the community at 0% LPSP, its minimal annualized total cost $(C_{ann,tot})$, levelized unit cost of energy (LCOE) and net present cost (NPC) was \$78708, \$0.166/kWh and $\$1.26 \times 10^6$ respectively.

Fig. 7.10 shows that the HRES LCOE can compete with the LCOE of a diesel alone energy system and the LCOE of the national grid. For example, at 0% LPSP, the HRES

LCOE is \$0.1657/kWh, but the LCOE for a diesel alone energy system was \$0.62/kWh [85]. Despite the national grid unreliability (see Fig. 5.6), the studied location 2019 residential customers reflective tariff (i.e., a tariff without subsidizes) was \$0.164/kWh [451]. Furthermore, if the HRES LPSP is increased to 3.7%, its LCOE is reduced to \$0.1623/kWh. So, for a LPSP of 3.7%, the HRES LCOE is less than the LCOE of the national grid. Meanwhile, the HRES LCOE will compete better with the LCOE of the national grid if more household loads are aggregated in the regional grid.

Power flow study of the effect of aggregating 5 regional loads show that load aggregation reduced the 5 regions peak load by 23%. Furthermore, power flow study of the regional grid shows that power losses minimization will be achieved when installed generators are not centralized but distributed in terms of the amount of apparent power drawn by each of the regional grid load buses. To identify and optimally control the regional grid apparent power losses, hourly power flow analysis of the regional grid shows that it is preferable to estimate the regional grid maximum apparent power losses in terms of its actual value (kVA) rather than its percentage values. This is because the calculated maximum apparent power percentage loss might not be actual value if it does not occur during the period of peak load. Estimation of the maximum apparent power percentage loss is relevant for estimating hourly deviation in apparent power losses and ensuring that hourly apparent power percentage loss does not exceed the acceptable benchmark for the studied location.

Chapter 8 CONCLUSION AND FUTURE WORK

This chapter summarizes the research performed in this thesis. This includes a summary of the research findings, and the recommendations for future research work.

8.1 Introduction

Electricity access rate is low, and the pace of rural electrification is slow in many sub-Saharan Africa (SSA) countries. For example, it is reported that SSA is were 90% those without electricity will live by 2030. For rapid rural electrification of communities beyond lighting or to supply reliable electricity to communities with electrical loads that are connected to an un-reliable national grid, communal grid is a viable approach for the supply of reliable electricity, as well as for the aggregation of the community electrical loads. The aim of this research is the design and evaluation of the use of clean energy technologies (i.e. integrated PV, biogas generator, and battery energy storage technologies) to supply reliable electricity to rural communities. A summary of the research carried in this thesis include Nigeria renewable energy assessment, reviews of literature on the design and evaluation of hybrid energy system, presentation of the methodology used for the design and evaluation of the hybrid energy system, occupancy-based survey of households energy consumption, stochastic modelling of community households load profiles, estimation of global solar radiation for photovoltaic application, optimal sizing of hybrid energy system components to guarantee reliable supply of electricity at minimal cost, and study of the effect of regional load aggregation on a regional grid.

8.2 Research findings

In presenting the research findings here, the research questions which define the research objectives are presented sequentially to show the process applied in achieving the research aim. After each research questions, the research procedures employed and the corresponding findings from the investigation carried out are also presented.

8.2.1 Research question one

What is Nigeria renewable energy potential and how does Nigeria's energy policies influence the deployment of renewable energy technologies?

The first research question was used to determine if Nigerian government support the use of renewable energy technologies for electrical energy generation and to assess Nigeria renewable energy resources availability. Therefore, in Chapter 2, Nigeria's position on the use of renewable energy technologies in resolving the country's energy crises was evaluated, and the approach that can be used in achieving the Nigeria's renewable energy target was examined. Assessment of Nigeria renewable energy resources and presentation of some factors that can influence the increase deployment of renewable energy technologies in Nigeria for the supply of reliable electricity beyond light was also presented in Chapter 2.

Outcomes from the study shows that there is a current drive by Nigeria government towards using PV system (i.e. 100% renewable energy technology) for rapid rural electrification. For example, Nigeria government plan to disburse 2/3rd of the $350 million electricity fund received from world bank in 2018 on solar technology related off-grid electricity project. Also, it was found that assessment of the country's solar radiation potential was necessary because there was discrepancy in the report of the country solar radiation potential. Despite the discrepancy, it was evident in the literature that Nigeria's solar radiation potential varies, therefore, in locations with lower solar radiation potential, the use of integrated PV and battery system to supply reliable electricity might not be a viable economic option. Consequently, integration of PV and battery system with other renewable energy resources might be a more viable economic option to supply reliable electricity to rural community. Specifically, the integration of PV and biogas systems can guarantee improve energy security as well as offer the possibility for improve community corporation or participation

8.2.2 Research question two

What is the energy consumption behaviour of rural areas?

The second research question was asked because an understanding of electricity consumption pattern is necessary for cost-effective supply of reliable electricity. Household occupants' energy consumption behaviour influence rural areas energy consumption patterns because residential electricity customers are the major electricity customers in rural areas. An occupancy-based stochastic load profile model is developed with the use of survey data on the number of bedrooms in a household, household population and classification, occupant' activity schedule and appliance ownership. The developed load model can be used to simulate load profiles that captures diversity between households or group of households, the effect of load coincidence, annual and diurnal variation, and short time-scale fluctuations is generated by the stochastic model.

Analysis of simulated load profiles show that incandescent bulbs accounts for 64% of the community's annual energy consumption. But when the commonly used incandescent bulbs were replace with CFL and LED bulbs, an annual energy savings of 53% (with CFL) or 57% (with LED bulbs) was achieved. Therefore, it is recommended that policies and regulations that would encourage the use of energy saving bulbs should be implemented because substantial energy savings in household energy consumption can be achieved by using energy saving bulbs. Furthermore, in-direct validation of the developed stochastic model with utility measured data shows that households' average daily consumption calculated from utility measured energy dispatch is 3.48 kWh day^{-1} and from the developed model, it is 3.13 kWh day^{-1}. It is hoped that the difference between the measured and simulated values can be reduced if energy consumption data were measured more closer to residential customers loads. Therefore, in developing countries without national measured time use data, this developed modelling approach can be applied to model the load profiles of households and communities.

8.2.3 Research question three

What is the amount of solar radiation that can be received in the studied location when a PV panel is either permanently fixed horizontally, permanently fixed at its optimal annual angle, or adjusted seasonally to its optimal angle?

Solar radiation datasets are required for the design and analysis of solar energy projects. In developing countries like Nigeria, solar radiation datasets are unavailable for many locations. Therefore, estimation models are used to predict the global solar radiation of these location. Even though several estimation solar radiation models have been developed, the rationale for selecting estimation models meteorological parameters and the influence that the selected meteorological parameters have on estimation models is often unclear. Meanwhile, performance evaluation of meteorological parameters used for constructing solar radiation estimation models was carried with 26 years (1993 – 2018) datasets and outcomes from the evaluation shows that temperature is an important meteorological parameter that should be used to estimate solar radiation in the survey location. Assessment of the minimum required duration of measured data to estimate past solar radiation shows that 2 years of recent data is required to achieve R^2 greater than 0.75, and more than 5 years of recent solar radiation data is required to achieve R^2 greater than 0.9

Diffused solar radiation data is required by most estimation models to determine the optimal angle to position a PV panel in a studied location. But because the few NiMet weather stations that measure solar radiation do not measure diffused solar radiation, the common practice (even though is not an optimal solution), is to use the solar project location latitude to determine PV panel inclination. However, this study shows that the annual optimal angel to position a PV panel in order to maximize the solar energy potential of the studied location was 11.6° rather than the studied location latitude of 6.8°.

8.2.4 Research question four

What is the studied location biomass potential?

Biomass availability and the size of the bio-digester are two important parameters that influence daily bio-energy production. Biomass availability is assessed by calculating the quantity of recoverable household and animal bio-waste in the studied location. Household and animal bio-waste were selected because they are usually disposed indiscriminately in rural areas. Therefore, the use of household and animal bio-waste for energy production will not disrupt living things food supply chain. Household and animal bio-waste has high moisture content, so, anaerobic digester is the most suitable technology for converting these bio-wastes into biogas [52]. Biomass availability assessment shows that the quantity of recoverable household and animal bio-waste in the studied location is limited. To reduce the quantity of outsourced bio-waste and minimize anaerobic digester volume, biogas generator is only used when energy demand is greater than 50% of its rated capacity.

8.2.5 Research question five

Can the integrated PV, biomass, and battery energy system LCOE compete with the LCOE of a diesel only energy system and the LCOE of the national grid?

This research question seeks to determine the best combination of hybrid energy system components that would guarantee reliable supply of electricity at minimal cost. Therefore, an hourly energy balance simulation was performance over a period one year to determine the optimum combination of PV, biogas generator and battery system. A quick, and simplified optimization technique called design space optimization technique was used to carry out the hourly simulation. Study on how different combinations of PV, biogas generator and battery systems affect the optimal sizing of battery shows that an optimally designed HRES requires a much smaller battery capacity than when a biogas generator and battery or a PV and battery are integrated for rural electrification in the studied location.

Outcomes from the techno-economic study shows that the optimal size of PV system, biogas generator, battery energy storage, and converter system that will guarantee

0% loss of power supply probability (LPSP) at minimal total cost were 40 kW_P, 160 kW, 32 kWh, and 24 kW respectively. Similarly, for a 0% LPSP, the hybrid energy system minimal annualized total cost ($C_{ann,tot}$), levelized unit cost of energy (LCOE) and net present cost (NPC) was \$78708, \$0.166/kWh and $\$1.26 \times 10^6$ respectively. The HRES LCOE can compete with the LCOE of a diesel alone energy system and the LCOE of the national grid because at 0% LPSP, HRES LCOE was \$0.1657/kWh, but the LCOE for a diesel alone energy system was \$0.62/kWh. Despite the national grid unreliability, the studied location 2019 residential customers reflective tariff (i.e., a tariff without subsidizes) was \$0.164/kWh [451]. Furthermore, if the HRES LPSP is increased to 3.7%, its LCOE is reduced to \$0.1623/kWh. So, for a LPSP of 3.7%, the HRES LCOE is less than the rural area residential customers tariff. Meanwhile, the HRES LCOE will compete better with the LCOE of the national grid if more household loads are aggregated in the regional grid.

8.2.6 Research question six

What is the effect of regional load aggregation on a regional grid?

The aggregation of regional load leads to peak load shaving (lower load diversity factor), but when the regional loads (regional load buses) of a regional grid are not close to each other, there will be substantial power losses in the network. Therefore, an energy system operating model was developed, and a power flow study was performed to evaluate if it is a better operating strategy to centralize or distribute generators in order to minimise the power losses in the network and guarantee the healthy operation of the regional grid. Power flow study of the effect of aggregating 5 regional loads show that load aggregation reduced the 5 regions peak load by 23%. Furthermore, power flow study of the regional grid shows that power losses minimization will be achieved when installed generators are not centralized but distributed in terms of the amount of apparent power drawn by each of the regional grid load buses. To identify and optimally control the regional grid apparent power losses, hourly power flow analysis of the regional grid shows that it is preferable to estimate the regional-grid maximum apparent power losses in terms of its actual value (kVA) rather than its percentage values. This is because the calculated maximum apparent power percentage loss might not be actual value if it does not

occur during the period of peak load. Estimation of the maximum apparent power percentage loss is relevant for estimating hourly deviation in apparent power losses and ensuring that hourly apparent power percentage loss does not exceed the acceptable benchmark for the studied country.

8.3 Recommendation for future work

In this section, further work possibilities are listed;

i) Modification of the developed stochastic load model to capture seasonal weather variation of locations with extreme weather conditions.

ii) Assessment of other regions NiMet's long-term meteorological data, in order to investigate if temperature will still be a dominant meteorological parameter for estimating solar radiation and to determine the minimum time span of meteorological data that is required by other regions to estimate solar radiation.

iii) Development of an electricity pricing plan that allows for the shifting of peak loads and a study of how the developed electricity pricing plan affects the integrated HRES levelized cost of electricity.

REFERENCES

[1] BP, ‘‘Energy outlook,’’ London, UK, 2018. [Online]. Available: https://www.bp.com/content/dam/bp-country/de_ch/PDF/Energy-Outlook-2018-edition-Booklet.pdf. [Accessed: Sep. 2, 2019].

[2] IMF, ‘‘World economic outlook: Less even expansion, rising trade tensions,’’ Washington, USA, 2018. [Online]. Available: https://www.imf.org/en/Publications/WEO/Issues/2018/07/02/world-economic-outlook-update-july-2018. [Accessed: Feb. 17, 2019].

[3] IEA, ‘‘Global energy & CO2 status report: The latest trends in energy and emissions,’’ Paris, France, 2018. [Online]. Available: https://webstore.iea.org/global-energy-co2-status-report-2018. [Accessed: Apr. 21, 2019].

[4] IEA, ‘‘Energy access outlook: From poverty to prosperity,’’ Paris, France, 2017. [Online]. Available: https://www.iea.org/ energyaccess/database/. [Accessed: Mar. 6, 2018].

[5] IEA, ‘‘World energy outlook: Electricity database,’’ Paris, France, 2017. [Online]. Available: https://www.iea.org/ energyaccess/database/. [Accessed: Oct. 14, 2018].

[6] World Bank, ‘‘World development indicators,’’ Washington, USA, 2019. [Online]. Available: https://data.worldbank.org/country/nigeria. [Accessed: Sep 2, 2019].

[7] E. Cecelski, ‘‘Enabling equitable access to rural electrification: Current thinking and major activities in energy, poverty and gender,’’ World Bank, Washington, USA, 2000. [Online]. Available: https://www.semanticscholar.org/paper/Enabling-equitable-access-to-rural-electrification. [Accessed: Nov 6, 2015].

[8] R. A. Cabraal, D. F. Barnes, and S. G. Agarwal, ‘‘Productive uses of energy for rural development,’’ *Annual Review of Environment and Resources*, vol. 30, pp. 117–144, 2005.

[9] D. F. Barnes, *The challenges of rural electrification: Strategies for developing countries*. Michigan: Routledge, 2007.

[10] M. Gustavsson, ‘‘Educational benefits from solar technology-Access to solar electric services and changes in children’s study routines, experiences from eastern province Zambia,’’ *Energy Policy*, vol. 35, pp. 1292–1299, 2007.

[11] World Bank, ‘‘The welfare impact of rural electrification: A reassessment of the costs and benefits,’’ World Bank, Washington, USA, 2008. [Online]. Available: https://siteresources. worldbank.org/EXTRURELECT/Resources/full_doc.pdf. [Accessed: Jan. 16, 2017].

[12] J. Finucane, S. V. Bogach, and L. E. Garcia, ‘Promoting productive uses of electricity in rural areas of Peru: Experience & lesons learned,’’ World Bank, Washington, USA, 2012. [Online]. Available: https://www.worldbank.org/en

/results/2013/04/10/pomoting-poductive-uses-electricity-rural-areas-peru. [Accessed: May 7, 2018].

[13] H. Ahlborg and L. Hammar, ‘‘Drivers and barriers to rural electrification in tanzania and mozambique - grid-extension, off-grid, and renewable energy technologies,’’ *Renewable Energy*, vol. 61, pp. 117–124, 2014.

[14] A. Yadoo and H. Cruickshank, ‘‘The role for low carbon electrification technologies in poverty reduction and climate change strategies: A focus on renewable energy mini-grids with case studies in Nepal, Peru and Kenya,’’ *Energy Policy*, vol. 42, pp. 591–602, 2012.

[15] S. R. Khandker, H. A. Samad, R. Ali, and D. F. Barnes, ‘‘Who benefits most from rural electrification? Evidence in India,’’ *The Energy Journal*, vol. 35, pp. 75–96, 2014.

[16] H. Zerriffi, *Rural Electrification Strategies for Distributed Generation*. London: Springer, 2011.

[17] D. S. Herran and T. Nakata, ‘‘Design of decentralized energy systems for rural electrification in developing countries considering regional disparity,’’ *Applied Energy*, vol. 91, pp. 130–145, 2012.

[18] E. O. Amrevurayire and V. N. Ojeh, ‘‘Consequences of rural-urban migration on the source region of Ughievwen clan Delta State Nigeria,’’ *European Journal of Geography*, vol. 7, pp. 42–57, 2016.

[19] A. Yadoo and H. Cruickshank, ‘‘The value of cooperatives in rural electrification,’’ *Energy Policy*, vol. 38, pp. 2941–2947, 2010.

[20] A. Zomers, ‘‘The challenge of rural electrification’’, *Energy for Sustainable Development*, vol. 7, pp. 69–76, 2003.

[21] S. O. Igbinovia and P. E. Orukpe, ‘‘Rural electrification: The propelling force for rural development of Edo State, Nigeria,’’ *Journal of Energy in Southern Africa*, vol. 18, pp. 18–26, 2007.

[22] J. Afa, ‘‘Problems of rural electrification in Bayelsa State,’’ *American Journal of Scientific and Industrial Research*, vol. 4, pp. 214–220, 2013.

[23] M. Torero, ‘‘The impact of rural electrification: Challenges and ways forward,’’ (in French) *Revue d’économie du développement*, vol. 23, pp. 49, 2015.

[24] D. Palit and A. Chaurey, ‘‘Off-grid rural electrification experiences from South Asia: Status and best practices,’’ *Energy for Sustainable Development*, vol. 15, pp. 266–276, 2011.

[25] K. Reiche, B. Tenenbaum, and C. T. Mastle, ‘‘Electrification and regulation: Principles and a model law,’’ World Bank, Washington, USA, 2006. [Online]. Available: http:// siteresources.worldbank.org/INTENERGY/Resources/ EnergyPaper18.pdf. [Accessed: Apr. 26, 2016].

[26] D. Schnitzer, D. S. Lounsbury, R. Carvallo, J. P. Deshmukh, J. Apt, and D. M. Kammen, ‘‘Microgrids for rural electrification: A critical review of best practices based on seven case studies,’’ United Nations Foundations, New York, USA, 2014. [Online]. Available: http:// energyaccess.org/wp-content/uploads/2015/07MicrogridsReportFINAL_ high.pdf. [Accessed: Nov.

8, 2017].

[27] D. F. Barnes, ‘‘Effective solutions for rural electrification in developing countries: Lessons from successful programs,’’ *Current Opinion in Environmental Sustainability*, vol. 3, pp. 260–264, 2011.

[28] N. Opiyo, ‘‘A survey informed PV-based cost-effective electrification options for rural sub-Saharan Africa,’’ *Energy Policy*, vol. 91, pp. 1–11, 2016.

[29] T. Levin and V. M. Thomas, ‘‘Energy for sustainable development can developing countries leapfrog the centralized electrification paradigm ?,’’ *Energy for Sustainable Development*, vol. 31, pp. 97–107, 2016.

[30] E. Terrado, A. Cabraal, and I. Mukherjee, ‘‘Designing sustainable off-grid rural electrification projects: Principles and practices,’’ World Bank, Washington, USA, 2008. [Online]. Available: http://siteresources.worldbank.org/ EXTENERGY2/Resources/OffgridGuidelines.pdf. [Accessed: Dec. 13, 2017].

[31] T. S. Ustun, C. Ozansoy, and A. Zayegh, ‘‘Recent developments in microgrids and example cases around the world - A review,’’ *Renewable and Sustainable Energy Reviews*, vol. 15, pp. 4030–4041, 2011.

[32] L. Parshall, D. Pillai, S. Mohan, A. Sanoh, and V. Modi, ‘‘National electricity planning in settings with low pre-existing grid coverage : Development of a spatial model and case study of Kenya,’’ *Energy Policy*, vol. 37, pp. 2395–2410, 2009.

[33] S. Szabo, K. Bodis, T. Huld, and M. Moner-Girona, ‘‘Energy solutions in rural Africa : mapping electrification costs of distributed solar and diesel generation versus grid extension,’’ *Environmental Research Letters*, vol. 6, pp. 1–9, 2011.

[34] N. U. Blum, R. S. Wakeling, and T. S. Schmidt, ‘‘Rural electrification through village grids — Assessing the cost competitiveness of isolated renewable energy technologies in Indonesia,’’ *Renewable and Sustainable Energy Reviews*, vol. 22, pp. 482–496, 2013.

[35] M-KOPA, ‘‘300,000 East African homes now on M-KOPA,’’ 2016. [Online]. Available: http:// www.m-kopa.com/ asante-sana-300000 -east- african-homes-now-on-m-kopa/. [Accessed: Nov. 19, 2017].

[36] E. Martinot and K. Reiche, ‘‘Regulatory approaches to rural electrification and renewable energy : Case studies from six developing countries,’’ World Bank, Washington, USA, 2000. [Online]. Available: http://citeseerx.ist.psu.edu/ viewdoc/summary?doi= 10.1.1.525.6348. [Accessed: Mar. 18, 2017].

[37] J. G. J. Olivier, K. M. Schure, and J. A. H. W. Peters, ‘‘Trends in global CO2 and total greenhouse gas emissions,’’ 2017. [Online]. Available: http://www. indiaenvironmentportal.org.in/files/file/pbl-2017-trends-in-global-co2- and-total-greenhouse-gas-emissons-2017-report.pdf. [Accessed: Aug. 19, 2018].

[38] M. Sharif Hossain, ‘‘Panel estimation for CO2emissions, energy consumption, economic growth, trade openness and urbanization of newly industrialized countries,’’ *Energy Policy*, vol. 39, pp. 6991–6999, 2011.

[39] UNPD, ‘‘World population prospects,’’ United Nations, New York, USA, 2017. [Online]. Available: https:// www.un.org/development/desa/publications/ world-population-prospects-the-2017-revision.html. [Accessed: Sep. 24, 2018].

[40] National population commission, ‘‘Nigeria's population hits 198M people,’’ Abuja, Nigeria 2018. [Online]. Available: http://population.gov.ng/nigerias-population-hit-198m-people-npopc-chairman/. [Accessed: Aug. 20, 2018].

[41] E. Gayawan, E. D. Arogundade, and S. B. Adebayo, ‘‘Possible determinants and spatial patterns of anaemia among young children in nigeria: A bayesian semi-parametric modelling,’’ *International Health*, vol. 6, pp. 35–45, 2014.

[42] PWC, ‘‘Powering Nigeria for the future,’’ London, UK, 2016. [Online]. Available: https://www.pwc.com/gx/en/growth-markets-centre/assets/pdf /powering-nigeria-future.pdf. [Accessed: Jun. 5, 2017].

[43] FGN, ‘‘Nigeria power baseline report,’’ Abuja, Nigeria, 2016. [Online]. Available: http://mypower.ng/wp-content/uploads/2018/01/Baseline-Report.pdf. [Accessed: Jan. 9, 2019].

[44] C. Adebayo, ‘‘How is 100% renewable energy possible for Nigeria?,’’ 2014. [Online]. Available: http://geni.org/globalenergy/research/renewable-energy-potential-of-nigeria/100-percent-renewable-energy-Nigeria.pdf. [Accessed: Nov. 29, 2016].

[45] S. C. Bhattacharyya, *Rural electrification through decentralised off-grid systems in developing countries*. London: Springer, 2012.

[46] S. Mandelli, J. Barbieri, R. Mereu, and E. Colombo, ‘‘Off-grid systems for rural electrification in developing countries: Definitions, classification and a comprehensive literature review,’’ *Renewable and Sustainable Energy Reviews*, vol. 58, pp. 1621–1646, 2016.

[47] T. O. Akinbulire, P. O. Oluseyi, and O. M. Babatunde, ‘‘Techno-economic and environmental evaluation of demand side management techniques for rural electrification in Ibadan, Nigeria,’’ *International Journal of Energy and Environmental Engineering*, vol. 5, pp. 375–385, 2014.

[48] L. Olatomiwa, S. Mekhilef, A. S. N. Huda, and O. S. Ohunakin, ‘‘Economic evaluation of hybrid energy systems for rural electrification in six geo-political zones of Nigeria,’’ *Renewable Energy*, vol. 83, pp. 435–446, 2015.

[49] O. O. Ajayi, O. D. Ohijeagbon, O. Mercy, and A. Ameh, ‘‘Potential and econometrics analysis of standalone RE facility for rural community utilization and embedded generation in North-East, Nigeria,’’ *Sustainable Cities and Society*, vol. 21, pp. 66–77, 2016.

[50] Nigeria Electricity Hub, ‘‘FG’s road map for solving Nigeria’s power crises,’’ 2016. [Online]. Available: http://www.nigeriaelectricityhub.com/2016/05/ 06/full-speech-fashola-unveils-fgs-road-map-for-solving-nigerias-power-crises/. [Accessed: Jul. 26, 2018].

[51] REA, ‘‘Energizing Economies,’’ Abuja, Nigeria, 2018. [Online]. Available: http://rea.gov.ng/ energizing-economies/. [Accessed: Aug. 7, 2018].

[52] M. Shaaban and J. O. Petinrin, ‘‘Renewable energy potentials in Nigeria: Meeting rural energy needs,’’ *Renewable and Sustainable Energy Reviews*, vol. 29, pp. 72–84, 2014.

[53] A. Agbongiarhuoyi, ‘‘Promoting renewable energy use in Nigeria,’’ 2015. [Online]. Available: https://www.vanguardngr.com/2015/08/promoting-renewable-energy-use-in-nigeria/. [Accessed: Oct. 29, 2018].

[54] Y. S. Mohammed, M. W. Mustafa, N. Bashir, and A. S. Mokhtar, ‘‘Renewable energy resources for distributed power generation in Nigeria: A review of the potential,’’ *Renewable and Sustainable Energy Reviews*, vol. 22, pp. 257–268, 2013.

[55] ECN and UNDP, ‘‘Renewable energy master plan: Final draft report,’’ 2005. [Online]. Available: http://www.ecowrex.org/sites/default/files/repository_old/2005%20RE%20Master%20Plan%20-%20Min%20Power.pdf. [Accessed: Mar. 3, 2016].

[56] A.S. Sambo, ‘‘The place of renewable energy in the Nigerian energy sector,’’ 2012. [Online]. Available: http://area-net.org/wp-content/uploads/2016/01 / Nigeria_renewable_energy_masterplan.pdf. [Accessed: Oct. 18, 2018].

[57] FGN, ‘‘National renewable energy and energy efficiency policy,’’ Abuja, Nigeria, 2015. [Online]. Available: http: // admin.theiguides.org / media / documents/NREEEP %20policy %202015-% 20FEC% 20approved%20copy. pdf. [Accessed: Feb. 7, 2018].

[58] A. S. Sambo and E. J. Bala, ‘‘Penetration of solar photovoltaic into Nigeria’s energy supply mix,’’ in Conf. *World Renewable Energy Forum Annual Conference*, Colorado, USA, 2012.

[59] O. Adeoti, B. A. Oyewole, and T. D. Adegboyega, ‘‘Solar photovoltaic-based home electrification system for rural development in Nigeria: domestic load assessment,’’ *Renewable Energy*, vol. 24, pp. 155–161, 2001.

[60] M. Usman, “Rural solar electrification in Nigeria: Renewable energy potentials distribution for rural development,” 2012. [Online]. Available: https://pdfs. semanticscholar.org/34d8/927ef0c09a96437a08b2818c984da8fd7e03.pdf. [Accessed: Aug. 18, 2019].

[61] D. O. Akinyele and R. K. Rayudu, ‘‘Distributed photovoltaic power generation for energy-poor households : The Nigerian perspective,’’ In Proc. *IEEE PES Asia-Pacific Power and Energy Engineering Conference*, Kowloon, China, 2013.

[62] S. Chakrabarti and S. Chakrabarti, ‘‘Rural electrification programme with solar energy in remote region – a case study in an island,’’ *Energy Policy*, vol. 30, pp. 33–42, 2002.

[63] R. M. Moharil and P. S. Kulkarni, ‘‘A case study of solar photovoltaic power system at Sagardeep Island , India,’’ *Renewable and Sustainable Energy Reviews*, vol. 13, pp. 673–681, 2009.

[64] O. S. Ohunakin, S. J. Ojolo, and O. O. Ajayi, ‘‘Small hydropower (SHP) development in Nigeria: An assessment,’’ *Renewable and Sustainable Energy Reviews*, vol. 15, pp. 2006–2013, 2011.

[65] I. A Adejumobi, O. I. Adebisi, and S. A Oyejide, ‘‘Developing small hydropower potentials for rural electrification,’’ *International Journal of Research and Reviews in Applied Sciences*, vol. 17, pp. 105–110, 2013.

[66] K. J. Simonyan and O. Fasina, ‘‘Biomass resources and bioenergy potentials in Nigeria’’, *African Journal of Agricultural Research*, vol. 8, pp. 4975–4989, 2013.

[67] Y. S. Mohammed, M. W. Mustafa, N. Bashir, M. A. Ogundola, and U. Umar, ‘‘Sustainable potential of bioenergy resources for distributed power generation development in Nigeria,’’ *Renewable and Sustainable Energy Reviews*, vol. 34, pp. 361–370, 2014.

[68] T. C. Ogwueleka, ‘‘Municipal solid waste characteristics and management solid waste characteristics and management in Nigeria,’’ *Iranian Journal of Environmental Health Science and Engineering*, vol. 6, pp. 173–180, 2009.

[69] C. Li *et al.*, ‘‘Carbon emission reduction potential of rural energy in China,’’ *Renewable and Sustainable Energy Reviews*, vol. 29, pp. 254–262, 2014.

[70] M. Balta, ‘‘Exergetic cost analysis and sustainability assessment of various low exergy heating systems,’’ *Energy and Buildings*, vol. 55, pp. 721–727, 2012.

[71] K. Annamalai, S. S. Thanapal, and D. Ranjan, ‘‘Ranking renewable and fossil fuels on global warming potential using respiratory quotient concept,’’ *Journal of Combustion*, vol. 1, pp. 1–16, 2018.

[72] H. Li, C. Jenkins-smith, C. L. Silva, R. P. Berrens, and K. G. Herron, ‘‘Public support for reducing US reliance on fossil fuels : Investigating household willingness-to-pay for energy research and development,’’ *Ecological Economics*, vol. 68, pp. 731–742, 2009.

[73] E. K. Stigka, J. A. Paravantis, and G. K. Mihalakakou, ‘‘Social acceptance of renewable energy sources: A review of contingent valuation applications,’’ *Renewable and Sustainable Energy Reviews*, vol. 32, pp. 100–106, 2014.

[74] H. Zhao, S. Guo, and L. Fu, ‘‘Review on the costs and benefits of renewable energy power subsidy in China,’’ *Renewable and Sustainable Energy Reviews*, vol. 37, pp. 538–549, 2014.

[75] REN21, ‘‘Renewables global status report,’’ Paris, France, 2018. [Online]. Available: http://www.ren21.net/gsr-2018/. [Accessed: Apr. 7, 2019].

[76] P. Mckendry, ‘‘Energy production from biomass (part 3): Gasification technologies,’’ *Bioresource Technology*, vol. 83, pp. 55–63, 2002.

[77] G. M. J. Herbert, S. Iniyan, E. Sreevalsan, and S. Rajapandian, ‘‘A review of wind energy technologies,’’ *Renewable and Sustainable Energy Reviews*, vol. 11, pp. 1117–1145, 2007.

[78] O. Ellabban, H. Abu-rub, and F. Blaabjerg, ‘‘Renewable energy resources: Current status , future prospects and their enabling technology,’’ *Renewable and Sustainable Energy Reviews*, vol. 39, pp. 748–764, 2014.

[79] J. G. Njiri and D. Söffker, ‘‘State-of-the-art in wind turbine control: Trends and challenges,’’ *Renewable and Sustainable Energy Reviews*, vol. 60, pp. 377–393, 2016.

[80] T. Tsoutsos, N. Frantzeskaki, and V. Gekas, ‘‘Environmental impacts from the solar energy technologies,’’ *Energy Policy*, vol. 33, pp. 289–296, 2005.

[81] J. A. Lesser and X. Su, ‘‘Design of an economically efficient feed-in tariff structure for renewable energy development,’’ *Energy Policy*, vol. 36, pp. 981–990, 2008.

[82] C. O. Okoye and U. Atikol, ‘‘A parametric study on the feasibility of solar chimney power plants in North Cyprus conditions,’’ *Energy Conversion and Management*, vol. 80, pp. 178–187, 2014.

[83] A. Soneye and A. Daramola, ‘‘Energy access in Nigeria: An assessment of solar utilization in Ibadan,’’ *International Journal of Renewable Energy Resources*, vol. 2, pp. 6–12, 2012.

[84] C. O. Okoye, O. Taylan, and D. K. Baker, ‘‘Solar energy potentials in strategically located cities in Nigeria: Review, resource assessment and PV system design,’’ *Renewable and Sustainable Energy Reviews*, vol. 55, pp. 550–566, 2016.

[85] O. D. Ohijeagbon and O. O. Ajayi, “Potential and economic viability of standalone hybrid systems for a rural community of Sokoto , North-west Nigeria,” *Front Energy*, vol. 8, pp. 145–159, 2014.

[86] E. J. Bala, ‘‘Implementing sustainable strategies in Nigeria renewable sector,’’ in Conf. *All-Energy Exhibition and Conference, Aberdeen, UK,* 2014., pp. 231-239.

[87] IRENA, ‘‘Renewable energy capacity statistics,’’ Abu Dhabi, UAE, 2018. [Online]. Available: https://www.irena.org/-/media/files/IRENA/agency/ publication/2018/ mar/IRENA_RE_capacity_statistics_2018. [Accessed:Feb. 4, 2019].

[88] GIZ, ‘‘The Nigerian energy sector,’’ Bonn, Germany, 2015. [Online]. Available: https:// www.giz.de/en/downloads/giz2015-en-nigerian-energy-sector.pdf. [Accessed: Oct. 8, 2016].

[89] WEC, ‘‘World energy resources,’’ London, UK, 2016. [Online]. Available: https: //www.worldenergy.org/publications/2016/world-energy-resources-2016. [Accessed:Dec. 13, 2016].

[90] FAO, ‘‘FAOSTAT,’’ Rome, Italy, 2018. [Online]. Available: http://www.fao.org/ faostat/ en/#data/QA. [Accessed: Feb. 23, 2019].

[91] Y. S. Mohammed, M. W. Mustafa, N. Bashir, and I. S. Ibrahem, ‘‘Existing and recommended renewable and sustainable energy development in Nigeria based on autonomous energy and microgrid technologies,’’ *Renewable and Sustainable Energy Reviews*, vol. 75, pp. 820–838, 2017.

[92] UNIDO, ‘‘Energy programme: Sustainable energy for inclusive development and climate action,’’ New York, USA, 2015. [Online]. Available: https://www. unido.org/ publications/2015/. [Accessed: Nov. 8, 2017].

[93] Y. S. Mohammed, A. S. Mokhtar, N. Bashir, and R. Saidur, ‘‘An overview of agricultural biomass for decentralized rural energy in Ghana,’’ *Renewable and Sustainable Energy Reviews*, vol. 20, pp. 15–25, 2013.

[94] J. Vasco-correa, S. Khanal, A. Manandhar, and A. Shah, ‘‘Anaerobic digestion

for bioenergy production : Global status , environmental and techno-economic implications , and government policies,'' *Bioresource Technology*, vol. 247, pp. 1015–1026, 2018.

[95] K. B. Cantrell, T. Ducey, K. S. Ro, and P. G. Hunt, ''Livestock waste-to-bioenergy generation opportunities,'' *Bioresource Technology*, vol. 99, pp. 7941–7953, 2008.

[96] M. N. I. Siddique and Z. A. Wahid, ''Achievements and perspectives of anaerobic co-digestion : A review,'' *Journal of Cleaner Production*, vol. 194, pp. 359–371, 2018.

[97] E. Ullah and A. R. Martin, ''Review of biogas digester technology in rural Bangladesh,'' *Renewable and Sustainable Energy Reviews*, vol. 62, pp. 247–259, 2016.

[98] T. V. Ramachandra, ''Geographical Information System Approach for Regional Biogas Potential Assessment,'' *Research Journal of Environmental Sciences*, vol. 2, pp. 170-184, 2008.

[99] S. F. Mayerle and J. N. de Figueiredo, ''Designing optimal supply chains for anaerobic bio-digestion/energy generation complexes with distributed small farm feedstock sourcing,'' *Renewable Energy*, vol. 90, pp. 46–54, 2016.

[100] G. He, B. Bluemling, A. P. J. Mol, L. Zhang, and Y. Lu, ''Comparing centralized and decentralized bio-energy systems in rural China,'' *Energy Policy*, vol. 63, pp. 34–43, 2013.

[101] C. E. Gutierrez, A. Xia, and J. D. Murphy, ''Can slurry biogas systems be cost effective without subsidy in Mexico ?,'' *Renewable Energy*, vol. 95, pp. 22–30, 2016.

[102] R. M. Jingura and R. Matengaifa, ''Optimization of biogas production by anaerobic digestion for sustainable energy development in Zimbabwe,'' *Renewable and Sustainable Energy Reviews*, vol. 13, pp. 1116–1120, 2009.

[103] V. K. Tyagi, L. A. Fdez-güelfo, Y. Zhou, C. J. Álvarez-gallego, L. I. R. Garcia, and W. J. Ng, ''Anaerobic co-digestion of organic fraction of municipal solid waste (OFMSW): Progress and challenges,'' *Renewable and Sustainable Energy Reviews*, vol. 93, pp. 380–399, 2018.

[104] C. Zhang, H. Su, J. Baeyens, and T. Tan, ''Reviewing the anaerobic digestion of food waste for biogas production,'' *Renewable and Sustainable Energy Reviews*, vol. 38, pp. 383–392, 2014.

[105] S. O. Oyedepo, ''Towards achieving energy for sustainable development in Nigeria,'' *Renewable and Sustainable Energy Reviews*, vol. 34, pp. 255–272, 2014.

[106] A. Giwa, A. Alabi, A. Yusuf, and T. Olukan, ''A comprehensive review on biomass and solar energy for sustainable energy generation in Nigeria,'' *Renewable and Sustainable Energy Reviews*, vol. 69, pp. 620–641, 2017.

[107] Z. A. Elum and A. S. Momodu, ''Climate change mitigation and renewable energy for sustainable development in Nigeria: A discourse approach,'' *Renewable and Sustainable Energy Reviews*, vol. 76, pp. 72–80, 2017.

[108] N. Abila, ‘‘Managing municipal wastes for energy generation in Nigeria,’’ *Renewable and Sustainable Energy Reviews*, vol. 37, pp. 182–190, 2014.

[109] T. O. Somorin, S. Adesola, and A. Kolawole, ‘‘State-level assessment of the waste-to-energy potential (via incineration) of municipal solid wastes in Nigeria,’’ *Journal of Cleaner Production*, vol. 164, pp. 804–815, 2017.

[110] M. Y. Suberu, N. Bashir, and M. W. Mustafa, ‘‘Biogenic waste methane emissions and methane optimization for bioelectricity in Nigeria,’’ *Renewable and Sustainable Energy Reviews*, vol. 25, pp. 643–654, 2013.

[111] L. Berga, ‘‘The role of hydropower in climate change mitigation and adaptation: A review,’’ *Engineering*, vol. 2, pp. 313–318, 2016.

[112] A. T. Brimmo, A. Sodiq, S. Sofela, and I. Kolo, ‘‘Sustainable energy development in Nigeria: Wind, hydropower, geothermal and nuclear (Vol. 1),’’ *Renewable and Sustainable Energy Reviews*, vol. 74, pp. 474–490, 2017.

[113] C. N. Emeribe, E. T. Ogbomida, O. A. Fasipe, O. Biose, I. Aganmwonyi, M. Isiekwe, and I. P. Fasipe, ‘‘Hydrological assessments of some rivers in Edo State, Nigeria for small-scale hydropower development,’’ *Nigerian Journal of Technology*, vol. 35, pp. 656 – 668, 2016.

[114] J. U. Abaka, T. B. Ibraheem, H. Salmanu, and O. Olokede, ‘‘Hydropower potential of Nigeria,’’ *International Journal of Modern Engineering Research*, vol. 7, pp. 52–58, 2017.

[115] L. L. Ladokun, B. F. Sule, K. R. Ajao, and A. G. Adeogun, ‘‘Resource assessment and feasibility study for the generation of hydrokinetic power in the tailwaters of selected hydropower stations in Nigeria,’’ *Water Science*, Vol. 32, pp. 338 - 354, 2018.

[116] M. B. Machina and S. Sharma, ‘‘Assessment of climate change impact on hydropower generation : A case study of Nigeria,’’ *International Journal of Engineering Technology Science Research*, vol. 4, pp. 753–762, 2017.

[117] J. A. Duffie and W. A. Beckman, *Solar engineering of thermal processes*, 4th ed. New Jersey: John Wiley & Sons, Inc., 2013.

[118] M. Iqbal, *An introduction to solar radiation.* Toronto: Academic Press, 1983.

[119] M. Adaramola, *Solar Energy: Application, economics, and public perception*. Oakville: Apple Academic Press, Inc, 2015.

[120] SolarGIS, ‘‘Nigeria global horizontal irradiation,’’ 2019. [Online]. Available: https://solargis.com/en/maps-and-gis-data/download/nigeria. [Accessed: Mar. 1, 2019].

[121] A. M. Khalid, I. Mitra, W. Warmuth, and V. Schacht, ‘‘Performance ratio – Crucial parameter for grid connected PV plants,’’ *Renewable and Sustainable Energy Reviews*, vol. 65, pp. 1139–1158, 2016.

[122] E. Elibol, Ö. T. Özmen, N. Tutkun, and O. Köysal, ‘‘Outdoor performance analysis of different PV panel types,’’ *Renewable and Sustainable Energy Reviews*, vol. 67, pp. 651–661, 2017.

[123] B. Herteleer, B. Huyck, F. Catthoor, J. Driesen, and J. Cappelle, ‘‘Normalised

efficiency of photovoltaic systems: Going beyond the performance ratio,'' *Solar Energy*, vol. 157, pp. 408–418, 2017.

[124] D. A. Quansah, M. S. Adaramola, G. K. Appiah, and I. A. Edwin, ''Performance analysis of different grid-connected solar photovoltaic (PV) system technologies with combined capacity of 20 kW located in humid tropical climate,'' *International Journal of Hydrogen Energy*, vol. 42, pp. 4626–4635, 2017.

[125] D. A. Fadare, ''Modelling of solar energy potential in Nigeria using an artificial neural network model,'' *Applied Energy*, vol. 86, pp. 1410–1422, 2009.

[126] World Bank, ''Nigeria: World bank ramps up support for human capital, governance, energy, and climate change,'' Washington, USA, 2018. [Online]. Available: https:// www.worldbank.org/en/news/press-release/2018/06/ 27/ nigeria -world- bank-ramps- up-support-for-human-capital-governance-energy-and-climate-change. [Accessed: May 1, 2019].

[127] REA, ''World bank approves $350m for REA off grid projects,'' Abuja, Nigeria, 2018. [Online]. Available: https://www.worldbank.org/en/news/press-release /2018/ 06/27 /nigeria-world-bank-ramps-up -support-for -human-capital-governance-energy-and-climate-change. [Accessed: Dec 6, 2018].

[128] IRENA, ''Renewable power generation costs,'' Abu Dhabi, UAE, 2017. [Online]. Available: https: // www.irena.org /publications /2018 / Jan / Renewable-power-generation-costs-in-2017. [Accessed: Jun. 19, 2018].

[129] O. S. Ohunakin, ''Wind resources in North-East geopolitical zone, Nigeria: An assessment of the monthly and seasonal characteristics,'' *Renewable and Sustainable Energy Reviews*, vol. 15, pp. 1977–1987, 2011.

[130] NiMet, ''Nigerian meteorological datasets,'' Lagos, Nigeria [Online]. Available: https:// nimet.gov.ng/.[Accessed: Nov. 13, 2018].

[131] B. U. Ngene, J. C. Agunwamba, I. T. Tenebe, and P. C. Emenike, ''Evaluation of spatial and temporal characteristics of wind and wind resources: A case study of some nigerian cities,'' *International Journal of Applied Engineering Research*, vol. 10, pp. 40153–40158, 2015.

[132] O. S. Ohunakin, "Wind resource evaluation in six selected high altitude locations in Nigeria," *Renewable Energy*, vol. 36, pp. 3273–3281, 2011.

[133] M. S. Adaramola, S. S. Paul, and S. O. Oyedepo, ''Assessment of electricity generation and energy cost of wind energy conversion systems in north-central Nigeria,'' *Energy Conversion and Management*, vol. 52, pp. 3363–3368, 2011.

[134] O. S. Ohunakin and O. O. Akinnawonu, ''Assessment of wind energy potential and the economics of wind power generation in Jos, Plateau State, Nigeria,'' *Energy for Sustainable Development*, vol. 16, pp. 78–83, 2012.

[135] O. O. Ajayi, R. O. Fagbenle, J. Katende, and J. O. Okeniyi, ''Availability of wind energy resource potential for power generation at Jos, Nigeria,'' *Frontiers in Energy*, vol. 5, pp. 376–385, 2011.

[136] C. I. Oriaku, J. C. Osuwa, A. D. Asiegbu, G. U. Chukwu, and C. O. Kanu,

''Frequency distribution analysis of available wind resources in Umudike, Abia state Nigeria for wind energy conversion system design,'' *Pacific Journal of Science and Technology*, vol. 8, pp. 203–206, 2007.

[137] A. Asiegbu and G. Iwuoha, ''Studies of wind resources in Umudike, South East Nigeria - An assessment of economic viability,'' *Journal of Engineering and Applied Sciences*, vol. 2, pp. 1539–1541, 2007.

[138] S. O. Oyedepo, M. S. Adaramola, and S. S. Paul, ''Analysis of wind speed data and wind energy potential in three selected locations in South-East Nigeria,'' *International Journal Energy and Environmental Engineering*, vol. 3, pp. 1–11, 2012.

[139] O. M. Amoo, ''Evaluation of the wind energy potential of two south west sites in Nigeria,'' *Frontiers in Energy*, vol. 6, pp. 237–246, 2012.

[140] O. O. Ajayi, R. O. Fagbenle, J. Katende, J. M. Ndambuki, D. O. Omole, and A. A. Badejo, ''Wind energy study and energy cost of wind electricity generation in Nigeria: Past and recent results and a case study for South West Nigeria,'' *Energies*, vol. 7, pp. 8508–8534, 2014.

[141] J. O. Okeniyi, O. S. Ohunakin, and E. T. Okeniyi, ''Assessments of wind-energy potential in selected sites from three geopolitical zones in Nigeria: Implications for renewable/sustainable rural electrification,'' *The Scientific World Journal*, vol. 2015, pp. 7–9, 2015.

[142] D. A. Fadare, ''A Statistical Analysis of Wind Energy Potential in Ibadan, Nigeria, Based on Weibull Distribution Function,'' *The Pacific Journal of Science and Technology*, vol. 9, pp. 110–119, 2008.

[143] U. Na, A. Oluleye, and I. Ka, ''Innovative Energy & Research Investigation of Wind Power Potential over Some Selected Coastal Cities in Nigeria,'' *Innovative Energy and Research*, vol. 6, pp. 1–12, 2017.

[144] O. S. Ohunakin, ''Wind characteristics and wind energy potential assessment in Uyo, Nigeria,'' *Journal of Engineering and Applied Sciences*, vol. 6, pp. 141–146, 2011.

[145] M. S. Adaramola, O. M. Oyewola, O. S. Ohunakin, and O. O. Akinnawonu, ''Performance evaluation of wind turbines for energy generation in Niger Delta, Nigeria,'' *Sustainable Energy Technologies and Assessments*, vol. 6, pp. 75–85, 2014.

[146] Wind turbines - Part 1: Design requirements, IEC 61400-1, Geneva, Switzerland, 2014.

[147] A. S. Aliyu, J. O. Dada, and I. K. Adam, ''Current status and future prospects of renewable energy in Nigeria,'' *Renewable and Sustainable Energy Reviews*, vol. 48, pp. 336–346, 2015.

[148] A. A. Mas'ud, A. V. Wirba, J. A. Ardila-Rey, R. Albarracin, F. Muhammad-Sukki, A. J. Duque, N. A. Bani, and A. B. Munir, ''Wind power potentials in Cameroon and Nigeria: Lessons from South Africa,'' *Energies*, vol. 10, pp. 1–19, 2017.

[149] Energy mix report, ''FG pushes ahead with 10MW Katsina wind, 215 MW Kaduna power projects,'' 2019. [Online]. Available: https://www.

energymixreport.com/fg-pushes-ahead-with-10mw-katsina-wind-215mw-kaduna-power-projects/. [Accessed: Jul. 27, 2019].

[150] N. V. Emodi, *Energy Policies for Sustainable Development Strategies*. Singapore: Springer, 2016.

[151] N. Edomah, ''On the path to sustainability: Key issues on Nigeria's sustainable energy development,'' *Energy Reports*, vol. 2, pp. 28–34, 2016.

[152] U. B. Akuru, I. E. Onukwube, O. I. Okoro, and E. S. Obe, ''Towards 100% renewable energy in Nigeria,'' *Renewable and Sustainable Energy Reviews*, vol. 71, pp. 943–953, 2017.

[153] C. G. Ozoegwu, C. A. Mgbemene, and P. A. Ozor, ''The status of solar energy integration and policy in Nigeria,'' *Renewable and Sustainable Energy Reviews*, vol. 70, pp. 457–471, 2017.

[154] J. Schallenberg-Rodriguez, ''Renewable electricity support systems: Are feed-in systems taking the lead?,'' *Renewable and Sustainable Energy Reviews*, vol. 76, pp. 1422–1439, 2017.

[155] IRENA, IEA, and REN21, ''Renewable Energy Policies in a Time of Transition,'' Abu Dhabi, UAE, 2018. [Online]. Available: https://www.irena.org/-/media/files/IRENA/ Agency/Publication/2018/Apr/IRENA_IEA_REN21_Policies_2018.pdf. [Accessed: Oct. 3, 2018].

[156] S. Sinha and S. S. Chandel, ''Review of software tools for hybrid renewable energy systems,'' *Renewable and Sustainable Energy Reviews*, vol. 32, pp. 192–205, 2014.

[157] M. Fadaeenejad, M. A. M. Radzi, M. Z. A Abkadir, and H. Hizam, ''Assessment of hybrid renewable power sources for rural electrification in Malaysia,'' *Renewable and Sustainable Energy Reviews*, vol. 30, pp. 299–305, 2014.

[158] J. G. Castellanos, M. Walker, D. Poggio, M. Pourkashanian, and W. Nimmo, ''Modelling an off-grid integrated renewable energy system for rural electrification in India using photovoltaics and anaerobic digestion,'' *Renewable Energy*, vol. 74, pp. 390–398, 2015.

[159] M. C. Mira, Z. Zhang, A. Knott, and M. A. E. Andersen, ''Analysis , Design , modeling , and control of an for hybrid renewable energy systems,'' *IEEE Transactions on Power Electronics*, vol. 32, pp. 1138–1155, 2017.

[160] S. Vazquez, J. Rodriguez, M. Rivera, L. G. Franquelo, and M. Norambuena, ''Model predictive control for power converters and drives: Advances and trends,'' *IEEE Transactions on Industrial Electronics*, vol. 64, pp. 935–947, 2017.

[161] R. R. Karasani, V. B. Borghate, P. M. Meshram, H. M. Suryawanshi, and S. Sabyasachi, ''A three-phase hybrid cascaded modular multilevel inverter for renewable energy environment,'' *IEEE Transactions on Power Electronics*, vol. 32, pp. 1070–1087, 2017.

[162] S. D'Arco, J. A. Suul, and O. B. Fosso, ''A Virtual Synchronous Machine implementation for distributed control of power converters in SmartGrids,'' *Electric Power Systems Research*, vol. 122, pp. 180–197, 2015.

[163] S. Li, J. Proano, and D. Zhang, ‘‘Microgrid power flow study in grid-connected and islanding modes under different converter control strategies,’’ in Proc. *IEEE power and energy society general meting*, San Diego, CA, USA, Jul. 22–26, 2012.

[164] E. Serban and H. Serban, ‘‘A control strategy for a distributed power generation microgrid application with voltage and current controlled source converter,’’ *IEEE Transactions on Power Electronics*, vol. 25, pp. 2981–2992, 2010.

[165] A. Chauhan and R. P. Saini, ‘‘A review on Integrated Renewable Energy System based power generation for stand-alone applications: Configurations, storage options, sizing methodologies and control,’’ *Renewable and Sustainable Energy Reviews*, vol. 38, pp. 99–120, 2014.

[166] R. Siddaiah and R. P. Saini, ‘‘A review on planning, configurations, modeling and optimization techniques of hybrid renewable energy systems for off grid applications,’’ *Renewable and Sustainable Energy Reviews*, vol. 58, pp. 376–396, 2016.

[167] M. D. A. Al-falahi, S S. D. G. Jayasinghe, and H. Enshaei, ‘‘A review on recent size optimization methodologies for standalone solar and wind hybrid renewable energy system,’’ *Energy Conversion and Management*, vol. 143, pp. 252–274, 2017.

[168] A. Maleki, M. G. Khajeh, and M. Ameri, ‘‘Optimal sizing of a grid independent hybrid renewable energy system incorporating resource uncertainty, and load uncertainty,’’ *International Journal of Electrical Power and Energy Systems*, vol. 83, pp. 514–524, 2016.

[169] S. R. Tito, T. T. Lie, and T. N. Anderson, ‘‘Optimal sizing of a wind-photovoltaic-battery hybrid renewable energy system considering socio-demographic factors,’’ *Solar Energy*, vol. 136, pp. 525–532, 2016.

[170] H. R. Baghaee, M. Mirsalim, G. B. Gharehpetian, and H. A. Talebi, ‘‘Reliability/cost-based multi-objective Pareto optimal design of stand-alone wind/PV/FC generation microgrid system,’’ *Energy*, vol. 115, pp. 1022–1041, 2016.

[171] H. Zahboune, S. Zouggar, G. Krajacic, P. S. Varbanov, M. Elhafyani, and E. Ziani, ‘‘Optimal hybrid renewable energy design in autonomous system using modified electric system cascade analysis and Homer software,’’ *Energy Conversion and Management*, vol. 126, pp. 909–922, 2016.

[172] M. H. Nehrir, C. Wang, K. Strunz, R. R. H. Aki, Z. M. J. Bing, Z. Miao, and Z. Salameh, ‘‘A review of hybrid renewable/alternative energy systems for electric power generation: configurations, control, and applications,’’ *IEEE Transactions on Sustainable Energy*, vol. 2, pp. 42–48, 2011.

[173] B. Zhao, X. Zhang, P. Li, K. Wang, M. Xue, and C. Wang, ‘‘Optimal sizing, operating strategy and operational experience of a stand-alone microgrid on Dongfushan Island,’’ *Applied Energy*, vol. 113, pp. 1656–1666, 2014.

[174] L. K. Gan, J. K. H. Shek, and M. A. Mueller, ‘‘Hybrid wind-photovoltaic-diesel-battery system sizing tool development using empirical approach, life-cycle

cost and performance analysis: A case study in Scotland,'' *Energy Conversion and Management*, vol. 106, pp. 479–494, 2015.

[175] A. Malheiro, P. M. Castro, R. M. Lima, and A. Estanqueiro, ''Integrated sizing and scheduling of wind/PV/diesel/battery isolated systems,'' *Renewable Energy*, vol. 83, pp. 646–657, 2015.

[176] S. Ahmadi and S. Abdi, ''Application of the hybrid big bang-big rrunch algorithm for optimal sizing of a stand-alone hybrid PV/wind/battery system,'' *Solar Energy*, vol. 134, pp. 366–374, 2016.

[177] A. Maleki, F. Pourfayaz, and M. A. Rosen, ''A novel framework for optimal design of hybrid renewable energy- based autonomous energy systems : A case study for Namin , Iran,'' *Energy*, vol. 98, pp. 168–180, 2016.

[178] A. S. O. Ogunjuyigbe, T. R. Ayodele, and O. A. Akinola, ''Optimal allocation and sizing of PV/wind/split-diesel/battery hybrid energy system for minimizing life cycle cost, carbon emission and dump energy of remote residential building,'' *Applied Energy*, vol. 171, pp. 153–171, 2016.

[179] S. A. Shezan, S. Julai, M. A. Kibria, K. R. Ullah, R. Saidur, W.T. Chong, and R. K. Akikur, ''Performance analysis of an off-grid wind-PV (photovoltaic)-diesel-battery hybrid energy system feasible for remote areas,'' *Journal of Cleaner Production*, vol. 125, pp. 121–132, 2016.

[180] A. Al-Sharafi, A. Z. Sahin, T. Ayar, and B. S. Yilbas, ''Techno-economic analysis and optimization of solar and wind energy systems for power generation and hydrogen production in Saudi Arabia,'' *Renewable and Sustainable Energy Reviews*, vol. 69, pp. 33–49, 2017.

[181] V. Indragandhi, V. Subramaniyaswamy, and R. Logesh, ''Resources, configurations, and soft computing techniques for power management and control of PV/wind hybrid system,'' *Renewable and Sustainable Energy Reviews*, vol. 69, pp. 129–143, 2017.

[182] A. Goetzberger, J. Knobloch, and V. Bernhard, *Crystalline silicon solar cells*. Chichester: John Wiley & Sons Ltd, 1998.

[183] T. Markvart and L. Castaner, *Solar Cells: Materials, manufacture and operation*. Oxford: Elsevier Ltd, 2005.

[184] H. Haberlin, *Photovoltaics : System design and practice*. Chichester: John Wiley & Sons Ltd, 2012.

[185] E. Skoplaki and J. A. Palyvos, ''On the temperature dependence of photovoltaic module electrical performance: A review of efficiency/power correlations,'' *Solar Energy*, vol. 83, pp. 614–624, 2009.

[186] T. Urmee, D. Harries, and H. G. Holtorf, *Photovoltaics for rural electrification in developing countries*. Geneva: Springer International Publishing, 2016.

[187] Canadian Solar, ''Poly crystalline silicon module,'' CS6U-355P datasheet, 2018.

[188] M. A. Green, Y. Hishikawa, E. D. Dunlop, D. H. Levi, J. Hohl-Ebinger, and A. W. Y. Ho-Baillie, ''Solar cell efficiency tables (version 52),'' *Progress in Photovoltaics: Research and Applications*, vol. 26, pp. 427–436, 2018..

[189] Evans, D. L., ‘‘Simplified method for predicting photovoltaic array Output’, *Solar Energy*,’’ vol. 26, pp. 555–560, 1981.

[190] A. H. Fathima and K. Palanisamy, ‘‘Optimization in microgrids with hybrid energy systems – A review,’’ *Renewable and Sustainable Energy Reviews*, vol. 45, pp. 431–446, 2015.

[191] R. Hosseinalizadeh, H. G. Shakouri, M. S. Amalnick, and P. Taghipour, ‘‘Economic sizing of a hybrid (PV – WT – FC) renewable energy system (HRES) for stand-alone usages by an optimization-simulation model : Case study of Iran,’’ *Renewable and Sustainable Energy Reviews*, vol. 54, pp. 139–150, 2016.

[192] J. Zhang, L. Zhao, S. Deng, W. Xu, and Y. Zhang, ‘‘A critical review of the models used to estimate solar radiation,’’ *Renewable and Sustainable Energy Reviews*, vol. 70, pp. 314–329, 2017.

[193] H. C. Bayrakçı, C. Demircan, and A. Keçebaş, ‘‘The development of empirical models for estimating global solar radiation on horizontal surface: A case study,’’ *Renewable and Sustainable Energy Reviews*, vol. 81, pp. 2771–2782, 2018.

[194] F. Besharat, A. A. Dehghan, and A. R. Faghih, ‘‘Empirical models for estimating global solar radiation: A review and case study,’’ *Renewable and Sustainable Energy Reviews*, vol. 21, pp. 798–821, 2013.

[195] M. A. Hassan, A. Khalil, S. Kaseb, and M. A. Kassem, ‘‘Independent models for estimation of daily global solar radiation: A review and a case study,’’ *Renewable and Sustainable Energy Reviews*, vol. 82, pp. 1565–1575, 2018.

[196] M. Despotovic, V. Nedic, D. Despotovic, and S. Cvetanovic, ‘‘Review and statistical analysis of different global solar radiation sunshine models,’’ *Renewable and Sustainable Energy Reviews*, vol. 52, pp. 1869–1880, 2015.

[197] S. Anis, B. Jamil, A. Ansari, and E. Bellos, ‘‘Generalized models for estimation of global solar radiation based on sunshine duration and detailed comparison with the existing : A case study for India,’’ *Sustainable Energy Technologies and Assessments*, vol. 31, pp. 179–198, 2019.

[198] A. Angstrom, ‘‘Solar and terrestrial radiation,’’ *Quarterly Journal of the Royal Meteorological Society*, vol. 50, pp. 121–126, 1924.

[199] F. E. Alsina, M. Bortolini, M. Gamberi, and A. Regattieri, ‘‘Artificial neural network optimisation for monthly average daily global solar radiation prediction,’’ *Energy Conversion and Management*, vol. 120, pp. 320–329, 2016.

[200] O. Celik, A. Teke, and B. H. Yildirim, ‘‘The optimized artificial neural network model with Levenberg-Marquardt algorithm for global solar radiation estimation in Eastern Mediterranean Region of Turkey,’’ *Journal of Cleaner Production*, vol. 116, pp. 1–12, 2016.

[201] K. Chiteka and C. C. Enweremadu, ‘‘Prediction of global horizontal solar irradiance in Zimbabwe using artificial neural networks,’’ *Journal of Cleaner Production*, vol. 135, pp. 701–711, 2016.

[202] R. C. Deo and M. Şahin, ‘‘Forecasting long-term global solar radiation with an ANN algorithm coupled with satellite-derived (MODIS) land surface

temperature (LST) for regional locations in Queensland,'' *Renewable and Sustainable Energy Reviews*, vol. 72, pp. 828–848, 2017.

[203] F. Baser and H. Demirhan, ''A fuzzy regression with support vector machine approach to the estimation of horizontal global solar radiation,'' *Energy*, vol. 123, pp. 229–240, 2017.

[204] Z. Ramedani, M. Omid, A. Keyhani, B. Khoshnevisan, and H. Saboohi, ''A comparative study between fuzzy linear regression and support vector regression for global solar radiation prediction in Iran,'' *Solar Energy*, vol. 109, pp. 135–143, 2014.

[205] M. Rizwan, M. Jamil, S. Kirmani, and D. P. Kothari, ''Fuzzy logic based modeling and estimation of global solar energy using meteorological parameters,'' *Energy*, vol. 70, pp. 685–691, 2014.

[206] J. M. Bakhashwain, ''Prediction of global solar radiation using support vector machines,'' *International Journal of Green Energy*, vol. 13, pp. 1467–1472, 2016.

[207] S. Belaid and A. Mellit, 'Prediction of daily and mean monthly global solar radiation using support vector machine in an arid climate,'' *Energy Conversion and Management*, vol. 118, pp. 105–118, 2016.

[208] K. Kaba, H. M. Kandirmaz, and M. Avci, ''Estimation of daily sunshine duration using support vector machines,'' *International Journal of Green Energy*, vol. 14, pp. 430–441, 2017.

[209] G. H. Hargreaves and Z. A. Samani, ''Estimating potential evapotranspiration,'' *Journal of the Irrigation and Drainage Engineering*, vol. 108, pp. 225–230, 1982.

[210] G. Olatona and A. Adeleke, ''Estimation of solar radiation over Ibadan from routine meteorological parameters,'' *The International Journal of Engineering and Science*, vol. 4, pp. 44–51, 2015.

[211] O. T. Kolebaje, A. Ikusika, and P. Akinyemi, ''Estimating solar radiation in Ikeja and Port Harcourt with relative humidity and temperature,'' *International Journal of Energy Production and Management*, vol. 1, pp. 253–262, 2016.

[212] O. O. Ajayi, O. D. Ohijeagbon, C. E. Nwadialo, and O. Olasope, ''New model to estimate daily global solar radiation over Nigeria,'' *Sustainable Energy Technologies and Assessments*, vol. 5, pp. 28–36, 2014.

[213] B. M. Olomiyesan and O. D. Oyedum, ''Comparative study of ground measured , satellite-derived, and estimated global solar radiation data in Nigeria,'' *Journal of Solar Energy*, vol. 1, pp. 1–7, 2016.

[214] S. C. Chukwu and A. N. Nwachukwu, ''Analysis of some meteorological parameters using artificial neural network method for Makurdi, Nigeria,'' *African Journal of Environmental Science and Technology*, vol. 6, pp. 182–188, 2012.

[215] L. Olatomiwa, S. Mekhilef, S. Shamshirband, and D. Petkovi, ''Adaptive neuro-fuzzy approach for solar radiation prediction in Nigeria,'' *Renewable and Sustainable Energy Reviews*, vol. 51, pp. 1784–1791, 2015.

[216] L. Olatomiwa, S. Mekhilef, S. Shamshirband, K. Mohammadi, D. Petkovic, and C. Sudheer, ‘‘A support vector machine–firefly algorithm-based model for global solar radiation prediction,’’ *Solar Energy*, vol. 115, pp. 632–644, 2015.

[217] A. Q. Jakhrani, S. R. Samo, A. Ragai, H. Rigit, and S. A. Kamboh, ‘‘Selection of models for calculation of incident solar radiation on tilted surfaces,’’ *World Applied Sciences Journal*, vol. 22, pp. 1334–1343, 2013.

[218] B. Jamil, A. T. Siddiqui, and N. Akhtar, ‘‘Estimation of solar radiation and optimum tilt angles for south-facing surfaces in humid subtropical climatic region of India,’’ *Engineering Science and Technology, an International Journal*, vol. 19, pp. 1826–1835, 2016.

[219] K. N. Shukla, S. Rangnekar, and K. Sudhakar, ‘‘Mathematical modelling of solar radiation incident on tilted surface for photovoltaic application at Bhopal, M. P., India,’’ *International Journal of Ambient Energy*, vol. 37, pp. 579–588, 2016.

[220] R. Tang and T. Wu, ‘‘Optimal tilt-angles for solar collectors used in China,’’ *Applied Energy*, vol. 79, pp. 239–248, 2004.

[221] M. D. Steven and M. H. Unsworth, ‘‘The angular distribution and interception of diffuse solar radiation below overcast skies,’’ *Quarterly Journal of the Royal Meteorological Society*, vol. 106, pp. 57–61, 1980.

[222] A. Skartveit and J. A. Olseth, ‘‘Modelling slope irradiance at high latitudes,’’ *Solar Energy*, vol. 36, pp. 333–344, 1986.

[223] T. M. Klucher, ‘‘Evaluation of models to predict insolation on tilted surfaces,’’ *Solar Energy*, vol. 23, pp. 111–114, 1979.

[224] D. T. Reindl, W. A. Beckman, and J. A. Duffie, ‘‘Evaluation of hourly tilted surface radiation models,’’ *Solar Energy*, vol. 45, pp. 9–17, 1990.

[225] J. E. Hay, ‘‘Calculation of monthly mean solar radiation for horizontal and inclined surfaces,’’ *Solar Energy*, vol. 23, pp. 301–307, 1979.

[226] V. Badescu, ‘‘A new kind of cloudy sky model to compute instantaneous values of diffuse and global solar irradiance,’’ *Theoretical and Applied Climatology*, vol. 72, pp. 127–136, 2002.

[227] P. S. Koronakis, ‘‘On the choice of the angle of tilt for south facing solar collectors in the Athens basin area,’’ *Solar Energy*, vol. 36, pp. 217–225, 1986.

[228] Y. Q. Tian, R. J. Davies-Colley, P. Gong, and B. W. Thorrold, ‘‘Estimating solar radiation on slopes of arbitrary aspect,’’ *Agricultural and Forest Meteorology*, vol. 109, pp. 67–74, 2001.

[229] F. Olmo, J. Vida, I. Foyo, Y. Castro-Diez, and L. Alados-Arboledas, ‘‘Prediction of global irradiance on inclined surfaces from horizontal global irradiance,’’ *Energy*, vol. 24, pp. 689–704, 1999.

[230] S. A. M. Maleki, H. Hizam, and C. Gomes, ‘‘Estimation of hourly, daily and monthly global solar radiation on inclined surfaces: Models re-visited,’’ *Energies*, vol. 10, p. 134, 2017.

[231] K. Bhumkittipich and W. Phuangpornpitak, ‘‘Optimal placement and sizing of distributed generation for power loss reduction using particle swarm

optimization,'' *Energy Procedia*, vol. 34, pp. 307–317, 2013.

[232] S. D. Biswas and A. Debbarma, ''Optimal operation of large power system by GA method,'' *Journal of Emerging Trends in Engineering and Applied Sciences*, vol. 3, pp. 1–7, 2012.

[233] S. M. Shahidehpour and S. K. Tong, ''An overview of power generation scheduling in the optimal operation of a large scale power system,'' *Electric Machines and Power Systems*, vol. 19, pp. 731–762, 1991.

[234] B. Jabeck, ''The impact of generator set underloading,'' 2013. [Online]. Available: https://www.cat.com/en_GB/by-industry/electric-power-generation/Articles/White-papers/the-impact-of-generator-set-underloading.html. [Accessed: Feb. 4, 2016].

[235] G. D. Najafpour, *Biochemical Engineering and Biotechnology*, 2nd ed. Oxford: Elsevier Ltd, 2015.

[236] T. R. Ayodele, A. S. O. Ogunjuyigbe, and M. A. Alao, ''Life cycle assessment of waste-to-energy (WtE) technologies for electricity generation using municipal solid waste in Nigeria,'' *Applied Energy*, vol. 201, pp. 200–218, 2017.

[237] A. S. O. Ogunjuyigbe, T. R. Ayodele, and M. A. Alao, ''Electricity generation from municipal solid waste in some selected cities of Nigeria: An assessment of feasibility, potential and technologies,'' *Renewable and Sustainable Energy Reviews*, vol. 80, pp. 149–162, 2017.

[238] S. A. Neshat, M. Mohammadi, G. D. Najafpour, and P. Lahijani, ''Anaerobic co-digestion of animal manures and lignocellulosic residues as a potent approach for sustainable biogas production,'' *Renewable and Sustainable Energy Reviews*, vol. 79, pp. 308–322, 2017.

[239] C. Mao, Y. Feng, X. Wang, and G. Ren, ''Review on research achievements of biogas from anaerobic digestion,'' *Renewable and Sustainable Energy Reviews*, vol. 45, pp. 540–555, 2015.

[240] K. C. Surendra, D. Takara, A. G. Hashimoto, and S. K. Khanal, ''Biogas as a sustainable energy source for developing countries: Opportunities and challenges,'' *Renewable and Sustainable Energy Reviews*, vol. 31, pp. 846–859, 2014.

[241] R. L. Grando, A. M. de Souza Antune, F. V. da Fonseca, A. Sánchez, R. Barrena, and X. Font, ''Technology overview of biogas production in anaerobic digestion plants: A European evaluation of research and development,'' *Renewable and Sustainable Energy Reviews*, vol. 80, pp. 44–53, 2017.

[242] F. Nardin and F. Mazzetto, ''Mapping of biomass fluxes: A method for optimizing Biogas-Refinery of livestock effluents,'' *Sustainability*, vol. 6, pp. 5920–5940, 2014.

[243] J. Edwards, M. Othman, and S. Burn, ''A review of policy drivers and barriers for the use of anaerobic digestion in Europe, the United States and Australia,'' *Renewable and Sustainable Energy Reviews*, vol. 52, pp. 815–828, 2015.

[244] I. S. Horváth, M. Tabatabaei, K. Karimi, and R. Kumar, ''Recent updates on biogas production - a review,'' *Biofuel Research Journal*, vol. 3, pp. 394–402,

2016.

[245] Z. Yong, Y. Dong, X. Zhang, and T. Tan, ‘‘Anaerobic co-digestion of food waste and straw for biogas production,’’ *Renewable Energy*, vol. 78, pp. 527–530, 2015.

[246] D. Divya, L. R. Gopinath, and P. Merlin Christy, ‘‘A review on current aspects and diverse prospects for enhancing biogas production in sustainable means,’’ *Renewable and Sustainable Energy Reviews*, vol. 42, pp. 690–699, 2015.

[247] N. Glanpracha and A. P. Annachhatre, ‘‘Anaerobic co-digestion of cyanide containing cassava pulp with pig manure,’’ *Bioresource Technology*, vol. 214, pp. 112–121, 2016.

[248] E. Naran, U. A. Toor, and D. J. Kim, ‘‘Effect of pretreatment and anaerobic co-digestion of food waste and waste activated sludge on stabilization and methane production,’’ *International Biodeterioration and Biodegradation*, vol. 113, pp. 17–21, 2016.

[249] E. J. Bowen, J. Dolfing, R. J. Davenport, F. L. Read, and T. P. Curtis, ‘‘Low-temperature limitation of bioreactor sludge in anaerobic treatment of domestic wastewater,’’ *Water Science and Technology*, vol. 69, pp. 1004–1013, 2014.

[250] T. Abbasi, S. Tauseef, and S. Abbasi, *Biogas Energy*. New York: Springers, 2012.

[251] M. N. Kinyua, L. E. Rowse, and S. J. Ergas, ‘‘Review of small-scale tubular anaerobic digesters treating livestock waste in the developing world,’’ *Renewable and Sustainable Energy Reviews*, vol. 58, pp. 896–910, 2016.

[252] M. Frisk, ‘‘Simulation and optimization of a hybrid renewable energy system for application on a Cuban farm,’’ Ph.D thesis, Department of Engineering Sciences, Uppsala University, Lägerhyddsvägen 1, Uppsala, 2017.

[253] M. M. Rahman, M. M. Hasan, J. V. Paatero, and R. Lahdelma, ‘‘Hybrid application of biogas and solar resources to fulfill household energy needs: A potentially viable option in rural areas of developing countries,’’ *Renewable Energy*, vol. 68, pp. 35–45, 2014.

[254] S. Cheng, Z. Li, H. P. Mang, E. M. Huba, R. Gao, and X. Wang, ‘‘Development and application of prefabricated biogas digesters in developing countries,’’ *Renewable and Sustainable Energy Reviews*, vol. 34, pp. 387–400, 2014.

[255] M. Westerholm, M. Hansson, and A. Schnürer, ‘‘Improved biogas production from whole stillage by co-digestion with cattle manure,’’ *Bioresource Technology*, vol. 114, pp. 314–319, 2012.

[256] K. Risberg, L. Sun, L. Levén, S. J. Horn, and A. Schnürer, ‘‘Biogas production from wheat straw and manure - Impact of pretreatment and process operating parameters,’’ *Bioresource Technology*, vol. 149, pp. 232–237, 2013.

[257] V. Moset, M. Poulsen, R. Wahid, O. Højberg, and H. B. Møller, ‘‘Mesophilic versus thermophilic anaerobic digestion of cattle manure: Methane productivity and microbial ecology,’’ *Microbial Biotechnology*, vol. 8, pp. 787–800, 2015.

[258] N. Zhai, T. Zhang, D. Yin, G. Yang, X. Wang, G. Ren, and Y. Feng, ‘‘Effect of initial

pH on anaerobic co-digestion of kitchen waste and cow manure,'' *Waste Management*, vol. 38, pp. 126–131, 2015.

[259] K. Hagos, J. Zong, D. Li, C. Liu, and X. Lu, ''Anaerobic co-digestion process for biogas production: Progress, challenges and perspectives,'' *Renewable and Sustainable Energy Reviews*, vol. 76, pp. 1485–1496, 2017.

[260] S. Guillaume and T. Lendormi, ''Anaerobic co-digestion of dairy cattle slurry and agro-industrial fats: Effect of fat ratio on the digester Efficiency,'' *The Canadian Journal of Chemical Engineering*, vol. 93, pp. 304–308, 2015.

[261] A. Y. Kallistova, G. Goel, and A. N. Nozhevnikova, ''Microbial diversity of methanogenic communities in the systems for anaerobic treatment of organic waste,'' *Microbiology*, vol. 83, pp. 462–483, 2014.

[262] K. Aboudi, C. J. Álvarez-Gallego, and L. I. Romero-García, ''Semi-continuous anaerobic co-digestion of sugar beet byproduct and pig manure: Effect of the organic loading rate (OLR) on process performance,'' *Bioresource Technology*, vol. 194, pp. 283–290, 2015.

[263] C. Rico, N. Muñoz, J. Fernández, and J. L. Rico, ''High-load anaerobic co-digestion of cheese whey and liquid fraction of dairy manure in a one-stage UASB process: Limits in co-substrates ratio and organic loading rate,'' *Chemical Engineering Journal*, vol. 262, pp. 794–802, 2015.

[264] C. Gou, Z. Yang, J. Huang, H. Wang, H. Xu, and L. Wang, ''Effects of temperature and organic loading rate on the performance and microbial community of anaerobic co-digestion of waste activated sludge and food waste,'' *Chemosphere*, vol. 105, pp. 146–151, 2014.

[265] M. S. Guney and Y. Tepe, ''Classification and assessment of energy storage systems,'' *Renewable and Sustainable Energy Reviews*, vol. 75, pp. 1187–1197, 2017.

[266] X. Luo, J. Wang, M. Dooner, and J. Clarke, ''Overview of current development in electrical energy storage technologies and the application potential in power system operation,'' *Applied Energy*, vol. 137, pp. 511–536, 2015.

[267] R. Hemmati and H. Saboori, ''Emergence of hybrid energy storage systems in renewable energy and transport applications – A review,'' *Renewable and Sustainable Energy Reviews*, vol. 65, pp. 11–23, 2016.

[268] K. S. Krishna and K. S. Kumar, "A review on hybrid renewable energy systems," *Renewable and Sustainable Energy Reviews*, vol. 52, pp. 907–916, 2015.

[269] S. Das and A. K. Akella, ''Power flow control of pv-wind-battery hybrid renewable energy systems for stand-alone application,'' *International Journal of Renewable Energy Research*, vol. 8, pp. 36–43, 2018.

[270] M. Y. Suberu, M. W. Mustafa, and N. Bashir, ''Energy storage systems for renewable energy power sector integration and mitigation of intermittency,'' *Renewable and Sustainable Energy Reviews*, vol. 35, pp. 499–514, 2014.

[271] H. Zhao, Q. Wu, S. Hu, H. Xu, and C. N. Rasmussen, ''Review of energy storage system for wind power integration support,'' *Applied Energy*, vol. 137, pp. 545–553, 2015.

[272] S. O. Amrouche, D. Rekioua, T. Rekioua, and S. Bacha, ‘‘Overview of energy storage in renewable energy systems,’’ *International Journal of Hydrogen Energy*, vol. 41, pp. 20914–20927, 2016.

[273] T. Bocklisch, “Hybrid energy storage approach for renewable energy applications,” *Journal of Energy Storage*, vol. 8, pp. 311–319, 2016.

[274] T. Bocklisch, ‘‘Hybrid energy storage systems for renewable energy applications,’’ *Energy Procedia*, vol. 73, pp. 103–111, 2015.

[275] L. W. Chong, Y. W. Wong, R. K. Rajkumar, R. K. Rajkumar, and D. Isa, ‘‘Hybrid energy storage systems and control strategies for stand-alone renewable energy power systems,’’ *Renewable and Sustainable Energy Reviews*, vol. 66, pp. 174–189, 2016.

[276] A Capasso, W. Grattieri, R. Lamedica, and A. Prudenzi, ‘‘A bottom-up approach to residential load modeling - Power Systems,’’ *IEEE Transactions on Power Systems*, vol. 9, pp. 957–964, 1994.

[277] F. McLoughlin, A. Duffy, and M. Conlon, ‘‘Characterising domestic electricity consumption patterns by dwelling and occupant socio-economic variables: An Irish case study,’’ *Energy and Buildings*, vol. 48, pp. 240–248, 2012.

[278] I. Richardson, M. Thomson, D. Infield, and C. Clifford, ‘‘Domestic electricity use: A high-resolution energy demand model. Energy and Buildings,’’ *Energy and Buildings*, vol. 42, pp. 1878–1887, 2010.

[279] J. Widén and E. Wäckelgård, ‘‘A high-resolution stochastic model of domestic activity patterns and electricity demand,’’ *Applied Energy*, vol. 87, pp. 1880–1892, 2010.

[280] U. Wilke, F. Haldi, J. L. Scartezzini, and D. Robinson, ‘‘A bottom-up stochastic model to predict building occupants’ time-dependent activities,’’ *Building and Environment*, vol. 60, pp. 254–264, 2013.

[281] I. Ahemen, A. N. Amah, and P. O. Agada, ‘‘A survey of power supply and lighting patterns in North Central Nigeria—The energy saving potentials through efficient lighting systems,’’ *Energy and Buildings*, vol. 133, pp. 770–776, 2016.

[282] R. V. Jones, A. Fuertes, and K. J. Lomas, ‘‘The socio-economic, dwelling and appliance related factors affecting electricity consumption in domestic buildings,’’ *Renewable and Sustainable Energy Reviews*, vol. 43, pp. 901–917, 2015.

[283] J. O’Doherty, S. Lyons, and R. S. J. Tol, ‘‘Energy-using appliances and energy-saving features: Determinants of ownership in Ireland,’’ *Applied Energy*, vol. 85, pp. 650–662, 2008.

[284] G. Wood and M. Newborough, ‘‘Dynamic energy-consumption indicators for domestic appliances: Environment, behaviour and design,’’ *Energy and Buildings*, vol. 35, pp. 821–841, 2003.

[285] Q. Xie, H. Ouyang, and X. Gao, ‘‘Estimation of electricity demand in the residential buildings of China based on household survey data,’’ *International Journal of Hydrogen Energy*, vol. 41, pp. 15879–15886, 2016.

[286] G. Huebner, D. Shipworth, I. Hamilton, Z. Chalabi, and T. Oreszczyn,

''Understanding electricity consumption: A comparative contribution of building factors, socio-demographics, appliances, behaviours and attitudes,'' *Applied Energy*, vol. 177, pp. 692–702, 2016.

[287] A. Kavousian, R. Rajagopal, and M. Fischer, ''Determinants of residential electricity consumption: Using smart meter data to examine the effect of climate, building characteristics, appliance stock, and occupants' behavior,'' *Energy*, vol. 55, pp. 184–194, 2013.

[288] B. Gao, X. Liu, and Z. Zhu, "A bottom-up model for household load profile based on the consumption behavior of residents," *Energies*, vol. 11, pp. 1–16, 2018.

[289] R. V. Jones and K. J. Lomas, ''Determinants of high electrical energy demand in UK homes: Appliance ownership and use,'' *Energy and Buildings*, vol. 117, pp. 71–82, 2016.

[290] M. Bedir, E. Hasselaar, and L. Itard, ''Determinants of electricity consumption in Dutch dwellings,'' *Energy and Buildings*, vol. 58, pp. 194–207, 2013.

[291] A. Grandjean, J. Adnot, and G. Binet, ''A review and an analysis of the residential electric load curve models,'' *Renewable and Sustainable Energy Reviews*, vol. 16, pp. 6539–6565, 2012.

[292] Y. Ge, C. Zhou, and D. M. Hepburn, ''Domestic electricity load modelling by multiple Gaussian functions,'' *Energy and Buildings*, vol. 126, pp. 455–462, 2016.

[293] A. Marszal-Pomianowska, P. Heiselberg, and O. K. Larsen, ''Household electricity demand profiles - A high-resolution load model to facilitate modelling of energy flexible buildings,'' *Energy*, vol. 103, pp. 487–501, 2016.

[294] N. Phuangpornpitak and W. Prommee, ''A study of load demand forecasting models in electric power system operation and planning,'' *Greater Mekong Subregion Academic and Research Network International Journal*, vol. 10, pp. 19–24, 2016.

[295] S. A. Soliman nd M. Al-Kandari, *Electrical load forecasting: Modeling and model construction*. Oxford: Elsevier Ltd, 2010.

[296] E. L. Ofetotse, E. A Essah, and R. Yao, ''Domestic energy models : Complexities in defining specific tools,'' in Conf. *International Conference in Sustainable Development in Building and Environment*, Chongqing, China, Oct. 28–30, 2013. [Online]. Available: https://www.researchgate.net/publication /275523347_Domestic_energy_models_complexities_in_defining_specific_ tools. [Accessed: Jan. 29, 2018].

[297] L. Suganthi a and A. A. Samuel, ''Energy models for demand forecasting - A review,'' *Renewable and Sustainable Energy Reviews*, vol. 16, pp. 1223–1240, 2012.

[298] W. Hong, ''Electric load forecasting by support vector model,'' *Applied Mathematical Modelling*, vol. 33, pp. 2444–2454, 2009.

[299] M. Grubb, J. Edmonds, P. Ten Brink, and M. Morrison, ''The costs of limiting fossil-fuel CO2 emissions : A survey and analysis,'' *Annual Review of Energy and the Environment*, vol. 18, pp. 397–478, 1993.

[300] R. B. Hiremath, B. Kumar, P. Balachandra, N. H. Ravindranath, and B. N. Raghunandan, ''Decentralised renewable energy: Scope, relevance and applications in the Indian context,'' *Energy for Sustainable Development*, vol. 13, pp. 4–10, 2009.

[301] A. Herbst, F. Toro, F. Reitze, and E. Jochem, ''Introduction to energy systems modelling,'' *Swiss Journal of Economics and Statistics*, vol. 148, pp. 111–135, 2012.

[302] M. Beaudin and H. Zareipour, ''Home energy management systems: A review of modelling and complexity,'' *Renewable and Sustainable Energy Reviews*, vol. 45, pp. 318–335, 2015.

[303] J. Widén, M. Lundh, I. Vassileva, E. Dahlquist, K. Ellegård, and E. Wäckelgård, ''Constructing load profiles for household electricity and hot water from time-use data–Modelling approach and validation,'' *Energy and Buildings*, vol. 41, pp. 753–768, 2009.

[304] L. G. Swan and V. I. Ugursal, ''Modeling of end-use energy consumption in the residential sector: A review of modeling techniques,'' *Renewable and Sustainable Energy Reviews*, vol. 13, pp. 1819–1835, 2009.

[305] T. Lee and R. Yao, ''Incorporating technology buying behaviour into UK-based long term domestic stock energy models to provide improved policy analysis,'' *Energy Policy*, vol. 52, pp. 363–372, 2013.

[306] M. Kavgic, A. Mavrogianni, D. Mumovic, A. Summerfield, Z. Stevanovic, and M. Djurovic-Petrovic, ''A review of bottom-up building stock models for energy consumption in the residential sector,'' *Building and Environment*, vol. 45, pp. 1683–1697, 2010.

[307] E. McKenna, M. Krawczynski, and M. Thomson, ''Four-state domestic building occupancy model for energy demand simulations,'' *Energy and Buildings*, vol. 96, pp. 30–39, 2015.

[308] F. Farzan, M. A. Jafari, J. Gong, F. Farzan, and A. Stryker, ''A multi-scale adaptive model of residential energy demand,'' *Applied Energy*, vol. 150, pp. 258–273, 2015.

[309] T. R. Ayodele, A. S. O. Ogunjuyigbe, and I. A. Atiba, ''Assessment of the impact of information feedback of prepaid meter on energy consumption of city residential buildings using bottom-up load modeling approach,'' *Sustainable Cities and Society*, vol. 30, pp. 171–183, 2017.

[310] M. Muratori, M. C. Roberts, R. Sioshansi, V. Marano, and G. Rizzoni, ''A highly resolved modeling technique to simulate residential power demand,'' *Applied Energy*, vol. 107, pp. 465–473, 2013.

[311] G. Raffio, O. Isambert, G. Mertz, C. Schreier, and K. Kissock, ''Targeting residential energy assistance,'' in *Proc. ASME energy sustainability conference*, CA, USA, Jul. 27–30, 2007, pp. 489–495.

[312] R. A. Douthitt, ''An economic analysis of the demand for residential space heating fuel in Canada,'' *Energy*, vol. 14, pp. 187–197, 1989.

[313] D. J. Aigner, C. Sorooshian, P. Kerwin, ''Conditional demand analysis for

estimating residential end-use load profiles,'' *The Energy Journal*, vol. 5, pp. 81–97, 1984.

[314] M. P. E. Lins, A. C. M. Da Silva, and L. P. Rosa, ''Regional variations in energy consumption of appliances: Conditional demand analysis applied to Brazilian households,'' *Annals of Operations Research*, vol. 117, pp. 235–246, 2002.

[315] G. Lafrance and D. Perron, ''Evolution of residential electricity demand by end-use in Quebec 1979-1989: A conditional demand analysis,'' *Energy Studies Review*, vol. 6, pp. 164–173, 1994.

[316] G. Mihalakakou, M. Santamouris, and A. Tsangrassoulis, ''On the energy consumption in residential buildings,'' *Energy and Buildings*, vol. 34, pp. 727–736, 2002.

[317] M. Aydinalp, V. I. Ugursal, and A. S. Fung, ''Modeling of the appliance, lighting and space-cooling energy consumption in the residential sector using neural networks,'' *Applied Energy*, vol. 71, pp. 87–110, 2002.

[318] R. Kadian, R. P. Dahiya, and H. P. Garg, ''Energy-related emissions and mitigation opportunities from the household sector in Delhi,'' *Energy Policy*, vol. 35, pp. 6195–6211, 2007.

[319] A. Parekh, ''Development of archetypes of building characteristcs libraries for simplified energy use evaluation of houses,'' in *Proc. 9th International Building Performance Simulation Association Conference*, Montreal, Canada, Aug. 15–18, 2005, pp. 921–928.

[320] Y. J. Huang and J. Brodrick, ''A Bottom-Up Engineering Estimate of the Aggregate Heating and Cooling Loads of the Entire US Building Stock,'' in Proc. American Council for an Energy-Efficient Economy *summer study on energy efficiency in buildings*, CA, USA, Aug. 2000, pp. 135–148.

[321] H. Farahbakhsh, V. I. Ugursal, and A. S. Fung, ''A residential end-use energy consumption model for Canada,'' *International Journal of Energy Research*, vol. 22, pp. 1133–1143, 1998.

[322] B. M. Larsen and R. Nesbakken, ''Household electricity end-use consumption: Results from econometric and engineering models,'' *Energy Economics*, vol. 26, pp. 179–200, 2004.

[323] I. Richardson, M. Thomson, and D. Infield, ''A high-resolution domestic building occupancy model for energy demand simulations,'' *Energy and Buildings*, vol. 40, pp. 1560–1566, 2008.

[324] R. Yao and K. Steemers, ''A method of formulating energy load profile for domestic buildings in the UK,'' *Energy and Buildings*, vol. 37, pp. 663–671, 2005.

[325] M. Stokes, M. Rylatt, and K. Lomas, ''A simple model of domestic lighting demand,'' *Energy and Buildings*, vol. 36, pp. 103–116, 2004.

[326] J. V. Paatero and P. D. Lund, ''A model for generating household electricity load profiles,'' *International Journal of Energy Research*, vol. 30, pp. 273–290, 2006.

[327] J. Torriti, ''A review of time use models of residential electricity demand,'' *Renewable and Sustainable Energy Reviews*, vol. 37, pp. 265–272, 2014.

[328] M. Stokes, ‘‘Removing barriers to embedded generation: A fine grained load a model to support low voltage network performance analysis,’’ Ph.D. thesis, Institute of Energy and Sustainabe Development, De Montfort University, Leicester, 2005.

[329] J. Widén, A. M. Nilsson, and E. Wäckelgård, ‘‘A combined Markov-chain and bottom-up approach to modelling of domestic lighting demand,’’ *Energy and Buildings*, vol. 41, pp. 1001–1012, 2009.

[330] D. Fischer, A. Härtl, and B. Wille-haussmann, ‘‘Model for electric load profiles with high time resolution for German,’’ *Energy and Buildings*, vol. 92, pp. 170–179, 2015.

[331] N. Good, L. Zhang, A. Navarro-Espinosa, and P. Mancarella, ‘‘High resolution modelling of multi-energy domestic demand profiles,’’ *Applied Energy*, vol. 137, pp. 193–210, 2015.

[332] I. Richardson, M. Thomson, D. Infield, and A. Delahunty, ‘‘Domestic lighting: A high-resolution energy demand model,’’ *Energy and Buildings*, vol. 41, pp. 781–789, 2009.

[333] J. Widén, ‘‘Distributed photovoltaics in the Swedish energy system,’’ Ph.D. thesis, Department of Engineering Sciences, Uppsala University, Lägerhyddsvägen 1, Uppsala, 2009.

[334] A. Maleki and F. Pourfayaz, ‘‘Sizing of stand-alone photovoltaic/wind/diesel system with battery and fuel cell storage devices by harmony search algorithm,’’ *Journal of Energy Storage*, vol. 2, pp. 30–42, 2015.

[335] H. Z. Al Garni, A. Awasthi, and M. A. M. Ramli, ‘‘Optimal design and analysis of grid-connected photovoltaic under different tracking systems using HOMER,’’ *Energy Conversion and Management*, vol. 155, pp. 42–57, 2018.

[336] A. Heydari and A. Askarzadeh, ‘‘Optimization of a biomass-based photovoltaic power plant for an off-grid application subject to loss of power supply probability concept,’’ *Applied Energy*, vol. 165, pp. 601–611, 2016.

[337] J.-H. Cho, M. G. Chun, and W. P. Hong, ‘‘Structure optimization of stand-alone renewable power systems based on multi object function,’’ *Energies*, vol. 9, pp. 649–667, 2016.

[338] S. Norbu and S. Bandyopadhyay, ‘‘Power pinch analysis for optimal sizing of renewable-based isolated system with uncertainties,’’ *Energy*, vol. 135, pp. 466–475, 2017.

[339] P. Y. Liew, S. R. Wan Alwi, S. W. Ho, Z. A. Manan, P. S. Varbanov, and J. J. Klemeš, ‘‘Multi-period energy targeting for total site and locally integrated energy sectors with cascade pinch analysis,’’ *Energy*, vol. 155, pp. 370–380, 2018.

[340] I. J. Esfahani, P. Ifaei, J. Kim, and C. Yoo, ‘‘Design of hybrid renewable energy systems with battery/hydrogen storage considering practical power losses : A MEPoPA (modified extended-power pinch analysis),’’ *Energy*, vol. 100, pp. 40–50, 2016.

[341] D. Jiang and S. Li, ‘‘Strategies of daily economical dispatch considering large-scale wind power integration and electricity contract,’’ In *Proc. International*

Conference on Computer Applications and System Modeling, Shanxi, China, Jul. 27–29, 2012, pp. 514–5177.

[342] H. Branco, R. Castro, and A. Setas Lopes, ''Battery energy storage systems as a way to integrate renewable energy in small isolated power systems,'' *Energy for Sustainable Development*, vol. 43, pp. 90–99, 2018.

[343] W.-T. Huang, K. C. Yao, and C. C. Wu, ''Using the direct search method for optimal dispatch of distributed generation in a medium-voltage microgrid,'' *Energies*, vol. 7, pp. 8355–8373, 2014.

[344] A. K. Al-Othman and K. M. El-Naggar, ''Application of pattern search method to power system security constrained economic dispatch with non-smooth cost function,'' *Electric Power Systems Research*, vol. 78, pp. 667–675, 2008.

[345] A. Mahor, V. Prasad, and S. Rangnekar, ''Economic dispatch using particle swarm optimization: A review,'' *Renewable and Sustainable Energy Reviews*, vol. 13, pp. 2134–2141, 2009.

[346] A. G. Marinopoulos, M. C. Alexiadis, and P. S. Dokopoulos, ''Energy losses in a distribution line with distributed generation based on stochastic power flow,'' *Electric Power Systems Research*, vol. 81, pp. 1986–1994, 2011.

[347] H. E. Farag, E. F. El-Saadany, R. El Shatshat, and A. Zidan, ''A generalized power flow analysis for distribution systems with high penetration of distributed generation,'' *Electric Power Systems Research*, vol. 81, pp. 1499–1506, 2011.

[348] A. C. Rueda-Medina, J. F. Franco, M. J. Rider, A. Padilha-Feltrin, and R. Romero, ''A mixed-integer linear programming approach for optimal type, size and allocation of distributed generation in radial distribution systems,'' *Electric Power Systems Research*, vol. 97, pp. 133–143, 2013.

[349] A. Vijayvargia, S S. Jain, S. Meena, V. Gupta, and M. Lalwani, ''Comparison between different load flow methodologies by analyzing various bus systems,'' *International Journal of Electrical Engineering*, vol. 9, pp. 127–138, 2016.

[350] D. J. Glover, T. J. Overbye, and S. S. Mulukutla, *Power system analysis & design*, 6th ed. Stamford: Cengage Learning, 2016.

[351] L. L. Grigsby, and W. Steveson, *Power system analysis*. Michigan: McGraw-Hill, 1994.

[353] Dharamjit and D. K. Tanti, "Load Flow Analysis on IEEE 30 bus System," *International Journal of Scientific and Research Publications*, vol. 2, pp. 1–6, 2012.

[354] C. A. Gross, *Power system analysis*, 2nd ed. John Wiley & Sons, Inc., 1986.

[355] Y. Levron, J. M. Guerrero, and Y. Beck, ''Optimal power flow in microgrids with energy storage,'' *IEEE Transactions on Power Systems*, vol. 28, pp. 3226–3234, 2013.

[356] A. Mahesh and K. S. Sandhu, ''Hybrid wind/photovoltaic energy system developments: Critical review and findings,'' *Renewable and Sustainable Energy Reviews*, vol. 52, pp. 1135–1147, 2015.

[357] S. M. Zahraee, M. Khalaji Assadi, and R. Saidur, ‘‘Application of artificial intelligence methods for hybrid energy system optimization,’’ *Renewable and Sustainable Energy Reviews*, vol. 66, pp. 617–630, 2016.

[358] D. Connolly, H. Lund, B. V. Mathiesen, and M. Leahy, ‘‘A review of computer tools for analysing the integration of renewable energy into various energy systems,’’ *Applied Energy*, vol. 87, pp. 1059–1082, 2010.

[359] S. Upadhyay and M. P. Sharma, “A review on configurations, control and sizing methodologies of hybrid energy systems,” *Renewable and Sustainable Energy Reviews*, vol. 38, pp. 47–63, 2014.

[360] F. A. Khan, N. Pal, and S. H. Saeed, ‘‘Review of solar photovoltaic and wind hybrid energy systems for sizing strategies optimization techniques and cost analysis methodologies,’’ *Renewable and Sustainable Energy Reviews*, vol. 92, pp. 937–947, 2018.

[361] S. Bandyopadhyay, ‘‘Design and optimization of isolated energy systems,’’ *Asia-Pacific Journal of Chemical Engineering*, pp. 518–526, 2011.

[362] S. R. Wan Alwi, N. E. M. Rozali, Z. A. Manan, and J. J. Klemeš, ‘‘A process integration targeting method for hybrid power systems,’’ *Energy*, vol. 44, pp. 6–10, 2012.

[363] S. R. Wan Alwi, S. O. Tin, N. E. M. Rozali, Z. A. Manan, and J. J. Klemes, ‘‘New graphical tools for process changes via load shifting for hybrid power systems based on Power Pinch Analysis,’’ *Clean Technologies Environmental Policy*, vol. 15, pp. 459–472, 2013.

[364] I. J. Esfahani, S. Lee, and C. Yoo, ‘‘Extended-power pinch analysis (EPoPA) for integration of renewable energy systems with battery/hydrogen storages,’’ *Renewable Energy*, vol. 80, pp. 1–14, 2015.

[365] N. E. M. Rozali, S. R. Wan Alwi, Z. A. Manan, and J. J. Klemeš, ‘‘Process integration for hybrid power system supply planning and demand management – A review,’’ *Renewable and Sustainable Energy Reviews*, vol. 66, pp. 834–842, 2016.

[366] E. N. M. Rozali, W. S. Ho, S. R. Wan Alwi, Z. A. Manan, J. J. Klemes, M. N. S. M. Yunus, and S. A. A. S. M. Zaki, ‘‘Peak-off-peak load shifting for optimal storage sizing in hybrid power systems using power pinch analysis considering energy losses,’’ *Energy*, vol. 156, pp. 299–310, 2018.

[367] K. Anoune, M. Bouya, A. Astito, and B. A. Abdellah, ‘‘Sizing methods and optimization techniques for PV-wind based hybrid renewable energy system: A review,’’ *Renewable and Sustainable Energy Reviews*, vol. 93, pp. 652–673, 2018.

[368] S. Sinha and S. S. Chandel, ‘‘Review of recent trends in optimization techniques for solar photovoltaic-wind based hybrid energy systems,’’ *Renewable and Sustainable Energy Reviews*, vol. 50, pp. 755–769, 2015.

[369] K. De Vos, J. Morbee, J. Driesen, and R. Belmans, ‘‘Impact of wind power on sizing and allocation of reserve requirements,’’ *IET Renewable Power Generation*, vol. 7, pp. 1–9, 2013.

[370] J. Chen and C. Rabiti, ‘‘Synthetic wind speed scenarios generation for probabilistic analysis of hybrid energy systems,’’ *Energy*, vol. 120, pp. 507–517, 2017.

[371] Y. V Makarov, P. Du, M. C. W. Kintner-meyer, C. Jin, and H. F. Illian, ‘‘Sizing energy storage to accommodate high penetration of variable energy resources,’’ *IEEE Transactions on Sustainable Energy*, vol. 3, pp. 34–40, 2012.

[372] Y. Ru, J. Kleissl, and S. Martinez, ‘‘Storage size determination for grid-connected photovoltaic systems,’’ *IEEE Transactions on Sustainable Energy*, vol. 4, pp. 68–81, 2013.

[373] M. Smaoui, A. Abdelkafi, and L. Krichen, ‘‘Optimal sizing of stand-alone photovoltaic/wind/hydrogen hybrid system supplying a desalination unit,’’ *Solar Energy*, vol. 120, pp. 263–276, 2015.

[374] A. Bagul, Z. Salameh, and B. Borowy, ‘‘Sizing of a standalone hybrid wind-photovoltaic system using a three event probability density approximation,’’ *Solar Energy*, vol. 56, pp. 323–335, 1996.

[375] G. Tina, S. Gagliano, and S. Raiti, ‘‘Hybrid solar/wind power system probabilistic modelling for long-term performance assessment,’’ *Solar Energy*, vol. 80, pp. 578–588, 2006.

[376] Y. M. Atwa, F. El–Saadany, M. M. A. Salama, and R. Seethapathy, ‘‘Optimal renewable resources mix for distribution system energy loss minimization,’’ *IEEE Transactions on Power Systems*, vol. 25, pp. 360–370, 2010.

[377] D. K. Khatod, V. Pant, and J. Sharma, ‘‘Analytical approach for well-being assessment of small autonomous power systems with solar and wind energy sources,’’ *IEEE Transactions on Energy Conversion*, vol. 25, pp. 535–545, 2010.

[378] S. Ashok, ‘‘Optimised model for community-based hybrid energy system,’’ *Renewable Energy*, vol. 32, pp. 1155–1164, 2007.

[379] H. Yang, L. Lu, and W. Zhou, ‘‘A novel optimization sizing model for hybrid solar-wind power generation system,’’ *Solar Energy*, vol. 81, pp. 76–84, 2007.

[380] B. Anderson, S. Lin, A. Newing, A. Bahaj, and P. James, ‘‘Computers, environment and urban systems electricity consumption and household characteristics : Implications for census-taking in a smart metered future,’’ *Computers, Environment and Urban Systems*, vol. 63, pp. 58–67, 2017.

[381] E. L. Ofetotse, E. A. Essah, and R. Yao, ‘‘Trends in domestic electricity consumption in Botswana,’’ *TMC Academic Journal*, vol. 9, pp. 83–104, 2015.

[382] H. Bagge and D. Johansson, ‘‘Measurements of household electricity and domestic hot water use in dwellings and the effect of different monitoring time resolution,’’ *Energy*, vol. 36, pp. 2943–2951, 2011.

[383] Y. G. Yohanis, J. D. Mondol, A. Wright, and B. Norton, ‘‘Real-life energy use in the UK : How occupancy and dwelling characteristics affect domestic electricity use,’’ *Energy & Buildings*, vol. 40, pp. 1053–1059, 2008.

[384] Y. Ge, ‘‘Modelling regional domestic load profile by multiple Gaussian functions,’’ Ph.D. thesis, School of Engineering and Building Environment, Glasgow Caledonian University, Glasgow, 2016.

[385] L. Suganthi and A. Samuel, ‘‘Energy models for demand forecasting—A review,’’ *Renewable and Sustainable Energy Reviews*, vol. 16, pp. 1223–1240, 2012.

[386] W. G. Cochran, *Sampling techniques*, 3rd ed. New York: John Wiley & Sons, Inc., 1977.

[387] H. Batih and C. Sorapipatana, ‘‘Characteristics of urban households’ electrical energy consumption in Indonesia and its saving potentials,’’ *Renewable and Sustainable Energy Reviews*, vol. 57, pp. 1160–1173, 2016.

[388] National population commission, ‘‘Nigerian housing and population census priority tables (LGA) Volume II: Housing characteristics and amenities tables,’’ Abuja, Nigeria, 2006. [Online]. Available: http://catalog.ihsn.org/ index.php/catalog/ 3340. [Accessed: Nov. 13, 2017].

[389] O. C. Ibe, *Markov processes for stochastic modeling,* 2nd ed. Oxford: Elsevier Ltd, 2009.

[390] H. Kobayashi, B. L. Mark, and W. Turin, *Probability, random processes, and statistical analysis*. Cambridge: Cambridge University Press,2012.

[391] E. Pardoux, *Markov processes and applications: Algorithms, networks, genome and finance*. Chichester: John Wiley & Sons, Ltd, 2008.

[392] S. Sherman, ‘‘Markov random fields and Gibbs random fields,’’ *Israel Journal of Mathematics*, vol. 14, pp. 92–103, 1973.

[393] L. B. Koralov, S. K. Nechaev, and Y. G. Sinai, ‘‘Limiting probability distribution for a random walk with topological constraints,’’ *Chaos: An Interdisciplinary Journal of Nonlinear Science*, vol. 1, pp. 131–133, 1991.

[394] E. J. Janse Van Rensburg, D. A. W. Sumners, E. Wasserman, and S. G. Whittington, ‘‘Entanglement complexity of self-avoiding walks,’’ *Journal of Physics A: Mathematical and General*, vol. 25, pp. 6557–6566, 1992.

[395] C. Zhang and D. Tao, ‘‘Risk bounds of learning processes for Lévy processes,’’ *Journal of Machine Learning Research*, vol. 14, pp. 351–376, 2013.

[396] P. Nowak and M. Romaniuk, ‘‘Application of Levy processes and Esscher transformed martingale measures for option pricing in fuzzy framework,’’ *Journal of Computational and Applied Mathematics*, vol. 263, pp. 129–151, 2014.

[397] F. Feroz and M. P. Hobson, ‘‘Multimodal nested sampling: An efficient and robust alternative to Markov Chain Monte Carlo methods for astronomical data analyses,’’ *Monthly Notices of the Royal Astronomical Society*, vol. 384, pp. 449–463, 2008.

[398] L. Appels, J. Baeyens, J. Degrève, and R. Dewil, ‘‘Principles and potential of the anaerobic digestion of waste-activated sludge,’’ *Progress in Energy and Combustion Science*, vol. 34, pp. 755–781, 2008.

[399] A. J. Ward, P. J. Hobbs, P. J. Holliman, and D. L. Jones, ‘‘Optimisation of the anaerobic digestion of agricultural resources,’’ *Bioresource Technology*, vol. 99, pp. 7928–7940, 2008.

[400] N. E. M. Rozali, S. R. Wan Alwi, Z. A. Manan, J. J. Klemeš, and M. Y. Hassan, ‘‘Process integration of hybrid power systems with energy losses considerations,’’ *Energy*, vol. 55, pp. 38–45, 2013.

[401] W. S. Ho, H. Hashim, M. H. Hassim, Z. A. Muis, and N. L. M. Shamsuddin, ‘‘Design of distributed energy system through electric system cascade analysis (ESCA),’’ *Applied Energy*, vol. 99, pp. 309–315, 2012.

[402] H. Hashim, W. S. Ho, J. S. Lim, and S. Macchietto, ‘‘Integrated biomass and solar town: Incorporation of load shifting and energy storage,’’ *Energy*, vol. 75, pp. 31–39, 2014.

[403] W. S. Ho, M. Z. W. M. Tohid, H. Hashim, and Z. A. Muis, ‘‘Electric system cascade analysis (ESCA): Solar PV system,’’ *Electrical Power and Energy Systems*, vol. 54, pp. 481–486, 2014.

[404] W. S. Ho, H. Hashim, and J. S. Lim, ‘‘Integrated biomass and solar town concept for a smart eco-village in Iskandar Malaysia (IM),’’ *Renewable Energy*, vol. 69, pp. 190–201, 2014.

[405] E. S. Sreeraj, K. Chatterjee, and S. Bandyopadhyay, ‘‘Design of isolated renewable hybrid power systems,’’ *Solar Energy*, vol. 84, pp. 1124–1136, 2010.

[406] A. K. Daud and M. S. Ismail, ‘‘Design of isolated hybrid systems minimizing costs and pollutant emissions,’’ *Renewable Energy*, vol. 44, pp. 215–224, 2012.

[407] V. Costanzo, R. Yao, E. Essah, L. Shao, M. Shahrestani, A. C. Oliveira, M. Araz, A. Hepbasli, and E. Biyik, “A method of strategic evaluation of energy performance of building integrated photovoltaic in the urban context,” *Journal of Cleaner Production*, vol. 184, pp. 82–91, 2018.

[408] R. Guerrero-Lemus, D. Cañadillas-Ramallo, T. Reindl, and J. M. Valle-Feijóo, “A simple big data methodology and analysis of the specific yield of all PV power plants in a power system over a long time period,” *Renewable and Sustainable Energy Reviews*, vol. 107, pp. 123–132, 2019.

[409] C. Ghenai and M. Bettayeb, “Modelling and performance analysis of a stand-alone hybrid solar PV/fuel cell/diesel generator power system for university building,” *Energy*, vol. 171, pp. 180–189, 2019.

[410] T. Jamal, C. Carter, T. Schmidt, G. M. Shafiullah, M. Calais, and T. Urmee, “An energy flow simulation tool for incorporating short-term PV forecasting in a diesel-PV-battery off-grid power supply system,” *Applied Energy*, vol. 254, pp. 113718–113740, 2019.

[411] M. Shahrestani, R. Yao, E. Essah, L. Shao, A. C. Oliveira, A. Hepbasli, E. Biyik, T. D. Caño, E. Rico, and J. L. Lechón, “Experimental and numerical studies to assess the energy performance of naturally ventilated PV façade systems,” *Solar Energy*, vol. 147, pp. 37–51, 2017.

[412] Q. Yu, M. Hu, J. Li, Y. Wang, and G. Pei, “Development of a 2D temperature-irradiance coupling model for performance characterizations of the flat-plate photovoltaic/thermal (PV/T) collector,” *Renewable Energy*, vol. 153, pp. 404–419, 2020.

[413] S. Watson, D. Bian, N. Sahraei, A. G. Winter, T. Buonassisi, and I. M. Peters, "Advantages of operation flexibility and load sizing for PV-powered system design," *Solar Energy*, vol. 162, pp. 132–139, 2018.

[414] S. P. Ayeng'o, H. Axelsen, D. Haberschusz, and D. U. Sauer, "A model for direct-coupled PV systems with batteries depending on solar radiation, temperature and number of serial connected PV cells," *Solar Energy*, vol. 183, pp. 120–131, 2019.

[415] S. Kaplanis and E. Kaplani, "Energy performance and degradation over 20 years performance of BP c-Si PV modules," *Simulation Modelling Practice and Theory*, vol. 19, pp. 1201–1211, 2011.

[416] Ö. Ayvazoğluyüksel and Ü. B. Filik, ''Estimation methods of global solar radiation, cell temperature and solar power forecasting: A review and case study in Eskişehir,'' *Renewable and Sustainable Energy Reviews*, vol. 91, pp. 639–653, 2018.

[417] M. S. Okundamiya, J. O. Emagbetere, and E. A. Ogujor, ''Evaluation of various global solar radiation models for Nigeria,'' *International Journal of Green Energy*, vol. 13, pp. 505–512, 2016.

[418] T. R. Ayodele and A. S. O. Ogunjuyigbe, ''Performance assessment of empirical models for prediction of daily and monthly average global solar radiation: the case study of Ibadan, Nigeria,'' *International Journal of Ambient Energy*, vol. 38, pp. 803–813, 2017.

[419] S. C. Nwokolo and J. C. Ogbulezie, ''A quantitative review and classification of empirical models for predicting global solar radiation in West Africa,'' *Beni-Suef University Journal of Basic and Applied Sciences*, vol. 7, pp. 367–396, 2018.

[420] J. A. Prescott, ''Evaporation from a water surface in relation to solar radiation,'' *Transactions and Proceedings of the Royal Society of South Australia*, vol. 64, pp. 114–118, 1940.

[421] K. N. Shukla, S. Rangnekar, and K. Sudhakar, ''Comparative study of isotropic and anisotropic sky models to estimate solar radiation incident on tilted surface: A case study for Bhopal, India,'' *Energy Reports*, vol. 1, pp. 96–103, 2015.

[422] B. Jamil and N. Akhtar, ''Empirical models for estimation of diffuse solar radiation based on measured data for humid-subtropical climatic region of India,'' *Journal of renewable sustainable energy*, vol. 9, pp. 1–19, 2017.

[423] P. Cooper, ''The absorption of radiation in solar stills,'' *Solar Energy*, vol. 12, pp. 333–346, 1969.

[424] J. W. Spencer, ''Fourier series representation of the position of the sun,'' *Applied Optics*, vol. 10, pp. 2569–2571, 1971.

[425] O. Behar, A. Khellaf, and K. Mohammedi, ''Comparison of solar radiation models and their validation under Algerian climate – The case of direct irradiance,'' *Energy Conversion and Management*, vol. 98, pp. 236–251, 2015.

[426] Y. El Mghouchi, A. El Bouardi, Z. Choulli, and T. Ajzoul, ''Models for obtaining the daily direct, diffuse and global solar radiations,'' *Renewable and*

Sustainable Energy Reviews, vol. 56, pp. 87–99, 2015.

[427] S. G. D. Iya, M. E. Toriman, M. B. Gazim, U. M. Gana, and M. G. Abdullahi, ‘‘The correlation functions and estimation of global solar radiation studies using sunshine based model for Kano , Nigeria,’’ *Advances in Physics Theories and Applications*, vol. 39, pp. 55–61, 2015.

[428] O. T. Kolebaje and O. L. Mustapha, ‘‘On the performance of some predictive models for global solar radiation estimate in tropical stations : Port Harcourt and Lokoja,’’ *The African Review of Physics*, vol. 7, pp. 145–163, 2012.

[429] O. S. Ohunakin, M. S. Adaramola, O. M. Oyewola, and R. O. Fagbenle, ‘‘Correlations for estimating solar radiation using sunshine hours and temperature measurement in Osogbo , Osun State,’’ *Frontiers Energy*, vol. 7, pp. 214–222, 2013.

[430] G. N. Okonkwo and A. O. C. Nwokoye, ‘‘Estimating global solar radiation from temperature data in Minna Location,’’ *European Scientific Journal*, vol. 10, pp. 254–264, 2014.

[431] O. T. Kolebaje, A. Ikusika, and P. Akinyemi, ‘‘Estimating solar radiation in Ikeja and Port-Harcourt via correlation with relative humidity and temperature,’’ *International Journal of Energy Production and Management*, vol. 1, pp. 253–262, 2016.

[432] S. O. Oyedepo, ‘‘Estimation of global and diffuse solar radiations for selected cities in Nigeria,’’ *International Journal of Energy and Environmental Engineering*, vol. 2, pp. 13–33, 2011.

[433] A. Whillier, ‘‘The determination of hourly values of total solar radiation from daily summations,’’ (in German) *Archiv für Meteorologie Geophysik und Bioklimatologie,* vol. 7, pp. 197–204, 1956.

[434] T. A. Newell, ‘‘Simple models for hourly to daily radiation ratio correlations,’’ *Solar Energy*, vol. 31, pp. 339–342, 1983.

[435] A. Baig, P. Akhter, and A. Mufti, ‘‘A novel approach to estimate the clear day global radiation,’’ *Renewable Energy*, vol. 1, pp. 119–123, 1991.

[436] P. C. Jain, ‘‘Estimation of monthly average hourly global and diffuse irradiation,’’ *Solar and Wind Technology*, vol. 5, pp. 7–14, 1988.

[437] H. P. Garg and S. N. Garg, ‘‘Improved correlation of daily and hourly diffuse radiation with global radiation for Indian stations,’’ *Solar and Wind Technology*, vol. 4, pp. 113–126, 1987.

[438] M. Collares-Pereira and A. Rabl, ‘‘The average distribution of solar radiation-correlations between diffuse and hemispherical and between daily and hourly insolation values,’’ *Solar Energy*, vol. 22, pp. 155–164, 1979.

[439] B. Y. H. Liu and R. C. Jordan, ‘‘The interrelationship and characteristic distribution of effect diffuse and total solar radiation,’’ *Solar Energy*, vol. 4, pp. 1–19, 1960.

[440] C. Gueymard, ‘‘Mean Daily Averages of Beam Radiation By the Atmosphere,’’ *Solar Energy*, vol. 37, pp. 261–267, 1986.

[441] R. Mejdoul M. Taqi, ‘‘The mean hourly global radiation prediction models investigation in two different climate regions in Morocco,’’ *International Journal of Renewable Energy Research*, vol. 2, pp. 608–617, 2012.

[442] T. Muneer, *Solar radiation and daylight models*, 2nd ed. Oxford: Elsevier Ltd, 2004.

[443] T. K. Poddar and G. T. Polley, ‘‘Heat exchanger design through parameter plotting,’’ *Chemical Engineering Research Design*, vol. 74, pp. 849–852, 1996.

[444] G. Strbac, ‘‘Demand side management: Benefits and challenges,’’ *Energy Policy*, vol. 36, pp. 4419–4426, 2008.

[445] M. E. Khodayar, ‘‘Rural electrification and expansion planning of off-grid microgrids,’’ *Electricity Journal*, vol. 30, pp. 68–74, 2017.

[446] C. Leonard, P. Klintenberg, C. Mbohwa, and F. Wallin, ‘‘Replicability and scalability of mini-grid solution to rural electrification programs in sub-Saharan Africa,’’ *Renewable Energy,* vol. 106, pp. 222–231, 2017.

[447] J. Bird, *Electrical and electronic principles and technology*, 3rd ed. Oxford: Elsevier Ltd, 2007.

[448] G. K. Kanji, *100 statistical tests*, 3rd ed. London: SAGE Publications Ltd, 2006.

[449] H. Wang and W. Yang, “An iterative load disaggregation approach based on appliance consumption pattern,” *Applied Sciences*, vol. 8, pp. 1–16, 2018.

[450] V. P. Kurmi, V. P. Gupta, and D. Sharma, ‘‘Impact of voltage variation on electrical and electronic loads and their power consumption,’’ *International Journal of Science, Engineering and Technology Research*, vol. 4, pp. 359–361, 2015.

[451] Nigerian electricity regulatory commission, ‘‘Commencement of 2015 multi year tariff order (MYTO),’’ Abuja, Nigeria, 2019. [Online]. Available: https:// nerc.gov.ng/ index.php/library/documents/MYTO-2015/. [Accessed: Oct. 2, 2019].

[452] CREDC, ‘‘Energy efficiency survey in Nigeria,’’ Abuja, Nigeria, 2009. [Online]. Available: https: // www.osti.gov / etdeweb / servlets / purl / 21328691. [Accessed: Apr. 17, 2015].

[453] T. Khatib and W. Elmenreich, “A model for hourly solar radiation data generation from daily solar radiation data using a generalized regression artificial neural network,” *International Journal of Photoenergy*, vol. 2015, pp. 1–13, 2015.

[454] D. O. Akpootu and Y. A. Sanusi, ‘‘A new temperature-based model for estimating global solar radiation in Port-Harcourt, South-South, Nigeria,’’ *The International Journal of Engineering and Science*, vol. 4, pp. 63–73, 2015.

[455] O. A. Ogbeide, ‘‘Meat industry development in Nigeria : Implications of the consumers’ perspective,’’ *Mayfair Journal of Agribusiness Management*, vol. 1, pp. 59–75, 2015.

[456] Central Bank of Nigeria, ‘‘Money and Credit Statistics - Central Bank of Nigeria,’’ Abuja, Nigeria, 2019. [Online]. Available: https://www.cbn.gov.ng/

rates/mnycredit.asp. [Accessed: Jun. 7, 2019].

[457] National Bureau of Statistics, ‘‘CPI and Inflation Report,’’ Jul., Abuja, Nigeria, 2019. [Online]. Available: https: // nigerianstat.gov.ng /elibrary ? queries [search]=. [Accessed: Aug. 22, 2019].

[458] E. Dioha, J. Dioha, and B. Nfor, ‘‘Operating and financing a family biogas plant,’’ *Journal of Energy Technologies and Policy*, vol. 2, pp. 25–37, 2012.

[459] E. K. Orhorhoro, P. O. Ebunilo, and G. E. Sadjere, ‘‘Experimental determination of effect of total solid (TS) and volatile solid (VS) on biogas yield,’’ *American Journal of Modern Energy*, vol. 6, pp. 131–135, 2017.

[460] F. Rosillo-Calle, P. de Groot, S. L. Hemstock, and J. Woods, *The biomass assessment handbook*. London: Earthscan, 2007.

[461] J. M. Lujano-Rojas, C. Monteiro, R. Dufo-López, and J. L. Bernal-Agustín, ‘‘Optimum load management strategy for wind/diesel/battery hybrid power systems,’’ *Renewable Energy*, vol. 44, pp. 288–295, 2012.

[462] J. M. Lujano-Rojas, C. Monteiro, R. Dufo-López, and J. L. Bernal-Agustín, ‘‘Optimum residential load management strategy for real time pricing (RTP) demand response programs,’’ *Energy Policy*, vol. 45, pp. 671–679, 2012.

[463] A. S. O. Ogunjuyigbe, T. R. Ayodele, and C. G. Monyei, ‘‘An intelligent load manager for PV powered off-grid residential houses,’’ *Energy for Sustainable Development*, vol. 26, pp. 34–42, 2015.

[464] Power cables with excluded insulation and their accessores for rated voltages, IEC 60502-2, Geneva, Switzerland, 2014.

[465] B. M. Weedy and B. A. Cory, *Electric Power Systems*, 4th ed. London: John Wiley & Sons Ltd, 1998.

[466] Power transformers - Part 5: Ability to withstand short circuits, IEC 60076-5, Geneva, Switzerland, 2007.

APPENDIX A: SURVEY ETHICAL APPROVAL

Research & Innovation Service
Level 11, Worsley Building
University of Leeds
Leeds, LS2 9NL
Tel: 0113 343 4873
Email: ResearchEthics@leeds.ac.uk

UNIVERSITY OF LEEDS

Efosa Osaghae
SCPE
University of Leeds

Leeds, LS2 9JT

MaPS and Engineering joint Faculty Research Ethics Committee (MEEC FREC)
University of Leeds

28 September 2019

Dear Efosa

Title of study **DEVELOPMENT AND INTEGRATION OF A BIOMASS AND PHOTOVOLTAIC SYSTEM FOR A RURAL AND URBAN ENERGY BRIDGE**
Ethics reference **MEEC 16-005**

I am pleased to inform you that the application listed above has been reviewed by the MaPS and Engineering joint Faculty Research Ethics Committee (MEEC FREC) and I can confirm a favourable ethical opinion as of the date of this letter. The following documentation was considered:

Document	*Version*	*Date*
MEEC 16-005 New ethical review form_v1_5-3 .doc	2	19/10/16
MEEC 16-005 signed off ethical review form.pdf	1	19/10/16
MEEC 16-005 investigation sheet .docx	1	19/10/16
MEEC 16-005 SURVEY QUESTIONNAIRE.docx	1	19/10/16
MEEC 16-005 VERBAL CONSENT SCRIPT.docx	1	19/10/16

Committee members made the following comments

- Any limits to withdrawal, eg once the results have been written up or published, should be made clear to participants in the survey introduction.
- Consider sharing your research data, eg by submitting it to the University of Leeds Research Data Repository for use in further research. Advice on how to do this can be found via: http://researchdata.leeds.ac.uk.

Please notify the committee if you intend to make any amendments to the original application as submitted at date of this approval as all changes must receive ethical approval prior to implementation. The amendment form is available at http://ris.leeds.ac.uk/EthicsAmendment.

Please note: You are expected to keep a record of all your approved documentation. You will be given a two week notice period if your project is to be audited. There is a checklist listing examples of documents to be kept which is available at http://ris.leeds.ac.uk/EthicsAudits.

We welcome feedback on your experience of the ethical review process and suggestions for improvement. Please email any comments to ResearchEthics@leeds.ac.uk.

Yours sincerely

Jennifer Blaikie
Senior Research Ethics Administrator, Research & Innovation Service
On behalf of Dr Dawn Groves, Chair, MEEC FREC

CC: Student's supervisor(s)

APPENDIX B: SURVEY QUESTIONNAIRE

Household characteristics (demographics)

1] Household class? Class _____
2] Participant name and/or telephone number (optional)? _____
3] House head occupation? _____
4] Number of bed rooms in the house? _____
5] Number of occupants _____

Household occupants' behaviour

6a] When do household occupants' go to bed? _____ to _____
6b] When do household occupants' get up from bed? _____ to _____
6c] When do household occupants' go to work? _____ to _____
6d] When do household occupants' get back from work? _____ to _____

Household activities

7a] When is household cleaning activity done? [AM] _____ to _____ [PM] _____ to _____
7b] When is household cooking activity done? [AM] _____ to _____ [PM] _____ to _____
7c] When is household leisure activity done? [AM] _____ to _____ [PM] _____ to _____

Energy usage and power availability

8a] Is your energy consumption the same for weekdays and weekends? Yes [ ] No [ ]
8b] If no, how significant is the difference in terms of the time of use? Yes [ ] No [ ]
9] Total daily average electricity supply duration? _____ hours
10] Household average monthly electricity bill? _____ hours

Household electrical appliances and appliance time of use

Household appliance	Quantity	Appliance on time (hour)	Appliance off time (hour)	Operating duration (minutes)
Sitting room bulb (Incandescent)				
Sitting room bulb (Energy saving)				
Bedroom bulb (Incandescent)				
Bedroom bulb (Energy saving)				
Outside/security bulb (Incandescent)				
Outside/security bulb (Energy saving)				
Mobile phone				
Sitting room fan				
Bedroom fan				
Television				
Digital video/versatile disc (DVD)				
Electric radio				
Refrigerator				
Electric iron				
Food blender				
Kindly list other household appliances and their appliance time of use				

APPENDIX C: MATLAB CODE FOR THE DEVELOPED STOCHASTIC DEMAND MODEL

```
%%%%%%%%%%%%%%%%%%%%%%%%%%%%%%%%%%%%%%
% set up all variables and constants %
%%%%%%%%%%%%%%%%%%%%%%%%%%%%%%%%%%%%%%
disp('loading data from excel survey file');
clear all;
close all;
total_number_of_household='enter the number of community residential customer';

%housing type fractions (from census data)
fraction_class(1)=0.114;
fraction_class(2)=0.253;
fraction_class(3)=0.508;
fraction_class(4)=0.125;

% house specific parameters
% the index provides the house class
survey_occupants_per_household = zeros(4,150);
survey_occupants_per_household(1,1:31)=xlsread('survey_data',1,'b2:b32')';
survey_occupants_per_household(2,1:69)=xlsread('survey_data',2,'b2:b70')';
survey_occupants_per_household(3,1:139)=xlsread('survey_data',3,'b2:b140')';
survey_occupants_per_household(4,1:34)=xlsread('survey_data',4,'b2:b35')';
survey_bedrooms_per_household = zeros(4,150);
survey_bedrooms_per_household(1,1:31)=xlsread('survey_data',1,'c2:c32')';
survey_bedrooms_per_household(2,1:69)=xlsread('survey_data',2,'c2:c70')';
survey_bedrooms_per_household(3,1:139)=xlsread('survey_data',3,'c2:c140')';
survey_bedrooms_per_household(4,1:34)=xlsread('survey_data',4,'c2:c35')';

%% cooking activities
survey_number_of_refrigerator = zeros(4,150);
survey_number_of_refrigerator(1,1:31) = xlsread('survey_data',1,'d2:d32')';
```

```
survey_number_of_refrigerator(2,1:69) = xlsread('survey_data',2,'d2:d70')';
survey_number_of_refrigerator(3,1:139)=xlsread('survey_data',3,'d2:d140')'
survey_number_of_refrigerator(4,1:34) = xlsread('survey_data',4,'d2:d35')';
power_of_refrigerator = 140; % in watts
survey_number_of_food_blender = zeros(4,150);
survey_number_of_food_blender(1,1:31) = xlsread('survey_data',1,'e2:e32')';
survey_number_of_food_blender(2,1:69) = xlsread('survey_data',2,'e2:e70')';
survey_number_of_food_blender(3,1:139) = xlsread('survey_data',3,'e2:e140')';
survey_number_of_food_blender(4,1:34) = xlsread('survey_data',4,'e2:e35')';
power_of_food_blender = 250; % in watts
mark_of_food_blender = 5;
space_of_food_blender = 55;
period_of_food_blender = mark_of_food_blender + space_of_food_blender;

%% cleaning activities
survey_number_of_electric_iron = zeros(4,150);
survey_number_of_electric_iron(1,1:31) = xlsread('survey_data',1,'f2:f32')';
survey_number_of_electric_iron(2,1:69) = xlsread('survey_data',2,'f2:f70')';
survey_number_of_electric_iron(3,1:139)=xlsread('survey_data',3,'f2:f140')'
survey_number_of_electric_iron(4,1:34) = xlsread('survey_data',4,'f2:f35')';
power_of_electric_iron = 1000; % in watts
mark_of_electric_iron = 10;
space_of_electric_iron = 50;
period_of_electric_iron = mark_of_electric_iron + space_of_electric_iron;

%% leisure activities
survey_number_of_television = zeros(4,150);
survey_number_of_television(1,1:31) = xlsread('survey_data',1,'g2:g32')';
survey_number_of_television(2,1:69) = xlsread('survey_data',2,'g2:g70')';
survey_number_of_television(3,1:139) = xlsread('survey_data',3,'g2:g140')';
survey_number_of_television(4,1:34) = xlsread('survey_data',4,'g2:g35')';
power_of_television = 50;% in watts
survey_number_of_dvd_player = zeros(4,150);
survey_number_of_dvd_player(1,1:31) = xlsread('survey_data',1,'h2:h32')';
```

```
survey_number_of_dvd_player(2,1:69) = xlsread('survey_data',2,'h2:h70')';
survey_number_of_dvd_player(3,1:139) = xlsread('survey_data',3,'h2:h140' )';
survey_number_of_dvd_player(4,1:34) = xlsread('survey_data',4,'h2:h35')';
power_of_dvd_player = 15; % in watts
survey_number_of_radio_player = zeros(4,150);
survey_number_of_radio_player(1,1:31) = xlsread('survey_data',1,'i2:i32')';
survey_number_of_radio_player(2,1:69) = xlsread('survey_data',2,'i2:i70')';
survey_number_of_radio_player(3,1:139) = xlsread('survey_data', 3,'i2:i140' )';
survey_number_of_radio_player(4,1:34) = xlsread('survey_data',4,'i2:i35')';
power_of_radio_player = 10; % in watts
survey_number_of_mobile_phone_charger = zeros(4,150);
survey_number_of_mobile_phone_charger(1,1:31)=xlsread
('survey_data',1,'j2:j32')';
survey_number_of_mobile_phone_charger(2,1:69)=xlsread
('survey_data',2,'j2:j70')';
survey_number_of_mobile_phone_charger(3,1:139)=xlsread
('survey_data',3,'j2:j140')';
survey_number_of_mobile_phone_charger(4,1:34)=xlsread
('survey_data',4,'j2:j35')';
power_of_mobile_phone_charger = 5; % in watts
survey_number_of_sitting_room_electric_fan = zeros(4,150);
survey_number_of_sitting_room_electric_fan(1,1:31)=xlsread
('survey_data',1,'k2:k32')';
survey_number_of_sitting_room_electric_fan(2,1:69)=xlsread
('survey_data',2,'k2:k70')';
survey_number_of_sitting_room_electric_fan(3,1:139)=xlsread
('survey_data',3,'k2:k140')';
survey_number_of_sitting_room_electric_fan(4,1:34)=xlsread
('survey_data',4,'k2:k35')';
power_of_sitting_room_electric_fan = 70; % in watts
survey_number_of_bed_room_electric_fan = zeros(4,150);
survey_number_of_bed_room_electric_fan(1,1:31)=xlsread
('survey_data',1,'l2:l32')';
survey_number_of_bed_room_electric_fan(2,1:69)=xlsread
('survey_data',2,'l2:l70')';
survey_number_of_bed_room_electric_fan(3,1:139)=xlsread
('survey_data',3,'l2:l140')';
```

```
survey_number_of_bed_room_electric_fan(4,1:34)=xlsread
('survey_data',4,'l2:l35')';
power_of_bed_room_electric_fan = 70; % in watts

%% lighting activities
survey_number_of_sitting_room_lights = zeros(4,150);
survey_number_of_sitting_room_lights(1,1:31)=xlsread('survey_data',1,'m2:m32')';
survey_number_of_sitting_room_lights(2,1:69)=xlsread('survey_data',2,'m2:m70')';
survey_number_of_sitting_room_lights(3,1:139)=xlsread
('survey_data',3,'m2:m140')';
survey_number_of_sitting_room_lights(4,1:34)=xlsread('survey_data',4,'m2:m35')';
power_of_sitting_room_lights = 60; % in watts
survey_number_of_bed_room_lights = zeros(4,150);
survey_number_of_bed_room_lights(1,1:31) = xlsread('survey_data',1, 'n2:n32')';
survey_number_of_bed_room_lights(2,1:69) =xlsread('survey_data',2, 'n2:n70')';
survey_number_of_bed_room_lights(3,1:139)=xlsread('survey_data',3, 'n2:n140')';
survey_number_of_bed_room_lights(4,1:34) = xlsread('survey_data',4, 'n2:n35')';
power_of_bed_room_lights = 60; % in watts
mark_of_bed_room_lights = 10; % in minutes
space_of_bed_room_lights = 50; % in minutes
period_of_bed_room_lights = mark_of_bed_room_lights + space_of_bed_room_lights;
survey_number_of_external_lights = zeros(4,150);
survey_number_of_external_lights(1,1:31) = xlsread('survey_data',1,'o2:o32' )';
survey_number_of_external_lights(2,1:69) = xlsread('survey_data',2,'o2:o70' )';
survey_number_of_external_lights(3,1:139)=xlsread('survey_data',3, 'o2:o140')';
survey_number_of_external_lights(4,1:34) = xlsread('survey_data',4,'o2:o35')';
power_of_external_lights = 60; % in watts

%% simulation duration
number_of_days = 1;
number_of_hours = number_of_days*24;
number_of_minutes = number_of_hours * 60;
number_cooking = zeros(number_of_hours,1);
number_cleaning = zeros(number_of_hours,1);
number_leisure = zeros(number_of_hours,1);
```

```
total_power = zeros(number_of_minutes,1);
community_power = zeros(number_of_minutes,1);

% appliance power usage initialization
power_refrigerator = zeros(number_of_minutes,1);
power_blender = zeros(number_of_minutes,1);
power_iron = zeros(number_of_minutes,1);
power_tv = zeros(number_of_minutes,1);
power_dvd = zeros(number_of_minutes,1);
power_radio = zeros(number_of_minutes,1);
power_phone = zeros(number_of_minutes,1);
power_sr_fan = zeros(number_of_minutes,1);
power_br_fan = zeros(number_of_minutes,1);
power_sr_bulb = zeros(number_of_minutes,1);
power_br_bulb = zeros(number_of_minutes,1);
power_external_bulb = zeros(number_of_minutes,1);

% applicance states initialization
tv_state = zeros(number_of_hours,1);
dvd_state = zeros(number_of_hours,1);
radio_state = zeros(number_of_hours,1);
mobile_phone_charging_state = zeros(number_of_hours,1);
sitting_room_fan_state = zeros(number_of_hours,1);
bed_room_fan_state = zeros(number_of_hours,1);
food_blender_state = zeros(number_of_hours,1);
electric_iron_state = zeros(number_of_hours,1);
sitting_room_bulb_state = zeros(number_of_hours,1);
bed_room_bulb_state = zeros(number_of_hours,1);
external_bulb_state = ones(number_of_minutes,1);
refrigerator_state= zeros(number_of_minutes,1);

%occupant states and activities
% occupant states
% occupant state 1: inactive at home (asleep)
```

```
% occupant state 2: active at home
% occupant state 3: away from home
% activities
% activity 1: cooking
% activity 2: cleaning
% activity 3: leisure
%% description and loading of the conditional probabilities
% cp1: this is the probability of getting up in the morning given that he is asleep
% cp2: this is the probability of going to work given that the occupant is
% awake at home
% cp3: this is the probability of coming home given that the occupant is
% away from home
% cp4: this is the probability of going to sleep given that the occupant is
% awake at home
cp1 = xlsread('survey_data',1,'c151:z151');
cp2 = xlsread('survey_data',1,'c152:z152');
cp3 = xlsread('survey_data',1,'c153:z153');
cp4 = xlsread('survey_data',1,'c154:z154');

%% description and loading of the activity's probabilities
% cpa1: this is the probability of cleaning given that there is one or more active
occupant
% cpa2: this is the probability of cooking given that there is one or more active
occupant
% cpa3: this is the probability of leisure given that there is one or more active
occupant
cpa1 = xlsread('survey_data',1,'c159:z159');
cpa2 = xlsread('survey_data',1,'c160:z160');
cpa3 = xlsread('survey_data_1100',1,'c161:z161');

%% description and loading of activities probabilities
cpfb = xlsread('survey_data',1,'c166:z166'); % food blender time-use probability
cpei = xlsread('survey_data',1,'c167:z167'); % probability of electric iron time-use
cptv = xlsread('survey_data',1,'c168:z168'); % probability of tv time-use
cpdvd = xlsread('survey_data',1,'c169:z169'); % probability of dvd time-use
```

```
cpradio = xlsread('survey_data',1,'c170:z170'); % probability of radio time-use
cpbf = xlsread('survey_data',1,'c171:z171'); % bedroom fan time-use probability
cpsf=xlsread('survey_data',1,'c172:z172'); % sitting room fan time-use probability
cpbb=xlsread('survey_data',1,'c173:z173'); % bedroom bulb time-use probability
cpsb=xlsread('survey_data',1,'c174:z174');% sitting room bulb time-use probability

% simulation on refrigerator time-use
refrigerator_success = 0.30;
for minute=1:number_of_minutes
        if refrigerator_success > rand
        refrigerator_state(minute)=refrigerator_state(minute)+1;
        end
end % end of simulation on refrigerator time-use

% daily sunrise and sunset related parameters
latitude=6.335; %latitude of the location in degrees
twilight =6/15*60;
declination_angle = zeros(number_of_days,1);
solar_angle = zeros(number_of_days,1);
sunrise = zeros(number_of_days,1);
sunset = zeros(number_of_days,1);
on_time = zeros(number_of_days,1);
off_time = zeros(number_of_days,1);

% check for probabilities that exceed 1
 if max(cp1) > 1
disp('error:p1 exceeds 1');
 end
if max(cp3) > 1
disp('error:p3 exceeds 1');
end
if max(cp2+cp4) > 1
disp('error: p2 + p4 exceeds 1');
end
```

```
%%%%%%%%%%%%%%%%%%%%%%%%%%%%%%%%
% calculate occupant states %
%%%%%%%%%%%%%%%%%%%%%%%%%%%%%%%%
power = zeros(number_of_hours*60,12,total_number_of_household);
for household = 1:total_number_of_household
        disp(['calculating household ' num2str(household)]);

        % select a class based on class fraction data
        r = rand();
        if r < fraction_class(1)
                class = 1;
        elseif r < (fraction_class(1) + fraction_class(2))
                class = 2;
        elseif r < (fraction_class(1) + fraction_class(2) + fraction_class(3))
                class = 3;
        else
                class = 4;
        end % end of the simulation that select a class based on class fraction data

        disp(['class ' num2str(class)]);

        % select a random house from the survey
        switch class
                case 1
                        household_sample = ceil(rand * 31);
                case 2
                        household_sample = ceil(rand * 69);
                case 3
                        household_sample = ceil(rand * 139);
                case 4
                        household_sample = ceil(rand * 34);
        end % end of the selection of a random house from the survey households
number_of_occupants=survey_occupants_per_household(class,household_sample);
disp(['number of occupants per household ' num2str( number_of_occupants)]);
```

```
number_of_bedrooms=survey_bedrooms_per_household(class,household_sample);
disp(['number of bedrooms ' num2str(number_of_bedrooms)]);
occupant_state = ones(number_of_occupants,number_of_hours+1);

% allocate number of appliances
number_of_refrigerator=survey_number_of_refrigerator(class,household_sample);
number_of_food_blender=survey_number_of_food_blender
(class,household_sample);
number_of_electric_iron=survey_number_of_electric_iron
(class,household_sample);
number_of_television = survey_number_of_television(class,household_sample);
number_of_dvd_player = survey_number_of_dvd_player(class,household_sample);
number_of_radio_player=survey_number_of_radio_player
(class,household_sample);
number_of_mobile_phone_charger=survey_number_of_mobile_phone_charger
(class,household_sample);
number_of_sitting_room_electric_fan=survey_number_of_sitting_room_electric_fan
(class,household_sample);
number_of_bed_room_electric_fan=survey_number_of_bed_room_electric_fan
(class,household_sample);
number_of_sitting_room_lights=survey_number_of_sitting_room_lights
(class,household_sample);
number_of_bed_room_lights=survey_number_of_bed_room_lights
(class,household_sample);
number_of_external_lights=survey_number_of_external_lights
(class,household_sample);

% determine occupant state for each occupant in each hour
        for occupant = 1:number_of_occupants
                for time = 1:number_of_hours
                        hour = rem(time,24);
                        if hour == 0
                                hour = 24;
                        end
                        random_number = rand;
                        new_state = occupant_state(occupant,time);
                switch occupant_state(occupant,time)
```

```
                    case 1 % inactive at home (asleep)
                    if cp1(hour)>random_number
                            new_state = 2;
                    end
                    case 2 % active at home
                    if cp2(hour)>random_number
                            new_state = 3;
                    end
                    if (1-cp4(hour))<random_number
                            new_state = 1;
                    end
                    case 3 % away from home
                    if cp3(hour)>random_number
                            new_state = 2;
                    end
            end % end of occupant state simulation
                    occupant_state(occupant,time+1) = new_state;
            end % end of simulation for each hourly time step
    end % end of simulation for each household occupant

%%%%%%%%%%%%%%%%%%%%%%%%%%%%%%%%
% calculate active occupancy %
%%%%%%%%%%%%%%%%%%%%%%%%%%%%%%%%
active_occupancy = sum(occupant_state(:,:) == 2);
home_occupancy = sum(occupant_state(:,:) == 1) + sum(occupant_state(:,:) == 2);
daily_average_hours_with_active_occupant=round
(((sum(active_occupancy(:)~=0))/number_of_days));
mark_of_mobile_phone_charger=round
((2*60)/daily_average_hours_with_active_occupant);
space_of_mobile_phone_charger = 60 - mark_of_mobile_phone_charger;
period_of_mobile_phone_charger=mark_of_mobile_phone_charger+
space_of_mobile_phone_charger;

%%%%%%%%%%%%%%%%%%%%%%%%%%%%%%%%
% calculate activities numbers %
```

```
%%%%%%%%%%%%%%%%%%%%%%%%%%%%%%%%%%%%
number_cooking(:) = 0;
number_cleaning(:) = 0;
number_leisure(:) = 0;
        for time = 1:number_of_hours
                hour = rem(time,24);
                if hour == 0
                        hour = 24;
                end
                if active_occupancy(time) ~= 0
                        for occupant = 1:active_occupancy(time)
                                if cpa1(hour) > rand
                                number_cleaning(time) = number_cleaning(time)+1;
                                end
                                if cpa2(hour) > rand
                                number_cooking(time) = number_cooking(time)+1;
                                end
                                if cpa3(hour) > rand
                                number_leisure(time) = number_leisure(time)+1;
                                end
                        end % end of simulation on number of occupants per activity
                end % end of simulation on number of active occupancy
        end % end of simulation on the number of active occupants for each time step

%%%%%%%%%%%%%%%%%%%%%%%%%%%%%%%%%%%%
% calculate appliance use %
%%%%%%%%%%%%%%%%%%%%%%%%%%%%%%%%%%%%

% simulation of appliances that are turned on per time
        for hour = 1:number_of_hours
                hour_of_day = rem(hour,24);
                if hour_of_day == 0
                        hour_of_day = 24;
                end
```

```
            tv_state(hour)=(active_occupancy(hour)>=1)&&  (cptv(hour_of_day)
            > rand);
            dvd_state(hour)=(number_leisure(hour)>=1)&&
            (cpdvd(hour_of_day) > rand);
            radio_state(hour)=(active_occupancy(hour)>=1)&&
            (cpradio(hour_of_day)>rand);
            mobile_phone_charging_state(hour)=(active_occupancy(hour) >= 1);
            sitting_room_fan_state(hour)=(number_leisure(hour)>=1)&&
            (cpsf(hour_of_day)>rand);
            bed_room_fan_state(hour) = (cpbf(hour_of_day) > rand);
            food_blender_state(hour)=(number_cooking(hour)>=1)&&
            (cpfb(hour_of_day)>rand);
            electric_iron_state(hour)  =  (number_cleaning(hour)  >=1)  &&
            (cpei(hour_of_day) > rand);
            sitting_room_bulb_state(hour)=(number_leisure(hour)>=1)&&
            (cpsb(hour_of_day)> rand);
            bed_room_bulb_state(hour)=(active_occupancy(hour)>=1)&&
            (cpbb(hour_of_day)> rand);
        end % end of simulation of appliances that are turned on per time

%%%%%%%%%%%%%%%%%%%%%%%%%%%
% minutely simulation of appliance load profile %
%%%%%%%%%%%%%%%%%%%%%%%%%%%

% set some random minute offsets for mark-space appliances to avoid
% repetition
minute_offset_fridge = ceil(rand * 60);
minute_offset_blender = ceil(rand * 60);
minute_offset_iron = ceil(rand * 60);
minute_offset_phone = ceil(rand * 60);
minute_offset_lights = ceil(rand * 60);

minute_offset = ceil(rand * 60) - 30;
        for minute = 1:number_of_minutes
            hour = ceil((minute + minute_offset) / 60);
            if hour == 0
                hour = 1;
```

```
        end
        if hour == (number_of_hours + 1)
                hour = number_of_hours;
        end

%% cooking activities
% fridge freezer
power_refrigerator(minute)=power_of_refrigerator*number_of_refrigerato*
refrigerator_state(minute);
% food blender
power_blender(minute)=power_of_food_blender*number_of_food_blender*
((rem(minute+minute_offset_blender,period_of_food_blender)<
mark_of_food_blender) && (food_blender_ state(hour)));

%% cleaning activities
% elecric iron
power_iron(minute)=power_of_electric_iron*number_of_electric_iron*
((rem(minute+minute_offset_iron,period_of_electric_iron)<
mark_of_electric_iron) && (electric_iron_state(hour)));

%% effect of leisure activities on demand
% television
power_tv(minute)=power_of_television*number_of_television*
tv_state(hour);
% dvd player
power_dvd(minute)=power_of_dvd_player*number_of_dvd_player*
dvd_state (hour);
% radio player
power_radio(minute)=power_of_radio_player*number_of_radio_player*
radio_state(hour);
% mobile phone charger
power_phone(minute)=power_of_mobile_phone_charger*
number_of_mobile_phone_charger*((rem(minute+
minute_offset_phone,period_of_mobile_phone_charger)<
mark_of_mobile_phone_charger)&&(mobile_phone_charging_state (hour)));
% sitting room electric fan
power_sr_fan(minute)=power_of_sitting_room_electric_fan*
number_of_sitting_room_electric_fan*sitting_room_fan_state(hour);
```

```
% bed room electric fan
power_br_fan(minute)=power_of_bed_room_electric_fan*
number_of_bed_room_electric_fan*bed_room_fan_state(hour);

%% effect of lighting on demand
% internal lights
% sitting room bulb
power_sr_bulb(minute)=power_of_sitting_room_lights*
number_of_sitting_room_lights*sitting_room_bulb_state(hour);
% bed room bulb
power_br_bulb(minute)=power_of_bed_room_lights*
number_of_bed_room_lights*((rem(minute+
minute_offset_lights,period_of_bed_room_lights)<mark_of_bed_room_lights)
&& (bed_room_bulb_state(hour)));

% external lights (outside/security bulbs)
% minutely simulation of external bulb time-us
    for day = 1:number_of_days
     declination_angle(day)=23.43*sin(deg2rad((360/365)*(284+day) ));
     solar_angle(day)=rad2deg(acos((tan(deg2rad
     (declination_angle(day)))*tan(deg2rad(latitude) ))));
     sunrise(day) = ceil((12-((12*solar_angle(day))/180))*60);
     sunset(day) = ceil((12+((12*solar_angle(day))/180))*60);
     on_time = sunset(day)+ceil(rand*twilight)+(day-1)*24*60;
     off_time = sunrise(day)-ceil(rand*twilight)+(day-1)*24*60;
     external_bulb_state(off_time:on_time) = zeros(on_time-off_time+1,1);
     end % end of minutely simulation of external bulb time-use
power_external_bulb(minute)=power_of_external_lights*
number_of_external_ lights*external_bulb_state(minute);

end% end of minutely simulation of the load profiles of household appliances

end % end of minutely simulation of the community residential load profile.
```